SHRP-A-404

Fatigue Response of Asphalt-Aggregate Mixes

Asphalt Research Program
Institute of Transportation Studies
University of California, Berkeley

Strategic Highway Research Program
National Research Council
Washington, DC 1994

SHRP-A-404
Contract A-003A
ISBN 0-309-05812-0
Product no.: 1019

Program Manager: *Edward T. Harrigan*
Project Manager: *Rita B. Leahy*
Program Area Secretary: *Juliet Narsiah*
Production Editor: *Margaret S. Milhous*

June 1994

key words:

controlled stress
controlled strain
diametral fatigue
dissipated energy
fatigue life
flexural beam fatigue
phase angle
stiffness
trapezoidal fatigue

Strategic Highway Research Program
National Research Council
2101 Constitution Avenue N.W.
Washington, DC 20418

(202) 334-3774

1.5M/NAP/594

Acknowledgments

The research described herein was supported by the Strategic Highway Research Program (SHRP). SHRP is a unit of the National Research Council that was authorized by section 128 of the Surface Transportation and Uniform Relocation Assistance Act of 1987.

This project, entitled "Performance Related Testing and Measuring of Asphalt-Aggregate Interactions and Mixtures," was conducted at the Institute of Transportation Studies, University of California at Berkeley, with Carl L. Monismith as Principal Investigator.

The flexural beam fatigue controlled-stress and controlled-strain testing was done at the University of California, Berkeley. Thanks are due to Bor-Wen Tsai, Elie Abijaoude, K. S. Yapa, Thomas Mills, and all other lab technicians and helpers for their efforts in specimen preparation and testing. Clarence Chan, Ed Nicks, and Todd Merport provided the necessary support for the manufacture, design, and repairs of the test equipment and electronics.

The trapezoidal, cantilever, controlled-stress and controlled-strain fatigue tests were conducted by SWK Engineering, University of Nottingham. The diametral fatigue tests were conducted at North Carolina State University. Statistical design of the laboratory testing program was prepared by the SHRP Project A-003A statistician, Lou Painter, under whose direction and guidance the fatigue data were statistically analyzed.

Contents

List of Figures

List of Tables

Abstract

This three-part report covers the development of accelerated performance tests for defining the fatigue response of asphalt-aggregate mixes and their use in mix analysis and design systems. The development process included a number of phases, which are described in the report. Included in this report are the following:

- A state-of-knowledge review for fatigue response of asphalt-aggregate mixes, including the identification of candidate tests to measure fatigue resistance that can be used for performance (fatigue cracking) prediction.

- A description of a pilot test program and its results to evaluate the candidate tests and to select suitable equipment and procedures to define mix fatigue response.

- A description of an expanded test program using the equipment and methodology selected in the pilot test program to 1) provide an expanded database, 2) validate the fatigue parameters included in the SHRP binder specifications, 3) explore relationships between mix properties, laboratory fatigue response, and anticipated pavement performance, and 4) develop surrogate models of fatigue behavior that, when appropriate, might substitute for laboratory testing.

- A description of a mix analysis and design system which can be used to mitigate fatigue cracking.

Executive Summary

The objectives of Strategic Highway Research Program (SHRP) Project A-003A were to develop a series of accelerated performance-related tests for asphalt-aggregate mixes, and to identify methods for analyzing asphalt-aggregate interactions which significantly affect pavement performance. The scope of the A-003A project included fatigue cracking, one of the major distress mechanisms that affects asphalt pavement performance.

This report includes the following:

- The methodology used to select the test for defining mix fatigue response (Part I).

- The use of the test method to 1) provide an expanded database for the fatigue response of 44 mixes containing conventional binders and information for the validation of the A-002A binder specification, 2) explore relationships between mix properties, laboratory fatigue response, and anticipated pavement performance, and 3) develop surrogate models of fatigue behavior that, when appropriate, might substitute for laboratory testing (Part II).

- Use of the test methodology and results to develop a mix analysis and design system to mitigate fatigue cracking (Part III).

To select the test methodology used for defining fatigue response, several candidate procedures were identified, including pulsed loading in flexure using third-point loading, sinusoidal loading in flexure using cantilever loading, sinusoidal loading in the uniaxial tension-compression mode, notched beam flexure loading and fracture mechanics (C*-line integral) considerations, and pulsed loading in the diametral mode.

The mix variables evaluated included asphalt type (temperature susceptibility), asphalt content, aggregate stripping potential, degree of compaction, temperature, and strain level. Sixty-four combinations were possible. To estimate the main effects and interactions 32 combinations were evaluated, and each cell was replicated for a total of 64 fatigue tests.

The evaluation highlighted many of the advantages and disadvantages of the candidate accelerated performance tests. Two of the candidate tests—uniaxial tension tests and fracture mechanics tests—were quickly eliminated after preliminary testing. Gripping the specimen is difficult in pure tension testing, and end-cap failure due to stress concentrations was a

persistent problem in the testing completed. Testing for fracture mechanics analysis is thought to be too extensive for routine mix analysis and design: repetitive fatigue tests are necessary to evaluate the crack initiation process as well as the crack growth rate, and notched-beam strength tests are necessary to evaluate the C*-line integral.

Among the remaining three candidate procedures, the diametral (indirect tension) test is appealing because of its ability to evaluate briquette-shaped specimens. The testing program demonstrated that, although diametral fatigue was reasonably reliable, it was generally inferior to flexural fatigue in the sensitivity of its measurements to mix composition. Measured stiffnesses were comparatively large—perhaps excessively so—and cycles to failure were unreasonably small. With the exception of the effect of aggregate type on stiffness, other mix and loading effects in the diametral testing were found to be reasonable.

In the final analysis, diametral testing is not suitable for routine mix analysis and design because of 1) the high incidence of unacceptable fracture patterns, 2) stress concentrations at the loading platens, and 3) its limitations under controlled-stress loading conditions. Moreover, its variable biaxial stress state, its inability to reverse stress fields, and the confounding influence of permanent deformations within test specimens on their resistance to repetitive tensile loading raise serious additional concerns.

The testing program revealed no striking differences between beam and cantilever testing. However, beam measurements were convincingly more sensitive to mix variables than cantilever measurements. With the exception of beam testing's failure to reasonably demonstrate the effect of asphalt content on cycles to failure and cantilever testing's questionable stiffness-temperature effects, the results of both tests were judged to be reasonable.

Although beam tests are advantageous because of their uniform stress distribution and the fact that gluing is unnecessary, the beam and cantilever tests are considered equivalent means for assessing the fatigue behavior of asphalt-aggregate mixes. Nevertheless, the beam test is preferred because of the authors' familiarity with it and because of the sophistication of its current design and its software interface.

A number of working hypotheses supported the study, and the report reflects on these. For example, one hypothesis stated that crack initiation in a given mix is related to stress or strain level as follows:

$$N_f = a(1/\epsilon)^b \quad \text{or} \quad N_f = c(1/\sigma)^d$$

where:

	N_f	=	number of load application to crack initiation,
	ϵ, σ	=	tensile strain and tensile stress, respectively, and
	a, b, c, d	=	experimentally determined coefficients dependent on test temperature.

These relationships were consistently confirmed for the ranges of stresses and strains to which the laboratory specimens were subjected. Replacing strain or stress with the energy

dissipated during an initial loading cycle, w_o, yielded an equally reliable and accurate expression as follows:

$$N_f = e(1/w_o)^f$$

where: e, f = experimentally determined coefficients dependent of test temperatures.

Early literature advanced the notion that a unique relationship might possibly exist between the number of cycles to failure and the cumulative energy dissipated to failure. If so, laboratory testing could be abbreviated, surrogates to testing appeared more promising, and compound loading could be handled more directly. Because of these advantages, considerable effort was made to investigate possible relationships between cycles to failure and cumulative dissipated energy. These efforts confirmed that, when strain is the only test variable, cycles to failure for a given mix are related to cumulative dissipated energy as follows:

$$W_N = A(N_f)^z$$

where: N_f = number of cycles to failure,
W_N = cumulative dissipated energy to failure, and
A, z = experimentally determined coefficients.

Unfortunately, the uniqueness of this relationship for different types and conditions of testing could not be substantiated. In fact, detailed investigation revealed that these relationships are different for different mixes and are affected by both test temperature and mode of testing.

Despite this disappointment, dissipated energy remains a useful concept in fatigue investigations. As noted above, the initial energy dissipated during each loading cycle—capturing effects not only of the imposed strain level but also of the dynamic mix properties—is a good predictor of cycles to failure and is thus a key component of surrogate models. Furthermore, dissipated energy is highly correlated with stiffness decrements during fatigue testing and helps to explain the effects of mode of loading on mix behavior.

The second portion of the study consisted of a series of laboratory fatigue tests and various wheel track tests conducted to validate the A-003A's accelerated performance test for fatigue. The laboratory test program tested 44 mixes that covered a range of asphalt and aggregate types. In addition, limited testing was conducted on mixes containing modified binders. The wheel track tests included those performed in the SWK laboratory wheel track device; a full-scale, Laboratoire Central des Ponts et Chaussées (LCPC) circular test track at Nantes; and the Federal Highway Administration (FHWA) Accelerated Loading Facility (ALF) at the Turner-Fairbank Highway Research Center in McLean, Virginia.

Improvements and changes in the test equipment and procedures significantly improved the repeatability of the laboratory fatigue test as indicated by a coefficient of variation of 40 percent for fatigue life versus the approximately 90 percent value observed during the pilot test program. These improvements in test repeatability allowed a short fatigue test procedure

to be developed in which a mix could be characterized in as little as 24 hours with a minimum of four fatigue tests.

The most extensive series of tests in this extended phase was the expanded test program, which included testing with eight Materials Reference Library (MRL) core asphalts and two MRL core aggregates. This series of tests provided vital information not only for evaluation and validation of the fatigue test itself, but also for confirmation of the SHRP Project A-002A fatigue hypothesis and the development of surrogate fatigue models.

Comparison of A-003A laboratory fatigue test results to those of the laboratory wheel track test results indicated that, for fatigue life, the ranking of core MRL asphalts from wheel track testing was similar to the ranking based on the fatigue life obtained from SHRP Project A-003A flexural beam fatigue tests.

For modified MRL asphalts, as well as for the non-MRL Nantes materials, validation results were inconclusive. However, it should be noted that, for the Nantes materials, rankings of mixes based on A-003A fatigue tests were similar to the rankings based on tests conducted by LCPC and those conducted by SHELL-Koninklijke Shell Laboratorium Amsterdam (SHELL-KSLA).

The results of the extended program provide the following observations:

- Conventional wisdom generally suggests that asphalt-aggregate mixes with lower stiffnesses are likely to demonstrate better fatigue resistance under controlled-strain loading than their counterparts with higher stiffnesses. Although binder effects on stiffness and fatigue life confirmed this concept, the effects of air-void content and aggregate type did not. Lower air-void content and crushed, rough-textured aggregates showed increased stiffness *and* increased fatigue life.

- A detailed analysis of asphalt effects indicated that the loss stiffness of the aged binder provides a good indication of the relative laboratory fatigue resistance of otherwise identical mixes. Accordingly, binder loss stiffness seems to be an attractive candidate for inclusion in binder specifications.

- The loss stiffness of the binder, however, is generally not a sufficient indication of the relative fatigue resistance of mixes. Other mix characteristics, such as asphalt content, aggregate type, and air-void content, also contribute significantly to laboratory fatigue resistance. Accordingly, a binder specification alone is insufficient to ensure satisfactory pavement performance.

- Although having laboratory test data on mixes is necessary for characterizing fatigue behavior, laboratory testing must be interpreted by using mechanistic analyses to determine how mixes are likely to perform in a pavement under anticipated traffic loads and environmental conditions. Accordingly, mix

specifications must address the composite effects of mix, structure, loading, and environment on pavement performance.

- Calibrations of surrogate fatigue models suggest that 1) the effects of initial mix stiffness and phase angle on fatigue life can be expressed with equivalent accuracy by the initial mix loss stiffness, 2) the effect of mix voids on fatigue life can be expressed with equivalent accuracy by either the air-void content or the percentage of voids filled with asphalt, and 3) the effects of initial strain level, mix stiffness, and phase angle on fatigue life can be expressed with equivalent accuracy by the initial dissipated energy per cycle.

- In general, the slope (K_2) of the strain-life relationship was found to be highly temperature sensitive and is expected to increase with an increase in the temperature susceptibility of asphalt binder.

- Fatigue life estimates from the strain- and energy-based surrogate fatigue models developed during the 8×2 expanded test program compared well with the life measurements in the temperature equivalency factors experiment. However, the surrogate models were unable to reproduce the observed effect of temperature on the strain-life slope (K_2).

- The ranking of six core MRL asphalts based on the fatigue life (N_1) from laboratory wheel track testing was similar to the ranking based on the fatigue life obtained from laboratory flexural beam fatigue tests.

- For LCPC-Nantes (non-MRL) materials, the SHRP A-003A flexural beam fatigue tests ranked mixes similar to those rankings based on the SHELL-KSLA flexural beam fatigue tests and the LCPC trapezoidal cantilever tests.

- The ranking of LCPC-Nantes mixes based on full-scale, circular wheel track results are not in agreement with the ranking of mixes based on any of the laboratory test results.

- Estimated pavement fatigue lives for the FHWA-ALF experiment based on the SHRP A-003A laboratory accelerated performance test as well as the surrogate models are in good agreement with the observed pavement fatigue life to surface crack initiation.

- Based on the combined laboratory fatigue data, the following strain-dependent model is used for surrogate analysis:

$$N_f = 2.738*10^5 \exp^{0.077\ VFB} (\epsilon_o)^{-3.624} (S_o'')^{-2.720}$$

where:
- N_f = fatigue life,
- ϵ_o = initial strain, in./in.,
- S_o'' = initial loss-stiffness, psi, and
- VFB = percent voids filled with asphalt.

- The following steps are recommended for the use of shear stiffness testing in the surrogate fatigue procedure:

    1. Convert the shear loss-stiffness (G''_o) at 20°C (68°F) and 10 Hz frequency to a flexural loss-stiffness (S''_o) at the same temperature and frequency.

    2. Estimate the fatigue resistance from the surrogate fatigue model.

- The effects of mix composition on fatigue resistance can be determined most accurately by laboratory fatigue testing; fatigue testing may be required in order to assess the fatigue resistance of new and unconventional mixes. At the same time, the fatigue resistance of unconventional mixes can be estimated, although often less accurately, by using precalibrated regression models.

The third portion of the report describes an innovative design and analysis system for evaluating the fatigue resistance of asphalt-aggregate mixes. This system provides an effective mechanism for interpreting laboratory fatigue measurements and determining the impact of asphalt-aggregate interactions on expected pavement performance. The system allows mix testing to take into consideration traffic loading (repetitions, wheel loads, and tire pressures), environmental conditions (temperature), and the pavement cross-section design.

Once a trial mix has been identified, traffic and environmental conditions have been determined, and the pavement cross-section has been designed, the analysis system seeks to judge, with predetermined reliability, whether the trial mix would perform satisfactorily in service. If the mix would not hold up, the designer can opt to redesign the mix, strengthen the pavement section, or repeat the analysis using more refined measurements and/or estimates.

For routine mix designs, the testing and analysis system has been simplified to the maximum extent possible. Laboratory testing is limited to stiffness measurements, and the primary analysis requires only a single estimate of in situ strains using traditional assumptions of linear elasticity. Unconventional mixes or uncommon applications, on the other hand, require more extensive testing and analysis for reliable decision making. Multiple-temperature fatigue testing must be performed, and analysis must address the complex thermal environment anticipated in situ.

Key features of the mix analysis system include the use of temperature conversion factors and quantitative reliability concepts. Temperature conversion factors—used to convert design equivalent single axle loads (ESALs) to their equivalents at a common reference temperature of 20°C (68°F)—have been found to be an effective but simple way of treating environmental temperature effects and of reducing the necessity for extensive multiple temperature testing. Reliability concepts provide a quantitative means for comparatively judging the adequacy of surrogate testing-regression models vis-à-vis laboratory fatigue testing; they thus permit and encourage a hierarchical approach to mix design which routinely simplifies the process but permits detailed analysis where necessary.

Conceptual development of the mix analysis system has been completed as part of SHRP Project A-003A, and considerable progress has been made toward establishing a readily implementable package for use by material engineers nationwide. In addition to completing the calibration process, one of the key remaining tasks is to validate the analysis system by demonstrating its ability to reliably discriminate among suitable and unsuitable mixes.

Part I Test Method Selection

Akhtarhusein A. Tayebali
John A. Deacon
John S. Coplantz
John T. Harvey
Carl L. Monismith

1

Introduction

1.1 Background

The fatigue resistance of an asphalt mix is its ability to withstand repeated bending without fracture. Fatigue, a common form of distress in asphalt-concrete pavement, manifests itself in the form of cracking from repeated traffic loading. It is important to have a measure of the fatigue characteristics of specific mixes over a range of traffic and environmental conditions so that fatigue considerations can be incorporated into the process of designing asphalt-concrete pavements.

The fatigue characteristics of asphalt mixes are usually expressed as relationships between the initial stress or strain and the number of load repetitions to failure—determined by using repeated flexure, direct tension, or diametral tests performed at several stress or strain levels. The fatigue behavior of a specific mix can be characterized by the slope and relative level of the stress or strain versus the number of load repetitions to failure and can be defined by a relationship of the following form (e.g., Monismith et al. 1985):

$$N_f = a\,(1/\epsilon_o)^b\,(1/S_o)^c \qquad (1.1)$$

where:

N_f	=	fatigue life,
ϵ_o	=	tensile strain,
S_o	=	initial mix stiffness, and
a, b, c	=	experimentally determined coefficients.

Based on laboratory test data presented in the form of Equation 1.1, several models have been proposed to predict the fatigue lives of pavements (Finn et al. 1977; Shell 1978; Asphalt Institute 1981). To develop these models, laboratory results have been calibrated by applying shift factors based on field observations to provide reasonable estimates of the in-service life cycle of a pavement based on limiting the amount of cracking due to repeated loads.

Several researchers (Chomton and Valayer 1972; van Dijk 1975; van Dijk and Visser 1977; van Dijk et al. 1978; Pronk and Hopmann 1990) have used the energy approach for predicting the fatigue behavior of the asphalt mixes. Van Dijk and Visser (1977) have suggested that the dissipated energy approach allows results of different types of tests, carried out under different test conditions with several types of asphalt mixes, to be described by a single mix-specific relationship that relates the number of cycles to failure to the cumulative dissipated energy. Therefore, such an approach would make it possible to predict the fatigue behavior of mixes in the laboratory over a wide range of conditions from the results of a few simple fatigue tests. Such a relationship can be characterized in the form of the following:

$$W_N = A\,(N_f)^z \tag{1.2}$$

where: N_f = fatigue life,
W_N = cumulative dissipated energy to failure, and
A, z = experimentally determined coefficients.

1.2 Purpose

This report provides preliminary recommendations for the laboratory studies associated with the "Development of Accelerated Performance Tests for Asphalt-Aggregate Mixes." The goal of this specific task was to identify suitable laboratory test procedure(s) to characterize the fatigue response of asphalt-aggregate mixes.

1.3 Hypotheses

As a result primarily of the initial literature review, a series of working hypotheses were developed early in the study. These hypotheses generally describe the fatigue behavior of asphalt-aggregate mixes both as tested in the laboratory and as reflected within analytical pavement models. They have served in part to orient and focus the investigations. Some became targets for detailed investigation because of their strong links to accelerated performance testing and mix analyses. The initial working hypotheses for the fatigue investigation are stated as follows:

Hypothesis 1. Fatigue cracking is caused by the repetitive application of traffic loads. For typical heavy-duty pavements, fatigue results from tensile stresses or strains at the underside of the asphalt-aggregate layer(s). The maximum principal tensile strain is considered the primary determinant of fatigue cracking.

Hypothesis 2. For the purposes of fatigue analysis, the critical stress or strain state in the pavement structure can be estimated with acceptable accuracy by the theory of linear elasticity, in which the mechanical behavior of the asphalt-aggregate mix is characterized by its modulus of elasticity and Poisson's ratio.

Hypothesis 3. Testing to destruction under cyclic loading is necessary in order to accurately measure the fatigue response of asphalt-aggregate mixes.

Hypothesis 4. In laboratory fatigue testing, pulsed loading is preferred to sinusoidal loading because the rest period permits stress relaxation similar to that permitted under in-service traffic loading.

Hypothesis 5. Although pavements become fatigued in response to repeated flexure, fatigue is basically a tensile phenomenon, and test specimens can be evaluated equally well under either tensile or flexural loading.

Hypothesis 6. Mode of loading is a critical concern in mix design systems because mix effects are quite different between controlled-stress and controlled-strain loading systems. The mode-of-loading effect is more likely due to differences in the rates of crack propagation than to differences in the times to crack initiation.

Hypothesis 7. Fatigue tests accelerated by the application of large stress or strain levels are satisfactory for mix analysis and design. That is, for practical purposes, mixes are ranked essentially the same at large and small stress or strain levels.

Hypothesis 8. Under simple loading, crack initiation in a given mix is related to strain or stress level as follows:

$$N_f = a\,(1/\epsilon)^b \quad \text{or} \quad N_f = c\,(1/\sigma)^d \tag{1.3}$$

where:
- N_f = number of load applications to crack initiation,
- ϵ, σ = tensile strain and stress, respectively, and
- a, b, c, d = experimentally determined coefficients dependent on test temperature.

Hypothesis 9. Under compound or mixed loading—due, for example, to multiple temperatures and/or stress or strain levels—cracking in a given mix is initiated when the linear summation of cycle ratios equals 1 as shown below:

$$\sum_i (n_i/N_i) = 1 \tag{1.4}$$

where:
- n_i = number of applications of stress σ_i or strain ϵ_i, and
- N_i = number of applications to failure at stress σ_i or strain ϵ_i.

Hypothesis 10. The principles of fracture mechanics represent the most feasible mechanistic approach for estimating rates of crack propagation in pavement structures.

2

Selection of Test Methods for Evaluation

Several test methodologies can be applied for measuring the fatigue behavior of asphalt-concrete. Brief descriptions along with the advantages and disadvantages and limitations of selected test methodologies can be found in SHRP's "Summary Report on Fatigue Response of Asphalt Mixes" (Tangella et al. 1990).

On the basis of the findings of the summary report and the prior experience of the research team, the following test methods were identified as the most promising for possible use in measuring those mix properties which significantly affect pavement performance:

Flexural fatigue tests	- third-point prismatic (beam) - trapezoidal cantilever
Tensile fatigue tests	- diametral - uniaxial tension compression
Fracture mechanics approach	- K, J, or C^*-line integral
Tensile strength and stiffness	- a surrogate for tensile fatigue effects

Flexural beam fatigue testing in controlled-stress and controlled-strain modes of loading, as well as the notched beam testing for the C^*-line integral approach, was done at the University of California, Berkeley (UCB). The trapezoidal cantilever fatigue tests in the controlled-stress mode of loading and a limited number of tests in the controlled-strain mode of loading, along with direct uniaxial tension compression tests on cylindrical specimens, were done by SWK Pavement Engineering at the University of Nottingham (SWK/UN). The diametral fatigue testing was done at North Carolina State University (NCSU). Table 2.1 gives an overview of the agencies involved and the test methods they evaluated.

Table 2.1. Test methods evaluated for fatigue program

Agency	Test
University of California, Berkeley	• Beam - pulsed loading (1.67 Hz), controlled stress and controlled strain • Direct tension - correlation with fatigue • Notched beam - C^*-line integral
SWK Pavement Engineering	• Trapezoidal - sinusoidal loading (20 Hz) controlled stress • Uniaxial tension compression - sinusoidal loading (20 Hz) controlled stress
North Carolina State University	• Diametral - pulsed loading (1.67 Hz) controlled stress and controlled strain

Criteria for test selection included the following:

- Sensitivity to mix variables, particularly asphalt properties.
- Reasonable simulation of field conditions.
- Prediction of fundamental properties that can be used in appropriate design or performance models.
- Ease and simplicity of use (user friendly).
- Time requirements.
- Ease of implementation and equipment cost.
- Reliability, accuracy, and precision.

Implicit in the criteria is also the relevancy of the test method to the specific distress under investigation. The overriding consideration is, however, the ability of the test to relate to pavement performance and be sensitive to material (asphalt and aggregate) properties.

It must be emphasized that simplicity is a relative term. For example, a test for fatigue may at first glance appear more complicated than current standard tests such as the Marshall or Hveem procedures. However, once the test method and equipment are developed, fatigue testing could actually be less complicated while at the same time yielding much more fundamental information. Procedures for specimen preparation and testing are expected to be highly automated, employing user-friendly computer software to control and reduce the data. Thus, test(s) will be as simple as possible and still be useful and reliable.

The research approach for Project A-003A has consistently emphasized that the primary requirements for developing tests to characterize asphalt-aggregate mixes relative to fatigue include

- characterization of the fatigue properties of asphalt-aggregate mixes and, from these tests,

- identification of the major chemical and physical properties of asphalt, aggregate, and mixes which influence fatigue properties.

Development and selection of test methods will also be based on the ability of test results to characterize material properties which can be used in mechanistic and/or mechanistic-empirical models. Procedures such as wheel track tests, although conceptually simple and capable of providing very useful information, are not viable candidates for the accelerated performance tests because fundamental properties are not measured. Test results are difficult to interpret fundamentally and may be useful for only a limited range of traffic, pavement, and environmental conditions. In developing and selecting the accelerated performance tests, primary emphasis will be given to prior knowledge of pavement performance, past research, and the consensus of researchers and advisors for the A-003A contract.

3

Selection of Variables and Materials

3.1 Variables Considered

The primary purpose of this study was to evaluate selected test systems for fatigue. Variables considered to affect the fatigue response of asphalt mixes are asphalt type (temperature susceptibility) and grade; aggregate type (stripping potential) and gradation; asphalt content; air-void content; temperature; and stress/strain level, aging, and moisture conditioning. Table 3.1 summarizes the significant variables considered in this study. Ten variables were considered of which four (aggregate gradation, grade of asphalt, aging, and moisture conditioning) were fixed. Each of the others was evaluated at two levels.

Table 3.1. Significant mix and test variables for fatigue study

Variable	Level of Treatment			No. of Levels
	1	2	3	
Aggregate				
Stripping Potential[a]	Low		High	2
Gradation		Medium		1
Asphalt				
Temperature Susceptibility[a]	Low		High	2
Content		Optimum	High	2
Compaction				
Air-Void Contents (percent)	4±1		8±1	2
Test Conditions				
Temperature	0°C		20°C	2
Stress/Strain Level	Low[b]		High[b]	2

[a]Based on the information from Materials Reference Library (MRL).
[b]Varies with temperature.

3.2 Mix Variables

The significant mix variables considered include the following:

- **Aggregates.** Two aggregate types—RB and RL—were used in this study. The RB aggregate exhibits a low level of stripping potential, whereas the RL aggregate exhibits a relatively higher level of stripping potential. Table 3.2 and Figure 3.1 show the California 3/4 in. medium gradation used in this study.

- **Asphalt.** Two asphalts were used: AAK-1 (an AC-30), with relatively lower temperature susceptibility (PI = -0.5), and AAG-1 (an AR-4000), with relatively higher temperature susceptibility (PI = -1.5).

- **Asphalt Content.** Two asphalt contents were used. For each asphalt-aggregate mix, the lower (optimum) asphalt content was determined by using the standard Hveem procedure. The upper asphalt content was set at a 0.6 percent higher level, corresponding approximately to the optimum asphalt content of the Marshall Corps of Engineers design procedure.[1] Table 3.3 shows the asphalt content used for the various mixes considered.

Table 3.2. Aggregate gradation used

Sieve Size	Percent Passing by Weight	Percent Retained on Each Sieve by Weight
1 in.	100	0
3/4 in.	95	5
1/2 in.	80	15
3/8 in.	68	12
No. 4	48	20
No. 8	35	13
No. 16	25	10
No. 30	17	8
No. 50	12	5
No. 100	8	4
No. 200	5.5	2.5
Pan		5.5

[1]Design criteria for 1380 kPa (200 psi) tires.

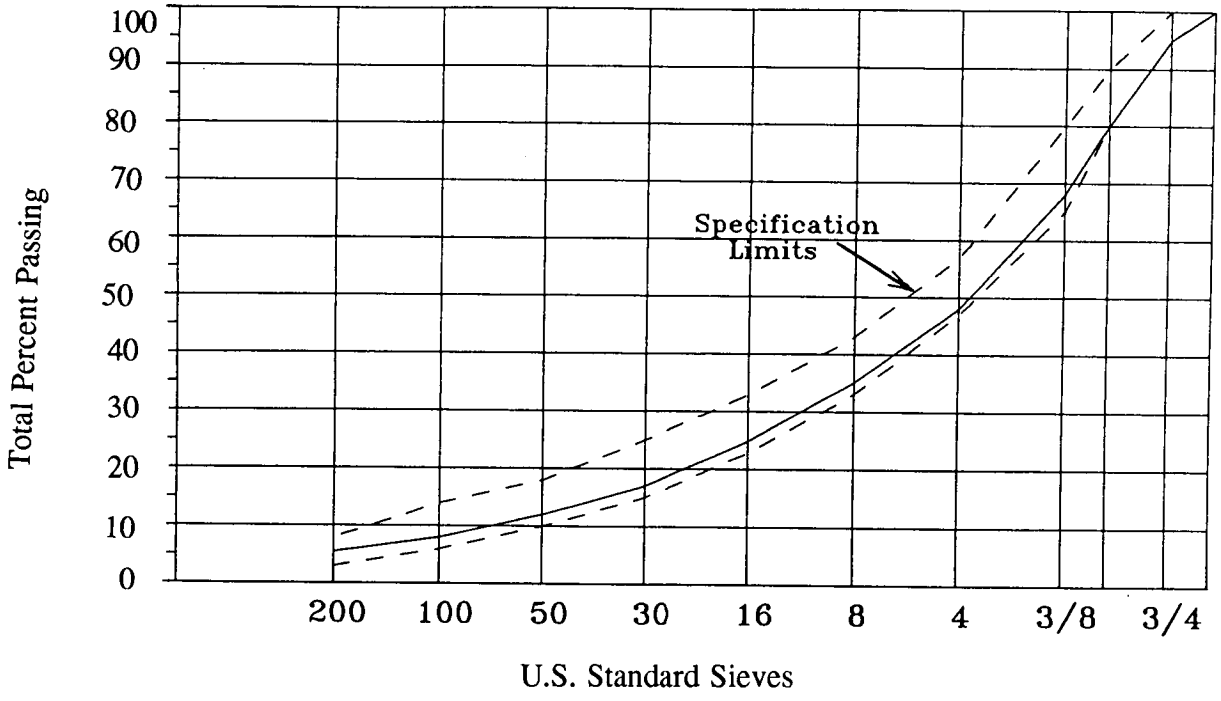

Figure 3.1. Aggregate gradation used

Table 3.3. Asphalt content used for various mixes

Aggregate Stripping Potential[b]	Temperature Susceptibility[a] Low (AAK, PI=-0.5) Asphalt Content[b]		High (AAG, PI=-1.5) Asphalt Content[b]	
	Optimum	High	Optimum	High
Low (RB)	5.1	5.7	4.9	5.5
High (RL)	4.3	5.0	4.1	4.8

[a]Based on the information from the Materials Reference Library (MRL).
[b]For beam specimens, the asphalt content used was by weight of aggregate. For trapezoidal specimens, the asphalt content used was by weight of mix.

- **Compaction.** Two levels of compactive effort were used. Low compactive effort was adjusted to provide a target air-void content of 8 percent in the specimen. The high level of compactive effort was adjusted to produce a target air-void content of 4 percent. A Triaxial Institute kneading compactor was used to fabricate beam specimens.

- **Test conditions.** Two temperatures (0° and 20°C [32° and 68°F]) and two stress and strain levels (high and low) were used for the controlled-stress and

controlled-strain tests, respectively. It should be noted that the target stress/strain levels were adjusted somewhat for the low and high temperatures to ensure failure in the specimens in a reasonable number of cycles. For all tests, unconditioned specimens (no aging and moisture conditioning) were used.

3.3 Experiment Design

The experiment design used in this study is the smallest fractional factorial design which permits the estimation of all two-factor interactions and the main effects of the variables being used. In this case, it was determined that one-half of the full factorial (i.e., 32 cells) would be necessary to estimate the main effects and interactions. To obtain estimates of purely experimental error, this 32-factorial combination was replicated twice for a total of 64 tests. Table 3.4 shows the experiment design used for the fatigue test program at UCB for flexural beam controlled-stress and controlled-strain tests, at SWK/UN for trapezoidal cantilever controlled-stress tests, and at NCSU for the diametral-fatigue tests.

Table 3.4. Fatigue experiment design

Experiment Design: $2^{5-1}*2$ Fractional Factorials in 32 Runs

A	B	C	D	E	F	A	B	C	D	E	F
0	0	0	0	0	0	0	0	0	0	0	1
1	0	0	0	1	0	1	0	0	0	1	1
0	1	0	0	1	0	0	1	0	0	1	1
1	1	0	0	0	0	1	1	0	0	0	1
0	0	1	0	1	0	0	0	1	0	1	1
1	0	1	0	0	0	1	0	1	0	0	1
0	1	1	0	0	0	0	1	1	0	0	1
1	1	1	0	1	0	1	1	1	0	1	1
0	0	0	1	1	0	0	0	0	1	1	1
1	0	0	1	0	0	1	0	0	1	0	1
0	1	0	1	0	0	0	1	0	1	0	1
1	1	0	1	1	0	1	1	0	1	1	1
0	0	1	1	0	0	0	0	1	1	0	1
1	0	1	1	1	0	1	0	1	1	1	1
0	1	1	1	1	0	0	1	1	1	1	1
1	1	1	1	0	0	1	1	1	1	0	1

Notes: A = Aggregate stripping potential (0=Low, 1=High)
B = Asphalt temperature susceptibility (0=Low, 1=High)
C = Asphalt content (0=Optimum, 1=High)
D = Compaction—air-void content (0=Low, 1=High)
E = Temperature (0=Low, 1=High)
F = Stress/strain (0=Low, 1=High)

This test matrix applies to both the controlled-stress and the controlled-strain fatigue experiments for all test types. All 32 combinations are repeated for a total of 64 tests.

4

Test Results

4.1 Stiffness, Fatigue Life, and Dissipated Energy

The stiffness at any number of load repetitions is computed from the tensile stress and strain at that specific value. Figure 4.1 shows a typical plot of stiffness ratio (defined as quotient of stiffness at the ith load repetition to the initial stiffness, S_i/S_o) versus the number of load repetitions for flexural beam fatigue tests in both controlled-stress and controlled-strain modes of loading. The fatigue life to failure (N_f) is dependent on the mode-of-loading condition. For controlled-stress tests, failure is well defined since specimens are cracked through at the end of the test. In controlled-strain testing, failure is not readily apparent; accordingly, the specimen is considered to have failed when its initial stiffness is reduced by 50 percent.

The dissipated energy per cycle for a beam specimen tested under pulsed loading is computed as the area within the stress-strain hysteresis loop. Figure 4.2 shows a typical stress-strain hysteresis loop for the controlled-strain mode of loading. Figure 4.3 shows the variation of dissipated energy per cycle with the number of load repetitions. The dissipated energy per cycle decreases with an increasing number of load repetitions in the controlled-strain fatigue tests; whereas, for the controlled-stress tests, the dissipated energy per cycle increases as the number of load repetitions increases. The cumulative dissipated energy to failure for a flexural beam fatigue test is the area under the curve between dissipated energy and number of cycles.

For the sinusoidal loading condition, dissipated energy per cycle (area within the hysteresis loop) is given by the following:

$$w_i = \pi \sigma_i \epsilon_i \sin\phi_i \qquad (4.1)$$

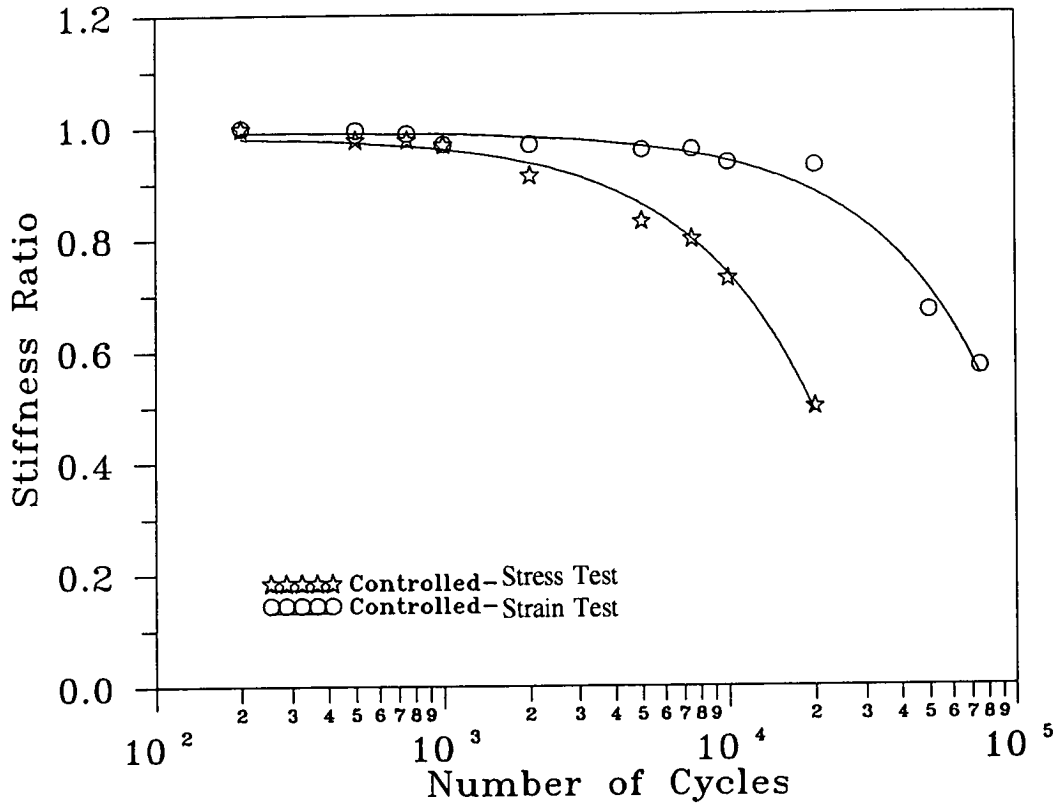

Figure 4.1. Stiffness ratio versus number of cycles, flexural beam fatigue controlled-stress and controlled-strain tests

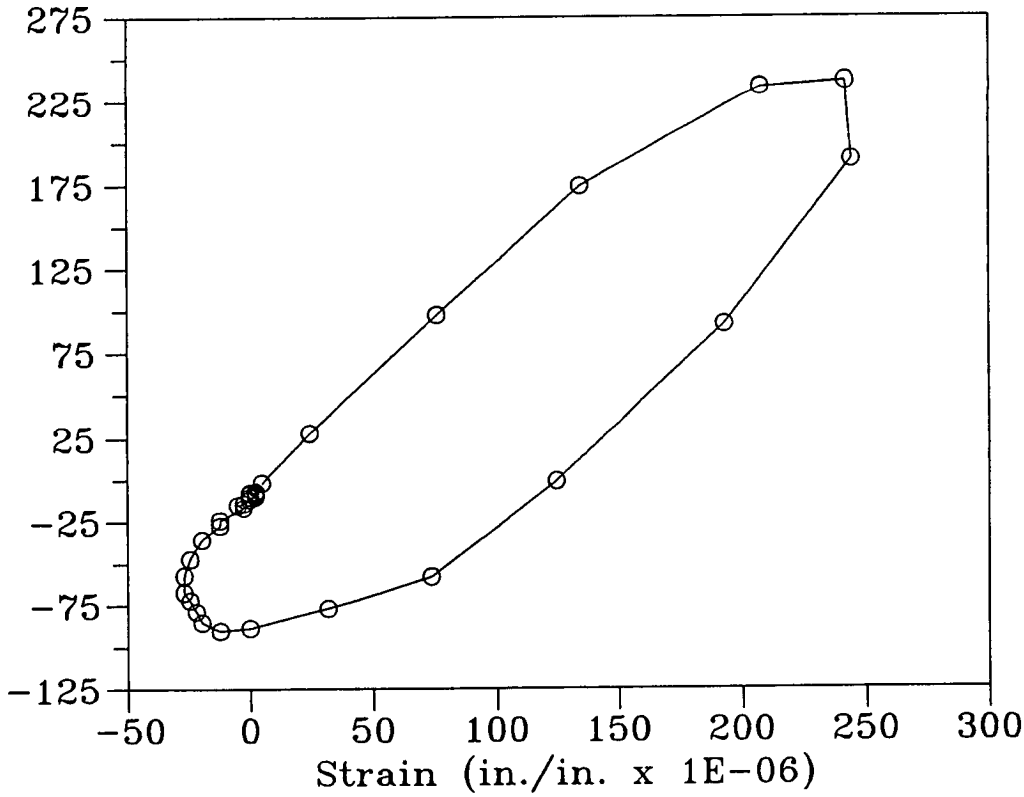

Figure 4.2. Stress-strain hysteresis loop, flexural beam fatigue controlled-strain test

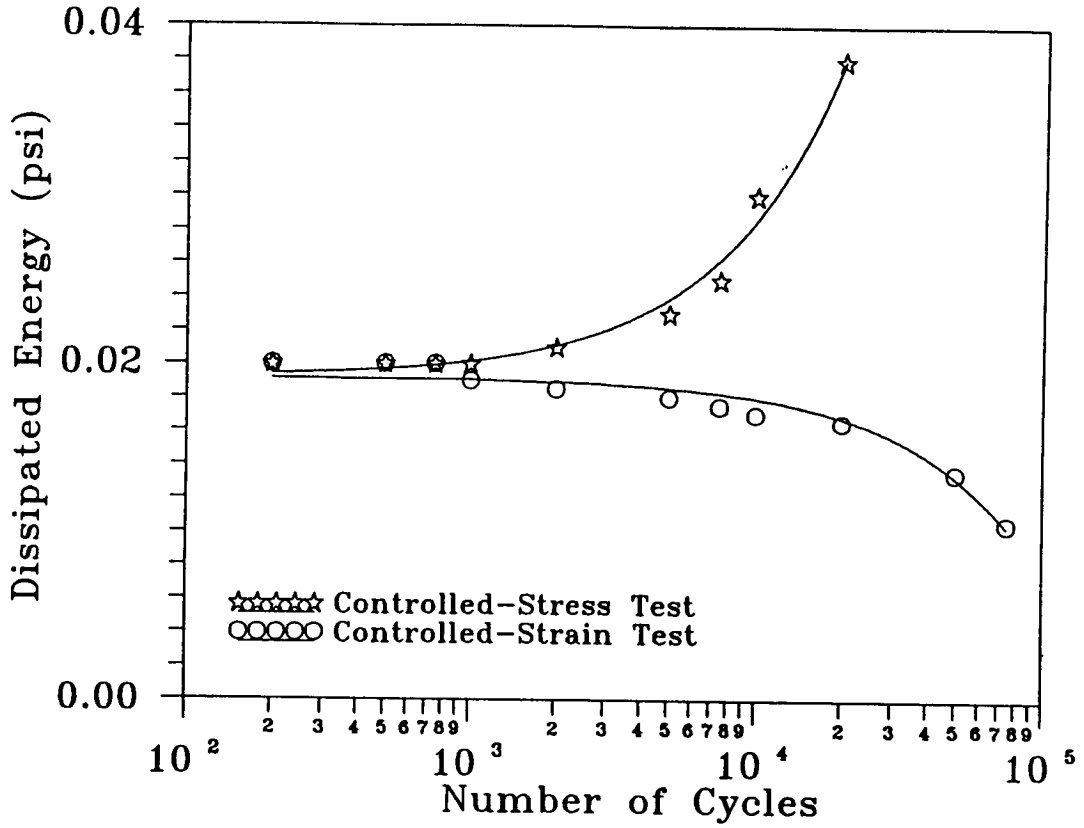

Figure 4.3. Dissipated energy per cycle versus number of cycles, flexural beam fatigue controlled-stress and controlled-strain tests

where:

w_i	=	dissipated energy at load cycle i,
σ_i	=	stress amplitude at load cycle i,
ϵ_i	=	strain amplitude at load cycle i,
ϕ_i	=	phase shift between stress and strain at load cycle i, and
π	=	3.142.

The cumulative dissipated energy to failure is defined by

$$W_N = \sum_i \pi \, \sigma_i \, \epsilon_i \, \sin\phi_i \qquad i = 1, N_f \tag{4.2}$$

4.2 Statistical Analysis of Test Results

In this section the results of the statistical analyses performed on the various fatigue data sets are summarized. The main purpose of these analyses was to determine the sensitivity of the fatigue tests methods to mix and test variables in characterizing the fatigue response of the asphalt-aggregate mixes. Of particular importance in the SHRP project was the sensitivity of the test methods to asphalt-aggregate mix properties.

As far as possible, the format for the statistical analysis was maintained across all data sets. The four data sets analyzed included the following:

- Flexural beam fatigue controlled-stress test.
- Flexural beam fatigue controlled-strain test.
- Trapezoidal cantilever fatigue controlled-stress test.
- Diametral fatigue controlled-stress tests.

The statistical analysis for each data set included the following sequence:

- Test for correlation among the independent variables (Pearson).
- Analysis of variance (ANOVA) of full models (all main factors and two-factor interactions) to determine the sensitivity of stiffness, fatigue life, and cumulative dissipated energy to mix and testing variables (for the diametral fatigue tests the dissipated energy was not available; therefore, only stiffness and fatigue life were evaluated).
- General linear modeling (GLM) to develop models for stiffness, fatigue life, and cumulative dissipated energy (these models were then used to compute the three parameters for a specific air-void content and applied stress/strain).
- Summaries of the effects of the experimental variables included in the experiment on stiffness, fatigue life, and cumulative dissipated energy based on the results of GLM.

One of the assumptions necessary for ANOVA and GLM is that the dependent and independent variables are normally distributed. Distributions for stress, strain, stiffness, cycles to failure, and cumulative dissipated energy were reviewed and found to be log-normally distributed. Therefore, log transformations (using natural logarithm, base e) were used in ANOVA and GLM through regression analysis.

Some independent variables which could not be precisely controlled but which were carefully measured (such as air-void contents) were normalized. The purpose of normalizing these variables was that they may be added or omitted in statistical models without adversely affecting the remaining model coefficients. Air-void contents, temperature, and the natural log of applied stress and strain were normalized as follows:

$$X_{normalized} = (X - X_{mean})/\{(X_{Hi} - X_{Lo})/2\} \quad (4.3)$$

where:
X = observed value,
X_{mean} = grand mean,
X_{Hi} = mean of the high values, and
X_{Lo} = mean of the low values.

The experiment design selected in this study is a fractional factorial which permits the estimation of the main effects of the experimental factors and all two-factor interactions. Accordingly, for ANOVA and GLM a log-linear model of the following type was utilized:

$$\begin{aligned} Y_i = \mu &+ \alpha_1*\text{Asph} + \alpha_2*\text{Aggr} + \alpha_3*\%\text{Asph} + \alpha_4*\text{Voids} + \alpha_5*\text{Temp} \\ &+ \alpha_6*\text{Stress/Strain} + \alpha_7*\text{Asph}*\text{Aggr} + \alpha_8*\text{Asph}*\%\text{Asph} + \alpha_9*\text{Asph}*\text{Voids} \\ &+ \alpha_{10}*\text{Asph}*\text{Temp} + \alpha_{11}*\text{Asph}*\text{Stress/Strain} + \alpha_{12}*\text{Aggr}*\%\text{Asph} \\ &+ \alpha_{13}*\text{Aggr}*\text{Voids} + \alpha_{14}*\text{Aggr}*\text{Temp} + \alpha_{15}*\text{Aggr}*\text{Stress/Strain} \\ &+ \alpha_{16}*\%\text{Asph}*\text{Voids} + \alpha_{17}*\%\text{Asph}*\text{Temp} + \alpha_{18}*\%\text{Asph}*\text{Stress/Strain} \\ &+ \alpha_{19}*\text{Voids}*\text{Temp} + \alpha_{20}*\text{Voids}*\text{Stress/Strain} + \alpha_{21}*\text{Temp}*\text{Stress/Strain} \end{aligned} \quad (4.4)$$

where:

Y_1	=	log-stiffness,
Y_2	=	log-cycles-to-failure,
Y_3	=	log-cumulative-dissipated-energy,
μ	=	constant (grand mean),
α_i	=	model coefficients,
Asph	=	asphalt type,
Aggr	=	aggregate type,
%Asph	=	asphalt content,
Voids	=	normalized percentage of air voids,
Temp	=	normalized temperature, and
Stress/Strain	=	normalized stress or strain.

Tables 4.1 to 4.3 show typical results for the Pearson correlation matrix, ANOVA, and GLM, respectively. The GLM is derived using a stepwise regression analysis technique. The SYSTAT Statistical Software Package was used to analyze the data.

Table 4.4 shows the summary statistics from GLM for stiffness, fatigue life, and cumulative dissipated energy. The summary statistics show good fit for the stiffness for all test types with an R^2 greater than 0.92. The coefficient of variation varies between 11 and 20 percent; trapezoidal cantilever tests show the lowest value (11.4 percent), and diametral tests show the highest value (19.7 percent).

The summary statistics for fatigue life show reasonable fits for all test types with an R^2 greater than 0.8 except for the trapezoidal cantilever controlled-stress tests which have an R^2 value of 0.73. The coefficients of variation based on model-fitted data are high for all test types. Diametral fatigue tests show the lowest coefficient of variation, 66 percent, followed by flexural beam tests showing 99 and 93 percent for the controlled-stress and controlled-strain loading, respectively. Trapezoidal cantilever tests show the highest coefficient of variation as a value of 172 percent. It may be noted that the coefficients of variation shown in Table 4.4 are measures of prediction error, random error, and testing errors. Computation based on actual data, not model-fitted data, have shown coefficients of variation of approximately 60 percent for the flexural beam fatigue controlled-stress test. The error in the prediction model accounts for the higher coefficients of variation. Data reported in the literature for fatigue life have shown coefficients of variation of approximately 80 percent based on fitted data.

Table 4.1. Pearson correlation matrix for the flexural beam fatigue controlled-stress test

	Asph	Aggr	% Asph	% Voids	Temp	Stress
Asph	1.000					
Aggr	0.000	1.000				
% Asph	0.000	0.000	1.000			
% Voids	-0.010	-0.012	0.001	1.000		
Temp	0.000	0.000	0.000	-0.024	1.000	
Stress	-0.004	0.009	0.000	0.020	-0.923	1.000

Note: Number of observations = 64.

Table 4.2. Full model ANOVA of log stiffness for beam fatigue controlled-stress test

Dep Var = Lnstiff N = 64 Multiple R = 0.994 Squared Multiple R = 0.989

Analysis of Variance

Source	Sum-of-Square	DF	Mean-Square	F-Ratio	P
Asph	6.735	1	6.735	463.673	0.000
Aggr	0.165	1	0.165	11.362	0.002
% Asph	0.005	1	0.005	0.361	0.551
% Voids	2.226	1	2.226	153.238	0.000
Temp	7.732	1	7.732	532.327	0.000
Stress	0.148	1	0.148	10.184	0.003
Asph * Aggr	0.002	1	0.002	0.167	0.685
Asph * % Asph	0.040	1	0.040	2.784	0.103
Asph * % Voids	0.109	1	0.109	7.480	0.009
Asph * Temp	0.143	1	0.143	9.814	0.003
Asph * Stress	0.028	1	0.028	1.936	0.171
Aggr * % Asph	0.007	1	0.007	0.497	0.485
Aggr * % Voids	0.006	1	0.006	0.434	0.514
Aggr * Temp	0.147	1	0.147	10.154	0.003
Aggr * Stress	0.047	1	0.047	3.209	0.080
% Asph * % Voids	0.008	1	0.008	0.557	0.460
% Asph * Temp	0.009	1	0.009	0.639	0.429
% Asph * Stress	0.004	1	0.004	0.250	0.620
% Voids * Temp	0.075	1	0.075	5.157	0.028
% Voids * Stress	0.031	1	0.031	2.106	0.154
Temp * Stress	0.002	1	0.002	0.133	0.718
Error	0.610	42	0.015		

Table 4.3. GLM of log stiffness for flexural beam fatigue controlled-stress test

Dep Var = Lnstiff N = 64 Multiple R = 0.992 Squared Multiple R = 0.985

	Lnstiff	Sum-of-Square	DF	Mean-Square	F-Ratio	P
Constant	13.746		1			
Asph AAG-1	0.363	8.443	1	8.443	563.596	0.000
Aggr RB	0.044	0.124	1	0.124	8.270	0.006
% Voids	-0.200	2.639	1	2.639	176.162	0.000
Temp	-0.918	7.959	1	7.959	531.287	0.000
Stress	-0.043	0.158	1	0.158	10.559	0.002
Asph AAG-1 * % Voids	0.040	0.103	1	0.103	6.869	0.011
Asph AAG-1 * Temp	0.074	0.345	1	0.345	23.030	0.000
Aggr RB * Temp	0.061	0.237	1	0.237	15.829	0.000
% Voids * Temp	-0.037	0.092	1	0.092	6.144	0.016
ERROR		0.809	54	0.015		

Table 4.4. Summary statistics from GLM for stiffness, fatigue life, and cumulative dissipated energy

Statistics	Beam Fatigue		Trapezoidal Fatigue	Diametral Fatigue
	Cont-stress	Cont-strain	Cont-stress	Cont-stress
Stiffness				
R^2	0.985	0.952	0.927	0.931
Root Mean Square Error (Ln)	0.123	0.158	0.114	0.195
Coefficient of Variation (%)	12.300	15.900	11.400	19.700
Fatigue Life				
R^2	0.844	0.818	0.729	0.842
Root Mean Square Error (Ln)	0.825	0.787	1.172	0.598
Coefficient of Variation (%)	98.700	92.700	171.800	65.500
Cumulative Dissipated Energy				
R^2	0.773	0.696	0.520	-
Root Mean Square Error (Ln)	0.780	0.777	1.096	-
Coefficient of Variation (%)	91.500	91.100	152.300	-

Note: R^2 = coefficient of determination.
Coefficient of variation = $100 * (e^{MSE} - 1)^{0.5}$
where: e = base of natural logarithms, and
MSE = mean square error.

The summary statistics for cumulative dissipated energy show fair fits with R^2 values of approximately 0.7 for flexural beam tests and less than 0.7 for the trapezoidal cantilever tests; the coefficients of variation are about 92 percent for the former and 152 percent for the latter.

Table 4.5 shows the effect of experiment design factors on the response variables (stiffness, fatigue life, and cumulative dissipated energy) for different test types. Tables 4.6 to 4.8 show the statistically significant effects at a 95 percent confidence level from GLM for the fatigue tests. Tables 4.9 to 4.13 show the average stiffness, cycles to failure, and cumulative dissipated energy from the GLM.

4.3 Stiffness

The statistical analysis for stiffness shows that all test types considered in this study are sensitive to asphalt type (Table 4.6); mixes containing AAG-1 had a higher stiffness than those containing AAK-1 (Tables 4.9 to 4.13). The percentage difference (expressed as a percentage of the higher value) between the mixes containing AAG-1 and AAK-1 ranges between 20 and 44 percent at 0°C (32°F) and 35 and 58 percent at 20°C (68°F). All test types show a significant interaction between asphalt type and temperature, which is expected because of the high temperature susceptibility of the AAG-1 asphalt.

Except the trapezoidal cantilever tests, all tests are sensitive to aggregate type. The flexural beam tests and trapezoidal cantilever tests show significant aggregate-temperature interaction; the latter test type also shows significant interaction between aggregate type and stress level. The flexural beam tests indicate that the average stiffness of mixes containing RL aggregate is approximately the same as those mixes containing the RB aggregate at the low temperature (0°C [32°F]), and significantly lower at the higher temperature (20°C [68°F]). In the trapezoidal cantilever tests, both mixes show approximately the same stiffness for the two temperatures. The diametral tests indicate that the stiffness of mixes containing RL aggregate is higher than for those mixes containing RB aggregate at both temperatures.

The stiffness trend for the flexural beam tests agrees with the results obtained from the axial resilient stiffness study conducted at UCB in which the axial resilient stiffness was compared to the diametral resilient stiffness for 32 mixes containing the AAG-1 and AAK-1 asphalts and RL and RB aggregates. The stiffness study indicated that, for the axial resilient stiffness, mixes containing RL aggregate exhibited similar stiffnesses to those mixes containing the RB aggregate at 0°C (32°F) and lower stiffnesses at 20°C (68°F). For the diametral resilient stiffness, RB aggregate mixes exhibited higher stiffness values than the RL aggregate mixes at 0°C (32°F), whereas at 20°C (68°F) the trend reversed—mixes containing RL aggregate exhibited higher stiffness than those containing RB aggregate.

For all tests except the flexural beam controlled-strain tests, asphalt content did not appear to have any influence on the stiffness, perhaps because of the narrow range in asphalt contents used as optimum and high for this study. For the flexural beam controlled-strain test, the mixes containing optimum asphalt content showed higher stiffnesses than those with the

Table 4.5. Summary effect of mix and test variables on the stiffness, fatigue life, and cumulative dissipated energy for different test types

Variable	Effect on	Beam Fatigue		Trapezoidal Fatigue	Diametral Fatigue
		Cont-stress	Cont-strain	Cont-stress	Cont-stress
Asphalt Type	Stiffness	AAG > AAK	AAG > AAK	AAG > AAK	AAG > AAK
	Fatigue Life	AAG > AAK	AAG < AAK	AAG > AAK	AAG > AAK
	Cumul. Energy	Temp. Dep.[a]	AAG < AAK	AAG > AAK	-
Asphalt Content	Stiffness	Opt = High	Opt > High	Opt = High	Opt = High
	Fatigue Life	Temp. Dep.[b]	Opt=High[d]	Opt = High	Opt = High
	Cumul. Energy	Temp. Dep.[b]	Opt = High	Opt = High	-
Aggregate Type	Stiffness	RB > RL[c]	RB > RL[c]	RB = RL[d]	RB < RL
	Fatigue Life	RB > RL	RB > RL	Temp. Dep.[e]	Temp. Dep.[e]
	Cumul. Energy	RB > RL	RB > RL	Temp. Dep.[e]	-
Air-Void Contents	Stiffness	Low > High	Low > High	Low > High	Low > High
	Fatigue Life	Low > High	Low > High	Low > High	Low > High
	Cumul. Energy	Low > High	Low > High	Low > High	-
Temperature	Stiffness	Low > High	Low > High	Low > High	Low > High
	Fatigue Life	Low > High	Low < High	Low > High	Low > High
	Cumul. Energy	Low > High	Low < High	Low > High	-
Stress/Strain	Stiffness	Low = High[d]	Low = High[d]	Low = High[d]	Low = High
	Fatigue Life	Low > High	Low > High	Low > High	Low > High
	Cumul. Energy	Low > High	Low > High	Low > High	-

[a]AAG > AAK at 0°C (32°F) and AAG < AAK at 20°C (68°F).
[b]Temperature dependent — Opt. > High at 0°C (32°F) and Opt. < High at 20°C (68°F).
[c]Negligible difference at 0°C (32°F).
[d]Negligible difference.
[e]RB > RL at 0°C (32°F) and RB < RL at 20°C (68°F).

Table 4.6. Statistically significant effect in GLM for fatigue tests, stiffness as response variable

Effect	Beam Fatigue		Trapezoidal Fatigue	Diametral Fatigue
	Cont-stress	Cont-strain	Cont-stress	Cont-stress
Intercept	Yes	Yes	Yes	Yes
Asphalt Type (Asph)	Yes	Yes	Yes	Yes
Aggregate Type (Aggr)	Yes	Yes		Yes
Asphalt Content (% Asph)		Yes		
Air-Void Content (% Voids)	Yes	Yes	Yes	Yes
Temperature (Temp)	Yes	Yes	Yes	Yes
Stress/Strain	Yes		Yes	
Asph * Aggr		Yes		
Asph * % Asph			Yes	
Asph * % Voids	Yes	Yes		
Asph * Temp	Yes	Yes	Yes	Yes
Asph * Stress/Strain				
Aggr * % Asph			Yes	
Aggr * % Voids				
Aggr * Temp	Yes	Yes	Yes	
Aggr * Stress/Strain			Yes	
% Asph * % Voids				
% Asph * Temp				
% Asph * Stress/Strain				
% Voids * Temp	Yes			
% Voids * Stress/Strain				
Temp * Stress/Strain				

Table 4.7. Statistically significant effects in GLM for fatigue tests, fatigue life as response variable

Effect	Beam Fatigue		Trapezoidal Fatigue	Diametral Fatigue
	Cont-stress	Cont-strain	Cont-stress	Cont-stress
Intercept	Yes	Yes	Yes	Yes
Asphalt Type (Asph)	Yes	Yes	Yes	Yes
Aggregate Type (Aggr)	Yes	Yes		
Asphalt Content (% Asph)				
Air-Void Content (% Voids)	Yes	Yes	Yes	Yes
Temperature (Temp)	Yes	Yes	Yes	Yes
Stress/Strain	Yes	Yes	Yes	Yes
Asph * Aggr				
Asph * % Asph		Yes		
Asph * % Voids				
Asph * Temp	Yes			Yes
Asph * Stress/Strain				
Aggr * % Asph				
Aggr * % Voids				
Aggr * Temp			Yes	Yes
Aggr * Stress/Strain				
% Asph * % Voids		Yes		
% Asph * Temp	Yes			
% Asph * Stress/Strain				
% Voids * Temp		Yes		
% Voids * Stress/Strain				
Temp * Stress/Strain	Yes	Yes	Yes	Yes

Table 4.8. Statistically significant effects in GLM for fatigue tests, cumulative dissipated energy as response variable

Effect	Beam Fatigue		Trapezoidal Fatigue
	Cont-stress	Cont-strain	Cont-stress
Intercept	Yes	Yes	Yes
Asphalt Type (Asph)		Yes	
Aggregate Type (Aggr)	Yes	Yes	
Asphalt Content (% Asph)			
Air-Void Content (% Voids)	Yes	Yes	Yes
Temperature (Temp)	Yes	Yes	Yes
Stress/Strain	Yes	Yes	Yes
Asph * Aggr		Yes	
Asph * % Asph		Yes	
Asph * % Voids			
Asph * Temp	Yes		
Asph * Stress/Strain			
Aggr * % Asph			
Aggr * % Voids			
Aggr * Temp			Yes
Aggr * Stress/Strain			
% Asph * % Voids			
% Asph * Temp	Yes		
% Asph * Stress/Strain			
% Voids * Temp		Yes	
% Voids * Stress/Strain			
Temp * Stress/Strain	Yes	Yes	

Table 4.9. Average results from GLM model, flexural beam fatigue controlled-stress tests

Effect	Level	Temperature of 0°C (32°F)			Temperature of 20°C (68°F)		
		Stiffness (psi)	Fatigue Life (cycles)	Cumul. Diss. Energy (psi)	Stiffness (psi)	Fatigue Life (cycles)	Cumul. Diss. Energy (psi)
Average		2,454,700	5,834,000	28,800	425,100	34,500	1100
Asphalt Type	AAK-1	1,837,000	2,183,000	17,100	274,300	29,600	1900
	AAG-1	3,280,200	15,591,200	48,500	658,600	40,200	700
	% Difference	44%	86%	65%	58%	26%	-63%
Asphalt Content	Optimum	2,454,700	8,262,300	42,800	425,100	24,300	800
	High	2,454,700	4,119,400	19,400	425,100	48,800	1700
	% Difference	0%	-50%	-55%	0%	50%	53%
Aggregate Type	RL	2,496,800	3,329,100	18,300	382,700	19,700	700
	RB	2,413,400	10,223,700	45,400	472,100	60,400	1800
	% Difference	-3%	67%	60%	19%	67%	61%
Air-Void Contents	4%	2,897,300	15,268,600	62,300	540,900	90,200	2500
	8%	2,079,800	2,229,100	13,400	334,000	13,200	500
	% Difference	-28%	-85%	-78%	-38%	-85%	-80%
Temperature	@ 150 psi	2,541,900	18,295,600	67,900	404,700	13,200	700
Stress	Low	2,541,900	18,295,600	67,900	446,500	89,700	1900
	High	2,370,500	1,860,300	12,200	404,700	13,200	700
	% Difference	-7%	-90%	-82%	-9%	-85%	-63%

Notes: Air-void contents normalized to 4 percent and 8 percent.
Stress normalized to 1033 and 1378 kPa (150 and 200 psi) for 0°C (32°F); and 100 and 150 for 20°C (68°F).
Averages based on logarithmic mean of regressed data.
Percent difference is the difference expressed as a percentage of the higher value.

Table 4.10. Average results from GLM model, flexural beam fatigue controlled-strain tests

Effect	Level	Temperature of 0°C (32°F)			Temperature of 20°C (68°F)		
		Stiffness (psi)	Fatigue Life (cycles)	Cumul. Diss. Energy (psi)	Stiffness (psi)	Fatigue Life (cycles)	Cumul. Diss. Energy (psi)
Average		2,048,500	45,400	700	789,100	87,400	1000
Asphalt Type	AAK-1	1,824,500	73,300	1000	536,500	141,200	1500
	AAG-1	2,229,900	28,100	500	1,160,500	54,100	700
	% Difference	18%	-62%	-50%	54%	-62%	-53%
Asphalt Content	Optimum	2,166,500	45,700	700	834,500	88,000	1000
	High	1,936,900	45,100	700	746,100	86,800	1000
	% Difference	-11%	-1%	0%	-11%	-1%	0%
Aggregate Type	RL	2,003,900	25,300	400	697,000	48,700	600
	RB	2,094,000	81,500	1200	893,200	156,900	1800
	% Difference	4%	69%	67%	22%	69%	67%
Air-Void Contents	4%	2,390,300	47,200	600	920,700	207,100	2500
	8%	1,755,500	43,600	700	676,200	36,900	400
	% Difference	-27%	-8%	14%	-27%	-82%	-84%
Strain (micron)	200	2,084,900	65,600	800	803,100	110,700	1100
	400	2,012,700	31,400	600	775,300	69,000	900
	% Difference	-3%	-52%	-25%	-3%	-38%	-18%

Notes: Air-void contents normalized to 4 percent and 8 percent.
Strain normalized to 200 and 400 micro in./in.
Averages based on logarithmic mean of regressed data.
Percent difference is the difference expressed as a percentage of the higher value.

Table 4.11. Average results from GLM model, flexural beam fatigue controlled-strain tests

Effect	Level	Temperature of 0°C (32°F)			Temperature of 20°C (68°F)		
		Stiffness (psi)	Fatigue Life (cycles)	Cumul. Diss. Energy (psi)	Stiffness (psi)	Fatigue Life (cycles)	Cumul. Diss. Energy (psi)
Average		1,983,700	3,644,400	6300	709,600	174,700	1400
Asphalt Type	AAK-1	1,694,500	2,744,600	6200	480,700	84,500	1200
	AAG-1	2,322,200	4,839,200	6400	1,047,600	361,400	1500
	% Difference	27%	43%	3%	54%	77%	20%
Asphalt Content	Optimum	2,112,700	4,977,800	7400	755,700	213,700	1500
	High	1,862,600	2,668,200	5400	666,300	142,800	1300
	% Difference	-12%	-46%	-27%	-12%	-33%	-13%
Aggregate Type	RL	2,005,600	2,141,500	3700	628,700	66,900	700
	RB	1,962,000	6,202,100	10,800	800,900	456,200	2800
	% Difference	-2%	65%	66%	22%	85%	75%
Air-Void Contents	4%	2,319,600	8,094,100	8700	829,800	672,100	4000
	8%	1,696,400	1,640,900	4500	606,800	45,400	500
	% Difference	-27%	-80%	-48%	-27%	-93%	-88%
Temperature	@ 150 psi	1,983,700	7,317,900	9000	709,600	93,200	1100
Stress	Low	1,983,700	7,317,900	9000	709,600	327,400	1700
	High	1,983,700	1,815,000	4400	709,600	93,200	1100
	% Difference	0%	-75%	-51%	0%	-72%	-35%

Notes: Air-void contents normalized to 4 percent and 8 percent.
Stress normalized to 1033 and 1378 kPa (150 and 200 psi) for 0°C (32°F); and 100 and 150 for 20°C (68°F).
Averages based on logarithmic mean of regressed data.
Percent difference is the difference expressed as a percentage of the higher value.

Table 4.12. Average results from GLM model, flexural trapezoidal cantilever fatigue controlled-stress tests

Effect	Level	Temperature of 0°C (32°F)			Temperature of 20°C (68°F)		
		Stiffness (psi)	Fatigue Life (cycles)	Cumul. Diss. Energy (psi)	Stiffness (psi)	Fatigue Life (cycles)	Cumul. Diss. Energy (psi)
Average		1,978,100	448,800	4500	1,063,100	42,400	1600
Asphalt Type	AAK-1	1,736,900	290,200	4500	856,500	27,400	1600
	AAG-1	2,252,700	694,000	4500	1,319,400	65,600	1600
	% Difference	23%	58%	0%	35%	58%	0%
Asphalt Content	Optimum	1,978,100	448,800	4500	1,063,100	42,400	1600
	High	1,978,100	448,800	4500	1,063,100	42,400	1600
	% Difference	0%	0%	0%	0%	0%	0%
Aggregate Type	RL	1,937,800	320,000	3000	1,096,800	59,500	2300
	RB	2,019,100	629,200	6500	1,030,400	30,300	1100
	% Difference	4%	49%	54%	-6%	-49%	-52%
Air-Void Contents	4%	2,270,800	1,009,800	7900	1,220,400	95,400	2800
	8%	1,723,100	199,400	2500	926,000	18,800	900
	% Difference	-24%	-80%	-68%	-24%	-80%	-68%
Temperature	@ 150 psi	1,952,800	1,007,400	6800	1,082,500	18,300	900
Stress	Low	1,952,800	1,007,400	6800	1,044,000	98,200	2900
	High	2,003,600	199,900	2900	1,082,500	18,300	900
	% Difference	3%	-80%	-57%	4%	81%	-69%

Notes: Air-void contents normalized to 4 percent and 8 percent.
Stress normalized to 1033 and 1378 kPa (150 and 200 psi) for 0°C (32°F); and 100 and 150 for 20°C (68°F).
Averages based on logarithmic mean of regressed data.
Percent difference is the difference expressed as a percentage of the higher value.

Table 4.13. Average results from GLM model, diametral fatigue controlled-stress tests

Effect	Level	Temperature of 0°C (32°F)		Temperature of 20°C (68°F)	
		Stiffness (psi)	Fatigue Life (cycles)	Stiffness (psi)	Fatigue Life (cycles)
Average		3,712,400	214,900	1,211,300	1300
Asphalt Type	AAK-1	2,955,600	84,200	862,200	1100
	AAG-1	4,663,100	548,600	1,701,800	1400
	% Difference	37%	85%	49%	21%
Asphalt Content	Optimum	3,712,400	214,900	1,211,300	1300
	High	3,712,400	214,900	1,211,300	1300
	% Difference	0%	0%	0%	0%
Aggregate Type	RL	4,347,900	160,300	1,418,600	1700
	RB	3,169,900	288,100	1,034,300	900
	% Difference	-27%	44%	-27%	-47%
Air-Void Contents	4%	4,111,000	366,400	1,341,300	2200
	8%	3,352,500	126,100	1,093,900	700
	% Difference	-18%	-66%	-18%	-68
Temperature	@ 150 psi	3,712,400	447,400	1,211,300	600
Stress	Low	3,712,400	447,400	1,211,300	2500
	High	3,712,400	103,300	1,211,300	600
	% Difference	0%	-77%	0%	-76%

Notes: Air-void contents normalized to 4 percent and 8 percent.
Stress normalized to 1033 and 1378 kPa (150 and 200 psi) for 0°C (32°F); and 100 and 150 for 20°C (68°F).
Averages based on logarithmic mean of regressed data.
Percent difference is the difference expressed as a percentage of the higher value.

higher asphalt content. For the trapezoidal cantilever tests, significant interactions between asphalt content and asphalt type and between asphalt content and aggregate type were noted.

As expected, both air-void content and temperature significantly influence the stiffness for all test types with lower voids and lower temperature, exhibiting higher stiffness than higher voids and higher temperature. As noted earlier, all test types show an interaction between asphalt type and temperature. Except for the diametral tests, an interaction between temperature and air-void content was also observed.

Stress/strain does not appear to influence the stiffness for diametral tests, and its effect was small on the stiffness for flexural beam tests and trapezoidal cantilever tests. However, it should be noted that for flexural beam fatigue tests, lower stiffness is associated with higher stress or strain; whereas for trapezoidal cantilever tests, higher stiffness is associated with a higher stress level. The initial stiffness for the flexural beam tests was defined as the stiffness at 200 load repetitions where specimens with relatively low fatigue lives (especially those containing higher voids, RL aggregate, and AAK-1 asphalt) could undergo significant damage, resulting in lower stiffness at a high stress level.

4.4 Fatigue Life (Cycles to Failure)

On the basis of the results of the statistical analysis, fatigue life as a response variable is sensitive to asphalt type for all test types (Table 4.7). Flexural beam controlled-stress and diametral fatigue tests both show a significant interaction between asphalt type and temperature. The flexural beam controlled-strain tests show an interaction between asphalt type and asphalt content.

The mixes containing AAG-1 asphalt used in the controlled-stress tests show higher fatigue life than the mixes containing AAK-1 asphalt. The percentage difference (expressed as a percentage of the higher value) between the mixes containing AAG-1 and AAK-1 asphalt varies between 58 percent for trapezoidal cantilever tests and 85 percent for the flexural beam and diametral fatigue tests.

For the flexural beam controlled-strain tests, mixes containing AAG-1 asphalt show lower fatigue lives than those mixes containing AAK-1 asphalt by a difference of 62 percent (Table 4.10) for data normalized to low and high levels of 200 and 400 micro in./in. For data normalized to low and high stress levels (Table 4.11), mixes containing AAG-1 asphalt show higher fatigue lives than the mixes containing AAK-1 asphalt. A similar observation was made of the controlled-stress tests.

Flexural beam tests exhibit sensitivity to aggregate type: mixes containing RL aggregate have a lower fatigue life than those mixes containing RB aggregate at both temperatures by about a 68 percent difference. For trapezoidal cantilever and diametral tests, aggregate type was not a significant variable; however, both these tests show significant interaction between aggregate type and temperature. At a low temperature (0°C [32°F]), specimens of mixes containing RL aggregate in the trapezoidal cantilever tests exhibit about 49 percent lower

fatigue lives than specimens of mixes containing RB aggregate. Diametral tests also show lower fatigue lives for mixes containing RL aggregate at 0°C (32°F); however, the stiffness for mixes containing RL aggregate is approximately 40 percent higher than for mixes containing RB aggregate at this temperature. This result is completely unexpected and violates an a priori notion for fatigue tests under controlled-stress conditions. That is, mixes with a higher stiffness are expected to have a higher fatigue life. At a higher temperature (20°C [68°F]), both the trapezoidal cantilever and the diametral tests indicate a higher fatigue life for mixes containing RL aggregate.

Asphalt content did not have a significant effect on fatigue life for any of the fatigue tests considered. For the flexural beam controlled-stress tests, interaction between asphalt content and temperature is significant; fatigue life is higher for mixes with optimum asphalt content at 0°C (32°F) and lower at 20°C (68°F) when compared to mixes containing high asphalt content. For flexural beam controlled-strain tests, asphalt content significantly interacts with asphalt type and air-void content.

Air-void content significantly influences fatigue life for all test types in that the fatigue life is higher for mixes with low voids than for mixes with high voids. Note that for the flexural beam controlled-strain tests, the effect of asphalt type (Tables 4.10 and 4.11) was such that those specimens exhibiting higher stiffness (mixes containing AAG-1 asphalt) had lower fatigue life than specimens having lower stiffness (mixes containing AAK-1 asphalt). The effect of air-void content is such that specimens with higher stiffness (lower air-void contents) exhibit higher fatigue life than specimens with lower stiffness (higher air-void contents). This negative effect of stiffness on fatigue life due to asphalt type and air-void content suggests that, *for a given asphalt type, **reducing the stiffness** (increasing the air-void content) will **decrease the fatigue life**; whereas, for a given **air-void content**, **decreasing the stiffness** (changing the asphalt type) will **increase the fatigue life**.*

Both temperature and stress or strain significantly influence fatigue life for all test types. For controlled-stress tests, fatigue life is higher at 0°C (32°F) than at 20°C (68°F). This result is expected since stiffness is higher at 0°C (32°F). For flexural beam controlled-strain tests, fatigue life is lower at 0°C (32°F) than at 20°C (68°F), which is also expected. Fatigue life for all test types decreases with an increase in stress or strain level.

For all test types, significant interaction between temperature and stress or strain level was noted and expected, since during testing the low and high stress or strain levels were varied depending on the temperature to ensure that the specimens failed in a reasonable number of cycles.

4.5 Cumulative Dissipated Energy

In general, the ranking observed for the cumulative dissipated energy is similar to that observed for fatigue life. Asphalt type was significant only for the flexural beam controlled-strain tests (Table 4.8). However, there is a significant asphalt type and temperature interaction for the flexural beam controlled-stress tests, indicating that the

ranking between AAG-1 and AAK-1 actually reverses at 20°C (68°F); mixes containing AAG-1 asphalt have lower cumulative dissipated energy although the fatigue life for an AAG-1 asphalt mix is higher at this temperature. This observation is important because a higher cumulative dissipated energy has generally been associated with a higher fatigue life; whereas, the above observation indicates that both fatigue life and the cumulative dissipated energy depend on asphalt type and temperature.

The flexural beam fatigue tests are sensitive to aggregate type, whereas the trapezoidal cantilever test is not. However, the latter test shows a significant interaction between aggregate type and temperature. Both the flexural beam and the trapezoidal cantilever tests are sensitive to air-void content, temperature, and stress or strain levels. The cumulative dissipated energy decreases with an increase in air-void content or stress or strain level.

4.6 Mode of Loading

Although the fatigue experiment was designed primarily for evaluating the different laboratory fatigue testing procedures, it also provides information useful for assessing the possible effects of mode of loading on fatigue behavior. Mode of loading may be important in mix analysis because, for similar initial conditions, fatigue life is typically greater in controlled-strain loading than in controlled-stress loading, and, even more important, mixes of greater stiffness tend to perform better in controlled-stress loading but worse in controlled-strain loading.

The analysis presented herein is based on the fatigue data obtained from flexural beam tests, since this test was the only type for which complete data sets for the experiment design were available for both modes of loading. It may be reiterated that the fatigue experiment included testing each of 16 mixes (Table 3.4) under both controlled-stress and controlled-strain loading at two load levels with full replication. One half of the mixes were tested at one temperature level and the other half at a second temperature. The mode-of-loading analysis was done with a least-squares calibration of models of the following type:

$$N_f = a \exp^{b\,MF} \exp^{c\,V_o} (\epsilon_o \text{ or } \sigma_o)^d (S_o)^e \qquad (4.5)$$

where:

	N_f	=	cycles to failure,
	MF	=	mode factor assuming values of 1 and -1 for controlled-strain and controlled-stress loading, respectively,
	V_o	=	initial air-void content in percentage,
	ϵ_o	=	initial flexural strain in in./in.,
	σ_o	=	initial flexural stress in psi,
	S_o	=	initial mix stiffness in psi, and
	a, b, c, d, e	=	regression constants.

Phase angle was excluded from the regression models because it was not measured during the flexural beam testing program. A separate model was calibrated for each mode of loading and each test temperature. Models were also calibrated for data sets combined over both temperatures and both modes of loading.

The summary of the regression analyses (Table 4.14) is based on calibrations in which outliers, defined as cases where the absolute values of the residuals (natural log of fatigue life) exceeded 1.1, were removed. Removal of outliers not only enhanced the accuracy of the models but, more important, improved their consistency and reasonableness. Predictor variables in each of the models of Table 4.14 were significant at a probability level of 0.05 or less.

A frequent question interpreting fatigue test data is whether the effects of temperature on fatigue behavior are fully accounted for by its related effects on mix stiffness. Those models of Table 4.14 in which strain was used as a predictor variable (instead of stress) certainly demonstrate differences between the models calibrated at 20°C (68°F) and those calibrated at 0°C (32°F). Most notably, the effects of air-void content and stiffness are statistically significant only at 20°C (68°F). However, extrapolations of the 20°C (68°F) controlled-strain calibrations to stiffnesses more characteristic of the 0°C (32°F) temperature compare nicely with the 0°C (32°F) calibrations (Figure 4.4). Whether the differences of Figure 4.4 are of practical significance probably depends on how the information will be used.

Overall, results of the regression analysis can be summarized as follows:

- At a given stress level in controlled-stress testing, stiffer mixes have greater fatigue resistance (positive stiffness power in controlled-stress models regressed on stress).

- At a given strain level in controlled-strain testing, stiffer mixes have lesser fatigue resistance (negative stiffness power in controlled-strain models regressed on strain).

- The effects of mix stiffness and air-void content are much less significant at 0°C (32°F) than at 20°C (68°F). Nevertheless, the effect of temperature on fatigue life can be accounted for by its related effect on stiffness, with some loss in accuracy.

- In general, fatigue life under controlled-strain loading is approximately 2.4 times greater than fatigue life under controlled-stress loading (from the combined model, $\exp^{0.4472\ MF}$ equals 0.639 for controlled-stress loading and 1.56 for controlled-strain loading).

The critical unknown in mix evaluation is whether the mode of loading selected for laboratory testing will influence the results of the evaluation process. For example, if Mix A is judged superior to Mix B on the basis of laboratory tests under one mode of loading, will it also be superior on the basis of results obtained under the opposite mode of loading? Prior speculation suggested that controlled-strain testing might be used to evaluate mixes for

Table 4.14. Comparative regression models for controlled-stress and controlled-strain testing

Model	Temp. (°C)	R^2	CV (%)
Controlled-Stress Models Regressed on Stress			
$N_f = 7.6527*10^{11} \exp^{-0.4975 V_o} (\sigma_o)^{-4.7425} (S_o)^{0.6816}$	20	0.87	73
$N_f = 8.6720*10^{-7} (\sigma_o)^{-5.7260} (S_o)^{3.9524}$	0	0.90	69
$N_f = 8.7309 \exp^{-0.2130 V_o} (\sigma_o)^{-3.7040} (S_o)^{2.119}$	Both	0.82	82
Controlled-Strain Models Regressed on Strain			
$N_f = 4.2554 \exp^{-0.4742 V_o} (\epsilon_o)^{-3.9200} (S_o)^{-1.4792}$	20	0.87	73
$N_f = 9.5223*10^{-11} (\epsilon_o)^{-4.0117}$	0	0.90	55
$N_f = 3.2513*10^{-4} \exp^{-0.2542 V_o} (\epsilon_o)^{-3.9211} (S_o)^{-0.8824}$	Both	0.85	66
Controlled-Stress Models Regressed on Strain			
$N_f = 7.8984*10^{11} \exp^{-0.4966 V_o} (\epsilon_o)^{-4.7620} (S_o)^{-4.0757}$	20	0.87	73
$N_f = 2.7755*10^{-12} (\epsilon_o)^{-4.2203}$	0	0.89	73
$N_f = 8.5292 \exp^{-0.2126 V_o} (\epsilon_o)^{-3.7148} (S_o)^{-1.5900}$	Both	0.82	82
Combined Models Regressed on Strain			
$N_f = 2.2934*10^{4} \exp^{0.5222 MF} \exp^{-0.4040 V_o} (\epsilon_o)^{-3.0091} (S_o)^{-1.6475}$	20	0.86	69
$N_f = 3.3596*10^{-11} \exp^{0.8611 MF} (\epsilon_o)^{-4.0336}$	0	0.90	55
$N_f = 0.9500 \exp^{0.4472 MF} \exp^{-0.2566 V_o} (\epsilon_o)^{-3.3669} (S_o)^{-1.1633}$	Both	0.84	75

Note: CV = coefficient of variation.

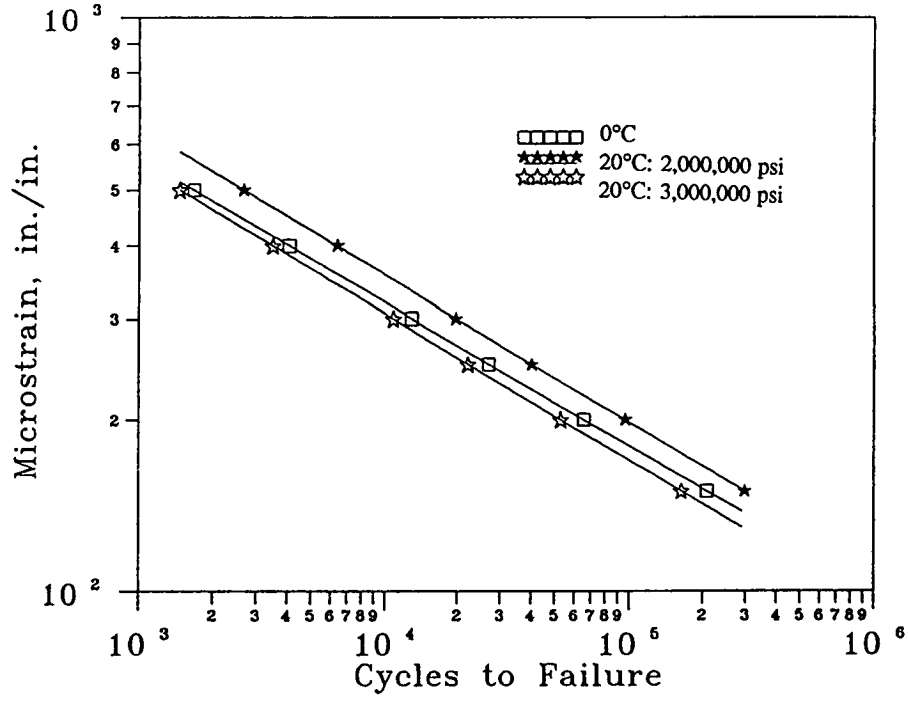

Figure 4.4. Effect of testing temperature on N_f-ϵ relationship

relatively thin pavements on stiff foundations and that controlled-stress testing might be more appropriate for thicker and relatively stiffer structures. Resolution of this issue is an important task of SHRP Project A-003A.

The fatigue behavior of the in situ mixes is determined by two key factors: the mixes' resistance to the destructive effects of repetitive stresses or strains and the levels of stress or strain to which it is subjected under traffic loading. Laboratory testing is necessary for establishing the fundamental fatigue behavior (N_f-ϵ_o relationship), and mechanistic analysis is necessary for establishing critical levels of stress or strain. A combination of fatigue testing and mechanistic analysis is required for evaluating likely in situ behavior.

Addressing the mode-of-loading issue thus required that mix performance be simulated for a suitable range of in situ pavement conditions. For convenience, the mechanistic analysis (ELSYM5) assumed linear elastic behavior in all pavement layers. The surface thickness of the two-layered structures ranged from 5 to 30.5 cm (2 to 12 in.) and subgrade moduli were varied, as indicated below, to exaggerate the relative stiffness of the surface layer to that of its support. Poisson's ratios of 0.35 and 0.30 were used for surface and subgrade layers, respectively. Loading consisted of 44 kN (10,000 lb) on 690 kPa (100 psi), dual tires, spaced 30.5 cm (12 in.) apart center to center.

Surface Thickness (in.)	**Subgrade Modulus (psi)**
2	30,000
4	25,000
6	20,000
8	15,000
10	10,000
12	5000

The first step in the simulations was to estimate the maximum principal tensile strains in the pavement structures for mixes that had been tested in the laboratory. These strains were then used with previously calibrated N_f versus ϵ_o relationships to determine the simulated cycles to failure in situ. Finally, the simulated cycles to failure were examined to determine if mixes were ranked identically depending on whether controlled-stress or controlled-strain data had been used.

The one complexity in the analysis stemmed from the fact that at 20°C (68°F) stiffnesses measured under controlled-stress loading were considerably smaller than those measured under controlled-strain loading. These differences may be due in part to the fact that step loads (0.1 second on followed by 0.5 second off) were used in the controlled-stress testing while haversine loads (also 0.1 second on followed by 0.5 second off) were used in the controlled-strain testing. Another contributing factor may have been the rather lengthy delay (up to eight months) between completion of the controlled-stress testing and completion of the controlled-strain testing. Limited evidence of stiffening due to steric hardening, particularly in specimens stored at room temperatures, was observed by A-003A investigators

at Oregon State University. In any case, in situ simulations are comparable only when identical stiffnesses are employed for each of the two laboratory modes of loading. This was rather easily accomplished by factoring controlled-stress stiffnesses so that the average stiffness for each mix tested under controlled-stress loading was the same as the average stiffness under controlled-strain loading.

Only three mixes, all tested at 20°C (68°F), were found which yielded acceptable calibrations[2] of the N_f-ϵ_o relationships. Over the range of pavement structures evaluated and with the use of either controlled-stress or controlled-strain data, the ranking of the three mixes was unchanged (Table 4.15). Mix 3 was always superior, and Mix 1 was always inferior. This limited analysis suggests, therefore, that the evaluation of mix performance may well be independent of laboratory mode of loading.

Table 4.15. Effect of laboratory mode of loading on the simulated fatigue life of three mixes

Mode of Loading	Surface Thickness (in.)	Simulated Fatigue Life		
		Mix 1 (575,000 psi)	Mix 2 (715,000 psi)	Mix 3 (1,013,000 psi)
Controlled-Stress Testing	2	2000	10,000	**40,000**
	4	6000	35,000	**213,000**
	6	17,000	107,000	**1,275,000**
	8	39,000	257,000	**5,524,000**
	10	77,000	528,000	**17,209,000**
	12	129,000	957,000	**40,394,000**
Controlled-Strain Testing	2	5000	11,000	**27,000**
	4	16,000	35,000	**65,000**
	6	50,000	96,000	**167,000**
	8	126,000	212,000	**363,000**
	10	269,000	408,000	**660,000**
	12	476,000	688,000	**1,035,000**

[2]For this purpose, a calibration was considered acceptable if, for both controlled-stress and controlled-strain loading, the coefficients of determination of the ln N_f-ln ϵ_o relationships exceeded 0.90 and the ln ϵ_o term was statistically significant at a probability level of 0.05 or smaller.

The analysis was extended to include four hypothetical mixes having stiffnesses of 2756 and 4134 MPa (400,000 and 600,000 psi) and air-void contents of 4 and 7 percent. Because of the hypothetical nature of these mixes, their fatigue response was estimated by regression models calibrated from testing at 20°C (68°F). For controlled-strain testing, the applicable model (Table 4.14) is as follows:

$$N_f = 4.2554 \exp^{-0.4742\ V_o} (\epsilon_o)^{-3.9200} (S_o)^{-1.4792} \quad (4.6)$$

For controlled-stress testing, a recalibration using adjusted stiffnesses yielded the following model:

$$N_f = 2.5263*10^5 \exp^{-0.2007\ V_o} (\epsilon_o)^{-3.4134} (S_o)^{-2.1239} \quad (4.7)$$

Once again, results of the simulation, summarized in Table 4.16, generally seem to be independent of mode of loading. For the same mix stiffness, low air-void mixes were always superior to high air-void mixes. As anticipated, stiffer mixes demonstrated inferior fatigue resistance for thin pavements, while stiffer mixes were preferred for thick pavements. The only difference between modes of loading is found when identifying the borderline between thin and thick pavements. Based on this analysis, this difference becomes important for surface thicknesses in the range of 7.6 to 12.7 cm (3 to 5 in.). The borderline thickness, however, is expected to vary depending on such factors as temperature, mix properties, and stiffness of the pavement surface layer relative to that of its support.

In summary, this analysis demonstrated the importance of mode of loading in the proper interpretation of laboratory fatigue data. It confirmed that fatigue lives under controlled-strain loading generally exceed those under controlled-stress loading and that, on casual inspection, effects of mix stiffness on fatigue life are generally reversed for the two modes of loading. However, when test results are interpreted in terms of the performance expected of the pavements in which the mixes are placed, it appears that controlled-stress and controlled-strain testing may yield similar mix rankings, especially for the substantial pavement structures characteristic of the nation's primary trucking highways.

4.7 Summary

Fatigue tests evaluated in this study were found to be sensitive to asphalt type as well as to aggregate type, either directly or through interactions with other mix or test variables for the three response variables—stiffness, fatigue life, and cumulative dissipated energy. For the diametral test, the cumulative energy was not available, and the response variables measured were stiffness and fatigue life only.

The regression fits for the stiffness are considered good; coefficients of determination vary between 0.93 for the diametral and trapezoidal cantilever controlled-stress tests and 0.98 and 0.95 for the flexural beam fatigue controlled-stress and controlled-strain tests, respectively. The coefficients of variation are between 12 and 19 percent, indicating that most of the variation in stiffness can be explained by the mix and test variables.

Table 4.16. Effects of laboratory mode of loading on the simulated fatigue life of hypothetical mixes of varying air-void contents and surface stiffnesses

Mode of Loading	Surface Thickness (in.)	Simulated Fatigue Life			
		4% Air-Void Contents		7% Air-Void Contents	
		400,000 psi	600,000 psi	400,000 psi	600,000 psi
Controlled-Stress Testing	2	46,000	30,000	25,000	16,000
	4	103,000	91,000	56,000	50,000
	6	290,000	294,000	159,000	161,000
	8	695,000	766,000	381,000	420,000
	10	1,324,000	1,641,000	725,000	899,000
	12	2,201,000	2,929,000	1,205,000	1,604,000
Controlled-Strain Testing	2	54,000	49,000	13,000	12,000
	4	137,000	174,000	33,000	42,000
	6	449,000	672,000	108,000	162,000
	8	1,225,000	2,021,000	295,000	487,000
	10	2,565,000	4,847,000	618,000	1,168,000
	12	4,599,000	9,425,000	1,109,000	2,272,000

Regression fits for the fatigue life and cumulative dissipated energy can be considered fair; the coefficient of determination is approximately 0.8 for fatigue life and 0.7 for cumulative dissipated energy. The coefficients of variation observed for fatigue life are greater than 90 percent for flexural tests and 66 percent for diametral tests, indicating that the variation in fatigue life or cumulative dissipated energy cannot be fully explained by just mix and test variables. It may be noted that the coefficient of variation measures prediction error, random error, and testing error. Computations based on actual data and not on fitted data have shown a coefficient of variation of approximately 60 percent for the controlled-stress beam fatigue test. The error in the prediction model accounts for the higher coefficients of variation.

The effects of mode of loading on the ranking of mixes were evaluated by simulating in situ pavement performance based on the flexural beam controlled-stress and controlled-strain data. Results of the analysis indicate that fatigue lives under controlled-strain loading generally exceed those under controlled-stress loading and that, the effects of mix stiffness on fatigue life are generally reversed for the two modes of loading. However, when test results are interpreted in terms of the performance expected of the pavements in which the mixes are placed, it appears that controlled-stress and controlled-strain testing may yield similar mix rankings, especially for the substantial pavement structure.

5

Comparison of Test Methods

5.1 Introduction

The test methods initially selected for detailed evaluation in SHRP Project A-003A included 1) flexural fatigue (both third-point loading of prismatic beams and cantilever loading of trapezoidal specimens), 2) tensile fatigue (both uniaxial and diametral configurations), 3) fracture mechanics, and 4) tensile strength and stiffness (as surrogates for repetitive testing to fracture). As work progressed, it became obvious that several of these methods could be eliminated from the laboratory testing program without seriously jeopardizing the study.

The uniaxial tension-compression testing, scheduled for completion by SWK/UN, was discontinued because of persistent specimen failures at or near the end caps, which rendered test results questionable. Finite element analysis of the test configuration confirmed that stress concentration would indeed occur at the ends of the specimen. It was decided that the effort required to correct this deficiency could be better spent expanding the trapezoidal cantilever test program at SWK/UN. Consequently, a limited number of controlled-strain trapezoidal cantilever tests were performed.

After having been started at the UCB, fracture mechanics testing was eventually eliminated in part because extensive testing would have been necessary to complete it. Moreover, for routine mix testing and evaluation, the fracture mechanics approach was judged excessively complex and difficult. Tensile strength testing, planned for UCB, was also eliminated in part because previous studies at LCPC (Bonnot 1991) indicate that tensile strength is not directly related to fatigue life and because of other more pressing testing needs at the laboratory. The search for a surrogate procedure to eliminate the need for repetitive fatigue testing focused instead on stiffness and phase angle measurements developed from frequency sweep testing of briquette and prismatic specimens in simple shear.

Remaining as viable test candidates were flexural beam fatigue, flexural cantilever fatigue, and diametral fatigue. An extensive testing program, detailed in Chapter 4, was conducted to aid in the evaluation of these test methods. This program provided an excellent

opportunity to fine-tune the equipment and procedures and to qualitatively evaluate the practicality and potential user acceptance of the three test procedures. It also developed the quantitative information necessary to 1) evaluate two of the preestablished evaluation criteria, namely, sensitivity to mix variables (particularly asphalt properties) and test reliability, and 2) determine the overall reasonableness of the test measurements. These quantitative evaluations are summarized in the following section. Thereafter, a second evaluation section, concentrates on more qualitative criteria, including reasonable simulation of field conditions; prediction of fundamental properties, which can be used in appropriate design or performance models; ease and simplicity of use; time requirements; and ease of implementation and equipment cost.

5.2 Test Measurements

The only comparative data available for evaluating the three primary test contenders were from the controlled-stress testing of the fractional factorial design described in Chapter 3. Because cumulative dissipated energy was not available for diametral testing, the most relevant response measures were limited to stiffness (modulus of resiliency) and cycles to failure (fatigue life). Examined herein are differences among the three test methods in the sensitivity of these response measures to mix variables and the reliability and reasonableness of test measurements.

5.2.1 Sensitivity to Mix Variables

One of the most important requirements of the accelerated performance tests being developed by Project A-003A was that the tests must be able to discriminate among asphalt-aggregate mixes based on expected field performance. To help assess this capability, the test program involved two asphalts, two aggregates, two asphalt contents, and two air-void contents. Although the difference between the two asphalt-content levels was relatively small, other mix variables were expected to strongly influence the test response of the different mixes and, by inference, their performance in situ.

One measure of the sensitivity of the test response to a given mix variable is the percentage difference between the response averages under low and high test conditions. Because air-void content[3] could not be precisely controlled, low and high averages corresponding to 4 percent and 8 percent air-void contents were computed from the GLM that had been fitted by stepwise-regression techniques to the test measurements. Only statistically significant main effects (variables) and two-level interactions were retained in these statistical models.

---

[3]Because of the extreme sensitivity of fatigue life to stress level and temperature and because of differences between the flexural tests and the diametral tests, the stresses at each of the two levels were not held constant for all testing. The GLM adjusted all test measurements to two constant stress levels: low and high.

Results indicating the sensitivities of the test responses to the four main mix effects are summarized in Table 5.1. Entries flanked by superscript a indicate effects that were not statistically significant. Superscript b indicates that statistically significant effects were limited to two-level interactions.

Table 5.1. Sensitivity of test response to mix variables (from GLM stepwise regression)

	Flexural Beam Fatigue	Flexural Cantilever Fatigue	Diametral Fatigue
Percent Difference in Average Stiffness			
Asphalt Type	51	29	43
Asphalt Content	0[a]	0[b]	0[a]
Aggregate Type	11	5[b]	27
Air-Void Content	33	24	18
Temperature	84	44	67
Stress	8	4	0[a]
Percent Difference in Average Cycles to Failure			
Asphalt Type	56	58	53
Asphalt Content	50[b]	0[a]	0[a]
Aggregate Type	67	49[b]	45[b]
Air-Void Content	85	80	67
Temperature	99	98	99
Stress	88	80	76

[a] Main effect and two-level interactions were not statistically significant
[b] Main effect was not statistically significant, but some interactions were statistically significant

Asphalt type is the mix variable of primary interest to the SHRP asphalt program. Flexural fatigue and diametral fatigue seem equally able to discriminate among mixes containing different asphalts based on both of their response measures, stiffness, and cycles to failure. For other mix variables, beam fatigue generally, yields the most sensitive measurements, followed in order by cantilever fatigue and diametral fatigue.

5.2.2. Reliability

Test reliability is generally related to the dispersion in the data when replicate specimens are tested under identical conditions. Under such conditions, the most reliable test is the one which produces the smallest coefficient of variation. The laboratory experiment yielded two measures which indicate test reliability. The first is the coefficient of variation which was

developed from the stepwise-regression calibration of the GLM. Although not a perfect measure since it includes prediction error and random error in addition to testing error, the coefficient of variation is relatively useful for measuring testing error in this case because of the low prediction error (indicated by large coefficients of determination) associated with most of these particular GLMs (Table 4.4). The one exception is the GLM for cycles to failure from trapezoidal fatigue testing.

A second measure of reliability is the variance of a set of replicate measurements. In the laboratory testing the 32 mix/testing combinations for each test method were replicated. An estimate of the variance for each method can be obtained by pooling the sample variances between these replicate tests.

As expected, coefficients of variation were much smaller for stiffness testing than for fatigue testing (Table 5.2). For both stiffness and cycles to failure, coefficients of variation were significantly different among test methods. Trapezoidal fatigue excelled for stiffness testing, followed in order by beam fatigue and finally diametral fatigue. For cycles to failure, the ordering of test methods was exactly reversed: diametral fatigue testing proved to be most reliable. Interestingly, earlier testing in flexural fatigue and diametral fatigue had yielded somewhat contrasting results (Sousa et al. 1991a). In the earlier testing, coefficients of variation for flexural and diametral testing, respectively, were 49.6 percent and 136.0 percent for cycles to failure and 16.7 percent and 36.6 percent for stiffness. Why the cycles-to-failure results are so different is particularly surprising and not easily understood.

Table 5.2. Accuracy of test measurements

	Flexural Beam Fatigue	Flexural Trapezoidal Fatigue	Diametral Fatigue
Stiffness			
Coefficient of Variation (%)	12.3	11.4	19.7
Sample Variance (ln psi)	0.010	0.014	0.015
Cycles to Failure			
Coefficient of Variation (%)	98.7	171.8	65.5
Sample Variance (ln cycles to failure)	0.282	1.696	0.213

Like the coefficients of variation, sample variances were also smaller for stiffness testing than for fatigue testing (Table 5.2). For stiffness testing, sample variance for the beam fatigue was the smallest, followed in order by trapezoidal fatigue and diametral fatigue. For fatigue testing, sample variance for the diametral fatigue was smallest, followed in order by beam fatigue and trapezoidal fatigue. It should be noted that the sample variance in

Table 5.2 was computed by linearly adjusting the stiffness and fatigue life for the variation in air-void levels and stress levels between replicates.

5.2.3. Reasonableness of Test Measurements

To be eligible for consideration as standards, the candidate accelerated performance tests for fatigue must produce reasonable results—results which are internally consistent and which conform with a priori expectations developed from prior experiences. Examined first are the highly aggregated results developed from the stepwise-regression GLM equations (Table 5.3).

Table 5.3. Average levels of stiffness and cycles to failure (from GLM stepwise regression)

	Flexural Beam Fatigue	Flexural Cantilever Fatigue	Diametral Fatigue
Average Stiffness (psi)			
0°C (32°F)	2,454,700	1,978,100	3,712,400
20°C (68°F)	425,100	1,063,100	1,211,300
Overall	1,439,900	1,520,600	2,461,850
Average Cycles to Failure			
0°C (32°F)	5,834,000	448,800	214,900
20°C (68°F)	34,500	42,400	1300
Overall	2,934,250	245,600	108,100

Most obvious from the average test measurements of Table 5.3 is the remarkable difference between diametral testing and flexural testing. The diametral testing yields average overall stiffnesses which exceed flexural stiffnesses by 60 to 70 percent. In turn, the average overall cycles to failure in flexure exceed those in indirect tension by a factor of approximately 27. It is clear that diametral specimens are considerably stiffer than flexural specimens but fail much more quickly under repetitive controlled-stress loading. These effects, particularly the possibility for stress stiffening, may be due in part to the biaxial state of critical stress in diametral specimens. The accumulation of permanent deformation during testing and the lack of stress reversal—uncharacteristic of mix loading in situ—contribute significantly to the reduced fatigue life of diametral specimens.

Both the stiffness and the cycles to failure results of the cantilever fatigue tests (Table 5.3) show less sensitivity to temperature than the results of either the beam fatigue or the diametral fatigue tests. Perhaps cantilever fatigue's more rapid loading frequency and sinusoidal waveform contributed to these differences. Nevertheless, the companion A-003A stiffness investigation generally confirms a more significant temperature dependence of stiffness than indicated by cantilever testing. For example, axial compression and diametral

tests of a similar array of mix types yielded average resilient moduli at 0°C (32°F) that were approximately 3.1 to 3.2 times the moduli at 20°C (68°F). The comparable ratio for the cantilever fatigue results reported in Table 5.3 is approximately 1.8. Furthermore, the 5.8 ratio observed for the beam fatigue tests seems excessive based on other test data.

In addition to the gross effects discussed above, the various mix and testing effects on stiffness and cycles to failure must also be reasonable. Table 5.4, also derived from the GLMs which were calibrated by stepwise regression, provide necessary information.

Table 5.4. Average effects of mix and test variables (from GLM stepwise regression)

		Flexural Beam Fatigue	Flexural Cantilever Fatigue	Diametral Fatigue
Average Stiffness				
Asphalt Type	AAK-1	1,055,650	1,296,700	1,908,900
	AAG-1	1,969,300	1,786,050	3,182,400
Asphalt Content	Low	1,439,900[a]	1,520,600[a]	2,461,800[a]
	High	1,439,900[a]	1,520,600[a]	2,461,800[a]
Aggregate Type	RL	1,439,750	1,517,300[b]	2,883,250
	RB	1,442,750	1,524,700[b]	2,102,100
Air-Void Content	4%	1,719,100	1,745,600	2,726,100
	8%	1,206,900	1,324,500	2,223,200
Temperature	0°C	2,541,900	1,952,800	3,712,400
	20°C	404,700	1,082,500	1,211,300
Stress	Low	1,494,200	1,498,400	2,461,800[a]
	High	1,387,600	1,543,000	2,461,800[a]
Average Cycles to Failure				
Asphalt Type	AAK-1	1,106,300	158,800	42,650
	AAG-1	7,815,700	379,800	275,000
Asphalt Content	Low	4,143,300[b]	245,600[b]	108,100[a]
	High	2,084,100[b]	245,600[b]	108,100[a]
Aggregate Type	RL	1,674,400	189,750[b]	81,000[b]
	RB	5,142,000	329,750[b]	144,100[b]
Air-Void Content	4%	7,679,400	552,600	184,300
	8%	1,121,150	109,100	63,400
Temperature	0°C	18,295,600	1,007,400	447,400
	20°C	13,200	18,300	600
Stress	Low	9,192,600	552,800	224,950
	High	936,750	109,100	51,950

[a]Main effect and two-level interactions were not statistically significant.
[b]Main effect was not statistically significant, but some interactions were statistically significant.

Regarding asphalt type, AAG mixes are generally stiffer than AAK mixes for each of the three test methods. The larger stiffnesses of AAG mixes at these test temperatures has been confirmed by A-003A's axial and diametral stiffness testing and by controlled-strain, beam fatigue testing. Since stiffer mixes are generally expected to survive longer at a fixed stress level in controlled-stress tests, AAG mixes are expected to perform better in this testing—the averages of Table 5.4 confirm that they do.

There is little basis for developing a priori expectations regarding the effects of asphalt content, primarily because the range between the low and high levels evaluated herein was relatively small. Over a wider range, however, the thicker films associated with higher asphalt contents are likely to influence the asphalt-aggregate bond, mix stiffness, strains within the asphalt binder, and the amount and distribution of air voids. The net effect could very well be an optimum air-void content for both stiffness and cycles to failure. In this study, however, test results show a generally negligible effect of asphalt content on both stiffness and cycles to failure. The one exception is the dramatic difference in average cycles to failure for the beam fatigue data, which were due solely to the interactive effects of asphalt content with temperature. This result is unexpected and unreasonable, given the results of the other testing, including the negligible effect of asphalt content on mix stiffness in beam fatigue.

Although of the same gradation, aggregates RL and RB are widely different. RB is a crushed, angular, rough surface texture aggregate that should prove stiffer and more resistant to controlled-stress loading than RL, which has a preponderance of naturally rounded particles and a smooth surface texture. Test results show surprisingly little aggregate effect on stiffness but a very significant effect—primarily due to two-level interactions—on cycles to failure. As expected, RB proved superior to RL. Average stiffnesses from the diametral tests indicate that RL mixes are stiffer—an unreasonable finding. This finding conflicts with the general principle that stiffer mixes should generally have greater fatigue resistance in controlled-stress testing.

The test effects of air-void content and temperature shed no additional information. Low voids and low temperatures translate into increased stiffness and increased cycles to failure under controlled-stress loading. These as-expected results were experimentally verified in each of the three testing configurations.

Finally, the test program confirmed that larger stresses mean lesser cycles to failure. The stress effects on mix stiffness were mixed, however, and although the axial and diametral stiffness testing program indicated a slight reduction in stiffness at a larger stress when testing at 20°C (68°F), a priori expectations provide no firm basis for selecting one test method over another.

5.3 Other Considerations

Addressed in this section are other preestablished criteria for comparing the three candidate test procedures, including 1) reasonable simulation of field conditions; 2) prediction of

fundamental properties that can be used in appropriate design or performance models; 3) ease and simplicity of use; 4) time requirements; and 5) ease of implementation and equipment cost. Beam and trapezoidal fatigue tests are addressed first, followed by a somewhat more detailed treatment of diametral tests.

First, though, it may be useful to identify some important similarities among the candidate procedures. Each procedure involves repetitive loading to failure of a small specimen, and, as a result, considerable laboratory testing effort is required. No procedure simulates exactly the stress fields under traffic loads, and none directly accounts for or simulates the progressive growth of cracks in real pavement structures. Temperature-control requirements, and consequently equipment, are similar for all tests. Although improvements and enhancements continue to be made, none of the tests is new, and test equipment, though not yet standardized, is generally available.

5.3.1 Beam and Trapezoidal Fatigue

Beam fatigue and trapezoidal fatigue share many common attributes, and there is little basis other than individual preference for choosing between the two.

Both simulate the flexural stress pattern found in situ but apply uniaxial rather than triaxial stresses. Both reverse the stresses (tension-compression), and neither permits the accumulation of permanent deformation with increasing numbers of load repetitions. Loading can be in either the controlled-stress or the controlled-strain mode to better simulate the range of conditions encountered in real pavements.

Response measures include not only stiffness, phase angle, and cycles to failure but also dissipated energy. The use of such measures in appropriate design or performance models has often been successfully demonstrated over the years by numerous agencies. Although test measurements generally do not seem subject to the extraneous influences that might threaten their validity, the beam test avoids the possible edge effects of bonding trapezoidal specimens to their end plates.

Experience with flexural fatigue testing is extensive: the beam test has been popular in the United States; the trapezoidal test, in Europe. As experience has developed, improvements have made the tests not only easier and simpler to perform but more accurate as well. Significant new enhancements have emerged as a result of SHRP Project A-003A, particularly in the area of computer control and data acquisition. In addition, hardware improvements have achieved notable improvements in test reliability as well. In each case operations have also been simplified and eased.

The shapes of the flexural test specimens generally require that they be sawed from larger compacted masses. Although sawing adds time and expense, experienced users do not find it burdensome, especially when they consider that test results are likely to be more reliable because of more uniform surface conditions and more homogeneous specimens. Compactors

designed to produce cylindrical briquettes are not generally suitable for preparing flexural fatigue specimens.

One advantage of beam fatigue under third-point loading over trapezoidal fatigue is that a larger portion of the specimen is subjected to a uniform maximum stress level. Thus the likelihood is greater in beam testing that test results will reflect the weaknesses that naturally occur in asphalt-aggregate mixes.

Test time, including specimen preparation, is similar for the beam and the trapezoidal tests except for the bonding of trapezoidal specimens to their end plates. For equipment comparable in accuracy and capability, there is no basis for estimating significant cost differentials between beam and trapezoidal tests.

5.3.2 Diametral Fatigue

In this section the advantages and disadvantages of the diametral test, as identified in an earlier SHRP Project A-003A investigation (Tangella et al. 1990), are first summarized. Then the types of failure patterns common to repetitive diametral testing are explained, and early SHRP A-003A testing experience is summarized. Finally, consideration is given to the circumstances for which the diametral test seems most well suited for use in evaluating the fatigue behavior of asphalt-aggregate mixes. The increased attention given here to diametral fatigue reflects primarily the attractiveness of its ability to test briquette specimens.

5.3.2.1 Prior Critique

A number of investigators have used the diametral test for asphalt mix evaluations and pavement analyses. The test is simple to perform and is considered by some to be effective for characterizing materials in terms of fundamental properties. Although the stress state within the specimen is complex, critical stresses and strains are readily computed if linear elastic behavior is assumed. A biaxial state of stress exists along the vertical load axis. Along this axis, the horizontal tensile stress is reasonably constant while the vertical compressive stress varies more significantly.

In addition to the biaxial state of stress, fundamental differences between flexural beam and diametral fatigue tests include the facts that 1) permanent deformation is usually prohibited in flexural tests but builds gradually under repetitive diametral loading, and 2) stress reversal is impractical in diametral tests. One significant effect of these differences is that fatigue life is much smaller under diametral testing than under flexural testing.

Advantages of the diametral test were found to include the following:

- The test is simple.

- The design of mixes and pavements for fatigue adequacy is possible in principle, using the diametral fatigue response together with field correlations.

- The equipment is applicable for other tests; for example, resilient modulus and indirect tensile strength.

- Failure is initiated in a region of relatively uniform tensile stress. However, it should be noted that, according to Porter and Kennedy (1975), the governing variable is the deviator stress, $\sigma_t - \sigma_c$. The uniform region for this variable is much more restricted than the uniform region for σ_t.

- A biaxial state of stress exists, possibly of a type better representing field conditions.

- Tests can be performed on field cores as well as laboratory briquettes.

Included among the disadvantages of the diametral test were the following:

- Although a biaxial stress state exists at the center of the specimen, it is impossible to vary the ratio of the vertical and horizontal components and, hence, to replicate the stress state at critical locations within in situ pavements.

- This method significantly underestimates fatigue life if the principal tensile stress is used as the damage determinant. Even when the stress difference, $(\sigma_t - \sigma_c)$, is used to predict fatigue life, the method still underestimates fatigue life relative to other laboratory methods.

- The absence of stress reversal and the accumulation of permanent deformation are of great concern.

- It is not possible to do controlled-strain testing.

5.3.2.2 Accumulation of Permanent Deformation and Failure Patterns in Diametral Fatigue

The repetitive diametral test was initially used in SHRP Project A-003A to evaluate laboratory compaction procedures (Sousa et al. 1991). The test evaluated the fatigue characteristics of a variety of mixes compacted by gyratory, kneading, and rolling-wheel procedures. The experiment design called for testing 144 specimens. Two-thirds of the tests were executed at 4°C (39.2°F); the other one-third, at 20°C (68°F).

The rationale for using the diametral test to measure fatigue response is that repetitive loading induces tensile stresses that will eventually split the specimens. Usually fatigue life is defined by the number of load repetitions required to burst or split the specimen. To detect failure, a metallic tape is placed on the specimens, which stops the test once it is

broken. For tests executed by the A-003A contractor, this system of detecting failure was replaced by setting limits on the total vertical deformation. A 1.25 cm (0.5 in.) vertical deformation was the limit set for testing at 20°C (68°F); a 0.50 cm (0.2 in.) deformation, at 4°C (39.2°F). Experience has shown that, even before these limits are reached, the specimen often fails catastrophically by bursting or splitting; that is, the specimen is broken into two pieces and the ram moves down under stress control and trips the limit switch, stopping the test. Nevertheless, using this procedure to define failure provided a unique opportunity to investigate the progressive accumulation of vertical permanent deformations in test specimens.

Figure 5.1 shows the evolution of permanent deformation with time (number of load repetitions) for six randomly chosen tests executed at 20°C (68°F). It is clear that there is a significant accumulation of permanent deformation during these fatigue tests. It was also observed that some tests reached the 1.25 cm (0.5 in.) vertical deformation limit before splitting occurred. It is therefore reasonable to assume that failure was often accompanied by a combination of permanent deformation and fatigue mechanisms. It was also observed that some of the specimens exhibited cracks starting at the edge of the loading strips (Figure 5.2) and not on the vertical centerline as expected.

Figure 5.3 shows the evolution of permanent deformation with time (number of load repetitions) for three randomly chosen tests executed at 4°C (39.2°F). The accumulation of permanent deformation is significantly smaller than that observed at 20°C (68°F). The mix is more brittle, and during the low-temperature testing, most of the specimens did in fact fail by splitting. However, many of them exhibited a peculiar failure zone directly beneath the loading platens (Figure 5.4). The specimen seems to have failed not by fatigue due to tensile stresses at the centerline of the specimen but by fatigue due to shear stresses occurring at the edge of the loading platens and rapidly propagating cracks toward the center of the specimen.

Several types of failure other than tensile rupture through the centerline, illustrated in Figure 5.5, have been reported by Hudson and Kennedy (1968). During the A-003A compaction study, failure patterns were predominantly of three types:

- Crack initiation at or near the center of the specimen, finally resulting in complete splitting of the specimen along the vertical plane. The initial cracking sometimes consisted of several parallel cracks within approximately 1 cm (2.54 in.) of the center of the specimen. Approximately 40 percent of the specimens failed this way, most at low temperature.

- Crack initiation at the top of the specimen (or in a few cases at the bottom of the specimen), which eventually spread progressively downward (or upward) until the specimen burst in half. The initial cracking usually was V-shaped, with the upper arms of the V originating at the outside edges of the loading platen and the bottom of the V approximately 1 to 2 cm (2.54 to 5.1 in.) below. Approximately 40 percent of the specimens failed this way.

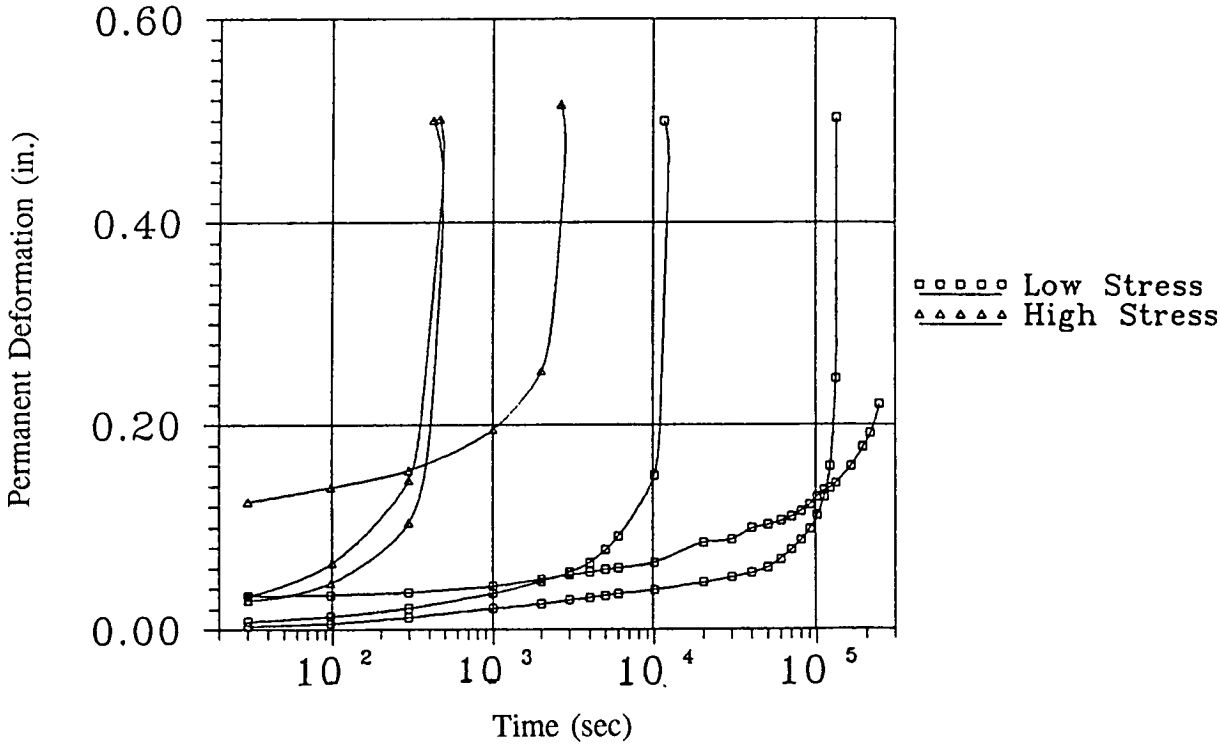

Figure 5.1. Variation of vertical permanent deformation in diametral repetitive tests at 20°C (68°F) (after Sousa et al. 1991)

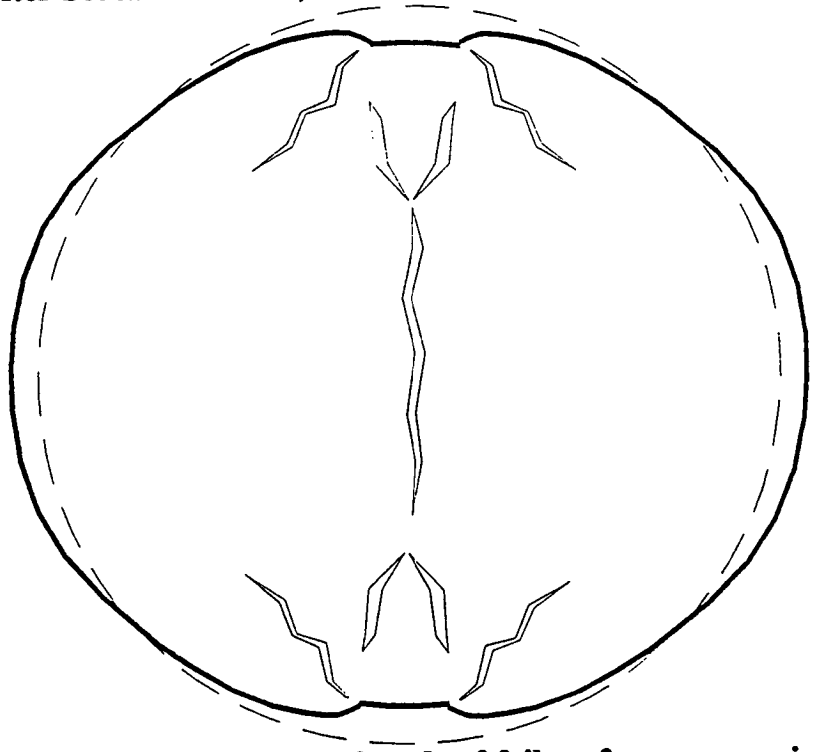

Figure 5.2. Schematic representation of mode of failure for some specimens at 20°C (68°F) (after Sousa et al. 1991)

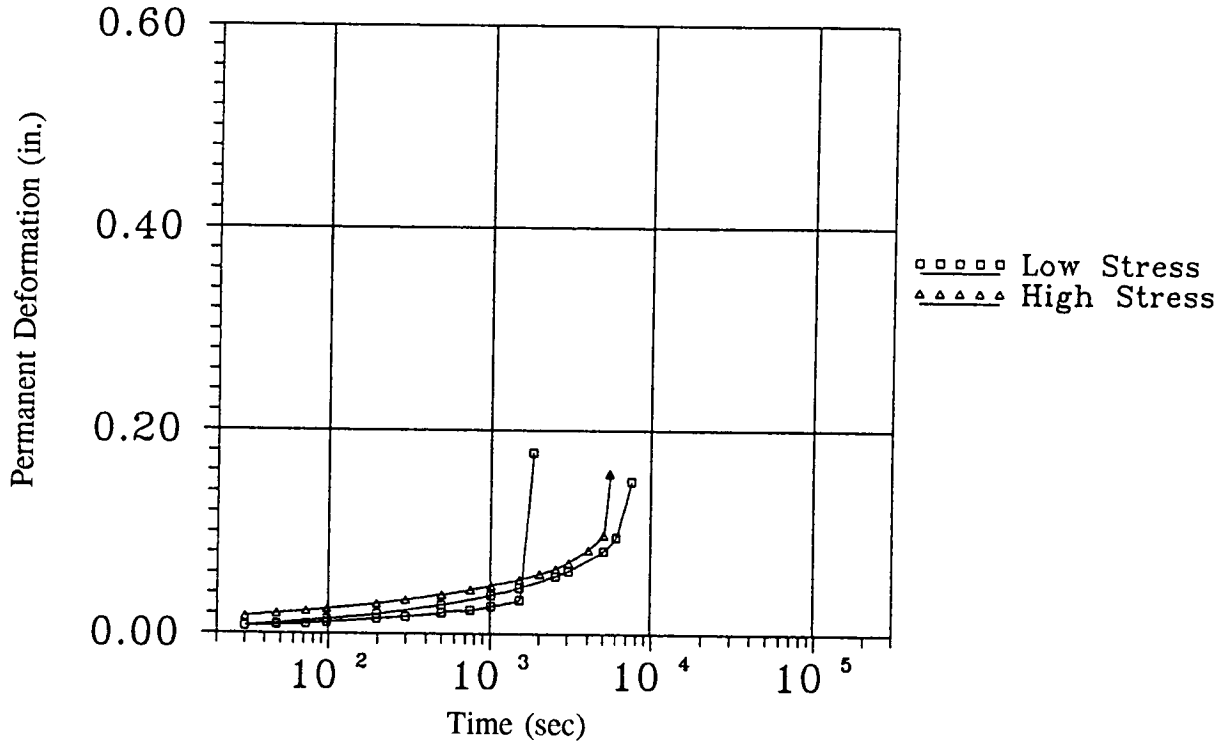

Figure 5.3. Variation of vertical permanent deformation in diametral repetitive tests at 4°C (39.2°F) (after Sousa et al. 1991)

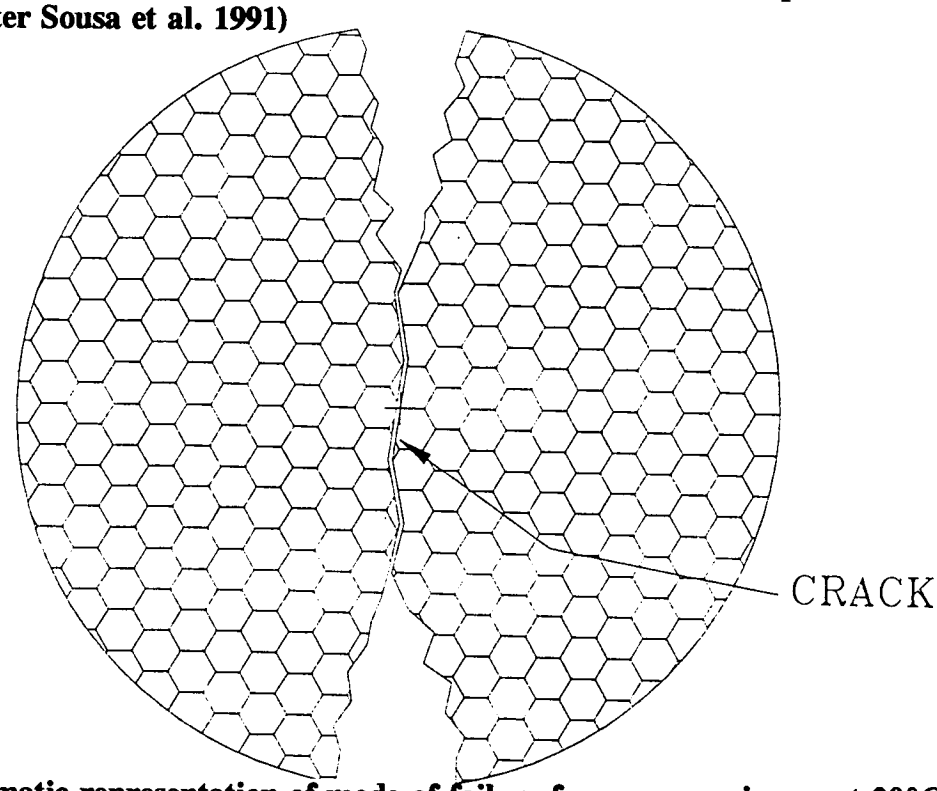

Figure 5.4. Schematic representation of mode of failure for some specimens at 20°C (68°F) (after Sousa et al. 1991)

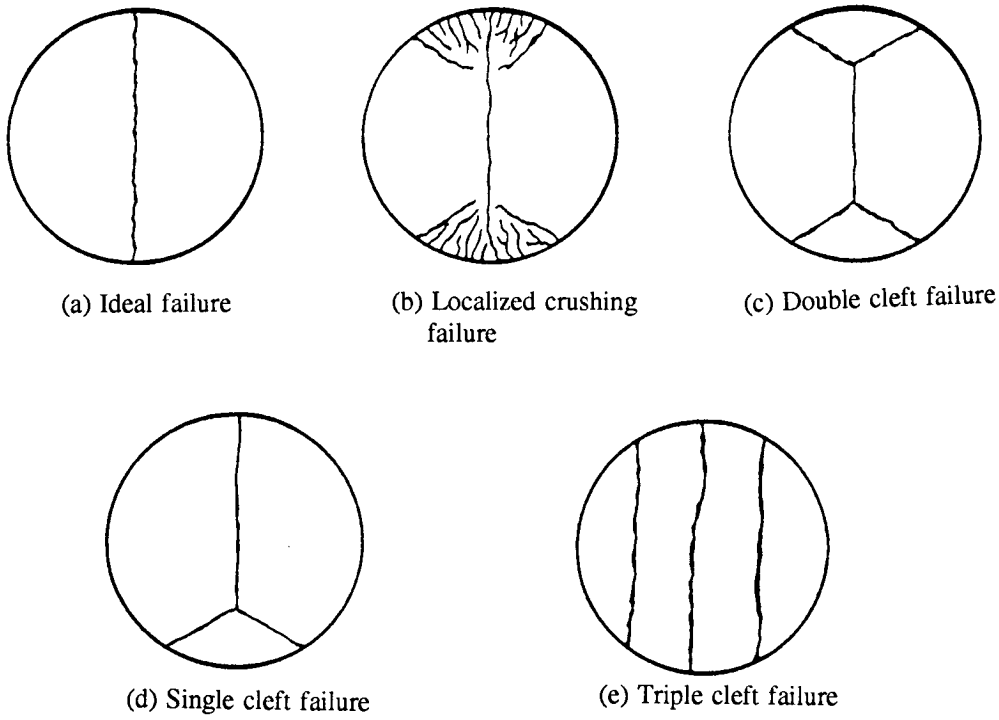

Figure 5.5. Previously observed failures (after Hudson and Kennedy 1968)

- No real cracking occurred. Instead, the specimen deformed plastically until the limiting vertical deformation was reached. The plastic deformation sometimes occurred in both a downward vertical direction and in an outward direction from the flat faces of the diametral specimen. Many specimens exhibited this type of failure at 20°C (68°F). All 11 of the 96 specimens that failed this way at 4°C (39.2°F) were fabricated by either gyratory or kneading compaction and had uncut surfaces. None of the specimens whose surfaces were smooth as a result of coring from rolling-wheel slabs exhibited this type of failure. Also, the specimens were generally evenly distributed among the two asphalt types, two aggregate types, two asphalt contents, and two air-void levels. This type of failure may be a phenomenon related to the presence of large uncut aggregates directly beneath the loading platens.

In many cases, as demonstrated earlier, some plastic deformation typically accompanied centerline cracking. In nearly all specimens that burst in half a V-shaped section of material was missing from the broken halves, approximately 1.2 cm (3.0 in.) wide across the top and 2.0 cm (5.1 in.) deep.

5.3.2.3 Testing Limitations

The diametral test is considered appropriate for obtaining a fundamental measure of the fatigue resistance of asphalt-aggregate mixes only under the following conditions:

- The type of failure observed under laboratory loading conforms with theoretical expectations.
- The laboratory mode of loading is similar to that expected in situ.
- Fatigue resistance is unaffected by stress reversal and the accumulation of permanent deformation.
- Mix and testing effects on fatigue resistance are reasonable and conform with a priori expectations.
- The measurement from which primary response (resilient tensile strain) is calculated is unaffected by spurious influences (such as plastic flow in the immediate vicinity of the load platens).
- The stress or strain behavior of a mix is proportionate to the stress-strain distribution at significant locations within the specimen for the test load that is imposed and the analysis that is performed.

These conditions impose the following specific restrictions on diametral fatigue testing:

- Results of diametral fatigue testing should be discarded if there is evidence either of crushing beneath the loading platens or of cracks initiating at the platens.
- Testing should be limited to applications where the in situ mode of loading approximates the controlled-stress condition; that is, thick and stiff bound layers or relatively weak underlying foundations or both.
- Testing should be limited to temperatures not much greater than 20°C (68°F) so that the resilient response will be reasonably linear and elastic and because of possible effects of stress concentrations near the loading platens on measurements of resilient vertical deformations, which are necessary for determining Poisson's ratio and, hence, the resilient tensile strains.
- Fatigue testing by indirect tension should be limited to specimens with cut surfaces to reduce the incidence of crack initiation outside the tensile failure zone.

Concern remains, however, about possible confounding effects related to stress reversal and the accumulation of permanent deformation. Early research by Raithby and Sterling (1972) documented significant stress-reversal effects on fatigue resistance, and data reported herein document that fatigue cracking under repetitive diametral loading cannot be isolated from permanent deformations accumulating in the specimen. Moreover, the fact remains that although a biaxial stress state exists at the center of the diametral specimen, it is impossible to vary the ratio of the vertical and horizontal components and, hence, to replicate the stress state at critical locations within in situ pavements. The fact that σ_t - σ_c cannot be varied

also eliminates the use of the diametral test in validating the hypothesis that deviatoric stress is the basic cause of fatigue distress in asphalt-aggregate mixes.

5.3.2.4 Summary

The diametral test can possibly be used for controlled-stress fatigue investigations at temperatures of approximately 20°C (68°F) or below, providing that specimen surfaces are cut, permanent deformations are small, and crack progression and crack patterns are indicative of fatigue failure. However, despite the diametral test's obvious appeal, it is not suitable for routine mix design and analysis because of 1) the high incidence of unacceptable fracture patterns, 2) stress concentrations at the loading platens, and 3) its limitation to controlled-stress loading conditions. Moreover, serious questions remain about the influences of the variable biaxial stress state, the inability to reverse stress fields, and the confounding influence of permanent deformation on the resistance to repetitive tensile loading.

5.4 Test Conditions

Both controlled-stress and controlled-strain testing have been included in A-003A's fatigue testing program to date. However, recommendations regarding mode of loading are being delayed pending additional testing and detailed analysis. The need to perform tests rapidly was instrumental in selecting a sinusoidal waveform, and modern hydraulic and control systems permitted its accurate and reliable use. The test frequency of 10 Hz is sufficiently large enough to permit rapid testing while still representing the load pulses generated by rapidly moving traffic. The test temperature is likely to depend on local environmental conditions. Temperature control systems capable of maintaining the test temperature within the range of 0° to 20°C (32° to 68°F) should prove sufficient.

5.5 Summary

This evaluation has highlighted many of the advantages and disadvantages of the candidate accelerated performance tests for fatigue. Despite the obvious appeal stemming from diametral testing versus capability to test specimen briquettes, it is not suitable for routine mix analysis and design because of 1) the high incidence of unacceptable fracture patterns, 2) stress concentrations at the loading platens, and 3) its limitation in controlled-stress loading conditions. Moreover, serious questions remain about the influences of the variable biaxial stress state, the inability to reverse stress fields, and the confounding influence of permanent deformations on the resistance to repetitive tensile loading.

The testing program demonstrated that, although the diametral test proved reasonably reliable, it was generally inferior to flexural fatigue in the sensitivity of its measurements to mix composition. Measured stiffnesses are comparatively large—perhaps excessively so—and cycles to failure are unreasonably small. With the exception of the effect of aggregate type

on stiffness, other mix and loading effects in the diametral testing were found to be reasonable.

The testing program revealed no striking differences between beam and cantilever testing. However, beam measurements were convincingly more sensitive to mix variables than cantilever measurements were. With the exception of beam testing's failure to logically demonstrate the effect of asphalt content on cycles to failure and questionable stiffness-temperature effects from the cantilever testing, the results of both tests were judged to be reasonable.

Although beam tests are advantageous because of their uniform stress distribution and because gluing is unnecessary, the beam and cantilever tests are considered equivalent means for assessing the fatigue behavior of asphalt-aggregate mixes. Nevertheless, the authors prefer the beam test because of their familiarity with it and because of the sophistication of its current design and of its software interface.

6

Energy Approach for Characterizing the Fatigue Behavior of Mixes

6.1 Introduction

Early literature, as indicated in Chapter 1, advanced the notion that a possibly unique relationship might exist between the number of cycles to failure and the cumulative dissipated energy to failure. If so, laboratory testing could be abbreviated, surrogates to testing would appear more promising, and compound loading could be handled more directly. Because of these advantages, possible relationships between cycles to failure and cumulative dissipated energy have been investigated and discussed in the following sections.

6.2 Dissipated Energy Versus Fatigue Life

Chomton and Valayer (1972) indicated that cumulative dissipated energy is the sole independent factor that predicts fatigue life, and this energy seems to be independent of the mix formulation. Van Dijk et al. (1972) also reported a similar relationship between cumulative dissipated energy and fatigue life, which was established from fatigue tests on different mixes tested at different temperatures and frequencies. Later work (van Dijk et al. 1975, 1977) suggests that the cumulative dissipated energy versus the number of cycles relationship is not independent of the mix formulation but is independent of test methods (two- and three-point bending), temperature (10° to 40°C [50°F to 104°F]), modes of loading (controlled-stress and controlled-strain), and frequency (10 to 50 Hz). Van Dijk (1975, 1977) and his colleagues have reported that the slope of the lines representing different mixes are nearly the same and similar to the 0.67 slope suggested by Chomton and Valayer (1972).

The cumulative dissipated energy versus the number of cycles to failure is usually characterized by relationship

$$W_N = A\,(N_f)^z \tag{6.1}$$

where:

N_f	=	fatigue life,
W_N	=	cumulative dissipated energy to failure, and
A, z	=	experimentally determined coefficients.

Figure 6.1 shows the cumulative dissipated energy versus the number of cycles to failure for the flexural fatigue beam controlled-stress tests at 0° and 20°C (32° and 68°F) for 16 different mixes containing the AAK-1 and AAG-1 asphalts and for RL and RB aggregates. The figure shows that all lines are not parallel and have different slopes. It should be noted that each line represents data from four tests: two specimens tested at high stress levels and two at low stress levels. The slopes and intercepts for these lines are presented in Table 6.1, which also shows the controlled-strain data for flexural beam fatigue tests and the controlled-stress data for the trapezoidal cantilever test. It may be noted that for the same mixes, the slope and intercepts for the controlled-stress and the controlled-strain tests appear to be different.

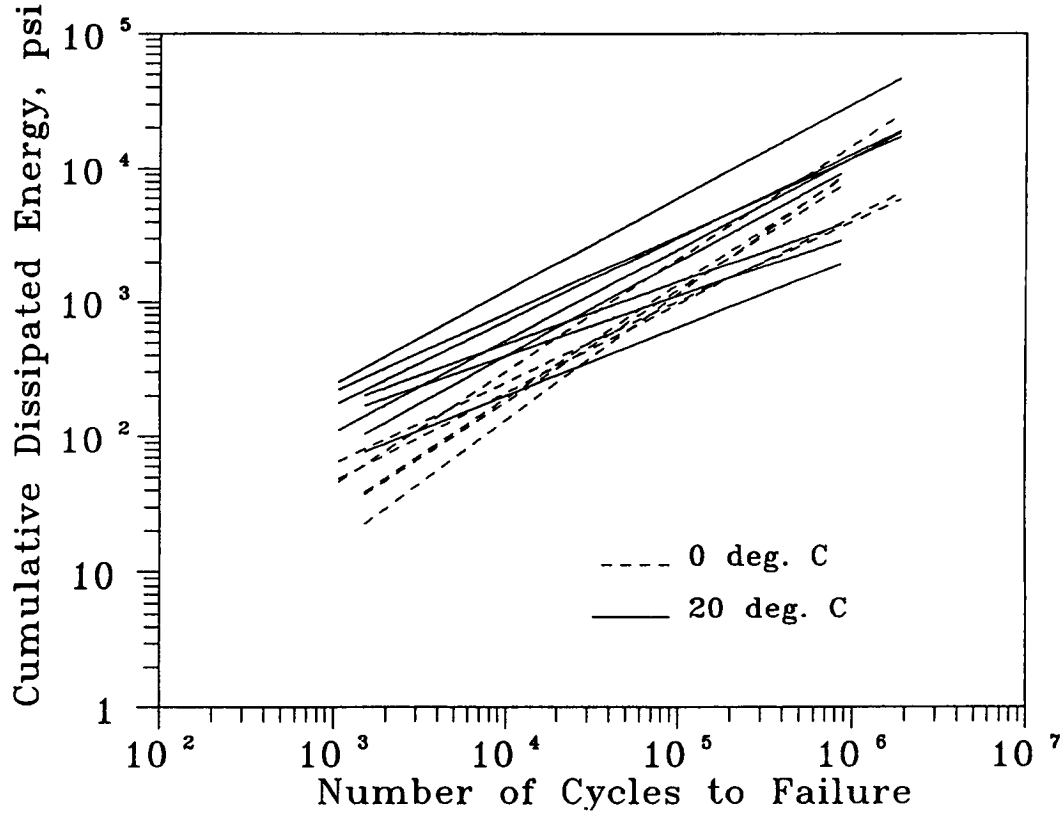

Figure 6.1. Cumulative dissipated energy versus number of cycles to failure, controlled-stress flexural beam fatigue tests, 0° and 20°C (32° and 68°F)

Table 6.1. Coefficients A and z for controlled-stress and controlled-strain tests

Mix Type					Flexural Beam Controlled-Stress Test			Flexural Beam Controlled-Strain Test			Flexural Trapezoidal Controlled-Stress Test	
AT	AC	AG	VO	TP	A	z	R^2	A	z	R^2	A	z
AAG	0	RL	1	1	1.88	0.507	0.99	4.15	0.414	0.76	2.3	0.739
AAG	1	RL	0	1	0.55	0.712	0.90	33.12	0.329	0.80	59.74	0.468
AAG	0	RB	0	1	6.85	0.461	0.68	1.07	0.666	0.98	9.57	0.654
AAG	1	RB	1	1	6.41	0.448	0.95	4.83	0.463	0.99	4.03	0.694
AAK	0	RL	0	1	2.29	0.624	0.97	0.33	0.752	0.91	8.04	0.736
AAK	1	RL	1	1	3.87	0.581	0.90	5.16	0.353	0.62	16.05	0.634
AAK	0	RB	1	1	0.96	0.682	0.98	20.33	0.360	0.67	5.61	0.731
AAK	1	RB	0	1	0.51	0.697	0.96	1.29	0.776	0.50	18.98	0.653
AAG	0	RL	0	0	0.09	0.832	0.99	0.19	0.677	0.79	1.30	0.804
AAG	1	RL	1	0	0.02	0.936	0.99	-	-	-	3.59	0.714
AAG	0	RB	1	0	0.08	0.845	0.98	2.88	0.479	0.80	0.65	0.841
AAG	1	RB	0	0	15.72	0.414	0.30	-	-	-	0.53	0.892
AAK	0	RL	1	0	0.50	0.657	0.95	0.45	0.720	0.98	0.94	0.816
AAK	1	RL	0	0	0.99	0.601	0.89	0.91	0.586	0.90	10.54	0.628
AAK	0	RB	0	0	0.48	0.718	0.99	1.69	0.655	0.95	2.81	0.800
AAK	1	RB	1	0	0.13	0.842	0.97	0.57	0.708	0.99	14.37	0.629

Note: AT = asphalt type; AC = asphalt content; AG = aggregate type; VO = air voids; TP = temperature.

Table 6.2 shows the average values of the slope based on the test temperature and the temperature susceptibility of asphalt (averages obtained from Table 6.1). Figure 6.2 shows the plot of controlled-stress data from Table 6.2. It appears that the slope for mixes containing asphalt AAG-1 is steeper than for those mixes containing asphalt AAK-1. Moreover, at 0°C (32°F) mixes containing asphalt AAG-1 exhibit a higher average slope than those mixes containing asphalt AAK-1. At 20°C (68°F) mixes containing asphalt AAK-1 show a higher average slope than mixes containing asphalt AAG-1. These results suggest that there is a strong asphalt type-temperature interaction, which is not surprising considering that asphalt AAG-1 is more temperature susceptible: its penetration index (PI) is approximately -1.5 versus asphalt AAK-1's PI of approximately -0.3.

Table 6.2. Average slope of W_N versus N_f relationships

Test Type	Temperature (°C)	Temperature Susceptibility	
		Low (AAK-1, PI=-0.3)[a]	High (AAG-1, PI=-1.5)[a]
Flexure - Beam			
Controlled-Stress	0	0.70	0.76
	20	0.65	0.53
Controlled-Strain	0	0.67	0.58
	20	0.55	0.47
Flexure - Trapezoidal			
Controlled-Stress	0	0.72	0.80
	20	0.69	0.64

[a]Average penetration index (PI) obtained at the University of California, Berkeley.

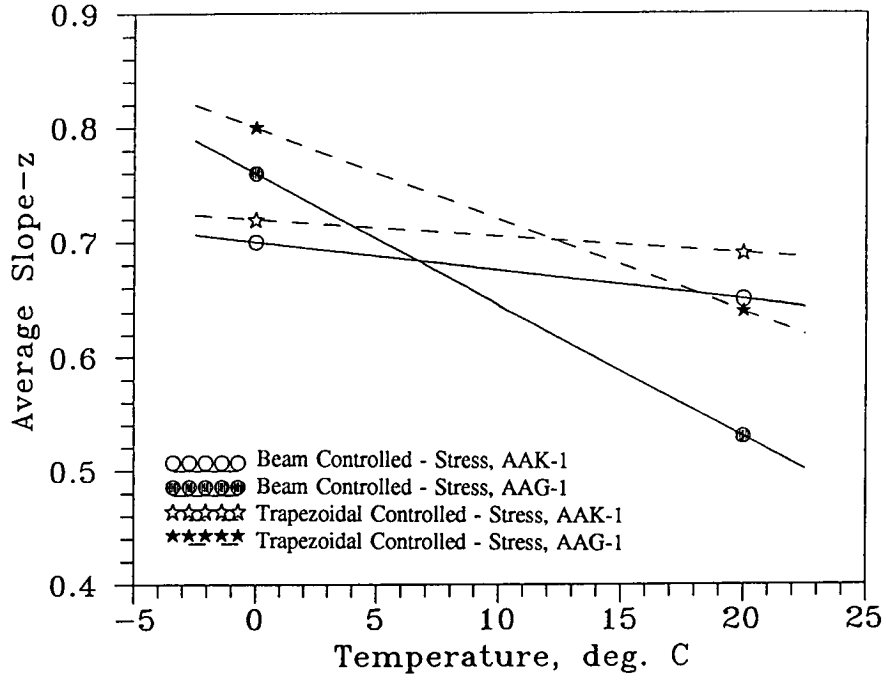

Figure 6.2. Average slope-z versus temperature for controlled-stress tests

Results of statistical analyses presented earlier in Chapter 4 support the observation that the slope is dependent on temperature. Both fatigue life and cumulative dissipated energy are sensitive to mix variables—asphalt type, aggregate type, and air-void content—and test variables—temperature and stress or strain level. In many cases there is significant interaction between temperature and asphalt type, aggregate type, air-void content, and asphalt content. It therefore follows that the cumulative dissipated energy versus fatigue life relationship is mix and temperature dependent, which confirms the findings of van Dijk (1975) and van Dijk and Vissert (1977). However, the results of this study show that the energy relationship also is dependent on temperature.

6.3 Prediction of Fatigue Life Using the Energy Approach

In general, for any mode of loading—controlled stress, controlled strain, or controlled energy—the cumulative dissipated energy to a given number of load repetitions can be computed using Equation 4.2. For controlled-stress tests, energy dissipated per cycle, w_i, increases with an increasing number of load cycles; whereas, for controlled-strain tests, it decreases with an increasing number of load cycles as shown in Figure 4.3. For controlled-energy tests, the dissipated energy per cycle ($w_i=w_o$) remains constant (constant loop size for the stress-strain hysteresis). In this case Equation 4.2 can be rewritten

$$W_N = N_f w_o$$

or

$$W_N = \pi N_f \sigma_o \epsilon_o \sin\phi_o \tag{6.2}$$

Since the stiffness is defined as the ratio of the stress to strain, an alternate form of Equation 6.2 is

$$W_N = \pi N_f \epsilon_o^2 S_o \sin\phi_o \tag{6.3}$$

Equating Equations 6.1 and 6.3, the following relationship is obtained under the assumption of constant dissipation of energy per cycle:

$$N_f = \{A/(\pi \epsilon_o^2 S_o \sin\phi_o)\}^{1/(1-z)} \tag{6.4}$$

where:

N_f	=	fatigue life,
w_o	=	initial dissipated energy per cycle,
ϵ_o	=	initial strain amplitude,
S_o	=	initial stiffness,
ϕ_o	=	initial phase shift between stress and strain, and
A, z	=	coefficients determined from Equation 6.1.

The product ($S_o \sin\phi_o$) represents the loss-stiffness (viscous component of the dynamic stiffness) of the material, and the fatigue life of a given mix depends primarily on the magnitude of the strain (or stress) used and the loss-stiffness of the mix—in effect, the initial energy dissipated during each cycle. For modes of loading other than controlled energy, a

mode-of-loading-dependent energy ratio factor (van Dijk 1975) is useful. The energy ratio factor, ψ, is defined as follows:

$$\psi = (N_f w_o)/W_N \tag{6.5}$$

Adding the energy ratio factor to Equation 6.4 yields

$$N_f = \{A\psi/(\pi \epsilon_o^2 S_o \sin\phi_o)\}^{1/(1-z)} \tag{6.6}$$

Equation 6.6 can be written as a general fatigue relationship with the following form:

$$N_f = a (\psi)^b (w_o)^c$$

or

$$N_f = d (\psi)^e (\epsilon_o)^f (S_o)^g (\sin\phi_o)^h \tag{6.7}$$

Use of a fatigue relationship in the form of Equation 6.7 as a surrogate for fatigue testing has been explored in detail in Parts II and III of this report.

6.4 Summary

In this section an effort was made to investigate possible relationships between cycles to failure and cumulative dissipated energy. These efforts confirmed that when strain is the only test variable, cycles to failure for a given mix are related to cumulative dissipated energy as presented in Equation 6.1:

$$W_N = A (N_f)^z$$

Unfortunately, the uniqueness of this relationship for different types of mixes and conditions of testing could not be substantiated. In fact, detailed investigation revealed that these relationships are different for different mixes and are affected by both test temperature and mode of loading.

Despite this disappointment, dissipated energy remains a useful concept in fatigue investigation, as will be discussed in Parts II and III of this report. The initial energy dissipated during each loading cycle—capturing effects not only of the imposed strain level but also of the dynamic mix properties—will be shown to be a good predictor of cycles to failure and is, thus, a key component of surrogate models. Furthermore, dissipated energy is highly correlated with stiffness decrements during fatigue testing and helps explain the effects of mode of loading on mix behavior.

7

Findings and Recommendations

The primary purpose of this investigation was to identify a suitable laboratory test procedure for characterizing the fatigue response of asphalt-aggregate mixes. This section not only summarizes the principal findings and recommendations regarding such a procedure but also reflects on the working hypotheses that have supported the work and highlights other considerations of fundamental importance to the mix analysis and design process.

7.1 Hypotheses

The investigations reported herein were influenced by a series of working hypotheses about the fatigue behavior of asphalt-aggregate mixes. Further insights regarding these hypotheses, developed as the investigation progressed, are summarized below.

Hypothesis 1. *Fatigue cracking is caused by the repetitive application of traffic loads. For typical heavy-duty pavements, fatigue results from tensile stresses or strains at the underside of the asphalt-aggregate layer(s). The maximum principal tensile strain is considered the primary determinant of fatigue cracking.*

Although it has not been subjected to rigorous evaluation, the maximum principal tensile strain is a convenient indication of expected fatigue damage, both for laboratory testing and pavement analysis. However, the energy dissipated during each loading cycle is also an excellent indicator of fatigue response. Furthermore, dissipated energy has greater conceptual appeal than a simple strain indicator because it captures both elastic and viscous effects.

Hypothesis 2. *For the purposes of fatigue analysis, the critical stress or strain state in the pavement structure can be estimated with acceptable accuracy by the theory of linear elasticity, in which the mechanical behavior of the asphalt-aggregate mix is characterized by its modulus of elasticity and Poisson's ratio.*

Because fatigue distress accumulates most rapidly under moderate to cool temperatures and rapid traffic loading, the theory of linear elasticity provides a reasonable indication of the response of pavement—particularly its asphalt-bound component—to traffic loads. Although the increased accuracy that can be achieved by a linear viscoelastic approach may be unnecessary, it appears that linear viscoelastic modeling may produce useful estimates of the energy dissipated during each loading cycle and, thus, might be the preferred approach to structural analysis.

Hypothesis 3. *Testing to destruction under cyclic loading is necessary in order to accurately measure the fatigue response of asphalt-aggregate mixes.*

The primary alternatives to destructive fatigue testing include tensile or flexural strength and stiffness measurements. Fatigue behavior is correlated with these properties, and regression models—calibrated using fatigue test results for a broad range of mixes—are useful for both mix and structural design. Fatigue testing is necessary, however, when high accuracy is required, when the candidate mix is only marginally suitable, and when the behavior of unconventional mixes and materials is being assessed.

Hypothesis 4. *In laboratory fatigue testing, pulsed loading is preferred to sinusoidal loading because the rest period permits stress relaxation similar to that permitted under in-service traffic loading.*

Although both pulsed and sinusoidal loading were used in the study, the experiments were designed neither to investigate possible effects of the different wave forms nor to document possible effects of rest periods. Test results confirmed, however, that mix effects on fatigue response were similar in either pulsed or sinusoidal loading. As a practical matter, accelerated performance testing in fatigue requires a loading frequency more rapid than the 1 to 2 Hz frequency characteristic of pulsed loading.

Hypothesis 5. *Although pavements become fatigued in response to repeated flexure, fatigue is basically a tensile phenomenon, and test specimens can be evaluated equally well under either tensile or flexural loading.*

Both flexural and tensile testing methods were evaluated herein. The tensile methods proved unacceptable in part because failure patterns frequently indicated undesirable end-cap or loading-platen influences. Fatigue response measured by indirect tension (diametral) loading differed significantly from that measured under flexural loading. Specimens failed much sooner in diametral testing because stresses are not reversed and because permanent deformations accumulate. Diametral testing was ultimately judged unsuitable for routine use. At the same time, once testing difficulties are overcome, direct uniaxial tension testing will likely yield accurate measurements of fatigue response.

Hypothesis 6. *Mode of loading is a critical concern in mix design systems because mix effects are quite different between controlled-stress and controlled-strain loading systems. The mode-of-loading effect is likely due more to differences in the rates of crack propagation than to differences in the times to crack initiation.*

The general pattern that stiffer mixes perform better under controlled-stress loading but worse under controlled-strain loading was confirmed by the testing reported herein. Although the importance of mode of loading to informed mix design systems cannot be overstated, proper interpretation of laboratory test results is expected to permit either controlled-stress or controlled-strain testing in the laboratory environment.

Hypothesis 7. *Fatigue tests accelerated by the application of large stress or strain levels are satisfactory for mix analysis and design. That is, for practical purposes, mixes are ranked essentially the same at large and small stress or strain levels.*

Mixes may be ranked differently at one loading level than at another; that is, the ϵ-N or w_o-N curves for different mixes are not always parallel. Thus, performance at a less destructive loading level cannot always be accurately inferred from testing at a more destructive level. Nevertheless, testing at *two or more* higher levels is sufficient to indicate the behavior at the lower levels to which typical paving mixes are subjected in situ.

Hypothesis 8. *Under simple loading, crack initiation in a given mix is related to strain or stress level as follows:*

$$N_f = a\,(1/\epsilon)^b \quad or \quad N_f = c\,(1/\sigma)^d$$

where: N_f = *number of load applications to crack initiation,*
ϵ, σ = *tensile strain and stress, respectively, and*
a, b, c, d = *experimentally determined coefficients dependent on test temperature.*

These relationships were consistently confirmed for the ranges of stresses and strains to which laboratory specimens were subjected. Replacing the strain or stress with the energy dissipated during an initial loading cycle, w_o, yields an equally reliable and accurate expression as follows:

$$N_f = e\,(1/w_o)^f$$

There has been no evidence of a fatigue limit, that is, a stress or strain below which repeated stressing does not eventually induce fatigue failure.

Hypothesis 9. *Under compound or mixed loading—due, for example, to multiple temperatures and/or stress or strain levels—cracking in a given mix is initiated when the linear summation of cycle ratios equals 1 as shown below:*

$$\Sigma_i\,(n_i/N_i) = 1$$

where: n_i = *number of applications of stress* σ_i *or strain* ϵ_i, *and*
N_i = *number of applications to failure at stress* σ_i *or strain* ϵ_i.

The linear-summation-of-cycle-ratios hypothesis was not examined in the current study and remains a viable technique with which to account for the effects of exposure to multiple

temperatures and/or stress or strain levels. Although cumulative dissipated energy initially seemed to be a promising replacement for the linear-summation-of-cycle-ratios procedure, its sensitivities both to temperature and to load level suggest that it is not a direct replacement for the linear summation of cycle ratios, that is, at the critical location:

$$\Sigma W_i \neq W_D$$

where: W_i = cumulative dissipated energy under temperature or load i, and
W_D = cumulative dissipated energy at failure.

Nevertheless, it seems reasonable that a relationship of the following type might be applicable to compound-loading situations:

$$\Sigma (W_i/W_{Di}) = 1$$

where: W_i = cumulative dissipated energy under temperature or load i, and
W_{Di} = cumulative dissipated energy to failure under temperature or load i.

Hypothesis 10. *The principles of fracture mechanics represent the most feasible mechanistic approach for estimating rates of crack propagation in pavement structures.*

SHRP A-003A investigations of fracture-mechanics principles stressed laboratory testing requirements instead of pavement analyses. Although the required laboratory testing was deemed unsuitable for routine use, fracture mechanics remains an attractive mechanistic approach for examining the rate of crack propagation in pavement structures. Fracture mechanics does not offer the potential to study crack initiation.

7.2 Laboratory Test Methods

This evaluation highlighted many of the advantages and disadvantages of the candidate accelerated performance tests. Two of the candidate tests, uniaxial tension tests and fracture mechanics tests, were quickly eliminated after preliminary testing. Gripping the specimen is difficult in pure tension testing, and end-cap failure due to stress concentrations was a persistent problem in the limited testing that was completed. Testing for fracture mechanics analysis is thought to be too extensive for routine mix analysis and design: repetitive fatigue tests are necessary to evaluate both the crack initiation process and the crack growth rate, and notched-beam strength tests are necessary to evaluate the C^*-line integral.

Among the remaining three candidate procedures, the diametral (indirect tension) test is obviously appealing because of its ability to evaluate briquette-shaped specimens. The testing program demonstrated that, although it was reasonably reliable, diametral fatigue was generally inferior to flexural fatigue in the sensitivity of its measurements to mix composition. Measured stiffnesses were comparatively large—perhaps excessively so—and cycles to failure were unreasonably small. With the exception of the effect of aggregate type

on stiffness, other mix and loading effects in the diametral testing were found to be reasonable.

In the final analysis, diametral testing is not suitable for routine mix analysis and design because of 1) the high incidence of unacceptable fracture patterns, 2) stress concentrations at the loading platens, and 3) its limitation to controlled-stress loading conditions. Moreover, its variable biaxial stress state, its inability to reverse stress fields, and the confounding influence of permanent deformations within test specimens on their resistance to repetitive tensile loading raise serious additional concerns.

The testing program revealed no striking differences between beam and cantilever testing. However, beam measurements were convincingly more sensitive to mix variables than cantilever measurements were. With the exception of beam testing's failure to logically demonstrate the effect of asphalt content on cycles to failure and cantilever testing's questionable stiffness-temperature effects, the results of both tests were judged to be reasonable.

Although beam tests are advantageous because of their uniform stress distribution and because gluing is unnecessary, the beam and cantilever tests are considered equivalent means for assessing the fatigue behavior of asphalt-aggregate mixes. Nevertheless, the authors prefer the beam test because they are familiar with it and because of the sophistication of the test's current design and its software interface.

7.3 Dissipated Energy

Early literature had advanced the notion that a possibly unique relationship might exist between the number of cycles to failure and the cumulative energy dissipated to failure. If so, laboratory testing could be abbreviated, surrogates to testing would appear more promising, and compound loading could be handled more directly. Because of these advantages, considerable effort was made to investigate possible relationships between cycles to failure and cumulative dissipated energy. These efforts confirmed that when strain is the only test variable, cycles to failure for a given mix are related to cumulative dissipated energy as follows:

$$W_N = A\,(N_f)^z$$

where:

	N_f	=	number of cycles to failure,
	W_N	=	cumulative dissipated energy to failure, and
	A, z	=	experimentally determined coefficients.

Unfortunately, the uniqueness of this relationship for different types and conditions of testing could not be substantiated. In fact, detailed investigation revealed that these relationships are different for different mixes and are affected by both test temperature and mode of loading.

Despite this disappointment, dissipated energy remains a useful concept in fatigue investigations. The initial energy dissipated during each loading cycle—capturing the effects not only of the imposed strain level but also of the dynamic mix properties—is a good predictor of cycles to failure and is thus a key component of surrogate models. Furthermore, dissipated energy is highly correlated with stiffness decrements during fatigue testing and helps to explain the effects of mode of loading on mix behavior.

Part II Extended Test Program

Akhtarhusein A. Tayebali
John A. Deacon
John S. Coplantz
Fred N. Finn
Carl L. Monismith

8

Introduction

8.1 Background

The primary objective of SHRP Project A-003A, entitled "Performance Related Testing and Measuring of Asphalt-Aggregate Interactions and Mixes," was the development of a series of accelerated performance tests for asphalt-aggregate mixes together with methods for analyzing asphalt-aggregate interactions which significantly affect pavement performance. Other important objectives of the A-003A project were to validate the accelerated performance tests and use the results of the validation to confirm the hypotheses being developed by the A-002A contractor and other SHRP investigators regarding asphalt binder properties, mix properties, and pavement performance.

Part I of this report identifies suitable laboratory test procedure(s) for characterizing the fatigue response of asphalt-aggregate mixes. For fatigue distress, the test methods which have been selected include the flexural beam and trapezoidal cantilever tests.

Part II details the laboratory studies conducted as part of SHRP Project A-003A in support of

- validation of a laboratory accelerated performance test for fatigue;
- validation of the A-002A hypotheses for fatigue;
- development of analytically based, surrogate fatigue modeling activities; and
- development of temperature equivalency factors for use in a mix design and analysis system.

Also included in this report is a brief description of improvements made to the fatigue test procedure and equipment.

8.2 Objective

The objective of this report is to document the results of all phases of fatigue testing and analysis of these test results under SHRP Project A-003A's extended test program activities, including both the laboratory fatigue tests as well as the laboratory and full-scale, field wheel track tests.

9

Flexural Beam Fatigue Test Equipment

Several alternative procedures for fatigue testing of asphalt-aggregate mixes were evaluated during the pilot test program (subsequently referred to as the 2×2 study, since it involved two asphalts and two aggregates) as outlined in Part I of this report. The flexural beam (third-point loading) fatigue test method in a controlled-strain mode of loading was selected for further evaluation by SHRP Project A-003A on the basis of 1) a review of the information in the technical literature, 2) recommendations that were based on the results of the pilot test program conducted for test method selection, and 3) the A-003A staff's experience with this test method. Furthermore, the controlled-strain mode of testing was selected because it was more compatible with the crack propagation concept and the pavement fatigue cracking prediction models that were being developed by SHRP Project A-005.

9.1 Improvements to Test Procedure and Equipment

Two major improvements were made to the flexural beam fatigue test procedure and equipment, the size of test specimen was increased, and a new fatigue beam module was designed and built that could be used as stand-alone test equipment or could be used as a module in the Universal Testing Machine (UTM) developed by SHRP Project A-003A for the permanent deformation test program. Specific goals for improving the equipment were to increase the ease, the simplicity, and the reliability of the fatigue test.

9.1.1 Specimen Size

The size of the test beam was increased from a 3.8 × 3.8 cm (1.5 × 1.5 in.) cross-section used in pilot test program to a rectangular cross-section with a 6.35 cm (2.5 in.) width and 5.0 cm (2.0 in.) height. The increase to a specimen width of 6.35 cm (2.5 in.) was the maximum achievable given the space restrictions of the fatigue module in the UTM. Similarly, the beam length was also restricted to 38.1 cm (15 in.); however, the beam span

(length between the reaction points) was increased from the original 30.5 to 35.6 cm (12 to 14 in.) in order to minimize shear deformation in the beam.[4] The selection of a maximum beam height of 5.0 cm (2.0 in.) resulted in approximately a 5 percent shear deformation (Tayebali 1991).

9.1.2 Test Equipment

Specific changes in the test equipment included the following:

- Design of the new test equipment to simplify and reduce the set-up time. This change was achieved by automating the specimen clamping procedure through the use of torque motors, which reduced the set-up time for each test from the approximately 30 to 45 minutes of the pilot test program to less than 5 minutes.

- Improvements in the linear and torsional bearings to minimize any extraneous stress, such as torsion, in the beam specimen and to maintain zero moment at the beam ends.

- Design of the various components to conform to the larger beam specimen and accommodation of the module within the UTM.

- Automation of temperature and test control, data acquisition, and data reduction.

The new fatigue test equipment, with its hydraulic pressure system, has a better response to and more precise control of the stress or strain induced in the specimen than its predecessor, which used an electropneumatic test system. Sinusoidal loads applied at up to 25 Hz frequency, with or without rest periods, can easily be achieved at temperatures ranging between -10° and 40°C (14° and 104°F). Once the specimen is mounted in the loading frame, the test itself, including temperature control, test control, data acquisition, and data reduction, is completely run by the computer. The equipment developed by UCB for SHRP A-003A uses the automated testing system software (Bronstein and Sousa 1987) for test control and data acquisition. A data analysis software package FATIGUE (Tsai and Tayebali 1992) was developed to facilitate fatigue data reduction for the A-003A project.

The improvements in the test equipment and procedure significantly improved the repeatability of the test in relation to the results from the pilot test program and reduced the overall testing time by a factor of approximately 6. Significant improvements in fatigue data repeatability using the new test equipment and procedure are indicated by a coefficient of variation of 40.2 percent for fatigue life versus approximately 90 percent for the pilot test program using the old equipment reported in Part I of this report. This reduction is most

---

[4]The ratio of shear to bending deformation in a beam specimen is proportional to the square of the height (h) to beam span (L) ratio. For shear deformations to be neglected, $(h/L)^2 << 1$.

likely due to improvements in control of the induced strain as well as to the use of larger beam specimens compacted by rolling-wheel compaction. The use of rolling-wheel compaction virtually eliminated fracturing of the aggregate, which was observed in the specimens compacted with kneading compaction in the pilot test program.

Figures 9.1 to 9.4 show the schematics of the flexural beam fatigue module and test apparatus. The specifications for the fatigue testing equipment are available from SHRP.

9.2 Fatigue Test Procedure

The fatigue test procedure developed in this investigation was divided into three tasks: specimen preparation, specimen testing, and analysis of results.

9.2.1 Specimen Preparation

Specimen preparation consists of proportioning the aggregate and asphalt binder, mixing, curing, compacting, and sawing. All beam specimens prepared for the extended test program study were sawed to the required dimensions from slabs prepared by means of rolling-wheel compaction. All the mixes were short-term aged in a forced draft oven at 135°C (275°F) for 4 hours. No water conditioning was included in this testing program. Sawed beam specimens were subjected to air-void content measurements before being accepted for testing. The acceptance criterion for air-void contents was the target air-void content percentage plus or minus 1 percent. Beam specimens, 6.35 cm (2.5 in.) wide, 5.1 cm (2.0 in.) high, and 38.1 cm (15 in.) long, were used in this test program. Specimen preparation details can be obtained from "Asphalt Concrete Specimen Preparation Protocol for SHRP Project A-003A" (Harvey 1990).

9.2.2 Specimen Testing

Beam specimens ready for testing were stored at the required temperature for at least 2 hours. All specimens in this test program were tested at 20°C (68°F), except for the temperature equivalency study, in which specimens were tested at four temperatures: 5°, 10°, 20°, and 25°C (41°, 50°, 68°, and 77°F). Specimens were tested at the required strain (deformation) level under the controlled-deformation mode of loading. All tests were conducted at 10 Hz frequency, corresponding to a total loading time under sinusoidal load of 0.1 seconds, with no rest periods. The loading applied imparted tension only at the extreme fiber. Initial peak-to-peak load amplitude was noted and the test terminated when the observed load amplitude was less than half the initial value. Sinusoidally varying load and deformation magnitudes and patterns were recorded and automatically saved on the computer hard drive at predefined cycles spaced at logarithmic intervals.

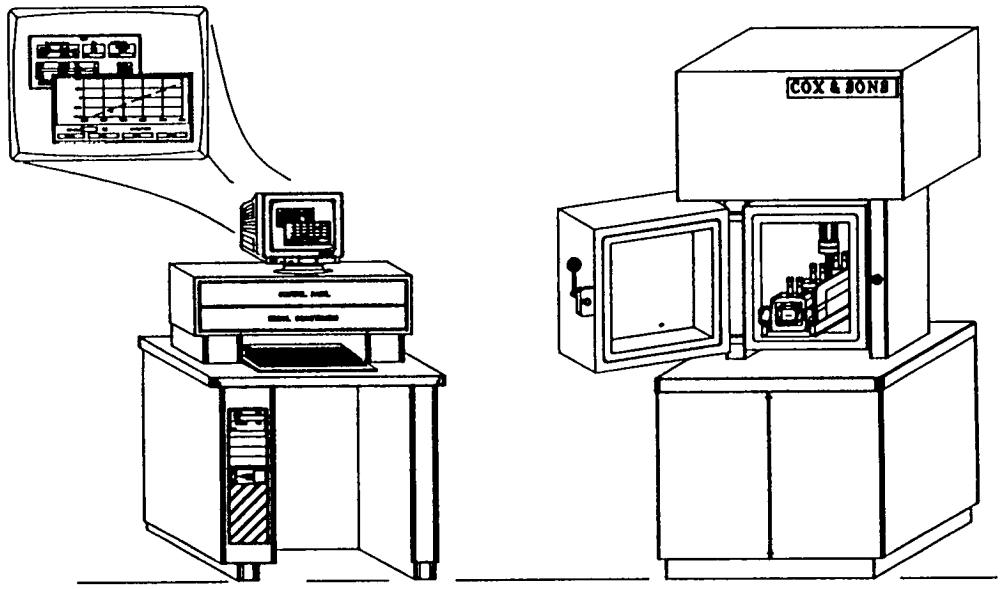

Figure 9.1. Schematic of flexural beam fatigue test apparatus

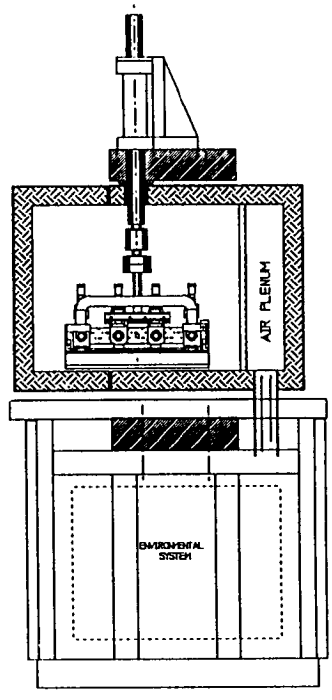

Figure 9.2. Schematic of flexural beam fatigue test apparatus, side view

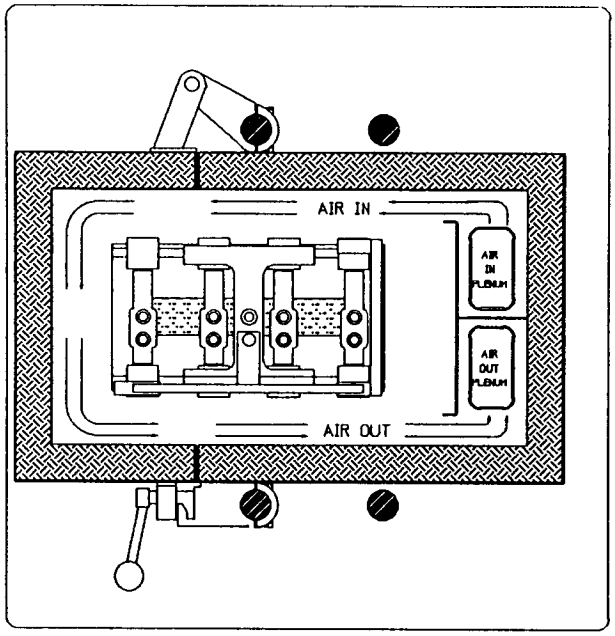

Figure 9.3. Schematic of flexural beam fatigue test apparatus, top view

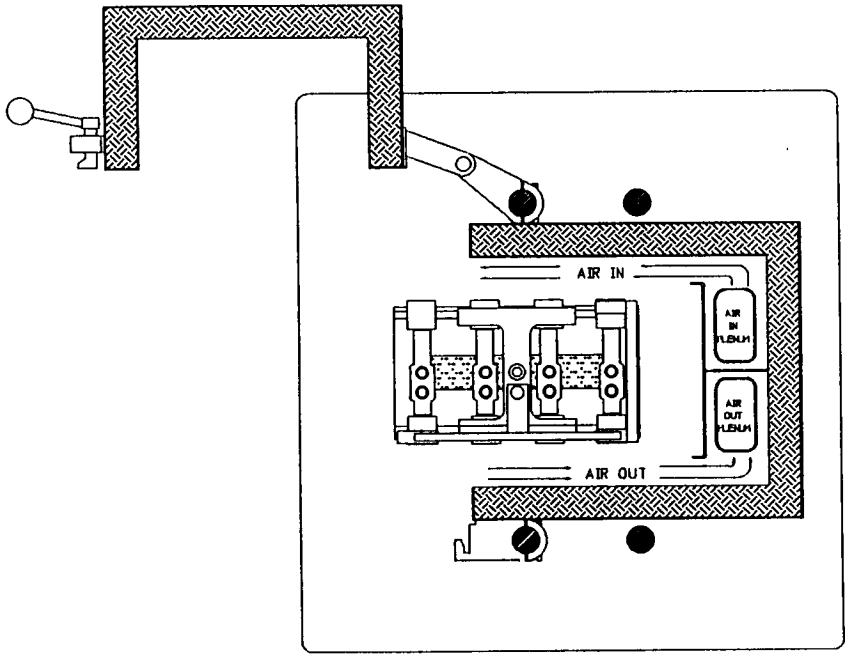

Figure 9.4. Schematic of flexural beam fatigue test apparatus, top view with door open

9.2.3 Analysis of Results

Test data were analyzed using by the FATIGUE computer program (Tsai and Tayebali 1992) to compute the stress, strain, stiffness, phase angle, and dissipated energy per cycle as functions of the number of load cycles, and the cumulative dissipated energy to a given load cycle. Fatigue life was defined as the number of cycles corresponding to a 50 percent reduction in initial stiffness; initial stiffness was measured at the 50th load cycle. Maximum stress, strain, and stiffness were computed by using the following relationships:

$$\text{Stress } (\sigma) = 3aP/(wh^2) \tag{9.1}$$

$$\text{Strain } (\epsilon) = 12h\delta/(3L^2-4a^2) \tag{9.2}$$

$$\text{Stiffness (S)} = \sigma/\epsilon \tag{9.3}$$

where:

	σ	=	peak-to-peak stress, psi,
	ϵ	=	peak-to-peak strain, in./in.,
	P	=	applied peak-to-peak load, lbf,
	S	=	stiffness, psi,
	L	=	beam span, in.,
	w	=	width of beam, in.,
	h	=	height of beam, in.,
	δ	=	beam deflection at neutral axis, in., and
	a	=	L/3.

The energy dissipated per cycle was computed as the area within the stress-strain hysteresis loop. The phase shift (angle) was estimated by using the following relationship:

$$w_i = 0.25\pi\epsilon_i^2 S_i \sin\phi_i \tag{9.4}$$

where:

	w_i	=	energy dissipated at load cycle i,
	ϵ_i	=	peak-to-peak strain at load cycle i,
	S_i	=	stiffness at load cycle i, and
	ϕ_i	=	phase angle between stress and strain at load cycle i.

Typical examples of raw and analyzed fatigue test results are presented in Tables 9.1 and 9.2, respectively.

9.3 A 24-Hour Procedure for Characterizing the Fatigue Response of an Asphalt-Aggregate Mix

A short fatigue test procedure for characterizing the fatigue behavior of mixes was developed that allows completion of all fatigue tests within 24 hours. This procedure involves testing four specimens, each at a different strain level, in the controlled-strain mode of loading at 10 Hz frequency.

Table 9.1. Typical fatigue test results, raw data file (only one cycle shown)

Digital_Control_Systems
Automatic_Testing_System_v.3.01

DYNAMIC_MODULUS_RESULT
SPECIMEN
BEAM_SPECIMEN

in
LOAD = 2
PRESS = -1
DISP = 1
HEIGHT = 2.025000
WIDTH = 2.538000
REACTION = 14.000000
LOADING = 4.667000

RAW_ATS_DATA
CHANNELS = 2

channel		1	2				
name		VERLVDT	LOAD				
sensit		4.92E-05	0.3757				
zero		0.00030609	-0.569043				
sec	cycle	in.	lb	sec	cycle	in.	lb
FREQUENCY = 10							
0	0	0.00808	3.19	1.0635	10	0.02121	12.20
1.0015	10	0.00872	-107.27	1.0655	10	0.02033	-11.09
1.0035	10	0.00911	-83.60	1.0675	10	0.01944	-33.63
1.0055	10	0.00970	-58.80	1.0695	10	0.01856	-55.42
1.0075	10	0.01034	-32.88	1.0715	10	0.01757	-76.08
1.0095	10	0.01113	-8.08	1.0735	10	0.01659	-95.62
1.0115	10	0.01196	18.22	1.0755	10	0.01565	-113.66
1.0135	10	0.01285	43.01	1.0775	10	0.01467	-129.43
1.0155	10	0.01383	67.81	1.0795	10	0.01374	-142.96
1.0175	10	0.01482	91.10	1.0815	10	0.01290	-154.98
1.0195	10	0.01575	112.52	1.0835	10	0.01201	-163.62
1.0215	10	0.01679	132.05	1.0855	10	0.01128	-169.63
1.0235	10	0.01777	149.71	1.0875	10	0.01054	-173.39
1.0255	10	0.01870	165.87	1.0895	10	0.01000	-173.77
1.0275	10	0.01969	180.52	1.0915	10	0.00951	-170.76
1.0295	10	0.02057	193.29	1.0935	10	0.00921	-165.13
1.0315	10	0.02146	204.19	1.0955	10	0.00896	-157.61
1.0335	10	0.02225	212.45	1.0975	10	0.00882	-148.22
1.0355	10	0.02298	218.84	1.0995	10	0.00882	-131.31
1.0375	10	0.02362	221.85	-	-	-	-
1.0395	10	0.02412	222.60	-	-	-	-
1.0415	10	0.02461	219.59	5.0015	50	0.00921	-112.90
1.0435	10	0.02485	213.58	-	-	-	-
1.0455	10	0.02500	205.69	-	-	-	-
1.0475	10	0.02515	193.29	-	-	-	-
1.0495	10	0.02505	176.76	-	-	-	-
1.0515	10	0.02480	158.35	-	-	-	-
1.0535	10	0.02451	136.19	-	-	-	-
1.0555	10	0.02402	113.27	3000.0935	30000	0.00882	-12.22
1.0575	10	0.02343	87.34	3000.0955	30000	0.00882	-11.84
1.0595	10	0.02274	62.55	3000.0975	30000	0.00887	-7.33
1.0615	10	0.02200	36.25	3000.0995	30000	0.00901	-2.07

Table 9.2. Typical analyzed fatigue test results

Period Number	Stress psi	Strain in./in.	Dynamic Stiffness psi	Phase Angle	Dissipated Energy psi	Cumulative Energy psi
10	533.2	8.00E-04	668903	34.5	1.89E-01	0.00E+00
25	517.5	8.10E-04	637793	34.7	1.88E-01	2.78E+00
50	475.1	7.70E-04	616286	35.9	1.69E-01	7.25E+00
75	469.5	7.80E-04	603469	36.2	1.70E-01	1.15E+01
100	465.0	7.90E-04	590378	36.5	1.71E-01	1.57E+01
200	450.8	8.00E-04	562192	37.5	1.73E-01	3.29E+01
300	441.7	8.20E-04	539603	38.2	1.76E-01	5.03E+01
500	394.7	7.70E-04	515233	38.7	1.48E-01	8.27E+01
750	383.1	7.70E-04	495429	39.4	1.48E-01	1.20E+02
1000	372.5	7.80E-04	475828	40.0	1.47E-01	1.57E+02
1500	353.8	8.00E-04	442496	41.0	1.46E-01	2.30E+02
2000	339.1	8.10E-04	419162	41.8	1.44E-01	3.02E+02
3000	313.9	8.30E-04	380079	42.7	1.38E-01	4.43E+02
3500	303.2	8.30E-04	366168	43.3	1.35E-01	5.11E+02
4000	273.9	7.60E-04	359804	43.3	1.12E-01	5.73E+02
5000	263.8	7.70E-04	343299	43.9	1.10E-01	6.85E+02
7500	238.5	7.80E-04	304737	45.2	1.04E-01	9.53E+02
10000	212.8	7.90E-04	270163	46.8	9.60E-02	1.20E+03
12500	181.9	7.90E-04	230320	47.9	8.38E-02	1.43E+03
15000	132.4	7.80E-04	170193	50.0	6.19E-02	1.61E+03
17500	86.9	7.70E-04	113470	51.7	4.11E-02	1.74E+03
20000	61.7	7.70E-04	80235	48.1	2.77E-02	1.82E+03
30000	26.3	7.60E-04	34520	34.8	8.97E-03	2.01E+03

Define Failure Criteria—Stiffness Reduction = 0.50
Smix at N50 = 616285.9 psi
Smix at Nf = 308142.9 psi
Nf = 7275.4 cycles
Accumulated Energy Between N50 and Nf = 921.23 psi
(*Mean Strain = 7.88E-0004*)

In this procedure, fatigue tests are performed over a range of strain levels (so that fatigue life varies between approximately 5000 cycles and 500,000 cycles). The specific testing procedure is as follows:

1. Conduct a test at a fairly high strain level so that the life of the specimen is between 5000 and 10,000 cycles. As a starting point, a strain level between 800 and 1000 micro in./in. should be used. If the fatigue life at this strain level is more than 10,000 cycles, then the strain is increased for the second fatigue test; otherwise, the strain level is decreased. Two tests at these strains are expected to take approximately 2 hours.

2. If the first two tests are conducted at different strain levels, then a crude estimate of the slope of the strain-versus-cycles relationship can be determined. By using this relationship, the strain level corresponding to a fatigue life of approximately 100,000 cycles can be determined. This test is expected to take approximately 4 hours.

3. With the result obtained from step 2, the strain-versus-cycles relationship can be better established and the strain level required for a life of approximately 350,000 to 500,000 cycles is estimated. This test is expected to take approximately 13 to 15 hours and should be done at the end of the work day so that the specimen will have reached its fatigue life by the next morning.

The variability associated with prediction of fatigue life at small strain levels from the results of this short test procedure and the effect of testing replicate specimens are explored in detail in Part III of this report. The standard test method for determining the fatigue life of compacted bituminous mixes subjected to repeated flexural bending described in SHRP test method M-009.

10

Expanded Fatigue Test Program

10.1 Objectives

In the pilot testing program the primary objective was to evaluate several methods and select a preferred method for fatigue testing asphalt-aggregate mixes. The expanded testing program was designed to expand the database relative to fatigue properties. Test results included eight Materials Reference Library (MRL) asphalts and two MRL aggregates. Specific objectives of this experiment program were as follows:

- To provide an expanded database for 1) evaluating improvements in the test method, 2) confirming and extending relationships found in the pilot testing phase, and 3) providing information for validation using wheel track test devices.
- To provide information for validation of A-002A hypotheses.
- To explore relationships between mix properties, laboratory fatigue response, and anticipated pavement performance.
- To develop surrogate models of fatigue behavior that, when appropriate, might substitute for laboratory testing.

10.2 Selection of Mix and Testing Variables

The mix and testing variables included in this expanded testing program included the following:

- **Asphalts.** Eight MRL asphalts were used: AAA-1, AAB-1, AAC-1, AAD-1, AAF-1, AAG-1, AAK-1, and AAM-1.

- **Aggregates.** Two MRL aggregates were used: RD, a limestone characterized as having low absorption, and RH, a Greywacke gravel. The limestone was 100 percent crushed material, while the gravel particles were partially crushed. Both products had a history of extensive use in their particular locale.

- **Asphalt Content.** A single asphalt content for each aggregate combination was incorporated in the mixes: 4.3 and 4.9 percent by weight of mix (4.5 and 5.2 percent by weight of aggregate) for RD and RH aggregates, respectively. These asphalt contents were selected according to the Hveem method, with a minimum Hveem stability of 35.

- **Air-Void Content.** Two levels of air-void content, 4 and 7 percent, were selected as targets with a tolerance of ± 1 percent.

- **Strain Levels.** Two strain levels were used: 400 and 700 micro in./in. Although these strains are higher than would normally be expected in heavy-duty pavements, they were selected to reduce the total testing time. Previous research has indicated that a linear relationship is appropriate between the log-number of cycles and the log-tensile strain. Thus, extrapolations to higher orders of cycles can be estimated from this type of relationship. The reliability of these extrapolations is discussed in Part III of this report.

- **Replicates.** Two replicate specimens were used at each strain level to study the repeatability of the test method.

- **Test Frequency.** All the tests were performed in the controlled-strain mode of loading at a frequency of 10 Hz with sinusoidal loading (no rest periods).

- **Test Temperature.** All tests were performed at 20°C (68°F).

- **Conditioning.** All mixes were short-term aged in a forced draft oven at 135°C (275°F) for 4 hours. No water conditioning was included in this program.

Features of this experiment, referred to as the 8×2 experiment since it includes eight different asphalts and two different aggregates, are summarized in Table 10.1. Table 10.2 identifies the asphalt binders and aggregates used. The aggregate gradation is identified in Table 10.3. The experiment design used in this study is a full factorial design consisting of 32 individual mixes. The experiment included testing all combinations for a total of 128 individual controlled-strain beam fatigue tests. The response variables (dependent variables) included were 1) initial flexural stiffness measured at the 50th load cycle, 2) fatigue life—the number of cycles to a 50 percent reduction in initial stiffness, 3) initial dissipated energy per cycle measured at the 50th load cycle, and 4) cumulative or total dissipated energy associated with the fatigue life. Test results are included in Appendix A of this report.

Table 10.1. Features of 8×2 fatigue experiment

Number of Asphalts	8 — MRL core asphalts (AAA-1, AAB-1, AAC-1, AAD-1, AAF-1, AAG-1, AAK-1, and AAM-1)
Number of Aggregates	2 — MRL aggregates (RH and RD)
Asphalt Content	1 — Optimum (Hveem) 5.2% and 4.5% by weight of aggregate for RH and RD aggregates, respectively
Air-Void Levels	2 — 4 ± 1 and 7 ± 1 percent
Strain Levels	2 — 400 and 700 micro in./in.
Replicates at Each Strain Level	2
Temperature	1 — 20°C (68°F)
Frequency	1 — 10 Hz (sinusoidal)
Specimen Size	2 in. (5.1 cm) height, 2.5 in. (6.35 cm) width, 15 in. (38.1 cm) length
Total Number of Mixes Tested	32
Total Number of Specimens Tested	128

Table 10.2. Asphalt binders and aggregates used in 8×2 experiment

Asphalts (MRL Code)	Grade	Penetration Index (PI)
AAA-1	150/200 Pen. Grade	0.7
AAB-1	AC-10	0.0
AAC-1	AC-8	-0.6
AAD-1	AR-4000	1.0
AAF-1	AC-20	-1.0
AAG-1	AR-4000	-1.4
AAK-1	AC-30	-0.5
AAM-1	AC-20	-0.2
Aggregate (MRL Code)	**Characteristics**	
RD	Limestone, low-absorption crushed quarry rock	
RH	Greywacke river gravel, partially crushed	

Table 10.3. Aggregate gradation

Sieve Size	Percentage Passing by Weight	ASTM Spec. (D 3515)
1 in.	100.0	100
3/4 in.	95.0	90-100
1/2 in.	80.0	-
3/8 in.	68.0	56-80
No. 4	48.0	35-65
No. 8	35.0	23-49
No. 16	25.0	-
No. 30	17.0	-
No. 50	12.0	5-19
No. 100	8.0	-
No. 200	5.5	2-8

10.3 Test Results

The method of statistical analysis for the 8×2 data set was identical to the procedure used in the 2×2 pilot test program reported in Part I of this study. A brief summary of the findings of the statistical analysis is included herein. Details of the statistical analysis of the 8×2 data are reported elsewhere (Coplantz and Tayebali 1992a).

10.3.1 Analysis of Variance and General Linear Modeling

Because of the variability associated with specimen preparation, it was not possible to exactly control the air-void contents for each specimen; therefore, the actual air-void content for each specimen were measured and the response variables (stiffness, fatigue life, and cumulative dissipated energy) were adjusted statistically to correspond to 4 percent and 7 percent air-void contents.

The response variables were adjusted by fitting general linear models to the measured data. The general linear modeling (GLM) included all main effects and two-factor interactions in the following general form:

$$\text{Log}(Y_i) = \mu + \alpha_1\text{*Asphalt Source} + \alpha_2\text{*Aggregate Source} + \alpha_3\text{*Centered Air-Void Contents} + \alpha_4\text{*Strain Level} + \alpha_5\text{*Asphalt Source*Aggregate Source} + \alpha_6\text{*Asphalt Source*Centered Air-Void Contents} + \alpha_7\text{*Asphalt Source*Strain Level} + \alpha_8\text{*Aggregate Source*Centered Air-Void Contents} + \alpha_9\text{*Aggregate Source*Strain Level} + \alpha_{10}\text{*Centered Air-Void Contents*Strain Level + error} \quad (10.1)$$

where:

Y_1 = initial flexural stiffness,
Y_2 = fatigue life,
Y_3 = cumulative dissipated energy,
μ = constant,
α_j = regression coefficients,
error = higher order interactions plus experimental error; and
Centered Air-Void Contents =

$$\{(\text{Measured Air-Void Contents} - 5.5 \text{ percent}) * 100\%\}/1.5\%. \quad (10.2)$$

The centering of air-void contents shown above was chosen so that air-void contents of 4 percent and 7 percent would result in transformed values of -1 and +1. A similar transformation for the strain level variable was not necessary for this experiment because of the more precise control of the applied strain level.

The results of an analysis of variance (ANOVA) on the general linear model above indicated that the dependent (response) variables (stiffness, fatigue life, and cumulative dissipated energy) could be explained by the main effects as represented by asphalt source, aggregate source, air-void contents, and their two-factor interactions shown in Table 10.4. Table 10.5 presents the summary statistics from the models for the three response variables. It is interesting to note that all the main effects for each response variable are significant at the 95-percent confidence level. Each response variable is also sensitive to the interaction of asphalt source and aggregate source, which suggests that fatigue behavior is mix dependent rather that just asphalt source dependent.

10.3.1.1 Repeatability

Since replicates were included in the experiment design, it was possible to estimate the variance associated with specimen preparation and testing. The coefficient of variation for log-normally-distributed data may be computed using the following relationship:

$$CV = 100 * (e^{VAR} - 1)^{0.5} \quad (10.3)$$

Table 10.4. Statistically significant effects in GLM for stiffness, fatigue life, and cumulative dissipated energy

Factor/Interaction	Initial Flexural Stiffness	Fatigue Life	Cumulative Dissipated Energy
Asphalt Source	H	H	H
Aggregate Source	H	H	S
Air-Void Content	H	H	H
Strain	H	H	H
Asphalt Source * Aggregate Source	H	H	S
Asphalt Source * Air-Void Contents	H	H	H
Asphalt Source * Strain			B
Aggregate Source * Air-Void Contents		H	H
Aggregate Source * Strain	B		
Air-Void Contents * Strain			

Notes:

Description:	Probability of type 1 error:
H = highly significant	less than 0.01
S = significant	0.01 to 0.05
B = barely significant	less than 0.10
Blank = not significant	greater than 0.10

Table 10.5. Summary statistics from GLM for stiffness, fatigue life, and cumulative dissipated energy

Statistics	Stiffness	Fatigue Life	Cumulative Dissipated Energy
R^2	0.960	0.950	0.860
Root Mean Square Error (Ln)	0.120	0.387	0.392
Coefficient of Variation (%)	11.90	40.20	40.70

Notes: R^2 = coefficient of determination; coefficient of variation = $100 * (e^{MSE} - 1)^{0.5}$; e = base of natural logarithm; and MSE = mean square error

where:

CV	=	coefficient of variation in percentage,
VAR	=	variance of log-transformed data or MSE from GLM,
e	=	base of natural logarithms, and
MSE	=	mean square error.

The mean square error (MSE) resulting from an ANOVA on natural-log-transformed data may be used as an estimate of variance. Coefficients of variation based on the GLM of natural-log-transformed data are summarized in Table 10.5.

The above results are similar to those based on the 2×2 pilot test program described in Part I, except that the coefficients of variation for fatigue life and cumulative dissipated energy are significantly reduced. As indicated earlier, this is most likely due to improvements in the test equipment, as well as the use of rolling-wheel compaction which virtually eliminated the fracturing of the aggregates which occurs in specimens prepared by kneading compaction.

10.3.1.2 Summary of Results from GLM

An overall summary of the response variables (adjusted to 4 percent and 7 percent air-void contents) is presented in Table 10.6. The effect of asphalt source on mix performance is explored in the following sections. Average stiffness of mixes containing RH aggregate was approximately 29 percent lower than that of mixes containing RD aggregate. The average fatigue life of mixes containing RH aggregate was observed to be approximately 35 percent greater than that of mixes containing RD aggregate. These results agree with the a priori notion that in the controlled-strain mode of loading, mixes exhibiting lower stiffness moduli outperform mixes with higher stiffness moduli. Similar to fatigue life, the average cumulative dissipated energy was also greater for mixes containing RH aggregate.

As for the effect of air-void contents, increasing the air-void content from 4 percent to 7 percent decreased the overall average stiffness of mixes by approximately 20 percent. Decreases in fatigue life and cumulative dissipated energy with increasing air-void content were also anticipated; the actual differences between the low- and high-void-content mixes were approximately 23 percent for fatigue life and 39 percent for cumulative dissipated energy, respectively. It is interesting to note that for the aggregate source, increased stiffness resulted in decreased fatigue life, whereas for air-void content, increased stiffness resulted in increased fatigue life. These trends in mix behavior for air-void effects are similar to those observed in the earlier 2×2 experiment. The aggregate and air-void effect for each individual asphalt depends on the asphalt source. The overall effect of aggregate and air-void contents is summarized below.

Table 10.6. Average stiffness, fatigue life, and cumulative dissipated energy across strain and replicates for 8×2 experiment

Effect	Flexural Stiffness (psi)	Fatigue Life (cycles)	Cumulative Dissipated Energy (psi)
Asphalt Source			
AAA-1	295,400	99,300	3100
AAB-1	409,900	70,300	2700
AAC-1	552,700	41,200	2100
AAD-1	386,200	74,400	2800
AAF-1	1,033,000	25,100	1800
AAG-1	1,172,700	7,200	600
AAK-1	592,800	46,200	2400
AAM-1	604,800	71,200	3400
% Difference[a]	75%	-93%	-79%
Aggregate Source			
RH	480,900	53,700	2300
RD	676,800	35,100	2000
% Difference	29%	-35%	-13%
Air-Void Contents			
4%	638,800	49,400	2800
7%	509,500	38,100	1700
% Difference	-20%	-23%	-39%

[a]Percentage difference between Asphalt Source AAA-1 and AAG-1

Notes: Air-void contents adjusted to 4 and 7 percent.
Averages based on the mean of log-transformed data.
Percentage difference is the expressed as a percentage of the larger value.

Effect	Flexural Stiffness	Fatigue Life	Cumulative Dissipated Energy
Aggregate Source	29% decrease from RD to RH	35% increase from RD to RH	13% increase from RD to RH
Air-Void Content	20% decrease from 4% to 7%	23% decrease from 4% to 7%	39% decrease from 4% to 7%

Table 10.7 summarizes the performance of two MRL asphalts, AAK-1 and AAG-1, in the two different (8×2 and 2×2) experiments. Although third-point flexural beam fatigue tests in the controlled-strain mode of loading at 20°C (68°F) were used in both experiments, all other variables, including aggregate source, strain level, test equipment, specimen size, and loading frequency and pattern, were different.

Table 10.7. Average stiffness, fatigue life, and cumulative dissipated energy for asphalt sources AAK-1 and AAG-1 for the 8×2 and 2×2 experiments

Test Type	Asphalt Source	Flexural Stiffness (psi)	Fatigue Life (cycles)	Cumul. Diss. Energy (psi)
	Flexural Fatigue 8×2 Experiment (20°C) (68°F)[a]			
Third-point sinusoidal loading, 10 Hz frequency, 2" x 2.5" x 15" specimen, RH and RD aggregates, rolling-wheel compaction, hydraulic test system	AAK-1	592,800	46,200	2400
	AAG-1	1,172,700	7200	660
	% Difference	49%	-85%	-73%
	Flexural Fatigue 2×2 Experiment (20°C) (68°F)[b]			
Third-point haversine pulse loading, 0.1 sec. loading time, 1.67 Hz frequency, 1.5" x 1.5" x 15" specimen, RB and RL aggregates, kneading compaction, pneumatic test system	AAK-1	536,500	141,200	1500
	AAG-1	1,160,500	54,100	700
	% Difference	54%	-62%	-53%

[a] Low and high strains correspond to 400 and 700 micro in./in.
Low and high air-void contents correspond to 4 and 7 percent.
[b] Low and high strains correspond to 200 and 400 micro in./in.
Low and high air-void contents correspond to 4 and 8 percent.

Notes: Averages based on the mean of log-transformed data.
Percentage difference is expressed as a percentage of the larger value.

Performance of these two MRL asphalts is identical in both experiments: mixes containing AAK-1 asphalt showed lower average stiffness moduli and higher average fatigue life and cumulative dissipated energy compared to mixes containing AAG-1 asphalt.

10.3.2 Performance Comparison of Mixes Containing Different Asphalts

A comparison of the performance of the various asphalts was accomplished through a combination of graphical and statistical analysis. All comparisons were made using response variables adjusted for air-void content and the comparisons of means were based on log-transformed response variables. The purposes of the comparisons were to classify the asphalts into groups of similar performance and attempt to distinguish asphalts which perform better than average from those that perform worse than average. A summary of the analysis results follows.

10.3.2.1 Flexural Stiffness

For flexural stiffness, mixes containing asphalts AAG-1 and AAF-1 were consistently stiffer, regardless of aggregate source or air-void levels. Similarly, the mixes containing asphalt AAA-1 consistently showed the lowest stiffness. The Tukey-pairwise-comparison matrix across aggregates, air-void contents, and replicates a) verified that mixes with asphalt AAA-1 had the lowest stiffness and b) showed that mixes with asphalt AAG-1 had higher stiffness than those containing asphalt AAF-1, with a significance of approximately 94 percent. The remaining mixes fell somewhere between these two extremes. Mixes containing asphalts AAC-1, AAK-1, and AAM-1 generally had higher stiffnesses than mixes with asphalts AAB-1 and AAD-1. On the basis of graphical results and confirmation with contrast statements, mixes were grouped by flexural stiffness across aggregates, air-void contents, strain, and replicates in the following manner:

(Lowest Stiffness)			**(Highest Stiffness)**
Group 1	**Group 2**	**Group 3**	**Group 4**
AAA-1	AAB-1	AAC-1	AAF-1
	AAD-1	AAK-1	AAG-1
		AAM-1	

10.3.2.2 Fatigue Life

For fatigue life, the relative performance of the asphalts is nearly opposite to that of the flexural stiffness. Since the 8×2 experiment was conducted in the controlled-strain mode of loading, this result was expected. Mixes containing asphalts AAG-1 and AAF-1 consistently showed the lowest fatigue lives. The Tukey-pairwise comparison across aggregate, air-void contents, strain, and replicates suggested that mixes with asphalt AAA-1 did not show a significantly higher fatigue life than mixes with asphalts AAB-1, AAD-1, and AAM-1; however, in contrast are mixes containing asphalt AAA-1 which have a higher fatigue life

than these same mixes taken as a group. Tukey comparisons of mixes containing asphalts AAG-1 and AAF-1 showed that they had significantly lower fatigue lives than the remainder of the mixes. As with flexural stiffness, the remaining mixes fell between the two extremes of mixes containing asphalt AAA-1 or AAG-1. Based on the results of the analysis, different mixes can be grouped in the following manner:

(Lowest Fatigue Life)				(Highest Fatigue Life)
Group 1	**Group 2**	**Group 3**	**Group 4**	**Group 5**
AAG-1	AAF-1	AAC-1	AAB-1	AAA-1
		AAK-1	AAD-1	
			AAM-1	

10.3.2.3 Cumulative Dissipated Energy

The relative performance of mixes is similar with regard to cumulative dissipated energy and fatigue life, as would be expected. However, the distinction between groups of mixes containing different asphalts is less clear. The mixes with asphalt AAG-1 continued to have the lowest performance, regardless of aggregate source. Mixes with asphalts AAA-1 and AAM-1 showed slightly better performance than mixes with asphalts AAB-1 and AAD-1 (approximately 92 percent significance). Likewise, mixes with asphalts AAB-1 and AAD-1 showed slightly better performance than mixes with asphalts AAC-1 and AAK-1 (approximately 95 percent significance) which in turn showed slightly better performance than mixes with asphalt AAF-1 (approximately 93 percent significance).

A more clear distinction (above 95 percent significance) can be made between mixes with asphalts AAA-1, AAB-1, AAD-1, and AAM-1 taken as a group in comparison with mixes containing asphalts AAC-1, AAF-1, and AAK-1, also taken as a group. Based on these findings the relative performance of mixes in terms of cumulative dissipated energy across aggregates, air-void contents, strain, and replicates may be grouped in either of two ways as follows:

(Lowest Cumulative Dissipated Energy)				(Highest Cumulative Dissipated Energy)
Group 1	**Group 2**	**Group 3**	**Group 4**	**Group 5**
AAG-1	AAF-1	AAC-1	AAB-1	AAA-1
		AAK-1	AAD-1	AAM-1

(Lowest Cumulative Dissipated Energy)		(Highest Cumulative Dissipated Energy)
Group 1	**Group 2**	**Group 3**
AAG-1	AAC-1	AAA-1
	AAF-1	AAB-1
	AAK-1	AAD-1
		AAM-1

10.3.3 Asphalt Binder Effects on Mix Performance

The SHRP A-002A contractor has hypothesized that the asphalt effect on fatigue resistance of asphalt-aggregate mixes can be explained largely on the basis of its loss stiffness, G″ ($G^* \sin\delta$),[5] for controlled-strain testing. Data from the 8×2 experiment were used to investigate this hypothesis. Measurements of G″ at 20°C (68°F) and 10 Hz frequency for thin film oven test (TFOT)-aged asphalt binders were provided by SHRP Project A-002A, the same temperature and frequency used in the fatigue testing. Table 10.8 presents the asphalt binder properties measured by using dynamic mechanical analysis (DMA). Relationships were evaluated between asphalt binder properties and

- laboratory-determined fatigue life of asphalt-aggregate mixes under third-point controlled-strain flexural beam fatigue testing, and
- in situ fatigue life of asphalt-aggregate mixes predicted by linear elastic layer analysis in which the maximum tensile strain was calculated in simulated pavements.

The detailed analysis is reported by Coplantz and Tayebali (1992a) and summarized in the following sections.

Table 10.8. Asphalt binder properties provided by A-002A (after TFOT, at 20°C [68°F] and 10 Hz)

Asphalt Source	G^* (kPa)	G″ ($G^*\sin\delta$) (kPa)	G′ ($G^* \cos\delta$) (kPa)	$\tan\delta$
AAA-1	3197	2732	1661	1.645
AAB-1	6098	4600	4001	1.150
AAC-1	9769	7295	6499	1.122
AAD-1	3845	3149	2205	1.428
AAF-1	18,321	12,326	13,551	0.910
AAG-1	23,517	17,975	15,179	1.183
AAK-1	10,833	8134	7150	1.138
AAM-1	8230	5609	6019	0.933

[5] G^* is the dynamic shear stiffness, and δ is the phase shift between stress and strain for the asphalt binder.

10.3.3.1 Binder Effects on Laboratory Mix Performance

Regression analysis was used to relate the asphalt binder loss stiffness ($G^* \sin\delta$) to the fatigue life of mixes at 20°C (68°F) and 10 Hz frequency. Table 10.9 shows the coefficients of determination (R^2) for the laboratory fatigue life versus binder loss stiffness and complex stiffness regressions, stratified by aggregate source and air-void content at the 400 micro in./in. strain level. For a given aggregate and air-void content, it can be seen that mix fatigue life (ln cycles to failure) correlates quite well with the loss stiffness of the aged asphalt binder (Figures 10.1 and 10.2). Increases in loss stiffness were accompanied by rather significant decreases in fatigue resistance. Aggregate type and air-void content were also important: RH aggregates generally produced more fatigue-resistant mixes than did RD aggregates, and mixes with low air-void content proved superior to those with high air-void contents. The loss stiffness of the aged binder was a slightly better predictor variable than the complex stiffness, as shown in Table 10.9.

Coefficients of determination from regressions on adjusted fatigue life (fatigue life adjusted to 4 percent and 7 percent air-void content) versus the binder loss stiffness as a function of aggregate source, air-void content, and strain level are summarized below:

Effect		**Coefficient of Determination Fatigue Life versus ($G^* \sin\delta$)**
Aggregate Source (across air-void contents, strain level, and replicates)	RH	0.97
	RD	0.64
Air-Void Contents (across aggregate source, strain level, and replicates)	4%	0.68
	7%	0.95
Strain Level (micro in./in.) (across aggregate source, air-void contents, and replicates)	400	0.81
	700	0.94

10.3.3.2 Binder Effects on In Situ Mix Performance

In situ mix performance was simulated by linear elastic layer analysis (ELSYM) of the response of three typical pavement structures to a 44.4 kN (10,000 lb) wheel load (12 in. center-to-center dual tires with 100 psi contact pressure). The first two structures were three-layered systems which consisted of 10.2 and 15.2 cm (4 and 6 in.) asphalt-aggregate surfaces with layer stiffnesses determined from laboratory flexural fatigue testing for each of the 32 asphalt-aggregate mixes (8 asphalts × 2 aggregates × 2 air-void contents) and an assumed Poisson's ratio of 0.35. A 40.6 and 30.5 cm (16 and 12 in.) base with a modulus of 138 MPa (20,000 psi) and Poisson's ratio of 0.3 were used for the 10.2 and 15.2 cm (4 and 6 in.) thick asphalt layers, respectively, over a subgrade with a modulus of 69 MPa (10,000 psi) and Poisson's ratio of 0.3. The third pavement was a two-layer structure with a 25.4 cm (10 in.) asphalt-aggregate surface placed directly on a weak subgrade with a modulus of 34.5 MPa (5000 psi) and Poisson's ratio of 0.4.

Table 10.9. Accuracy of regressions for laboratory measurements of mix fatigue life[a] versus loss stiffness and complex stiffness of binder

Aggregate	Voids	Coefficient of Determination Fatigue Life Versus	
		Binder Loss Stiffness ($G^* \sin\delta$)	Binder Complex Stiffness (G^*)
RD	Low	0.68	0.59
RD	High	0.86	0.82
RH	Low	0.90	0.85
RH	High	0.94	0.95
All Aggregates and Air-Void Contents		0.78	0.74

[a]Natural logarithmic function (Ln) of cycles to failure at 400 micro in./in. strain.

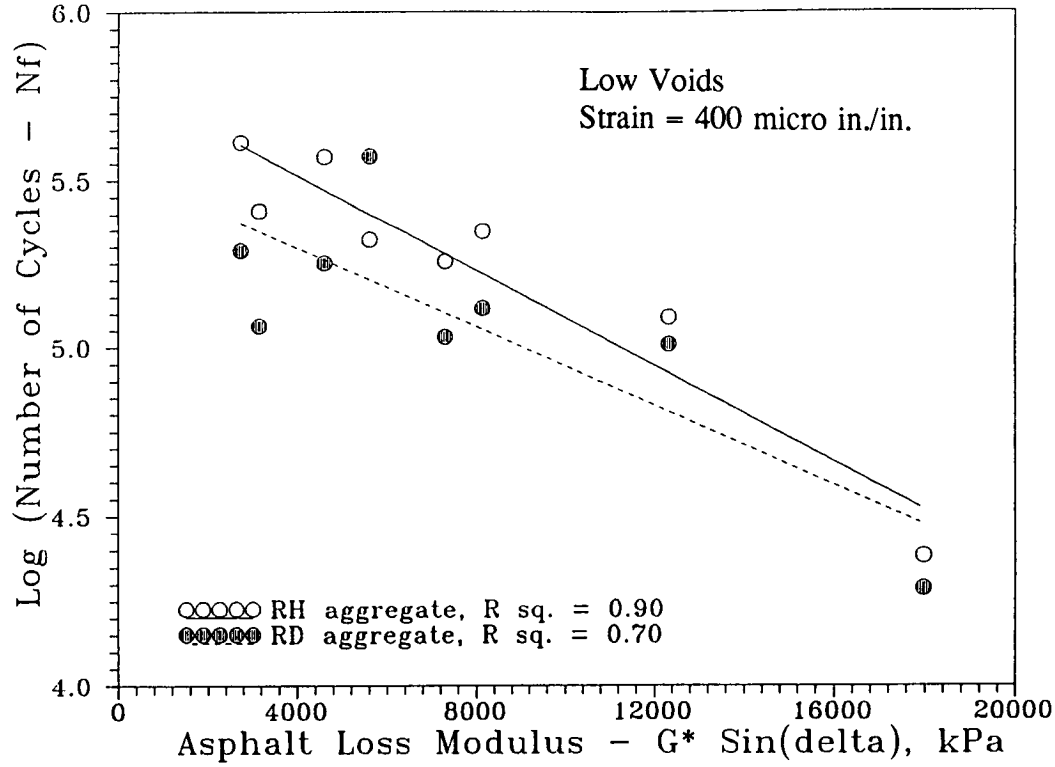

Figure 10.1. Effect of asphalt binder loss stiffness and aggregate source on laboratory cycles to failure for low-void mixes

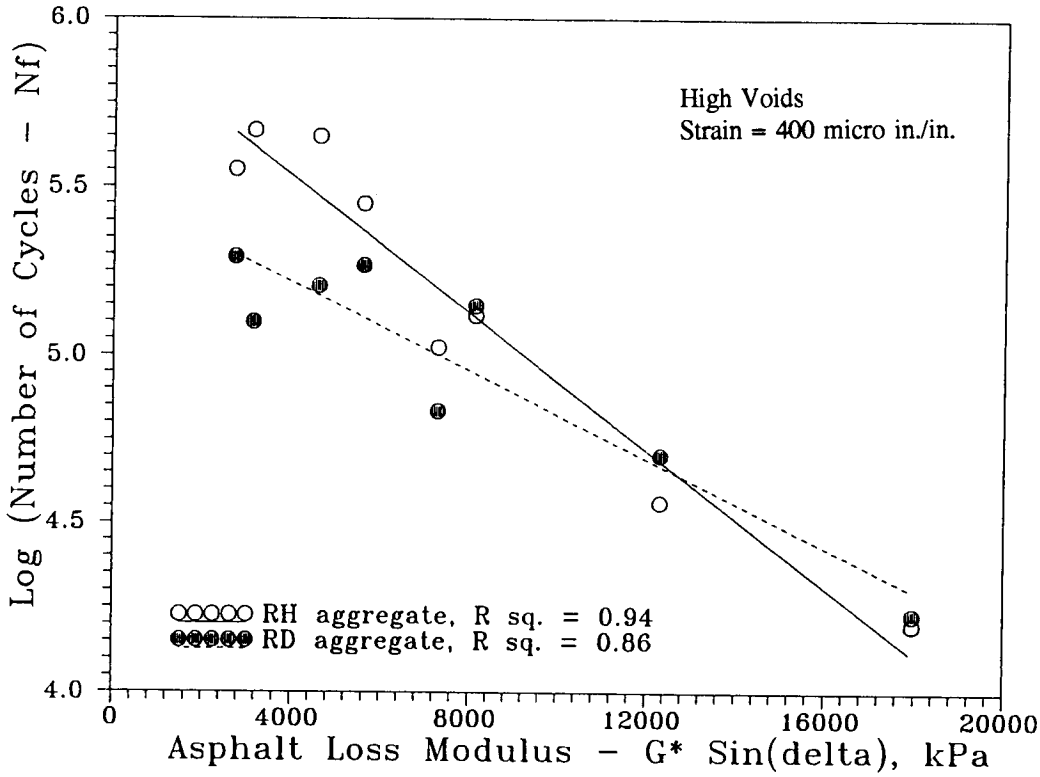

Figure 10.2. Effect of asphalt binder loss stiffness and aggregate source on laboratory cycles to failure for high-void mixes

For each pavement structure, the maximum tensile strain at the bottom of the asphalt layer was determined from elastic analysis for the 32 asphalt-aggregate mixes (a total of 96 ELSYM simulations for the three pavement sections under consideration).

For each of the 32 asphalt-aggregate mixes, laboratory fatigue life versus tensile strain regression models of the following form were determined:

$$N_f = K_1 (1/\epsilon)^{K2} \tag{10.4}$$

where: N_f = laboratory fatigue life,
ϵ = initial tensile strain, and
K_1 and K_2 = experimentally determined regression coefficients.

By using the tensile strain at the bottom of the asphalt-aggregate layer as determined from the elastic pavement analysis and the laboratory fatigue relationships between the initial tensile strain and fatigue life, cycles to failure in the simulated pavement structures for the 32 asphalt-aggregate mixes were determined. The cycles to failure for the simulated structures were then correlated to binder loss stiffness.

The analysis indicated that the binder loss stiffness was not well correlated with simulated pavement performance (Table 10.10) with or without stratification by aggregate type and air-void content. Typical relationships between the binder loss stiffness and simulated field cycles to failure for a three-layered structure with a 15.2 cm (6 in.) asphalt-aggregate layer

Table 10.10. Accuracy of regressions for field simulations of mix fatigue life[a] versus loss stiffness and complex stiffness of binder

Aggregates	Voids	Coefficient of Determination Fatigue Life Versus	
		Binder Loss Stiffness ($G^* \sin\delta$)	Binder Complex Stiffness (G^*)
Three-Layer Structure (10.2 cm [4 in.] Asphalt-Aggregate Layer)			
RD	Low	0.02	0.01
RD	High	0.04	0.02
RH	Low	0.03	0.06
RH	High	0.21	0.32
All Aggregates and Air-Void Contents		0.00	0.00
Three-Layer Structure (15.2 cm [6 in.] Asphalt-Aggregate Layer)			
RD	Low	0.02	0.06
RD	High	0.07	0.10
RH	Low	0.09	0.14
RH	High	0.12	0.12
All Aggregates and Air-Void Contents		0.01	0.02
Two-Layer Structure (25.4 cm [10 in.] Asphalt-Aggregate Layer)			
RD	Low	0.07	0.12
RD	High	0.17	0.22
RH	Low	0.24	0.30
RH	High	0.00	0.00
All Aggregates and Air-Void Contents		0.06	0.08

[a]Ln cycles to failure under 88.8 kN (20,000 lb) axle load.

are presented in Figures 10.3 and 10.4. It is interesting that the effects of binder loss stiffness, aggregate type, and air-void content on fatigue resistance were different depending on how the fatigue response was measured. Using laboratory fatigue life (natural logarithmic function (Ln) of cycles to failure at 400 micro in./in.), a superior response was associated with smaller binder loss stiffness, RH aggregate, and low air-void content (Figures 10.1 and 10.2). Using field simulations of cycles to failure, a superior response was associated with larger binder loss stiffness, RD aggregate, and high air-void contents (Figures 10.3 and 10.4).

Accuracy of the regressions was found to improve slightly with an increase in asphalt layer thickness (Table 10.10), but all trends were similar for the three pavement structures. These

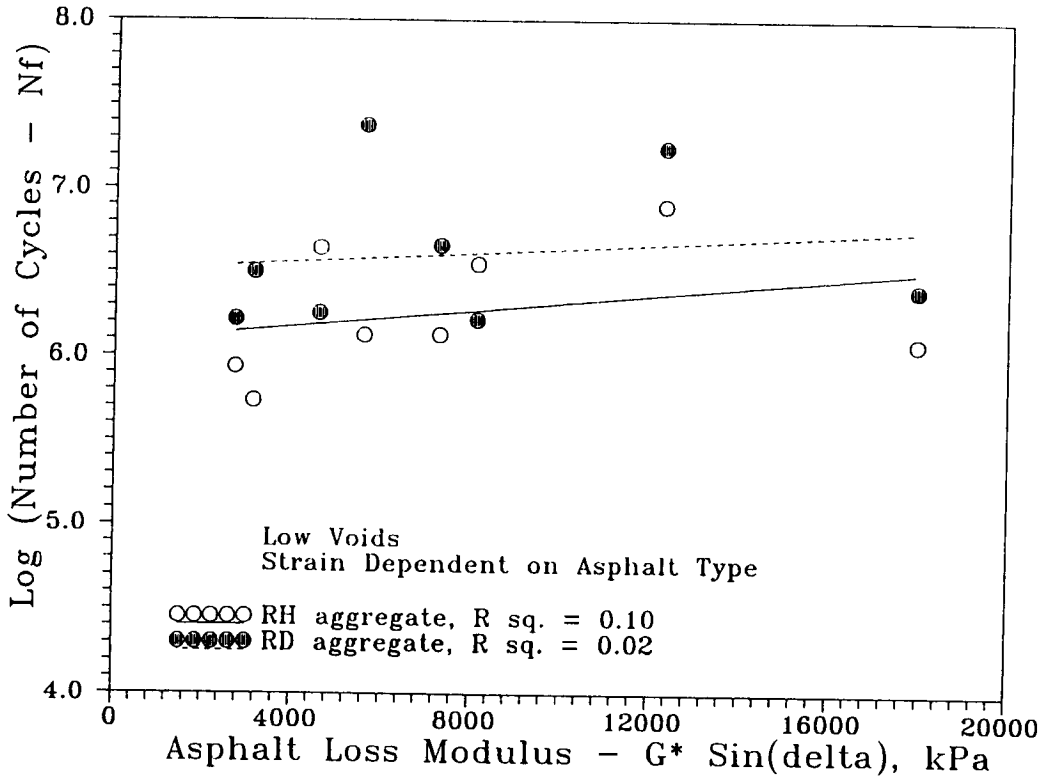

Figure 10.3. Effect of asphalt binder loss stiffness and aggregate source on simulated field cycles to failure for low-void mixes (structure with 15.2 cm [6 in.] asphalt layer)

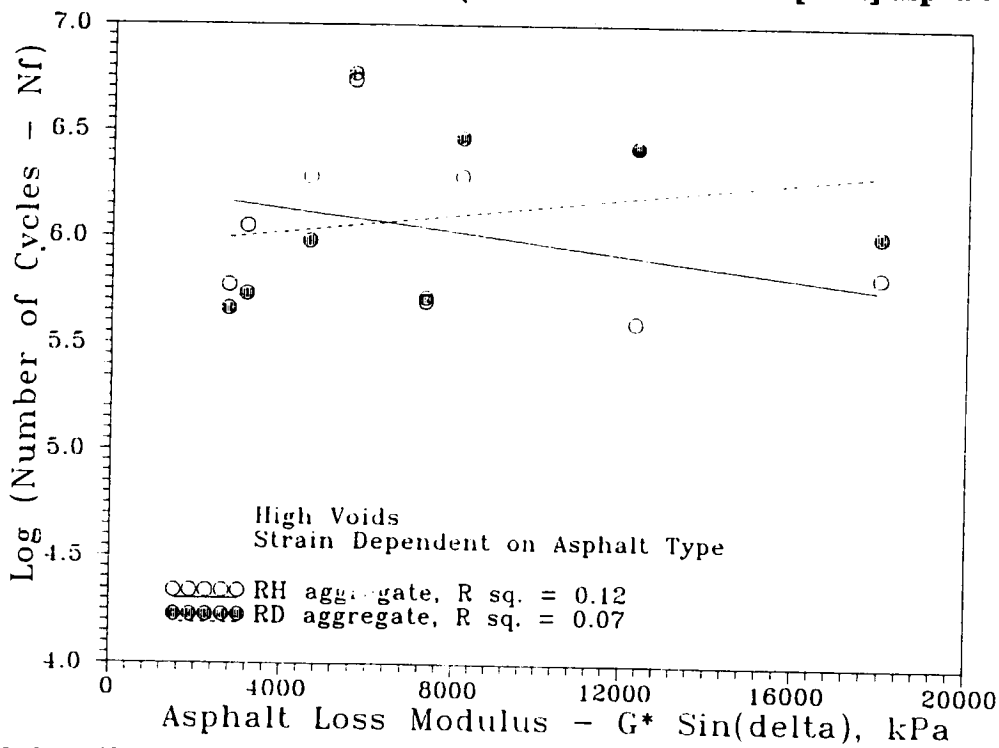

Figure 10.4. Effect of asphalt binder loss stiffness and aggregate source on simulated field cycles to failure for high-void mixes (structure with 15.2 cm [6 in.] asphalt layer)

findings underscore the importance of using mechanistic analyses to properly interpret laboratory fatigue data.

10.3.3.3 Summary of the Asphalt Binder Effects on Mix Performance

The investigating results of the effect of asphalt binder loss stiffness on laboratory- and field-simulated asphalt-aggregate mix fatigue performance can be summarized as follows:

- The laboratory fatigue resistance of asphalt-aggregate mixes is sensitive to the type of asphalt binder. The loss stiffness of the aged binder provides a good indication of the relative laboratory fatigue resistance of otherwise identical mixes. Accordingly, the binder loss stiffness seems to be an attractive candidate for inclusion in binder specifications.

- The loss stiffness of the binder, however, is generally not a sufficient indicator of the relative fatigue resistance of asphalt-aggregate mixes. Other mix characteristics, such as aggregate type and air-void content, also significantly contribute to laboratory fatigue resistance. Accordingly, a binder specification alone is insufficient to ensure satisfactory fatigue performance of pavements in situ.

- Having laboratory test data on mixes is a necessary condition for characterizing fatigue behavior. However, laboratory testing must be supplemented by mechanistic analyses to determine how mixes are likely to perform in the pavement structure under anticipated traffic loads and environmental conditions. Accordingly, mix specifications must address the composite effects of the mix properties, structure, traffic loading, and environment on pavement performance.

10.4 Models of Fatigue Response

Modeling the laboratory fatigue response was of great interest not only because of insights developed during the model-building process and in interpreting its results but also because of the possibility that a sufficiently accurate model—one that captured the essential effects of mix properties on fatigue behavior—would lessen the requirements for laboratory fatigue testing in the mix design process. Models based on dissipated-energy concepts seemed particularly appealing because of their promise of rather simply and accurately capturing a range of mix and testing effects.

The model-building process is briefly described in this section. Addressed first is the conceptual advancement that seeks a common understanding of the strain-based and energy-based approaches to fatigue modeling. Following are a presentation of calibration results for several alternative models and recommendations regarding two of the most promising.

10.4.1 Fatigue Life Relationships

It has been accepted for many years that the fatigue behavior of asphalt-aggregate mixes can be characterized by a relationship of the form:

$$N_f = a\,(1/\epsilon_o)^b \tag{10.5}$$

where: N_f = fatigue life,
ϵ_o = initial tensile strain, and
a, b = experimentally determined coefficients.

The above relationship is applicable to *a given asphalt mix*. Some researchers (e.g., Monismith et al. 1985) have suggested that a relationship which is more applicable to asphalt-aggregate mixes in general is the following:

$$N_f = a\,(1/\epsilon_o)^b\,(1/S_o)^c \tag{10.6}$$

where: N_f = fatigue life,
ϵ_o = initial tensile strain,
S_o = initial mix stiffness, and
a, b, c = experimentally determined coefficients.

Based on the laboratory test data presented in the form of Equation 10.6, several strain-based models have been proposed to predict pavement fatigue life (Finn et al. 1977; SHELL 1978; Asphalt Institute 1981).

Other researchers (Chomton and Valayer 1972; van Dijk 1975; van Dijk and Visser 1977; Pronk and Hopman 1990; Tayebali et al. 1992b) have used an energy approach for describing fatigue behavior and have shown that the total or, cumulative, dissipated energy to failure is related to fatigue life as follows:

$$W_N = A\,(N_f)^z \tag{10.7}$$

where: N_f = fatigue life,
W_N = cumulative dissipated energy to failure, and
A, z = experimentally determined coefficients.

In Equations 10.5 and 10.6, fatigue life is related to initial test conditions, namely, the initial strain and initial mix stiffness. In Equation 10.7, fatigue life is related to a terminal test condition, namely, the cumulative dissipated energy to failure. Neither approach directly recognizes how damage to the mix actually develops as loading proceeds from beginning to end. The cumulative dissipated energy to failure, W_N, is related to the energy dissipated during the ith load cycle, w_i, as follows:

$$W_N = \sum_{i}^{N_f} w_i \tag{10.8}$$

For a sinusoidal loading condition

$$w_i = \pi \epsilon_i^2 S_i \sin\phi_i \tag{10.9}$$

where:

N_f	=	fatigue life,
w_i	=	dissipated energy at load cycle i,
ϵ_i	=	strain amplitude at load cycle i,
S_i	=	mix stiffness at load cycle i,
ϕ_i	=	phase shift between stress and strain at load cycle i, and
π	=	3.142.

For controlled-strain loading, the dissipated energy per cycle (w_i) decreases with an increasing number of load repetitions. For controlled-energy loading, the dissipated energy per cycle (w_i) remains constant during testing, and the cumulative dissipated energy is simply the product of the initial dissipated energy per cycle, w_o, and the number of cycles to failure, N_f. That is,

$$W_N = w_o N_f \tag{10.10}$$

or

$$W_N = \pi N_f \epsilon_o^2 S_o \sin\phi_o \tag{10.11}$$

where:

N_f	=	fatigue life,
W_N	=	cumulative dissipated energy to failure,
w_o	=	initial dissipated energy per load cycle,
ϵ_o	=	initial strain amplitude,
S_o	=	initial mix stiffness,
ϕ_o	=	initial phase shift between stress and strain, and
π	=	3.142.

Combining Equations 10.7 and 10.11, the following relationship is obtained under the assumption of constant dissipation of energy per cycle (controlled-energy loading):

$$N_f = \{A/(\pi \epsilon_o^2 S_o \sin\phi_o)\}^{1/(1-z)} \tag{10.12}$$

For modes of loading other than controlled energy, a mode-of-loading-dependent energy ratio factor (van Dijk 1975) is useful. The energy ratio factor, ψ, is defined as follows:

$$\psi = (N_f w_o)/W_N \tag{10.13}$$

Adding the energy ratio factor to Equation 10.12 yields

$$N_f = \{A\psi/(\pi \epsilon_o^2 S_o \sin\phi_o)\}^{1/1-z} \tag{10.14}$$

and generalizing for the purpose of regression analyses yields

$$N_f = a\,(\psi)^b\,(\epsilon_o)^c\,(S_o)^d\,(\sin\phi_o)^e \qquad (10.15)$$

or, replacing initial dissipated energy per cycle, w_o, for ϵ_o, S_o, and $\sin\phi_o$ yields

$$N_f = d\,(\psi)^f\,(w_o)^g \qquad (10.16)$$

Equations 10.15 and 10.16 indicate that, for the controlled-strain mode of loading, the fatigue life is a function of the strain and the loss stiffness ($S_o \sin\phi_o$, the viscous component of dynamic stiffness) of the mix, in effect, the energy that is dissipated during the initial load cycle.

10.4.2 Surrogate Fatigue Models

All the surrogate fatigue models evaluated herein were developed on the basis of Equations 10.15 and 10.16. Van Dijk and Visser (1977) and Tayebali et al. (1992b) have shown that the coefficients A and z in Equations 10.7 and 10.14 are mix dependent. A term expressing the possible effects of voids was added to Equations 10.15 and 10.16 because of 1) concern that w_o (or ϵ_o, S_o, and ϕ_o) and ψ would not fully capture the significant effects of mix voids, and 2) the effects of air-void contents on fatigue resistance are not explained by their related effects on mix stiffness. Two alternative measures of mix voids were evaluated: the initial air-void content and the initial percentage of voids filled with asphalt.

Calibrations of surrogate models were based on the data from the 8×2 test program described previously. While the mixes had quite different fatigue behaviors, they are considered representative of the range of conventional paving mixes being used in the United States. As noted earlier, testing was limited to controlled-strain loading with a frequency of 10 Hz applied at a temperature of 20°C (68°F). Pearson correlations for the dependent and independent variables are shown in Table 10.11. The model calibrations are summarized in Table 10.12.

The main findings from these calibrations are summarized as follows:

- The effects of initial mix stiffness and phase angle on cycles to failure can be expressed with equal accuracy by an initial mix loss modulus.
- The effect of mix voids on cycles to failure can be expressed with equal accuracy by either the air-void content or the percentage of voids filled with asphalt.
- The effects of initial strain level, mix stiffness, and phase angle can be expressed with equal accuracy by the initial dissipated energy per cycle.

Table 10.11. Pearson correlation matrix for the dependent and independent variables

	Ln (N_f)	Ln (w_o)	Ln (ϵ_o)	Ln (S_o)	Ln ($\sin\phi_o$)	Ln (ψ)	V_o	VFB
Ln (N_f)	1.000							
Ln (w_o)	-0.887	1.000						
Ln (ϵ_o)	-0.760	0.859	1.000					
Ln (S_o)	-0.429	0.442	-0.054	1.000				
Ln ($\sin\phi_o$)	0.318	-0.268	0.112	-0.889	1.000			
Ln (ψ)	0.371	-0.320	-0.018	-0.681	0.690	1.000		
V_o	-0.118	-0.152	0.010	-0.194	-0.026	0.116	1.000	
VFB	0.132	0.114	-0.012	0.138	0.047	-0.101	-0.979	1.000

Table 10.12. Calibrations of fatigue life models

Model	R^2	Coefficients of Variation (%)
Strain-Dependent		
$N_f = 1.012*10^5 (V_o)^{-1.351} (\psi)^{1.81} (\epsilon_o)^{-3.901} (S_o)^{-2.279} (\sin\phi_o)^{-2.666}$	0.87	58
$N_f = 1.495*10^{-4} (VFB)^{3.481} (\psi)^{1.913} (\epsilon_o)^{-3.921} (S_o)^{-2.010} (\sin\phi_o)^{-2.169}$	0.86	61
$N_f = 4.148*10^4 \exp^{-0.266 V_o} (\psi)^{1.896} (\epsilon_o)^{-3.901} (S_o)^{-2.274} (\sin\phi_o)^{-2.691}$	0.87	58
$N_f = 12.23 \exp^{0.052 VFB} (\psi)^{1.891} (\epsilon_o)^{-3.920} (S_o)^{-2.023} (\sin\phi_o)^{-2.186}$	0.86	61
Strain-Dependent With Loss Modulus		
$N_f = 1.619*10^4 (V_o)^{-1.283} (\psi)^{1.474} (\epsilon_o)^{-3.935} (S_o'')^{-2.137}$	0.87	58
$N_f = 1.052*10^{-4} (VFB)^{3.410} (\psi)^{1.768} (\epsilon_o)^{-3.936} (S_o'')^{-1.956}$	0.86	61
$N_f = 6.136*10^3 \exp^{-0.252 V_o} (\psi)^{1.530} (\epsilon_o)^{-3.938} (S_o'')^{-2.123}$	0.87	58
$N_f = 6.732 \exp^{0.051 VFB} (\psi)^{1.742} (\epsilon_o)^{-3.935} (S_o'')^{-1.967}$	0.86	61
Energy-Dependent		
$N_f = 927.97 (V_o)^{-1.241} (\psi)^{1.751} (w_o)^{-1.995}$	0.86	59
$N_f = 7.515*10^{-5} (VFB)^{3.416} (\psi)^{1.748} (w_o)^{-1.966}$	0.86	61
$N_f = 451.24 \exp^{-0.245 V_o} (\psi)^{1.781} (w_o)^{-1.994}$	0.87	58
$N_f = 4.19 \exp^{0.051 VFB} (\psi)^{1.742} (w_o)^{-1.967}$	0.86	61
Energy-Dependent Without Energy Ratio Factor		
$N_f = 1.270*10^3 (V_o)^{-1.206} (w_o)^{-2.075}$	0.85	62
$N_f = 1.705*10^{-4} (VFB)^{3.308} (w_o)^{-2.046}$	0.84	63
$N_f = 632.1 \exp^{-0.237 V_o} (w_o)^{-2.075}$	0.85	61
$N_f = 6.719 \exp^{0.049 VFB} (w_o)^{-2.047}$	0.84	63
Strain-Dependent Without Energy Ratio Factor		
$N_f = 1.651*10^5 \exp^{-0.255 V_o} (\epsilon_o)^{-3.957} (S_o)^{-2.348} (\sin\phi_o)^{-2.259}$	0.86	60
$N_f = 63.69 \exp^{0.050 VFB} (\epsilon_o)^{-3.976} (S_o)^{-2.101} (\sin\phi_o)^{-1.762}$	0.85	63
Strain-Dependent With Loss Modulus and Without Energy Ratio Factor		
$N_f = 3.038*10^5 \exp^{-0.259 V_o} (\epsilon_o)^{-3.950} (S_o'')^{-2.395}$	0.86	60
$N_f = 466.38 \exp^{0.052 VFB} (\epsilon_o)^{-3.948} (S_o'')^{-2.270}$	0.85	63

Although the energy ratio factor (ψ) is statistically significant at the 95 percent confidence level, it improves the coefficient of determination only marginally. Because all data used for model calibrations were obtained under controlled-strain loading, the energy ratio factor may be omitted from the surrogate fatigue models. According to van Dijk (1977), the energy ratio factor is related to both mode of loading and mix stiffness. The stiffness effect, illustrated in Figure 10.5, is relatively small (with a coefficient of determination of less than 0.5).

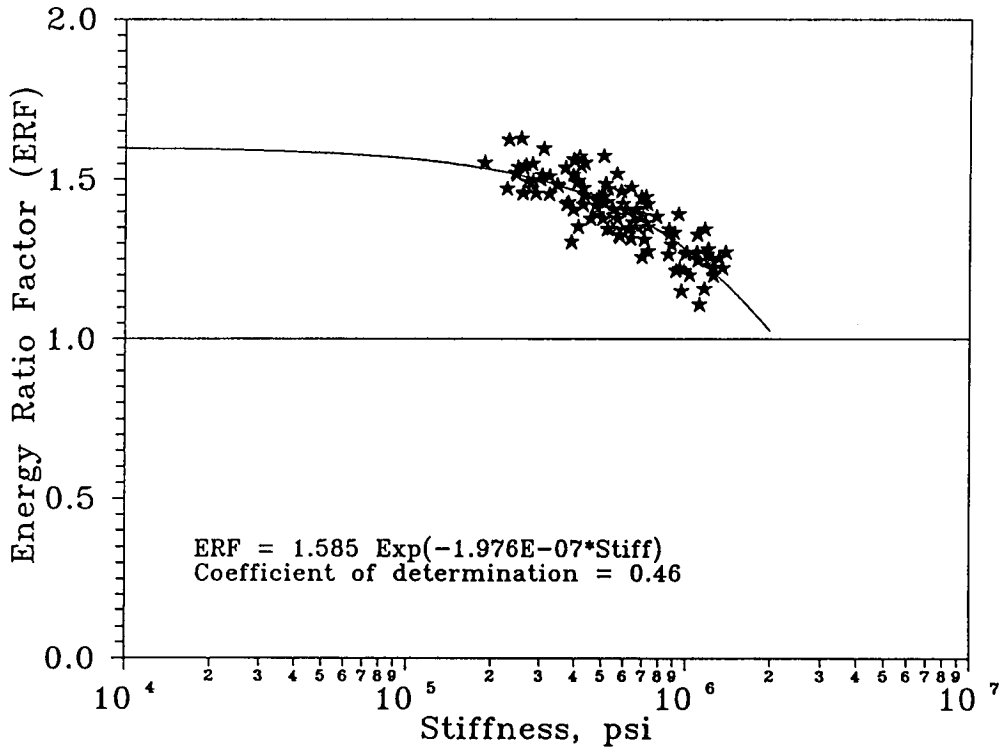

Figure 10.5. Effect of mix stiffness on energy ratio factor

Although not illustrated herein, the influence of mode of loading on the energy ratio factor is expected to be greater than the influence of stiffness.

Strain-dependent and energy-dependent models recommended for use in surrogate mix analysis based on the 8×2 experiment are the following:[6]

$$N_f = 466.4 \exp^{0.052\ VFB} (\epsilon_o)^{-3.948} (S_o'')^{-2.270} \quad (10.17)$$

or

$$N_f = 6.72 \exp^{0.049\ VFB} (w_o)^{-2.047} \quad (10.18)$$

where:

N_f	=	fatigue life,
ϵ_o	=	initial strain, in./in.,
S_o''	=	initial loss stiffness, psi,

[6]More general models based on combined data from all SHRP Project A-003A fatigue test experiments are presented in later chapters.

w_o = initial dissipated energy per cycle, psi, and
VFB = percent voids filled with bitumen.

Results of the regression analysis for the strain- and energy-based models of Equations 10.17 and 10.18 are presented in Tables 10.13 and 10.14. Figures 10.6 and 10.7 graphically illustrate the energy-dependent model of Equation 10.18. Figure 10.6 shows the effect of strain level and percentage voids filled with asphalt on the fatigue life for a mix loss stiffness of 2411 MPa (350,000 psi). Figure 10.7 shows the effect of strain level and mix loss stiffness on fatigue life for a mix having 70 percent of its voids filled with asphalt.

Table 10.13. Results of the regression analysis for the strain-based surrogate model

Dep Var = $Ln(N_f)$ N = 128 Multiple R = 0.920 Squared Multiple R = 0.846
Adjusted Squared Multiple R = 0.842 Standard Error of Estimate = 0.579

Variable	Coefficient	STD Error	STD Coef	Tolerance	T	P (2 Tail)
Constant	6.145	2.381	0.000	.	2.581	0.011
Ln (ϵ_o)	-3.948	0.183	-0.762	0.999	-21.599	0.000
Ln (S''_o)	-2.270	0.159	-0.519	0.941	-14.275	0.000
VFB	0.052	0.008	0.249	0.941	6.842	0.000

Analysis of Variance

Source	Sum-of-Squares	DF	Mean-Square	F-Ratio	P
Regression	227.687	3.000	75.896	226.66	0.000
Residual	41.521	124.000	0.335		

Table 10.14. Results of the regression analysis for the energy-based surrogate model

Dep Var = $Ln(N_f)$ N = 128 Multiple R = 0.918 Squared Multiple R = 0.843
Adjusted Squared Multiple R = 0.840 Standard Error of Estimate = 0.582

Variable	Coefficient	STD Error	STD Coef	Tolerance	T	P (2 Tail)
Constant	1.905	0.568	0.000	.	3.353	0.001
Ln(w_o)	-2.047	0.080	-0.914	0.987	-25.591	0.000
VFB	0.049	0.007	0.236	0.987	6.607	0.000

Analysis of Variance

Source	Sum-of-Squares	DF	Mean-Square	F-Ratio	P
Regression	226.810	2.000	113.405	334.353	0.000
Residual	42.397	125.000	0.339		

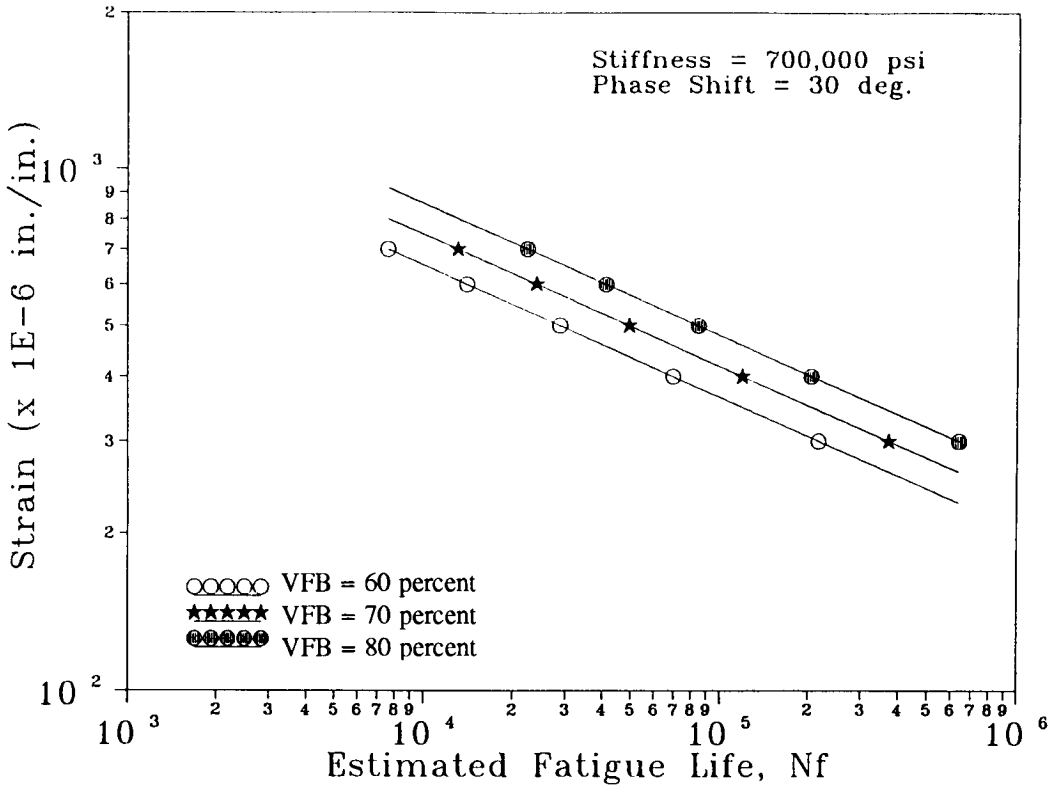

Figure 10.6. Surrogate fatigue model: effect of percent voids filled with asphalt

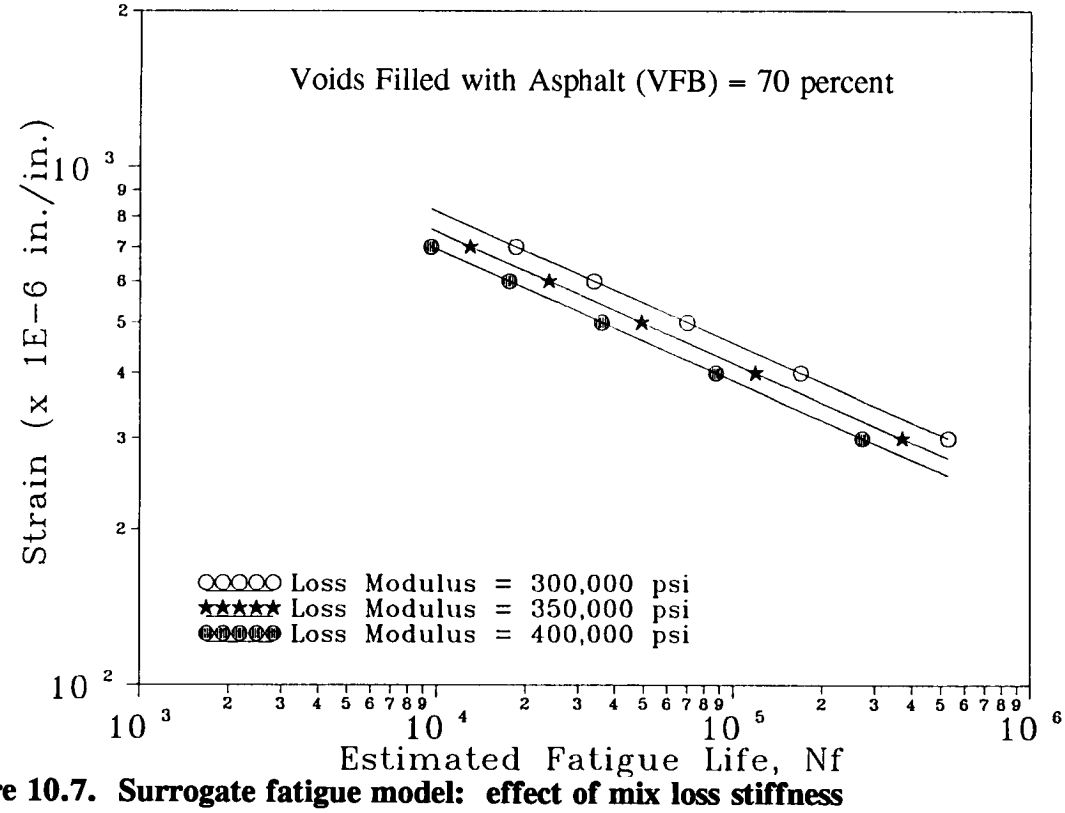

Figure 10.7. Surrogate fatigue model: effect of mix loss stiffness

10.4.3 Implications for Mix Design

When surrogate models such as Equations 10.17 and 10.18 are used in the mix design process, laboratory testing is only required to determine mix stiffness and phase angle. Elimination of the need for more extensive fatigue testing is the primary advantage of surrogate models.

The strain-dependent model, Equation 10.17, requires the use of elastic-layered system models, such as ELSYM, for the mechanistic analysis of in situ pavement structures, while the energy-dependent model, Equation 10.18, requires viscoelastic analysis. Both models properly account for the effects of mix voids (at least within the calibration range of 55 to 80 percent of the voids filled with asphalt) and yield an accuracy which may be sufficient in evaluating many mixes, with a coefficient of determination of 0.85 to 0.86 and a coefficient of variation in the range of 60 to 63 percent. In comparison, however, fatigue testing as currently practiced in SHRP Project A-003A yields superior accuracy as indicated by a coefficient of variation of approximately 40 percent.

Such surrogate models may eventually be useful for evaluating dense-graded mixes with conventional binders—mixes similar to those for which the models were calibrated. When a mix is judged inadequate through a surrogate model, the designer may choose to redesign the mix, strengthen the pavement structure, or obtain a more accurate estimate of fatigue behavior by laboratory fatigue testing. In any case, laboratory fatigue testing continues to be essential for evaluating unconventional mixes and those mixes that incorporate modified binders. Detailed treatment of the use of surrogate models vis-à-vis fatigue testing and their effects on the mix design and analysis system are presented in Part III of this report.

10.4.4 Relationship Between Shear and Flexural Stiffness and Phase Angles

Level 1 of the abridged procedure for the mix design and analysis system for fatigue, outlined in Part III of this report, requires an estimate of the flexural stiffness of the asphalt-aggregate mixes at 20°C (68°F). This estimate is used with multilayer elastic analysis to determine the critical strain that the mix is subjected to under the traffic load and to determine the fatigue life of the mix using surrogate fatigue models.

The SHRP materials testing protocol is expected to specify the use of the shear frequency sweep test for Level 1 of the abridged procedure. Regression calibrations for estimating flexural stiffness and phase angle from the shear stiffness and shear phase angle at 20°C (68°F) and 10 Hz frequency are presented in this section.

In order to calibrate these models, shear stiffness tests were conducted on prismatic specimens, 5.1 cm (2.0 in.) height, 6.4 cm (2.5 in.) width, and 15.2 cm (6.0 in.) length. One specimen from each of the same 32 mixes used in the 8×2 fatigue experiment (Table 10.1) was subjected to shear stiffness testing at 20°C (68°F) and 10 Hz frequency—the same temperature and frequency used in the fatigue experiment.

Each prismatic shear stiffness specimen was subjected to two preconditioning cycles before testing. Each preconditioning cycle consisted of loading the specimen at 10 Hz—100 micro in./in. strain level—in the controlled-strain mode of loading for 100 cycles. Following the preconditioning cycles, the shear stiffness measurements were made at the same frequency and strain level as used for preconditioning. Initial shear stiffness (G_o) was defined to be the stiffness at the 50th load cycle, to correspond with the initial flexural stiffness (S_o) also defined at the 50th cycle in the flexural beam fatigue test in the 8×2 experiment. Stiffness data used for the regression calibration are presented in Appendix B. Further details are presented by Tayebali (1992a).

Model calibrations using linear regression yielded the following relationships:

$$S_o = 3.586 \exp^{-0.045\ V_o} (G_o)^{1.002} \qquad R^2 = 0.834 \quad S_e = 0.227 \qquad (10.19)$$

$$S_o = 1.178 \exp^{0.010\ VFB} (G_o)^{1.015} \qquad R^2 = 0.835 \quad S_e = 0.226 \qquad (10.20)$$

$$\sin\phi_{S_o} = 1.15 (\sin\phi_{G_o})^{0.892} \qquad R^2 = 0.820 \quad S_e = 0.100 \qquad (10.21)$$

where:

S_o	=	initial flexural stiffness, psi,
G_o	=	initial shear stiffness, psi,
ϕ_{S_o}	=	initial phase angle between stress and strain in flexure,
ϕ_{G_o}	=	initial phase angle between stress and strain in shear,
V_o	=	percentage of air-void content,
VFB	=	percentage of voids filled with asphalt, and
S_e	=	standard error of estimate for natural-log-transformed data.

In Equations 10.19 through 10.21 the shear stiffness and sine of the phase angle were statistically significant at the 95 percent confidence level. The air-void contents and voids filled with binder were statistically significant at the 94 percent confidence level.

The steps recommended for using shear stiffness testing in the surrogate fatigue procedure are as follows:

1. Convert the shear stiffness (G_o) at 20°C (68°F) and 10 Hz frequency to a flexural stiffness (S_o) at the same temperature and frequency using Equations 10.19 or 10.20.

2. Convert the sine of the phase angle from the shear test ($\sin\phi_{G_o}$) at 20°C (68°F) and 10 Hz frequency to the sine of the phase angle in flexure ($\sin\phi_{S_o}$) at the same temperature and frequency using Equation 10.21.

3. Estimate the fatigue resistance from a regression model such as Equation 10.17 or 10.18.

More general stiffness models based on combined data from all stiffness experiments will be presented in a later chapter.

10.5 Summary and Conclusion

The expanded test program, also referred to as the 8×2 experiment, was designed to expand the database of information relative to fatigue properties and included laboratory testing of mixes prepared with combinations of eight core MRL asphalts and two core MRL aggregates at two air-void contents. Specific objectives of this experiment were to 1) evaluate improvements in the test method; 2) confirm the effects of mix and test variables found in the 2×2 pilot test program; 3) validate SHRP A-002A hypotheses regarding binder effects on the fatigue response of mixes; 4) explore relationships between mix properties, laboratory fatigue response, and anticipated pavement performance; and 5) develop surrogate models of fatigue and stiffness behavior that, when appropriate, might substitute for laboratory testing.

Major findings and conclusions of these investigations include the following:

- Conventional wisdom generally suggests that lower stiffness asphalt-aggregate mixes are more likely to demonstrate better fatigue resistance under controlled-strain loading than their higher stiffness counterparts. Although binder effects on stiffness and fatigue life confirmed this concept, the effects of air-void content and aggregate type did not. Lower air-void content and crushed, rough-textured aggregates exhibited increased stiffness *and* increased fatigue life.

- A detailed analysis of asphalt effects indicated that the loss stiffness of the aged binder provides a good indication of the relative laboratory fatigue resistance of otherwise identical mixes. Accordingly, the binder loss stiffness seems to be an attractive candidate for inclusion in binder specifications.

- However, the loss stiffness of the binder is not a sufficient indication of the relative fatigue resistance of mixes generally. Other mix characteristics, such as aggregate type and air-void content, also contribute significantly to laboratory fatigue resistance. Accordingly, a binder specification alone is insufficient to ensure satisfactory mix and pavement performance.

- Having laboratory test data on mixes is needed to characterize fatigue behavior. However, laboratory testing must be interpreted by using mechanistic analyses to determine how mixes are likely to perform in a pavement structure under anticipated traffic loads and environmental conditions. Accordingly, mix specifications must address the composite effects of the mix, pavement structure, traffic loading, and environment on pavement performance.

- Calibrations of surrogate fatigue models suggest the following: 1) the effects of initial mix stiffness and phase angle on fatigue life can be expressed with equivalent accuracy by the initial mix loss stiffness; 2) the effect of mix voids on fatigue life can be expressed with equivalent accuracy by either the air-void content or the percentage of voids filled with asphalt; and 3) the effects of initial strain level, mix stiffness, and phase angle on fatigue life can be expressed with equivalent accuracy by the initial dissipated energy per cycle.

- The effects of mix composition on fatigue resistance can be determined most accurately by laboratory fatigue testing, and fatigue testing may be required in order to assess the fatigue resistance of new and unconventional mixes. At the same time, the fatigue resistance of conventional mixes can be estimated, although often less accurately, by using precalibrated regression models.

- Based on the 8×2 study, strain-dependent and energy-dependent models that could be used for surrogate mix analysis are the following:

$$N_f = 466.4 \exp^{0.052\ VFB} (\epsilon_o)^{-3.948} (S''_o)^{-2.270}$$

or

$$N_f = 6.72 \exp^{0.049\ VFB} (w_o)^{-2.047}$$

where:

N_f	=	fatigue life,
ϵ_o	=	initial strain, in./in.,
S''_o	=	initial loss stiffness, psi,
w_o	=	initial dissipated energy per cycle, psi, and
VFB	=	percentage of voids filled with bitumen.

Either model can be used with equivalent accuracy. The strain-dependent model requires the use of elastic-layered system models, such as ELSYM, for the mechanistic analysis of in situ pavement structures; the energy-dependent model requires the use of viscoelastic analysis.

- On the basis of the 8×2 study, regression models that could be used for estimating flexural stiffness and phase angles from shear stiffness and shear phase angles are the following:

$$S_o = 3.586 \exp^{-0.045\ V_o} (G_o)^{1.002}$$

$$S_o = 1.178 \exp^{0.010\ VFB} (G_o)^{1.015}$$

$$\sin\phi_{S_o} = 1.15 (\sin\phi_{G_o})^{0.892}$$

where:

S_o	=	initial flexural stiffness, psi,
G_o	=	initial shear stiffness, psi,
ϕ_{S_o}	=	initial phase angle between stress and strain in flexure,

ϕ_{G_o} = initial phase angle between stress and strain in shear,
V_o = percentage of air-void content, and
VFB = percentage of voids filled with asphalt.

11

Mix Design Study

11.1 Introduction

The scope of SHRP Project A-003A included the development of laboratory tests for asphalt-aggregate mixes, which permit the estimation of mix performance in situ. The mix design study was conducted by Project A-003A to evaluate 1) a new approach for mix design in which the effects of asphalt content and air-void content can be individually evaluated, 2) recommended procedures and equipment for specimen fabrication, and 3) fatigue and permanent deformation characteristics of an example asphalt-aggregate mix using the new mix design methodology and equipment.

In the Marshall and Hveem mix design methodologies, a standard compaction effort is applied to mixes with varying asphalt contents, resulting in an experiment design in which combinations of asphalt content and air-void content are such that the two variables are completely dependent (Sousa et al. 1993). The disadvantage of this type of approach is that the standard compaction level used for specimen preparation may be more or less than that achieved by the contractor during an individual project. The effects of higher or lower levels of compaction and variation in asphalt content on pavement performance, cannot be evaluated individually.

To overcome these problems, a new mix design procedure was proposed (Sousa et al. 1993) in which both asphalt content and air-void content are independent variables, resulting in a rectangular matrix as shown in Table 11.1. This experiment design allows the effects of asphalt content and air-void content to be evaluated individually, thus allowing performance analysis of each candidate asphalt content over a range of possible air-void contents in the field.

In the 2×2 pilot test program two asphalt contents were used—optimum and high. The optimum asphalt content corresponded to that obtained using the Hveem mix design procedure. The high asphalt content was the optimum plus 0.6 percent (by weight of aggregate), approximately the design asphalt content obtained by using the Marshall mix

Table 11.1. Average air-void content for matrix of asphalt content and air-void level used in the mix design study for fatigue

Void Level (%)	Asphalt Content (%) by wt. of Aggregate			
	4.5	5.0	5.5	6.0
4 - 5	4.7	—	—	4.3
5 - 6	5.8	—	—	5.0
6 - 7	—	—	—	—
7 - 9	7.9	—	—	7.7

Table 11.2. Mix design fatigue experiment

Number of Asphalts	1 — MRL core asphalt AAG-1
Number of Aggregates	1 — MRL aggregate RB
Asphalt Content	2 — 4.5 and 6.0% by weight of aggregate
Air-void Levels	3 — 4-5, 5-6, and 7-9%
Strain Levels	Variable — 200 to 700 micro in./in.
Replicates at Each Strain Level	None
Temperature	1 — 20°C (68°F)
Frequency	1 — 10 Hz (sinusoidal)
Specimen Size	2 in. (5.1 cm) height, 2.5 in. (6.35 cm) width, 15 in. (38.1 cm) length
Total Number of Mixes Tested	6
Total Number of Specimens Tested	22

design procedure. Statistical analysis of the fatigue test results from flexural beam controlled-stress and controlled-strain tests, trapezoidal cantilever controlled-stress tests, and diametral controlled-stress tests indicated that asphalt content did not significantly affect fatigue life for these factor levels. This finding was probably the result of the very narrow range of asphalt contents selected as optimum and high. In the 8×2 expanded test program (Table 11.2), asphalt content was not a variable; therefore, the evaluation of the effect of asphalt content on fatigue, as measured with the new SHRP A-003A equipment and procedures, was a primary objective of this mix design study.

The mix design study results for fatigue also allowed to some extent the validation of the surrogate fatigue models developed during the 8×2 expanded test program detailed in Chapter 10. Although the mix design study involved both fatigue and permanent deformation characteristics, the presentation herein is limited to fatigue.

11.2 Selection of Mix and Testing Variables

The mix and test variables included in this study were following:

- **Asphalts.** One MRL asphalt was used: AAG-1.
- **Aggregates.** One MRL aggregate was used: RB, a crushed granite. This material has been used in a large number of SHRP experiments. The aggregate gradation used conformed to that shown in Table 10.3.
- **Asphalt Content.** Two asphalt contents were used: 4.5 and 6 percent, by weight of aggregate.
- **Air-Void Content.** Three levels of air-void content were used: 4 to 5 percent, 5 to 6 percent, and 7 to 9 percent.
- **Strain Levels.** Four strain levels were used: 200, 300, 400, and 700 micro in./in.
- **Replicates.** None.
- **Test Frequency.** All tests were performed in the controlled-strain mode of loading at a frequency of 10 Hz with sinusoidal loading (no rest periods).
- **Test Temperature.** Tests were performed at 20°C (68°F).
- **Conditioning.** All mixes were short-term aged in a forced draft oven at 135°C (275°F) for 4 hours. No water conditioning was included in this test program.

Specimens, 6.35 cm (2.5 in.) wide, 5.1 cm (2.0 in.) tall, and 38 cm (15.0 in.) long, were sawed from slabs prepared using the UCB rolling-wheel compaction method. The response variables (dependent variables) measured included 1) initial flexural stiffness measured at the 50th load cycle, 2) fatigue life—the number of cycles to a 50 percent reduction in initial flexural stiffness, 3) initial dissipated energy per cycle measured at the 50th load cycle, and 4) cumulative or total dissipated energy associated with the fatigue life.

11.3 Test Results

The method of statistical analysis for the mix design test results is similar to the procedure used earlier for the 2×2 pilot test program and the 8×2 expanded test program. A summary of the analysis and related findings follows. Test results for the mix design study are included in Appendix C of this report.

11.3.1 General Linear Modeling

In this study the independent variables were asphalt content, air-void content, and strain level. Of these three variables, the effect of asphalt content was the most important consideration since the effects of air-void content and strain level had been previously established in both the 2×2 pilot test program and the 8×2 expanded test program. Tables 11.3 through 11.5 present a summary of stepwise-regression modeling, or general linear modeling (GLM) for the three response variables. Table 11.6 shows the significant independent variables in the GLM for the three response variables. The summary statistics are presented in Table 11.7.

The ANOVA results on the GLM indicated that fatigue life and cumulative dissipated energy could be explained well by the main effects of asphalt content, air-void content, and strain level as indicated by the coefficients of determination (R^2) of 0.98 and 0.93 and coefficients of variation of 29.4 and 30.0 percent for fatigue life and cumulative dissipated energy, respectively (Table 11.7). These results are similar to those obtained for the 8×2 expanded test program presented in Table 10.5. Initial flexural stiffness could not be explained well by the main effects and their two-factor interactions, as indicated by a coefficient of determination of 0.66, which is lower than the 0.96 obtained for the 8×2 expanded test program.

11.3.2 Summary of the Results from GLM

The ANOVA for the main effects and their two-factor interactions are shown in Table 11.6. It is interesting that all the main effects and two-factor interactions were significant at the 95 percent confidence level. Table 11.8 contains the average values of stiffness, fatigue life, and cumulative dissipated energy computed by using the regression models presented in Tables 11.3 through 11.5. Comparisons of average values were made at asphalt contents of 4.5 and 6.0 percent, air-void contents of 4 and 8 percent, and strain levels of 200 and 700 micro in./in. and summarized below:

Table 11.3. Results of the GLM for stiffness, mix design study

Dep Var = $Ln(S_o)$ N = 22 Multiple R = 0.812 Squared Multiple R = 0.660
Adjusted Squared Multiple R = 0.603 Standard Error of Estimate = 0.134

Variable	Coefficient	STD Error	STD Coef	Tolerance	T	P (2 Tail)
Constant	16.688	0.849	0.000	.	19.659	0.000
AC (%)	-0.448	0.158	-1.621	0.0577	-2.833	0.011
V_o (%)	-0.447	0.137	-3.215	0.0195	-3.266	0.004
AC * V_o	0.066	0.026	2.743	0.0164	2.553	0.020

Analysis of Variance

Source	Sum-of-Squares	DF	Mean-Square	F-Ratio	P
Regression	0.623	3	0.208	11.642	0.000
Residual	0.321	18	0.018		

Table 11.4. Results of the GLM for fatigue life, mix design study

Dep Var = $Ln(N_f)$ N = 22 Multiple R = 0.988 Squared Multiple R: 0.977
Adjusted Squared Multiple R = 0.973 Standard Error of Estimate = 0.288

Variable	Coefficient	STD Error	STD Coef	Tolerance	T	P (2 Tail)
Constant	-19.391	1.167	0.000	.	-16.613	0.000
$Ln(\epsilon_o)$	-3.302	0.130	-0.913	0.9976	-25.419	0.000
AC (%)	0.743	0.082	0.326	0.9872	9.021	0.000
V_o (%)	-0.148	0.041	-0.129	0.9849	-3.572	0.002

Analysis of Variance

Source	Sum-of-Squares	DF	Mean-Square	F-Ratio	P
Regression	62.880	3	20.960	253.118	0.000
Residual	1.491	18	0.083		

Table 11.5. Results of the GLM for cumulative dissipated energy, mix design study

Dep Var = $Ln(W_D)$ N = 22 Multiple R = 0.964 Squared Multiple R = 0.929
Adjusted Squared Multiple R = 0.918 Standard Error of Estimate = 0.293

Variable	Coefficient	STD Error	STD Coef	Tolerance	T	P (2 Tail)
Constant	-7.043	1.187	0.000	.	-5.933	0.000
$Ln(\epsilon_o)$	-1.356	0.132	-0.643	0.9976	-10.267	0.000
AC (%)	0.774	0.084	0.583	0.9872	9.250	0.000
V_o (%)	-0.223	0.042	-0.333	0.9849	-5.287	0.000

Analysis of Variance

Source	Sum-of-Squares	DF	Mean-Square	F-Ratio	P
Regression	20.318	3	6.773	79.081	0.000
Residual	1.542	18	0.086		

Table 11.6. Statistically significant effects in GLM for stiffness, fatigue life, and cumulative dissipated energy

Factor/Interaction	Initial Flexural Stiffness	Fatigue Life	Cumulative Dissipated Energy
Asphalt Content	S	H	H
Air-Void Content	H	H	H
Strain		H	H
Asphalt Content * Air-Void Content	S		
Asphalt Content * Strain			
Air-Void Content * Strain			

Notes:	Description	Probability
	H = highly significant	less than 0.01
	S = significant	0.01 to 0.05
	B = barely significant	less than 0.10
	Blank = not significant	greater than 0.10

Table 11.7. Summary statistics from GLM for stiffness, fatigue life, and cumulative dissipated energy

Statistics	Stiffness	Fatigue Life	Cumulative Dissipated Energy
R^2	0.660	0.977	0.930
Root Mean Square Error (Ln)	0.134	0.288	0.293
Coefficient of Variation (%)	13.5	29.40	30.00

Notes: R^2 = coefficient of determination; coefficient of variation = $100 * (e^{MSE} - 1)^{0.5}$; e = base of natural logarithm; and MSE = Mean square error.

Table 11.8. Average stiffness, fatigue life, and cumulative dissipated energy

Effect	Flexural Stiffness (psi)	Fatigue Life (cycles)	Cumulative Dissipated Energy (psi)
Asphalt Content			
4.5%	957,400	9100	330
6.0%	885,500	27,900	1100
Difference	-8%	67%	70%
Air-Void Content			
4.0%	1,125,800	21,500	920
8.0%	753,100	11,900	380
Difference	-33%	-45%	-59%
Strain Level			
200 micro in./in.	921,000	126,200	1390
700 micro in./in.	921,000	2000	250
Difference	0%	-98%	-82%

Notes: Air-void contents adjusted to 4 and 8%.
Averages based on the mean of log-transformed data.
Percentage difference is expressed as a percentage of the larger value.

Effect	Flexural Stiffness	Fatigue Life	Cumulative Dissipated Energy
Asphalt Content	8% decrease from 4.5% to 6%	67% increase from 4.5% to 6%	70% increase from 4.5% to 6%
Air-Void Contents	33% decrease from 4% to 8%	45% decrease from 4% to 8%	59% decrease from 4% to 8%
Strain (micro in./in.)	Not affected	98% decrease from 200 to 700	82% decrease from 200 to 700

Asphalt content significantly affected the three response variables. Average flexural stiffness decreased with increasing asphalt content. Both fatigue life and cumulative dissipated energy increased with increasing asphalt content. For flexural stiffness, an interaction between asphalt content and air-void content was noted.

As anticipated, the effect of void content was significant for all three response variables. The only interaction between the dependent variables as noted before was between asphalt content and air-void content. Although the actual air-void content in the mix design experiment varied approximately between 4 and 8 percent, comparisons were made at 4 percent and 8 percent voids only. As observed earlier in the 8×2 expanded test program, the effect of air-void content on all three response variables was that of decreasing values of average stiffness, fatigue life, and cumulative dissipated energy with an increase in void content.

The effect of strain level was significant for fatigue life and cumulative dissipated energy. Both the fatigue life and cumulative dissipated energy decreased as the strain level increased. Stiffness did not change significantly between the strain extremes of 200 and 700 micro in./in. used in the experiment.

11.4 Validation of Surrogate Fatigue Model Using the Mix Design Experiment

The mix design study data presented an opportunity for validating the surrogate fatigue model developed from the 8×2 expanded test program. The strain-based surrogate model used is as follows:

$$N_f = 466.38 \exp^{(0.052\ VFB)} (\epsilon_o)^{-3.948} (S''_o)^{-2.270} \qquad (11.1)$$

where: N_f = fatigue life,
ϵ_o = initial tensile strain, in./in.,
S''_o = initial flexural loss stiffness, psi,
VFB = percent voids filled with binder, and
exp = exponent of natural logarithm.

In general, fatigue life estimates from the surrogate model exceeded measurements in the mix design study by a factor of approximately 6. Figure 11.1 shows the relationship between predicted and measured cycles to failure. When modeling fatigue behavior, the strain exponent for the mix design data appeared to be different from that for the 8×2 expanded test program (Table 11.9).

Figure 11.2 shows fatigue life, estimated by using the models of Table 11.1 at 400 micro in./in. strain from each group of the test (i.e., each level of air-void contents and each level of asphalt content). The results are consistent and reasonable: fatigue life decreases with increased air-void contents and lower asphalt contents.

The effects of air-void and asphalt contents on average flexural stiffness are shown in Figure 11.3. For the higher asphalt content, there appears to be an optimum air-void content for maximum stiffness. Whether such an optimum is real or a result of testing variability or error cannot be determined.

A stepwise-regression model fitted to the mix-design-fatigue-life data is as follows:

$$N_f = 638.42 \exp^{(0.107\ VFB)} (\epsilon_o)^{-3.309} (S''_o)^{-2.309} \qquad R^2 = 0.94 \qquad CV = 50\% \qquad (11.2)$$

This model was judged to be adequate with the percentage of voids filled with asphalt, strain, and loss stiffness as independent variables. The form model was similar to that obtained from the 8×2 expanded test program (Equation 11.1), with loss stiffness being significant at the 91 percent confidence level and the two other variables being significant at the 95 percent confidence level. When percentage of voids filled with asphalt was replaced by air-void content, the loss stiffness did not remain statistically significant in the model; however, the stepwise-regression results indicated that asphalt content was highly significant. The following model resulted:

$$N_f = 3.79 \times 10^{-9} \exp^{(0.743\ AC\ -\ 0.148\ V_o)} (\epsilon_o)^{-3.302} \qquad R^2 = 0.98 \qquad CV = 30\% \qquad (11.3)$$

where: N_f = fatigue life,
ϵ_o = initial tensile strain, in./in.,
S''_o = initial flexural loss stiffness, psi,
V_o = air-void content,
AC = asphalt content by weight of aggregate,
exp = exponent of natural logarithm, and
CV = coefficient of variation.

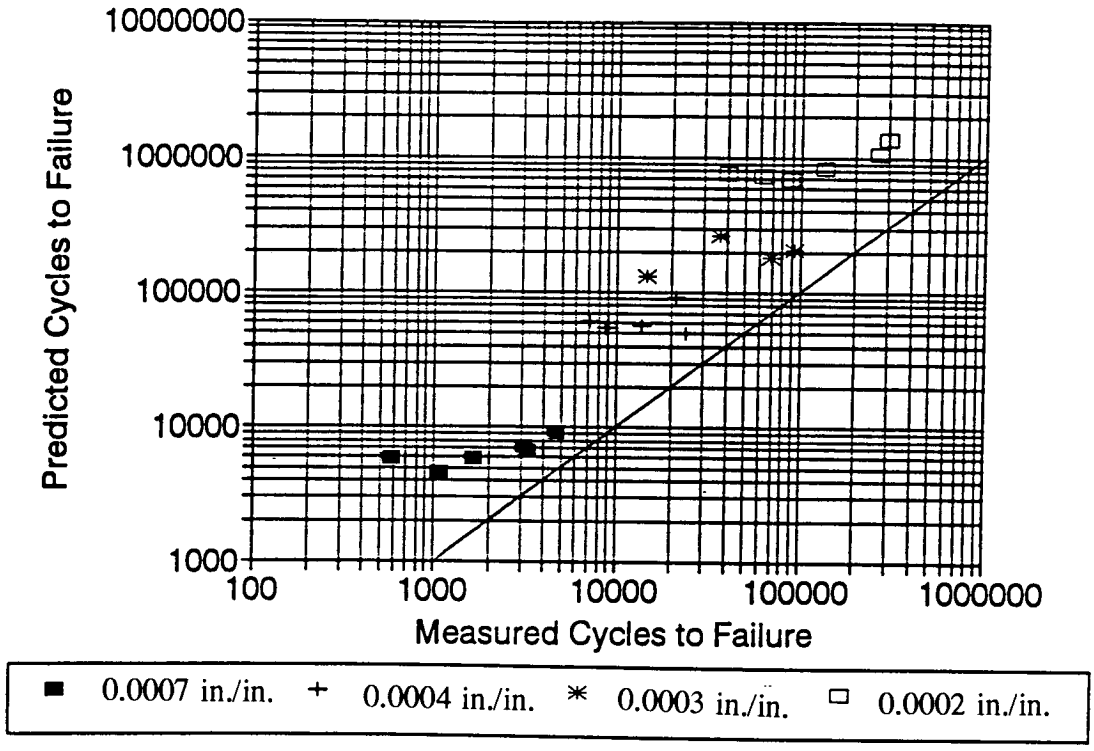

Figure 11.1. Predicted versus measured cycles to failure in the mix design experiment

Table 11.9. Fatigue life versus strain calibrations, mix design study

Asphalt Content (% by wt. of aggregate)	Average Air - Void Content (%)	Fatigue-Life-Strain Relationship		R^2
		K_1	K_2	
4.5	4.7	5.6565×10^{-8}	-3.3071	0.96
4.5	5.8	8.1051×10^{-8}	-3.2216	0.99
4.5	7.8	2.2117×10^{-8}	-3.3468	0.92
6.0	4.3	1.1525×10^{-7}	-3.3442	0.98
6.0	5.0	1.1292×10^{-8}	-3.6339	0.99
6.0	7.7	4.4955×10^{-7}	-3.1225	0.95

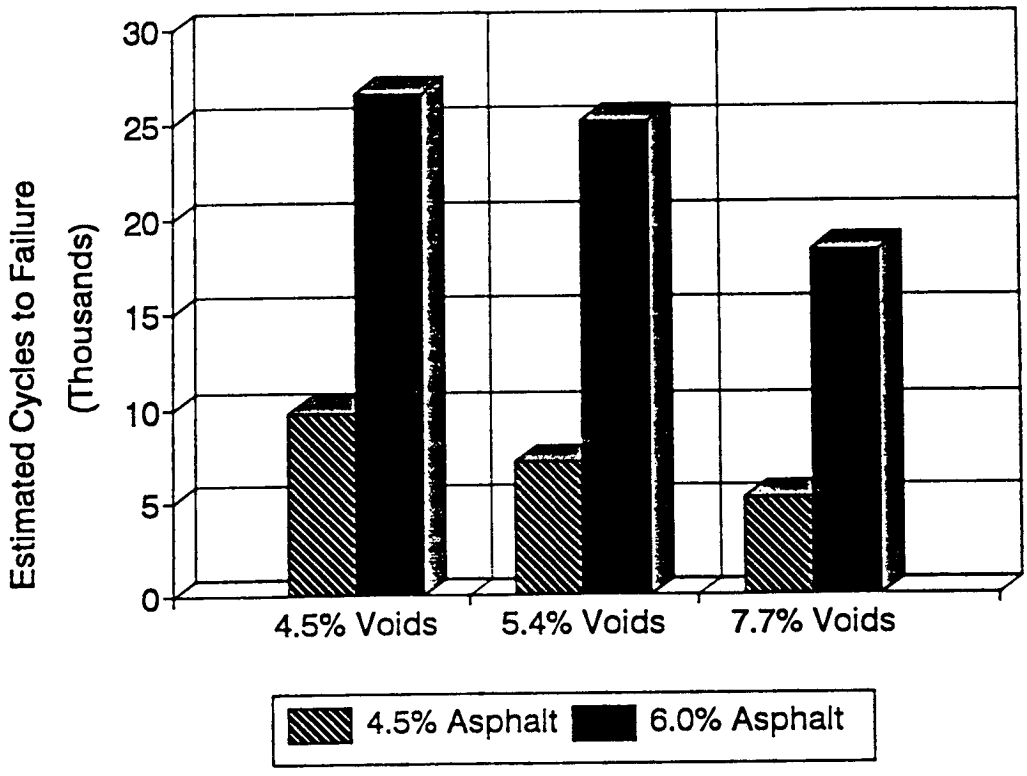

Figure 11.2. Estimated cycles to failure (at 400 micro in./in. strain) versus air-void content

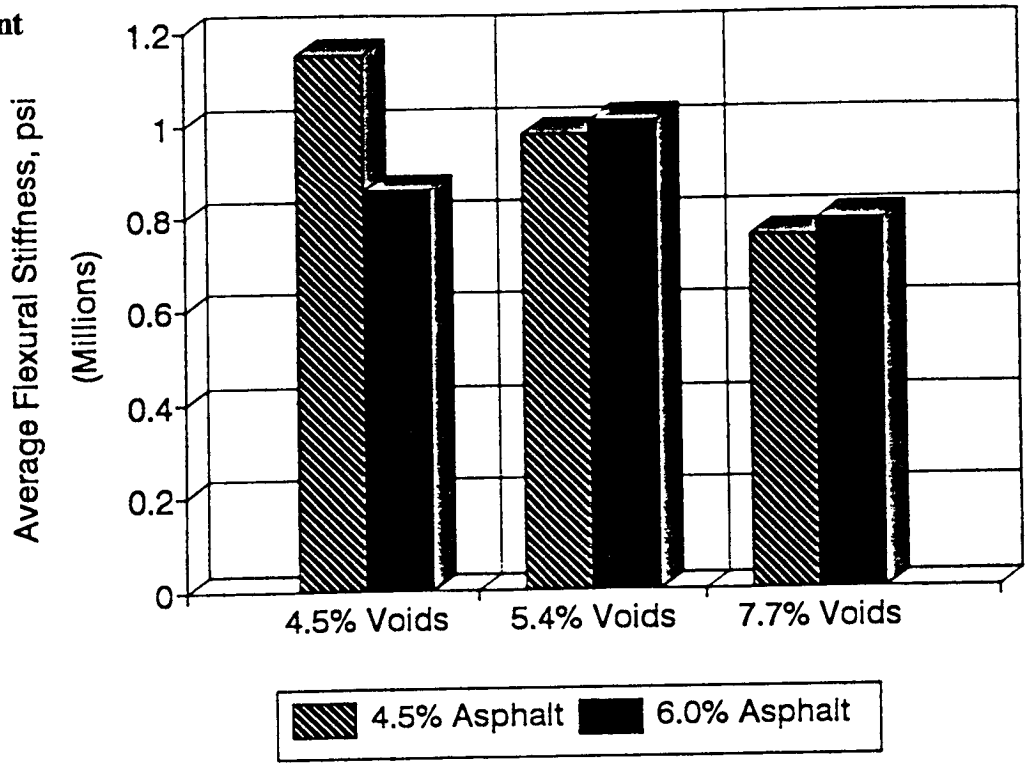

Figure 11.3. Average stiffness versus asphalt content

As discussed earlier, the effect of increasing asphalt content was to decrease stiffness and to increase fatigue life. The effect of increasing air-void content was to decrease both stiffness and fatigue life. Moreover, results from the 2×2 pilot test program and 8×2 expanded test program indicate that the effect of increased stiffness due to changes in asphalt or aggregate source results in decreased fatigue life in the controlled-strain mode of loading.

These results suggest that the effects of asphalt content on the fatigue resistance of mixes are not fully explained by their effects on mix stiffness. The percentage of voids filled with asphalt appears to better account for the effects of both the air-void and the asphalt contents; consequently, surrogate fatigue models calibrated with strain, loss stiffness, and the percentage of voids filled with asphalt are superior to models calibrated with strain, loss stiffness, and air-void contents.

Even though the testing protocol and equipment were the same in the mix design experiment and the 8×2 expanded test program, models developed during the expanded test program did not accurately simulate the behavior observed during the mix design experiment. Differences between the performance of the two aggregates—RB in the mix design experiment and RH and RD in the 8×2 expanded test program—were noted but cannot be attributed to specific aggregate characteristics. Whether the differences between the fatigue lives found using the surrogate model and those observed in the mix design study are large enough to be of practical significance has not been determined.

11.5 Summary

The mix design experiment examined the effects of asphalt content and air-void content on fatigue life for a single combination of asphalt and aggregate. Both variables had significant effects on all three response variables—initial flexural stiffness, fatigue life, and cumulative dissipated energy. Increasing asphalt content resulted in decreasing stiffness and an increase in both the fatigue life and cumulative dissipated energy. Increases in air-void content resulted in decreases in all three response variables.

On average, estimates from the strain-based surrogate model developed during the 8×2 expanded test program exceeded measurements in the mix design experiment by a factor of approximately 6, even though the testing protocol and equipment for both experiments were the same. Differences between the performance of the two aggregates—RB in the mix design experiment and RH and RD in the 8×2 expanded test program—were noted but could not be attributed to specific aggregate characteristics. Whether the differences between model-estimated fatigue lives and the experimentally observed lives are large enough to be of practical significance was not determined.

Model fitting on the mix design data was generally judged to be adequate. The effects of asphalt content, air-void content, and strain level on the response variables were found to be reasonable and consistent with the results of prior studies. Strain-based, fatigue life, surrogate models with the variable percentage of voids filled with asphalt, incorporating the

effects of both the air-void and asphalt contents, appear to be superior to models which include only the variable of air-void content.

12

Temperature Equivalency Factors Experiment

12.1 Introduction

Conventional fatigue analyses typically accommodate variations in temperature by means of the linear-summation-of-cycle-ratios hypothesis. According to this methodology, the temperature environment is approximated by a limited number of discrete categories (such as average temperature by month), and the ratio of the predicted to permissible fatigue damage is summed over all categories. The design is considered satisfactory if the summation does not exceed unity. Although such procedures have been reasonably successful, they are considered too cumbersome for routine mix analysis. Instead, the SHRP Project A-003A mix design and analysis system proposes to limit, where possible, fatigue testing or other estimates of fatigue life to a single temperature and to express the destructive effects of anticipated traffic in the field as ESALs at that temperature. These tasks are accomplished through the use of temperature equivalency factors (TEFs). This approach is expected to simplify testing, with a resulting increase in productivity and reduced costs.

To support the development of TEFs detailed in Part III of this report, an experimental fatigue testing program—the TEF experiment—was carried out. The two objectives of this experiment were 1) to develop a strain-versus-fatigue-life (ϵ-N_f) relationship for different temperatures, and 2) to develop a relationship between stiffness and temperature.

To a lesser extent, the TEF experiment also allowed the surrogate fatigue models developed during the 8×2 expanded study to be validated and allowed the applicability of the models to temperatures other than the 20°C (68°F) used in the 8×2 expanded test study to be assessed.

12.2 Selection of Mix and Testing Variables

The mix and test variables included in this study were the following:

- **Asphalts.** One MRL asphalt was used: AAD-1.

- **Aggregates.** One MRL aggregate was used: RH, a partially crushed Greywacke river gravel. The aggregate gradation used conformed to that shown in Table 10.3.

- **Asphalt Content.** One asphalt content was used: 5.2 percent, by weight of aggregate.

- **Air-Void Content.** The target air-void content used was 4 percent plus or minus 1 percent.

- **Strain Levels.** Strain levels selected varied between 300 and 1200 micro in./in., such that the fatigue life of the specimens ranged between 10,000 and 500,000 cycles.

- **Replicates.** Testing replicate specimens was not planned in this study; however, some replicates were tested at 5°, 10°, and 20°C (41°, 50°, and 68°F) at selected strain levels.

- **Test Frequency.** All tests were performed in the controlled-strain mode of loading at a frequency of 10 Hz with sinusoidal loading (no rest periods).

- **Test Temperature.** Tests were performed at four temperatures: 5°, 10°, 20°, and 25°C (41°, 50°, 68°, and 77°F).

- **Conditioning.** All mixes were short-term aged in a forced draft oven at 135°C (275°F) for 4 hours. No water conditioning was included in this test program.

Features of the TEF experiment are summarized in Table 12.1. Specimens, 6.35 cm (2.5 in.) wide, 5.1 cm (2 in.) tall, and 38 cm (15.0 in.) long, were sawed from slabs prepared by rolling-wheel compaction. The response variables (dependent variables) measured included 1) initial flexural stiffness measured at the 50th load cycle, 2) fatigue life—the number of cycles to 50 percent reduction in initial flexural stiffness, 3) initial dissipated energy per cycle measured at 50th load cycle, and 4) cumulative or total dissipated energy associated with the fatigue life.

12.3 Test Results

Test results for the TEF experiment are presented in Appendix D. Fatigue-life-versus-strain (ϵ-N_f) relationships for each temperature are shown in Figure 12.1 and summarized below and in Table 12.2.

Table 12.1. Features of the TEF Experiment

Number of Asphalts	1 — MRL core asphalt AAD-1
Number of Aggregates	1 — MRL aggregate RH
Asphalt Content	1 — Optimum (Hveem), 5.2% by wt. of aggregate
Air-Void Content	1 — 4 ± 1 percent
Strain Levels	Variable — 300 to 1200 micro in./in.
Replicates at Each Strain Level	None
Temperature	4 — 5°, 10°, 20°, and 25°C (41°, 50°, 68°, and 77°F)
Frequency	1 — 10 Hz (sinusoidal)
Specimen Size	2 in. (5.1 cm) height, 2.5 in. (6.35 cm) width, 15 in. (38 cm)
Total Number of Mixes Tested	1
Total Number of Specimens Tested	23

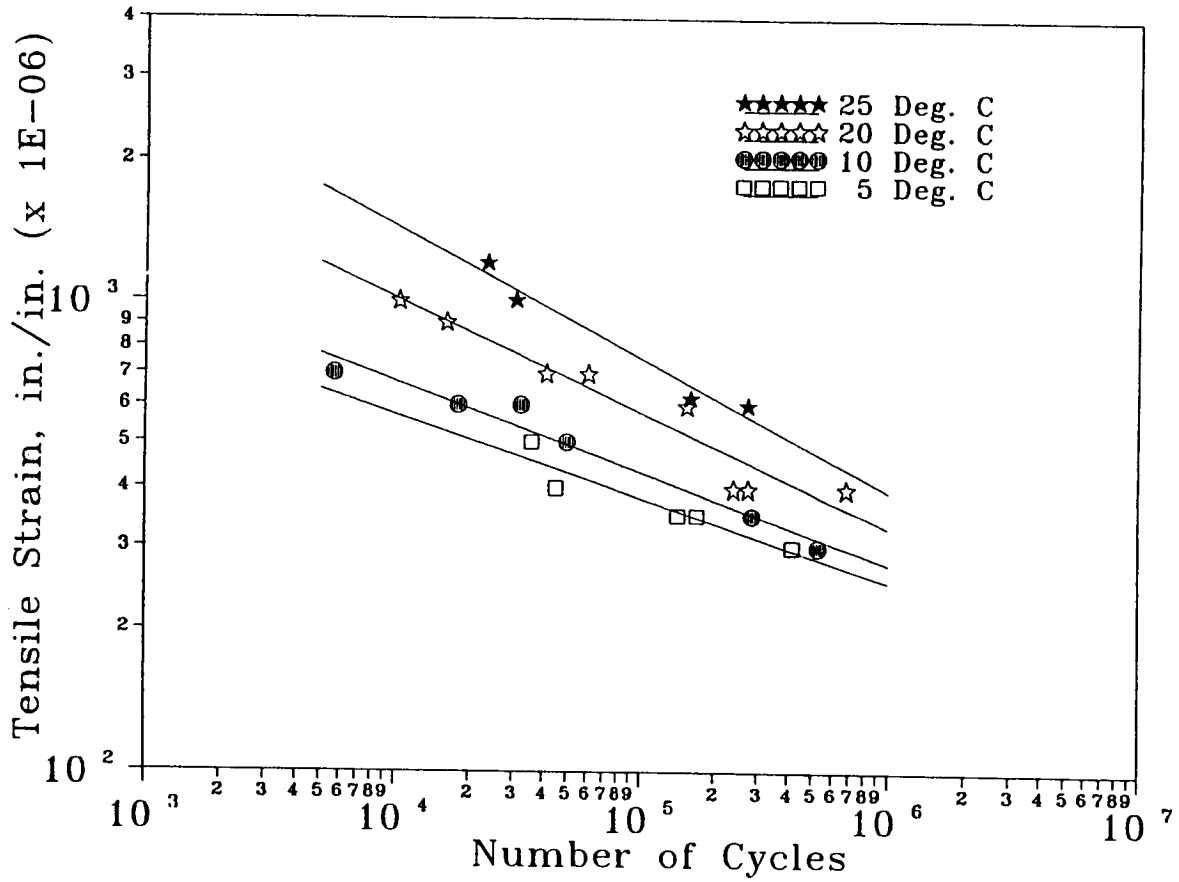

Figure 12.1. Strain-versus-fatigue-life relationships for different temperatures

Table 12.2. Fatigue-life-versus-strain calibrations from TEF Experiment

Temperature (°C)	K_1	K_2	R^2	CV (%)
5	$1.088 * 10^{-12}$	-4.963	0.881	42
10	$1.610 * 10^{-12}$	-4.988	0.966	36
20	$5.600 * 10^{-8}$	-3.783	0.922	46
25	$2.043 * 10^{-6}$	-3.422	0.964	29

Temperature	Model	R^2	CV (%)
25°C (77°F)	$N_f = 2.043*10^{-6} (\epsilon_o)^{-3.422}$	0.964	29
20°C (68°F)	$N_f = 5.600*10^{-8} (\epsilon_o)^{-3.783}$	0.922	46
10°C (50°F)	$N_f = 1.610*10^{-12} (\epsilon_o)^{-4.988}$	0.966	36
5°C (41°F)	$N_f = 1.088*10^{-12} (\epsilon_o)^{-4.963}$	0.881	42

where: N_f = fatigue life to 50-percent reduction in initial stiffness, and
ϵ_o = strain in./in.

Each fatigue relationship is a linear regression calibration of the form

$$N_f = K_1 \epsilon_o^{K2} \quad (12.1)$$

where: N_f and ϵ_o are as defined previously, and
K_1 and K_2 = experimentally determined coefficients.

The model fits are strong: coefficients of determination (R^2) vary between 0.88 and 0.97 and coefficients of variation vary between 29 and 46 percent. The coefficients of variation compare well with those observed in the 8×2 expanded test program and the mix design study. It should be noted that air-void contents or voids filled with asphalt were not statistically significant for these models developed for *each temperature*. Moreover, stiffness or loss stiffness (loss modulus) was not statistically significant for these models either. *The stiffness or voids were not expected to be statistically significant in these models since, for a given mix at a given temperature, both of these parameters are essentially constant.* However, for a combined fatigue model the stiffness (or loss stiffness) is expected to be significant since mix stiffness varies with temperature.

The absolute value of the strain-life slope (K_2) of the fatigue-life-versus-strain relationships (Table 12.2) varies with temperature and generally increases with decreasing temperature. The dependence of K_2 on temperature, shown in Figure 12.2, appears to be fairly linear with temperature. Because of the stiffness-temperature relationship of asphalt mixes (Figure 12.3), K_2 also varies with the stiffness of the mix, as shown in Figure 12.4. Strong

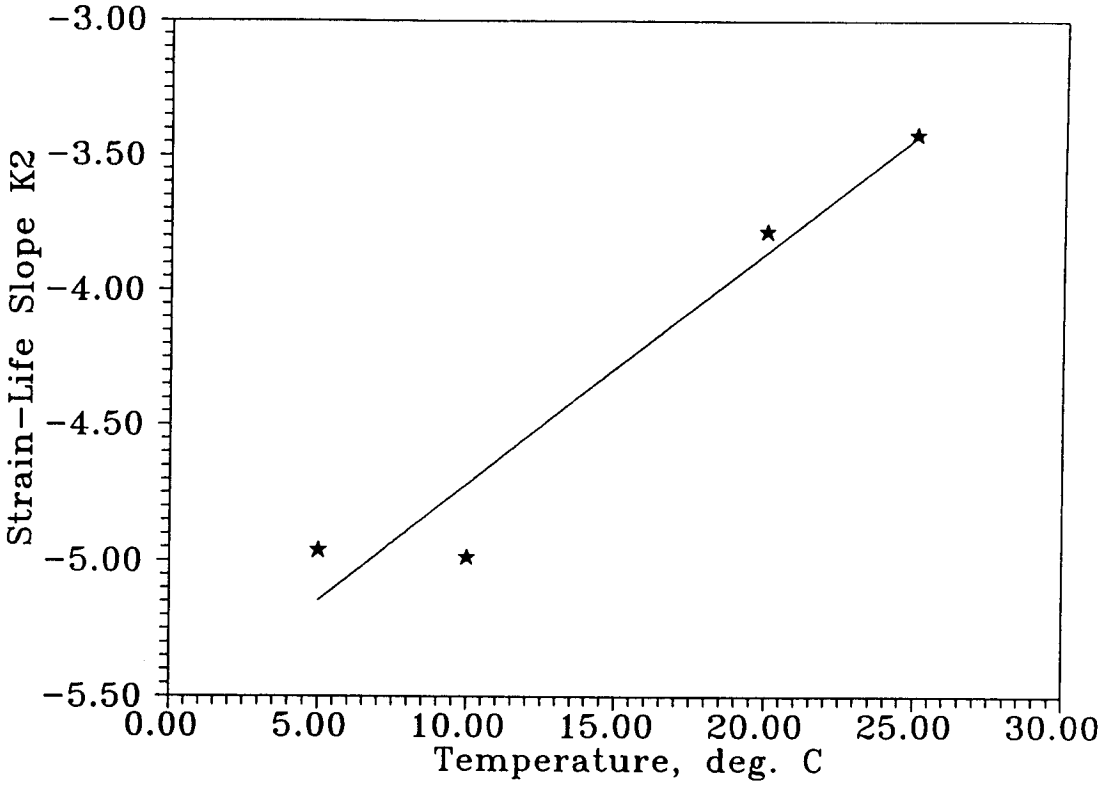

Figure 12.2. Strain-life slope K_2 versus temperature

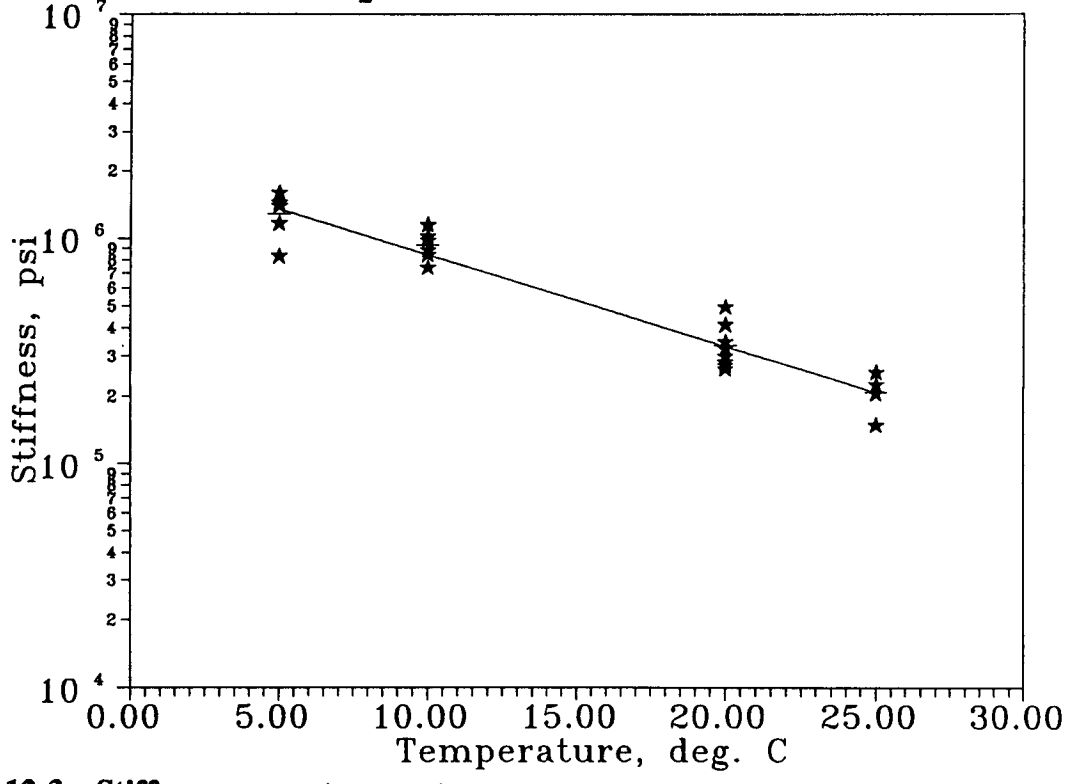

Figure 12.3. Stiffness versus temperature

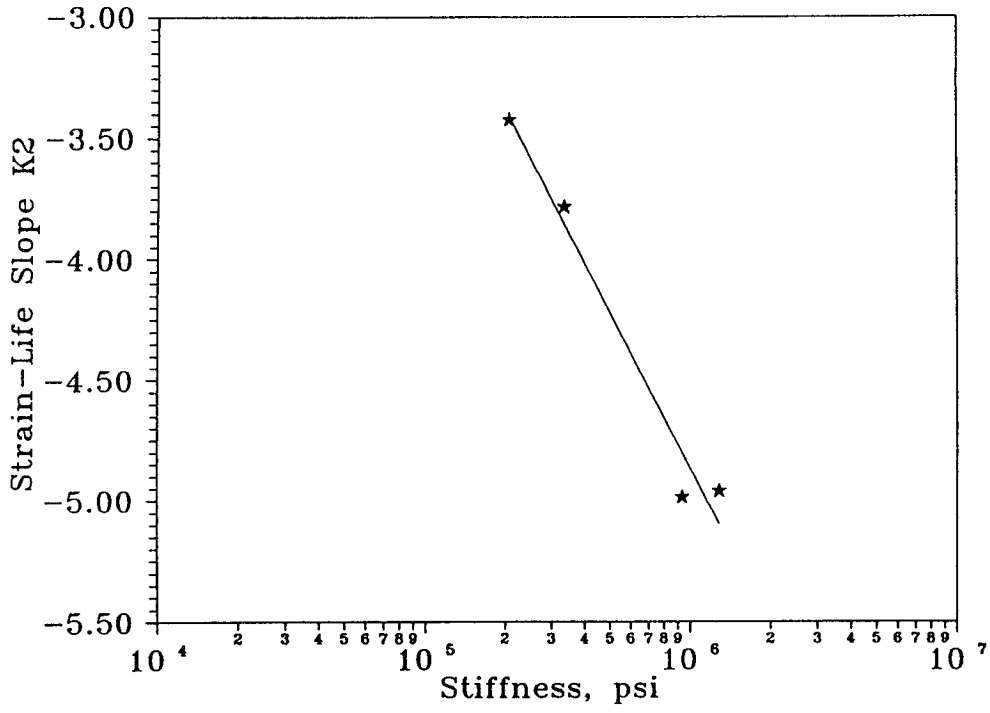

Figure 12.4. Strain-life slope versus stiffness

regression model fits between K_2, temperature, and stiffness are indicated by high coefficients of determination for the following relationships:

$$K_2 = 0.086*\text{Temp} - 5.575 \qquad R^2 = 0.97 \qquad (12.2)$$

and

$$K_2 = 7.753 - 2.104 \log(S_o) \qquad R^2 = 0.94 \qquad (12.3)$$

where:
K_2 = strain-life slope,
Temp = temperature in °C, and
S_o = initial flexural stiffness, psi.

12.4 Model Calibrations

The modeling effort for the TEF data included calibrations of the stiffness, phase angle, and loss stiffness versus temperature relationships and development of temperature-dependent fatigue life models. Results of the model calibrations are summarized in the following sections.

12.4.1 Stiffness, Phase Angle, and Loss Stiffness as Functions of Temperature

As anticipated, stiffness, phase angle, and loss stiffness correlated well with temperature. Linear regression calibrations resulted in the following relationships:

$$S_o = 2{,}162{,}986 \exp^{-0.094\ Temp} \qquad R^2 = 0.92 \qquad (12.4)$$

$$\phi_o = 9.667 + 1.627\ Temp \qquad R^2 = 0.93 \qquad (12.5)$$

$$S''_o = 560{,}173 \exp^{-0.048\ Temp} \qquad R^2 = 0.86 \qquad (12.6)$$

where:

Temp	=	temperature, °C,
S_o	=	initial loss stiffness, psi,
ϕ_o	=	phase angle between stress and strain,
S''_o	=	initial loss stiffness, psi, and
exp	=	exponent of natural logarithm.

Phase angle was also found to be highly correlated with initial mix stiffness:

$$\phi_o = 260.096 - 17.172\ Ln(S_o) \qquad R^2 = 0.98 \qquad (12.7)$$

where: Ln = base of the natural logarithm.

While Figure 12.3 shows the stiffness-temperature relationship, Figures 12.5 and 12.6 show the phase angle and loss stiffness versus temperature relationships, respectively. The relationship of phase angle versus stiffness is presented in Figure 12.7.

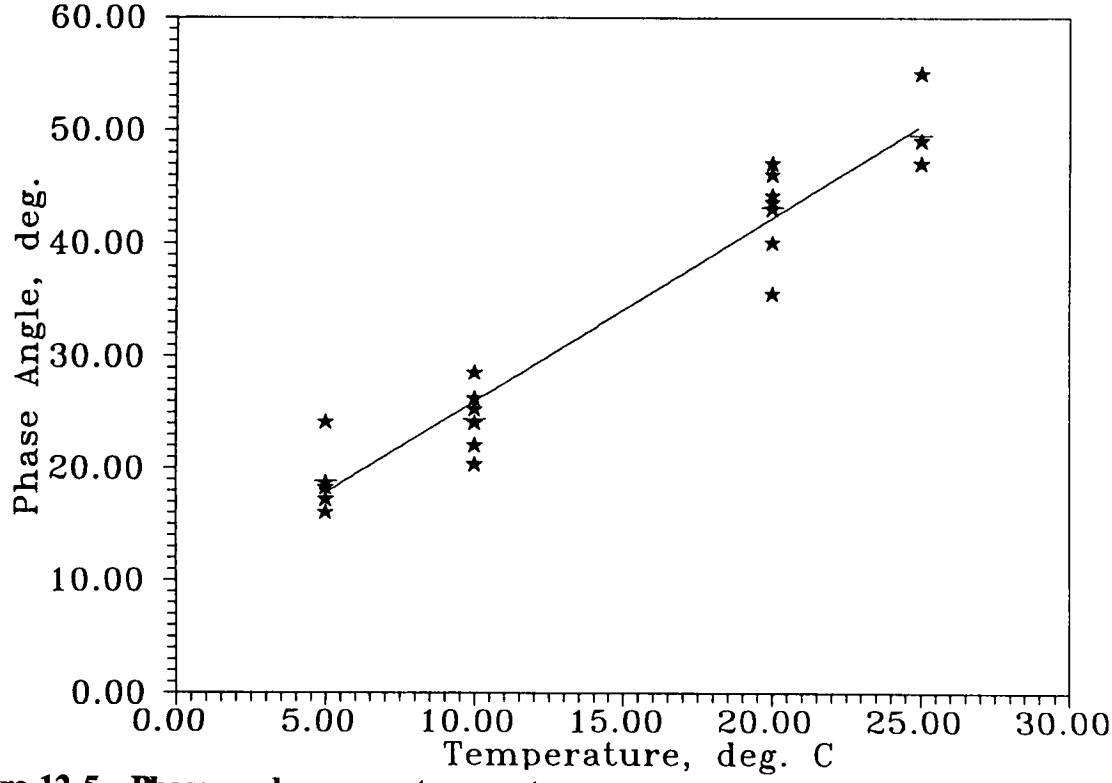

Figure 12.5. Phase angles versus temperature

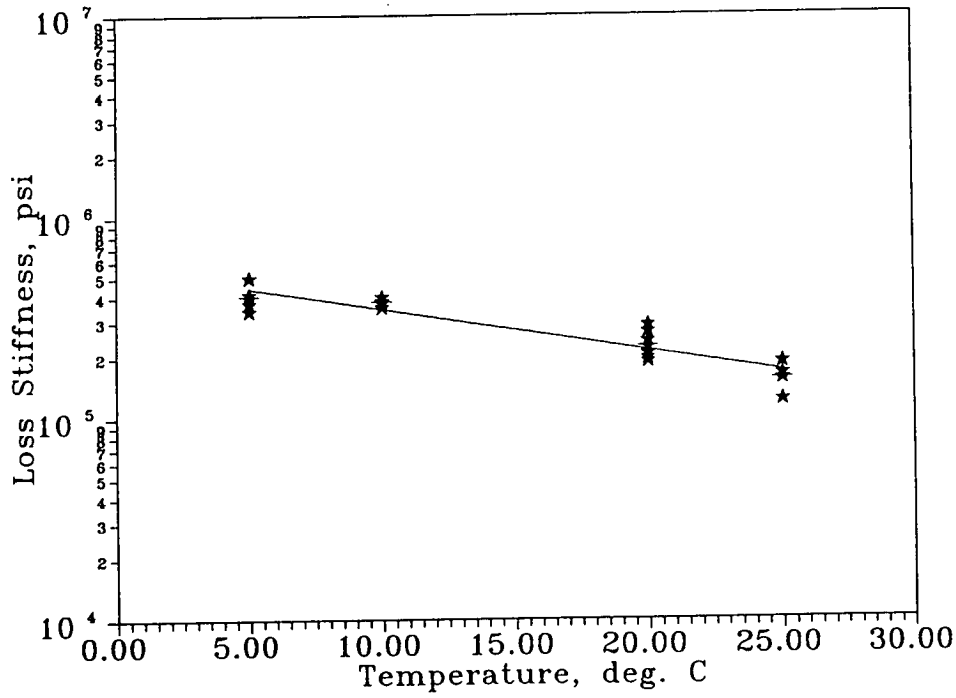

Figure 12.6. Loss stiffness versus temperature

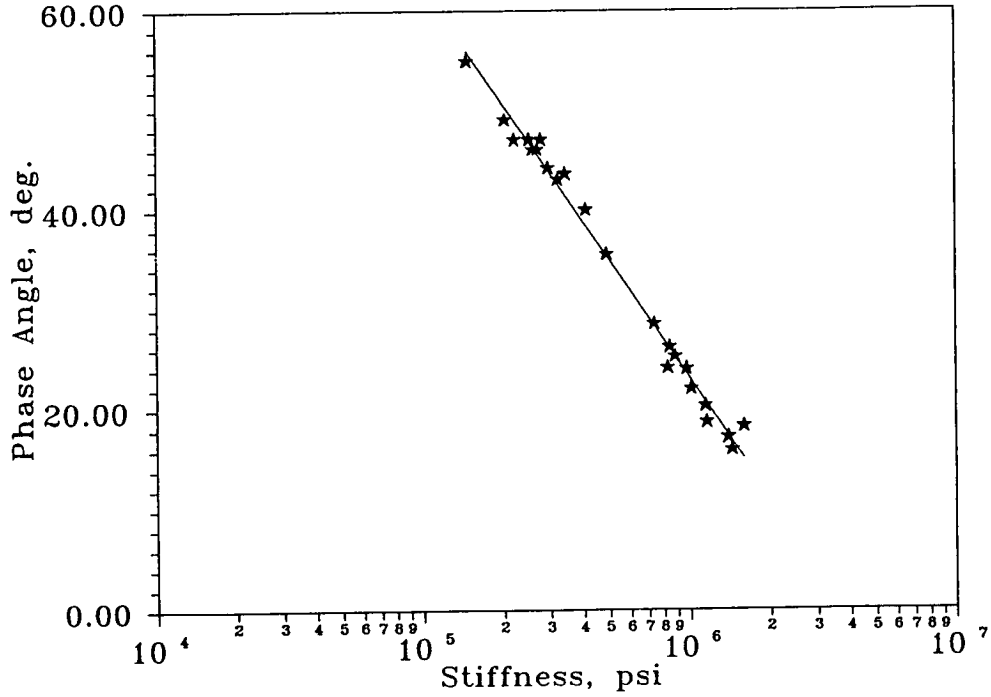

Figure 12.7. Phase angle versus stiffness

12.4.2 Energy-, Strain-, and Loss-Stiffness-Based Fatigue Life Models

The calibrated strain- and energy-based fatigue models for the TEF results across all temperatures were as follows:

$$N_f = 3.342*10^4 \, (\epsilon_o)^{-3.968} \, (S_o'')^{-2.316} \qquad R^2 = 0.81 \quad CV = 67\% \qquad (12.8)$$

$$N_f = 368.34 \, (w_o)^{-1.937} \qquad R^2 = 0.80 \quad CV = 67\% \qquad (12.9)$$

These models are comparable to the following surrogate fatigue models developed from the 8×2 expanded test program:

$$N_f = 466.4 \, \exp^{0.052 \, VFB} \, (\epsilon_o)^{-3.948} \, (S_o'')^{-2.270} \qquad R^2 = 0.85 \quad CV = 63\% \qquad (12.10)$$

$$N_f = 6.72 \, \exp^{0.049 \, VFB} \, (w_o)^{-2.047} \qquad R^2 = 0.84 \quad CV = 63\% \qquad (12.11)$$

where:

N_f	=	fatigue life,
ϵ_o	=	initial strain, in./in.,
S_o''	=	initial loss stiffness, psi,
w_o	=	initial dissipated energy per cycle, psi,
VFB	=	percent voids filled with bitumen, and
exp	=	exponent of natural logarithm.

The constants in these two sets of models are different since in the TEF experiment only one mix was tested, and air-void content or the percentage of voids filled with asphalt was constant. The coefficients of determination are slightly lower, and the coefficients of variation are slightly higher for the TEF models than for the surrogate models from the 8×2 expanded test program. The strain exponent in Equation 12.8 is a constant value, whereas earlier it was stated that the strain-life slope K_2 was dependent on temperature. In order to account for the temperature (or stiffness) dependency of the strain exponent, the temperature effects on the strain exponent were taken into account when the fatigue life models were calibrated. These calibrations are presented in the following sections.

12.4.3 Temperature-, Strain-, and Stiffness-Based Fatigue Life Models

A temperature-based fatigue life model of the following form was calibrated, assuming that the log of fatigue life varies linearly with temperature and log of strain:

$$N_f = 10^{(K_1+K_2*Temp)} * \epsilon_o^{(K_3+K_4*Temp)} \qquad (12.12)$$

where:

N_f	=	fatigue life,
ϵ_o	=	initial tensile strain,
Temp	=	temperature, and
K_1 to K_4	=	experimentally determined coefficients.

On the basis of the TEF data, linear regression calibration yielded the following:

$$N_f = 10^{(20.034-0.226*Temp)} * \epsilon_o^{(-5.914+0.106*Temp)} \qquad R^2 = 0.94 \quad CV = 36\% \quad (12.13)$$

Since mix stiffness varies with temperature, replacing the temperature with stiffness in Equation 12.13 resulted in the following relationship:

$$N_f = 4.730*10^{-10} * S_o^{4.495}\ \epsilon_o^{(7.912-2.123\ Log(S_o))} \qquad R^2 = 0.83 \quad CV = 59\% \quad (12.14)$$

where: ϵ_o = initial tensile strain, micro in./in.,
S_o = initial flexural stiffness, psi, and
Temp = temperature, °C.

The temperature- and strain-based model (Equation 12.13) was used to develop the TEFs detailed in Part III of this report.

12.5 Validation of Surrogate Fatigue Model Using the TEF Experiment

Results of the TEF experiment (which included fatigue life measurements at four different temperatures) provided an opportunity for assessing the applicability of the strain- and energy-based surrogate models from the 8×2 expanded test program, which were developed based on a single temperature of 20°C (68°F). Equations 12.10 and 12.11 were used for this purpose.

Estimates from the surrogate model compare well with the measurements in the TEF experiment as shown in Figure 12.8. Pearson correlations between the estimated fatigue life and TEF measurements are presented in Table 12.3. Correlation between observed and estimated lives for both strain- and energy-based models is good (R^2 = approximately 0.9), indicating that the surrogate models from the 8×2 expanded test program provide reasonable results for this multitemperature data set. A correlation coefficient of 0.99 between predicted lives using the strain and energy models indicates that the two models can estimate fatigue life with similar accuracy. Estimated and measured fatigue lives at each of the four temperatures are shown in Figures 12.9 to 12.12.

12.6 Summary

The TEF experiment was conducted in order to develop temperature equivalency factors for the mix design and analysis system. This experiment examined the effects of temperature on fatigue life and strain relationships for a single mix containing AAD-1 asphalt and an RH aggregate. The temperature- and strain-based fatigue life model developed from the TEF data and used to develop TEFs was the following:

$$N_f = 10^{(20.034-0.226*Temp)} * \epsilon_o^{(-5.914+0.106*Temp)}$$

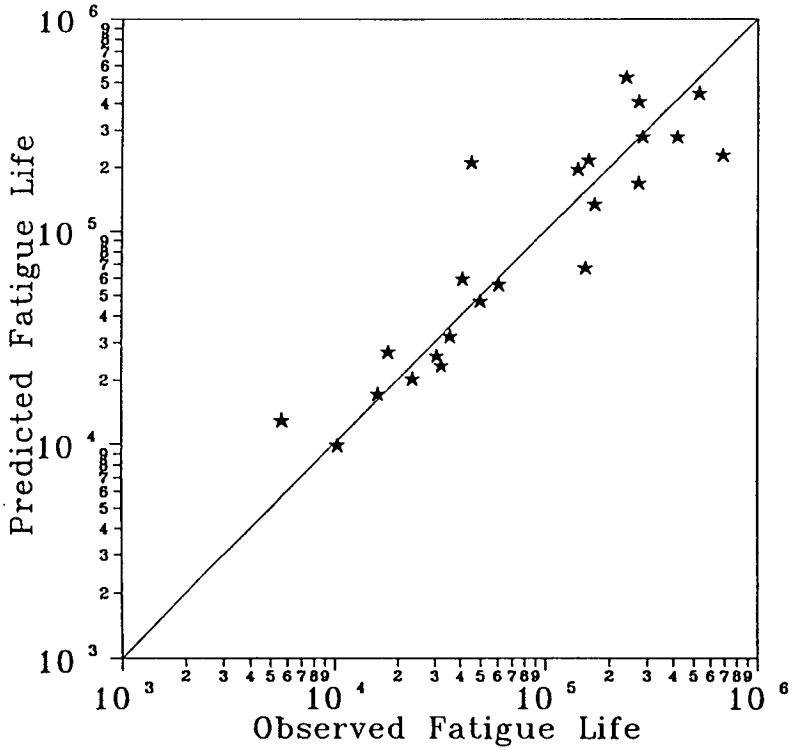

Figure 12.8. Predicted versus observed fatigue lives in TEF experiment

Table 12.3. Pearson correlation matrix for estimated (8×2 surrogate model) versus observed (TEF measurements) fatigue lives

	Ln (TEF Measurement)	Ln (Estimate from 8×2 Strain-Based Model)	Ln (Estimate from 8×2 Energy-Based Model)
Ln (Observed Life)	1.000		
Ln (Estimate from 8×2 Strain-Based Model)	0.908	1.000	
Ln (Estimate from 8×2 Energy-Based Model)	0.902	0.994	1.000

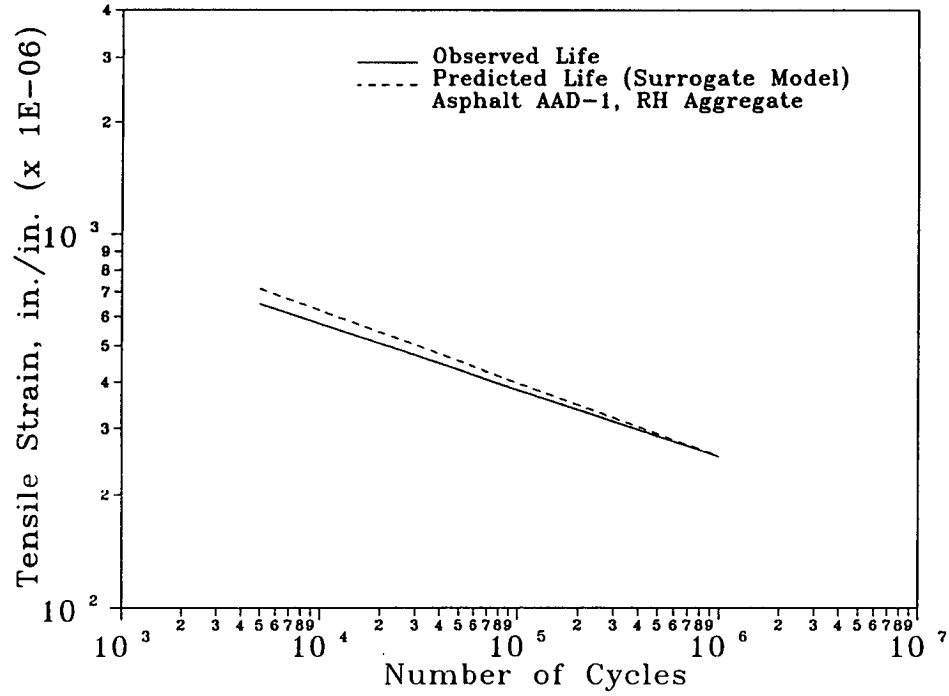

Figure 12.9. Strain-life relationships between observed and predicted fatigue lives at 5°C (41°F)

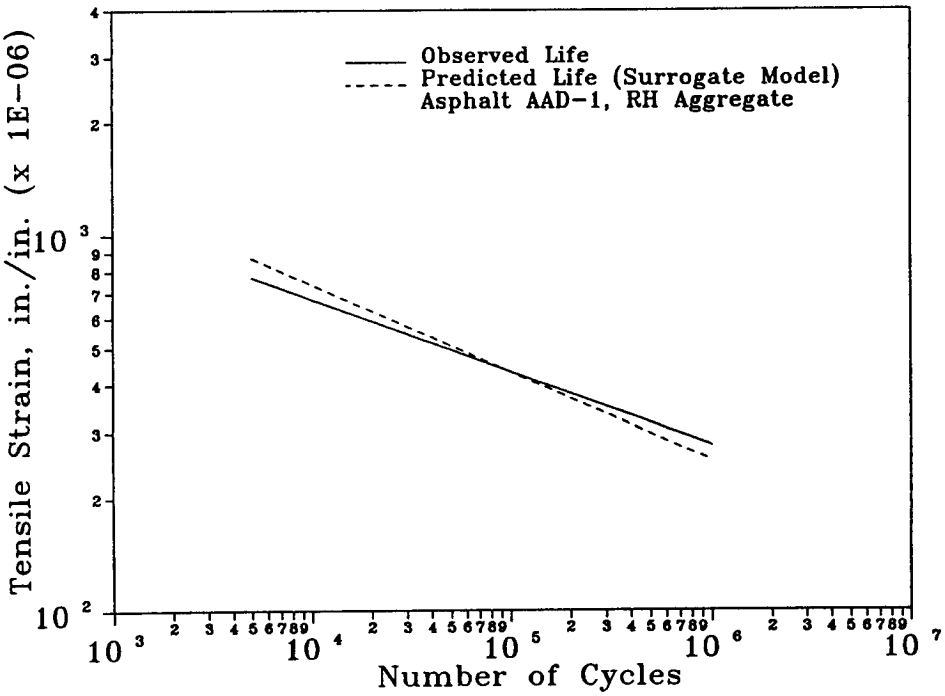

Figure 12.10. Strain-life relationships between observed and predicted fatigue lives at 10°C (50°F)

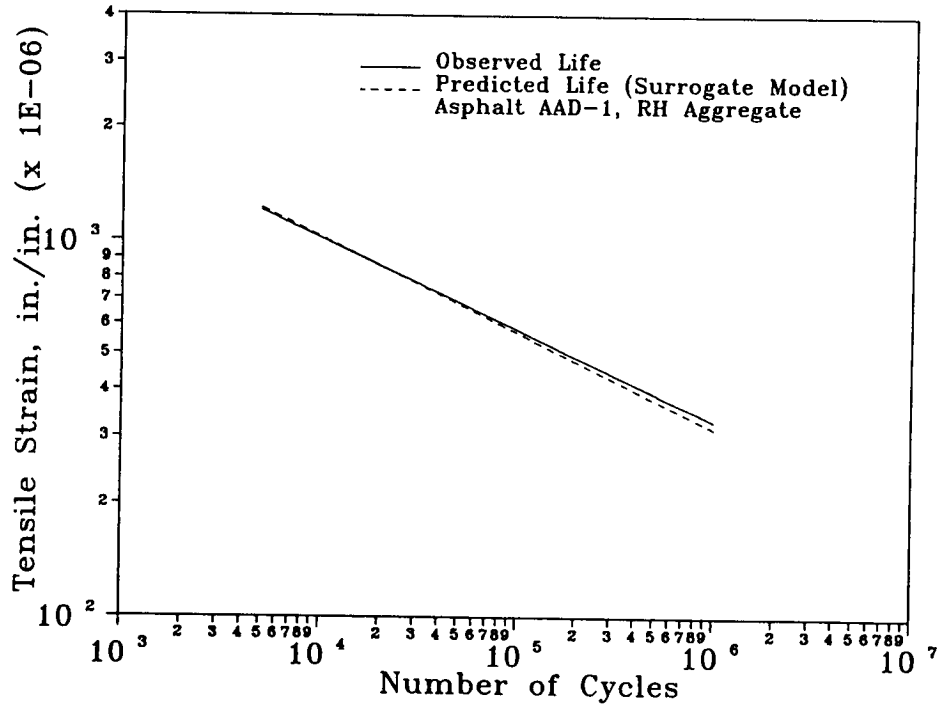

Figure 12.11. Strain-life relationships between observed and predicted fatigue lives at 20°C (68°F)

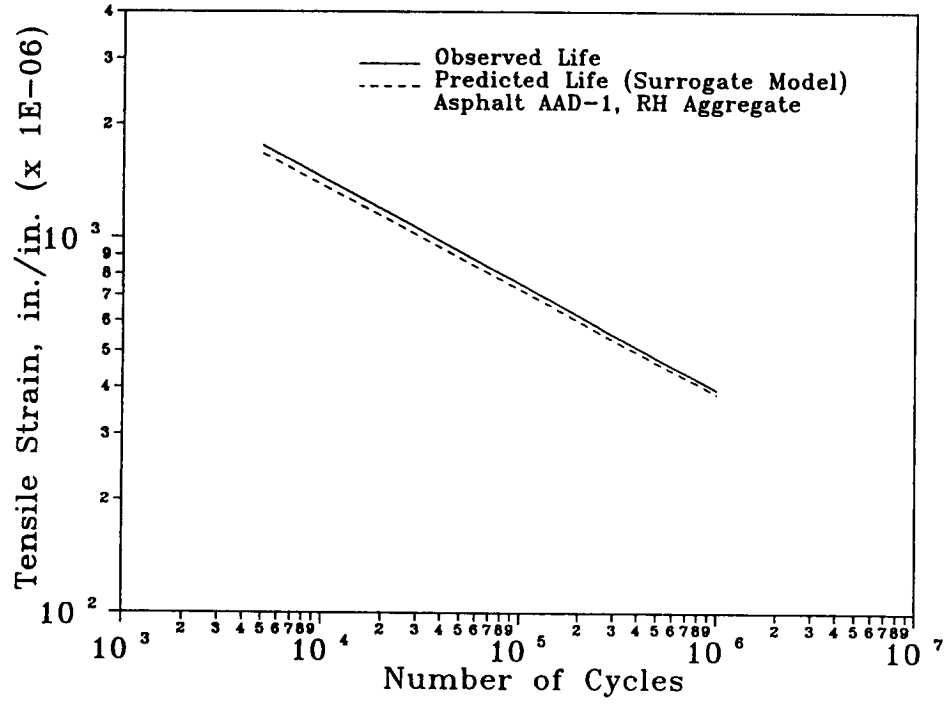

Figure 12.12. Strain-life relationships between observed and predicted fatigue lives at 25°C (77°F)

Test results indicated that the strain-life slope (K_2) is highly temperature sensitive. Model fitting on TEF data was generally judged adequate. As anticipated, mix stiffness increased and phase angles decreased with decreasing temperature. For the controlled-strain mode of loading used in this experiment, fatigue life decreased with increasing stiffness (decreasing temperature).

In general, fatigue life estimates from the strain- and energy-based surrogate fatigue models developed during the 8×2 expanded test program compared well with the measurements in the TEF experiment. However, the strain-based surrogate model was unable to reproduce the observed effect of temperature on the strain-life slope.

13

Modified Asphalt Mixes Experiment

13.1 Introduction

The modified asphalt mixes experiment (subsequently referred to as MAME) was conducted as part of SHRP Project A-003A to investigate whether the new fatigue equipment and procedure were sensitive to changes in fatigue characteristics caused by the presence of modifiers. The experiment design included three MRL core asphalts and three modifiers. Specimens were prepared using kneading compaction at Southwestern Laboratories (SWL) in Houston and shipped to UCB. Specimens were sawed to the required height and tested at UCB.

13.2 Selection of Mix and Testing Variables

The mix and test variables included in this study were as follows:

- **Asphalts.** Three MRL asphalts were used: AAF-1, AAG-1, and AAK-1.
- **Modifiers.** Three modifiers—M-405, M-415, and M-416—were used for this study. Asphalt AAF-1 was modified with M-405 only, whereas asphalts AAG-1 and AAK-1 were modified with all three modifiers.
- **Aggregates.** One MRL aggregate was used: RB, a crushed granite. The aggregate gradation used conformed to that shown in Table 10.3.
- **Asphalt Content.** One asphalt content was used for this investigation: 5.0 percent for the unmodified asphalt mixes and 5.2 percent for the modified asphalt mixes, by weight of aggregate.
- **Air-Void Content.** One air-void level was used: 7 percent plus or minus 1 percent.

- **Strain Levels.** Two strain levels were used: 400 and 700 micro in./in.
- **Replicates.** Two replicate specimens were tested at each strain level.
- **Test Frequency.** All tests were performed in the controlled-strain mode of loading at a frequency of 10 Hz with sinusoidal loading (no rest periods).
- **Test Temperature.** Tests were conducted at 20°C (68°F).
- **Conditioning.** All mixes were short-term aged in a forced draft oven at 135°C (275°F) for 4 hours. No water conditioning was included in this test program.

The MAME design is summarized in Table 13.1. Specimens 6.4 cm (2.5 in.) wide, 5.1 cm (2 in.) tall, and 40.7 cm (15.0 in.) long were sawed from 7.6 × 7.6 × 40.7 cm (3 × 3 × 16 in.) specimens prepared using the kneading compaction method. The response (dependent) variables measured included 1) initial flexural stiffness measured at the 50th load cycle, 2) fatigue life—the number of cycles to 50 percent reduction in initial flexural stiffness, 3) initial dissipated energy per cycle measured at the 50th load cycle, and 4) cumulative or total dissipated energy associated with fatigue life.

Table 13.1. Features of modified asphalt mixes experiment

Number of Asphalts	3 — MRL core asphalts AAF-1, AAG-1, and AAK-1
Number of Aggregates	1 — MRL aggregate RB
Asphalt Content	1 — 5.0 and 5.2 percent for unmodified and modified mixes, by weight of aggregates
Number of Modifiers	3 — Modifiers identified as M-405, M-415, and M-416
Air-Void Levels	1 — 7 ± 1 percent
Strain Levels	2 — 400 and 700 micro in./in.
Replicates at Each Strain Level	2
Temperature	1 — 20°C (68°F)
Frequency	1 — 10 Hz (sinusoidal)
Specimen Size	2 in. (5.1 cm) height, 2.5 in. (6.4 cm) width, 15 in. (40.7 cm) length
Method of Compaction	Kneading compaction
Total Number of Mixes Tested	10
Total Number of Specimens Tested	39

13.3 Test Results

The MAME results are presented in Appendix E. Fatigue life versus strain relationships are presented in Table 13.2. Each fatigue relationship is a linear regression calibration of the following form:

$$N_f = K_1 \epsilon_o^{K2} \quad (13.1)$$

where: N_f = fatigue life,
ϵ_o = initial tensile strain, in./in., and
K_1, K_2 = experimentally determined coefficients.

Table 13.2. Fatigue life versus strain calibrations from modified asphalt mix experiment

Mix Type			K_1	K_2	R^2	CV (%)
Asphalt Source	Modifier	Aggregate Source				
AAF-1	None	RB	$5.463*10^{-12}$	-4.618	0.968	34.50
AAG-1	None	RB	$5.982*10^{-10}$	-3.894	0.814	84.80
AAK-1	None	RB	$2.244*10^{-7}$	-3.267	0.852	58.00
AAF-1	M-405	RB	$3.493*10^{-17}$	-6.110	0.958	54.10
AAG-1	M-405	RB	$1.266*10^{-9}$	-3.673	0.774	92.30
AAK-1	M-405	RB	$5.883*10^{-18}$	-6.359	0.958	56.60
AAG-1	M-415	RB	$1.104*10^{-11}$	-4.270	0.930	49.20
AAK-1	M-415	RB	$2.210*10^{-6}$	-3.110	0.953	27.90
AAG-1	M-416	RB	$1.202*10^{-7}$	-3.119	0.990	3.30
AAK-1	M-416	RB	$5.311*10^{-8}$	-3.670	0.990	6.20

The relationships of cumulative dissipated energy versus fatigue life are summarized in Table 13.3. Each relationship is a linear regression calibration of the following form:

$$W_N = A (N_f)^z \quad (13.2)$$

where: W_N = cumulative dissipated energy with fatigue life,
N_f = fatigue life, and
A, z = experimentally determined coefficients.

Table 13.3. Cumulative dissipated energy versus fatigue life calibrations from modified asphalt mix experiment

Mix Type						
Asphalt Source	Modifier	Aggregate Source	A	z	R^2	CV (%)
AAF-1	None	RB	1.891	0.572	0.935	28.70
AAG-1	None	RB	1.060	0.643	0.835	51.80
AAK-1	None	RB	15.480	0.352	0.800	25.00
AAF-1	M-405	RB	0.416	0.675	0.950	39.60
AAG-1	M-405	RB	1.015	0.520	0.972	14.70
AAK-1	M-405	RB	0.098	0.828	0.980	31.80
AAG-1	M-415	RB	0.503	0.665	0.955	25.70
AAK-1	M-415	RB	6.191	0.472	0.990	15.00
AAG-1	M-416	RB	10.000	0.326	0.952	10.50
AAK-1	M-416	RB	12.780	0.429	0.957	13.30

Table 13.4 presents the average values of the stiffness, fatigue life, and cumulative dissipated energy for each of the mixes containing straight- and modified-asphalt binders. Fatigue lives in Table 13.4 were computed at a strain level of 500 micro in./in. using the fatigue life and strain relationships presented in Table 13.2. The cumulative dissipated energy associated with the fatigue life was estimated using the energy-life relationships presented in Table 13.3. Results are discussed in the following sections.

Table 13.4. Average values of stiffness, fatigue life (at 500 micro in./in.), and cumulative dissipated energy from modified asphalt mix experiment

Mix Type	Stiffness (psi)	Fatigue Life (N_f) (at 500 micro in./in.)	Cumulative Dissipated Energy to N_f (psi)	Voids (%)	VFB (%)
AAF-1	581,500	9600	360	7.0	62
AAF/M-405	681,600	5200	130	6.6	64
AAG-1	785,100	4300	230	6.4	64
AAG/M-405	635,700	1700	50	6.6	64
AAG/M-415	606,600	1400	60	6.4	65
AAG/M-416	710,900	2400	130	6.6	64
AAK-1	416,200	13,700	440	6.8	63
AAK/M-405	473,300	5800	130	7.1	63
AAK/M-415	263,700	40,800	930	7.3	62
AAK/M-416	254,150	69,200	1530	7.0	63

13.3.1 Stiffness

For conventional asphalt binders, mixes containing asphalt AAG-1 exhibited the highest average stiffness, followed by mixes containing asphalt AAF-1 and asphalt AAK-1. This behavior is similar to that observed in the 8×2 expanded study. The effect of adding modifiers on the mix stiffness is summarized below, showing the percentage difference in stiffness between the conventional and the modified asphalt mixes. In general, mix stiffness was observed to decrease between 10 and 39 percent, except for mixes with asphalts AAF-1 and AAK-1, which showed increases of approximately 12 to 15 percent in stiffness with modifier M-405. Figures 13.1 to 13.4 show the effect of modifier type on the average stiffness of the various mixes.

Asphalt Source	**Modifier Type**		
	M-405	M-415	M-416
AAF-1	+15%	-	-
AAG-1	-19%	-23%	-10%
AAK-1	+12%	-37%	-39%

Note: Percentage difference computed as percentage of the larger value.

13.3.2 Fatigue Life

The fatigue life of mixes containing asphalt AAK-1 was observed to be the highest, followed by mixes containing asphalts AAF-1 and AAG-1. This ranking agrees with that observed in the 8×2 expanded test program. Moreover, the conventional notion that stiffer mixes under controlled-strain fatigue testing performed poorer than their less stiff counterparts was also confirmed for the conventional unmodified mixes. However, the modified mixes did not follow this pattern. The effect of adding modifiers on fatigue life is summarized below.

Asphalt Source	**Modifier Type**		
	M-405	M-415	M-416
AAF-1	-46%	-	-
AAG-1	-61%	-67%	-44%
AAK-1	-58%	+66%	+80%

Note: Percentage difference computed as percentage of the larger value.

Modifier M-405 was detrimental to the fatigue performance when it was added to each of the three asphalts. Addition of this modifier to asphalts AAF-1 and AAK-1 increased the stiffness by about 12 percent as indicated before but decreased the fatigue life by approximately 46 and 58 percent for mixes containing asphalts AAF-1 and AAK-1, respectively. The stiffness of mixes containing asphalt AAG-1 decreased by approximately

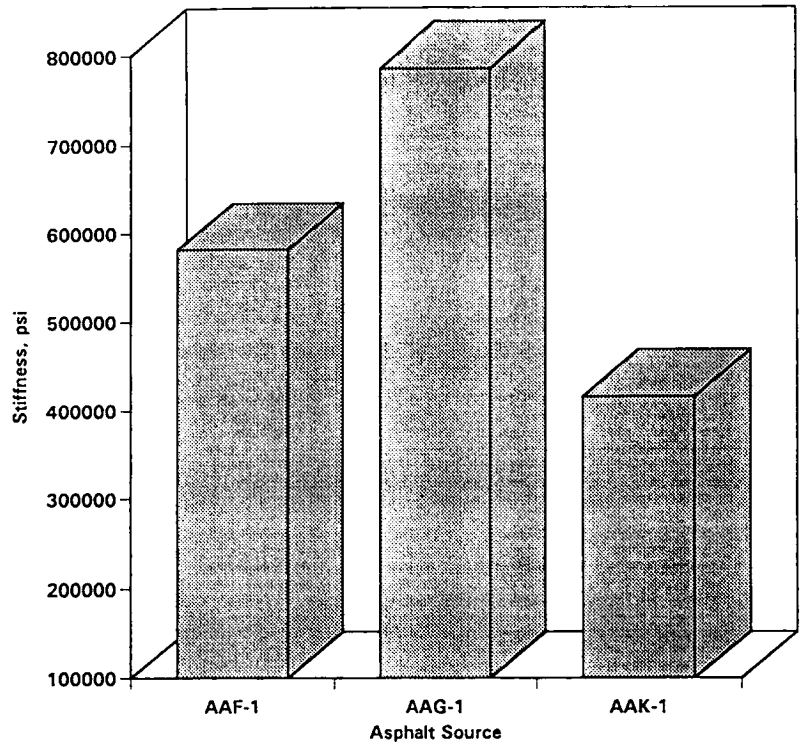

Figure 13.1. Average stiffness versus asphalt source

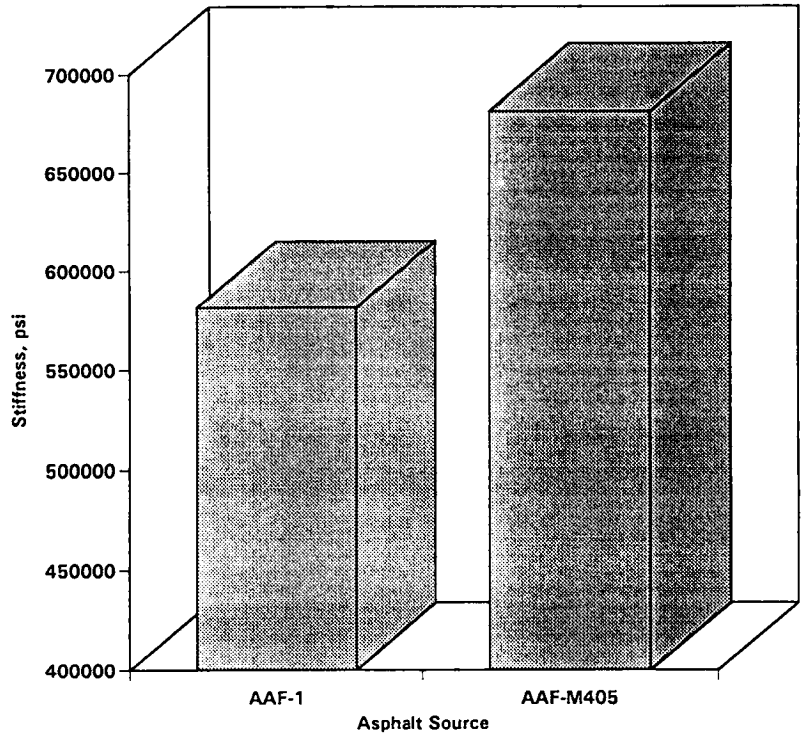

Figure 13.2. Effect of modifier type on average stiffness for mixes containing AAF-1 asphalt binder and M-405 modifier

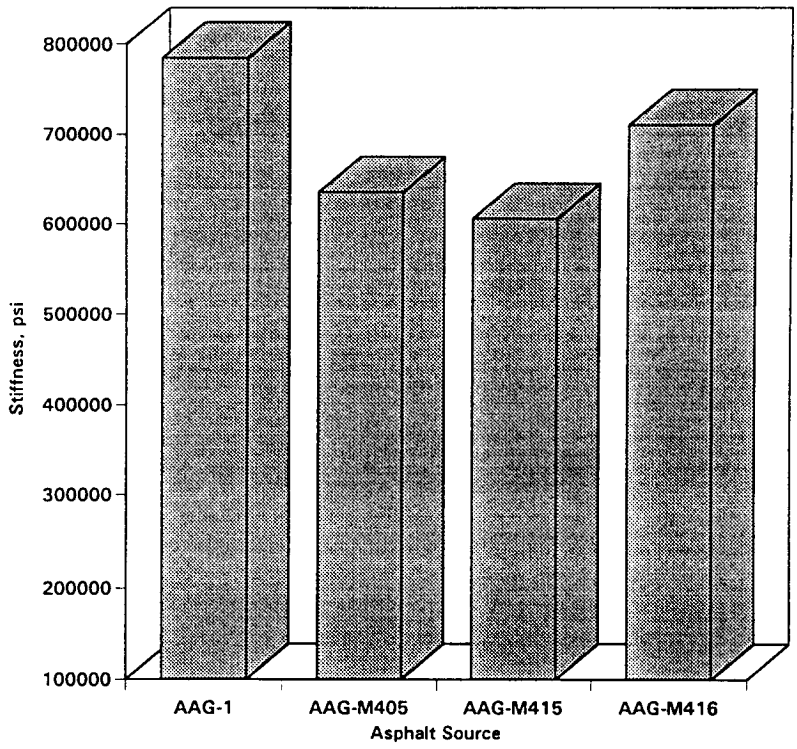

Figure 13.3. Effect of modifier type on average stiffness for mixes containing AAG-1 asphalt binder and M-405, M-415, and M-416 modifiers

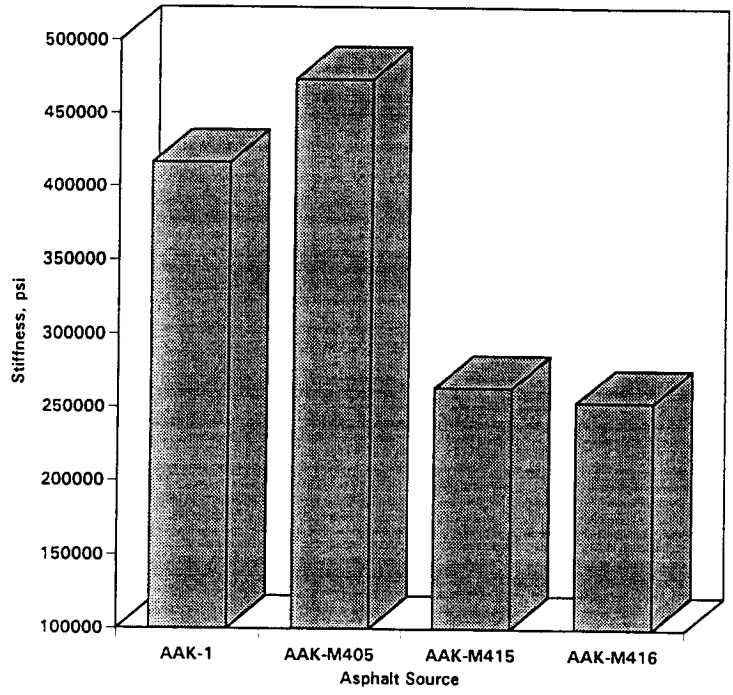

Figure 13.4. Effect of modifier type on average stiffness for mixes containing AAK-1 asphalt binder and M-405, M-415, and M-416 modifiers

19 percent; however, with this decrease in stiffness, the anticipated increase in fatigue life was not observed. Instead, the fatigue life decreased by approximately 61 percent.

Modifiers M-415 and M-416 produced changes in performance similar to those of modifier M-405 on mixes containing asphalt AAG-1. Addition of both modifiers resulted in reduced fatigue life, although mix stiffness was observed to decrease.

For mixes containing asphalt AAK-1, the addition of modifiers M-415 and M-416 resulted in substantially increased fatigue life as indicated by respective increases of approximately 66 and 80 percent. In both cases, mix stiffness was observed to decrease by about 38 percent. Figures 13.5 to 13.8 show the effect of modifier type on the fatigue life of the various mixes.

The effects of modifiers on cumulative dissipated energy are similar to those observed for fatigue life.

13.3.3 Effect of Compaction Method on Repeatability

Because specimens in this study were prepared using kneading compaction, the variability associated with specimen preparation and testing was computed for comparison with the variability in the 8×2 expanded test program in which specimens were compacted by rolling-wheel compaction. Higher variability was expected for specimens prepared using kneading compaction since there is more aggregate breakage, which reduces fatigue life. Except for the difference in specimen preparation, all other aspects of testing were the same, including specimen size, test equipment, and procedure.

MAME involved 10 mixes tested at each of two strain levels with full replication. The 20 pairs provided the following means for estimating the sample variance by pooling variances between replicate tests:

$$s^2 = \{\Sigma \tfrac{1}{2}[\ln(N_{rep1}/N_{rep2})]^2\}/(\#\ \text{Obs}) \qquad (13.3)$$

where:
- s^2 = sample variance of ln cycles to failure associated with fatigue testing,
- N_{rep1} = fatigue life of first replicate,
- N_{rep2} = fatigue life of second replicate, and
- # Obs = number of replicates.

The coefficient of variation was computed using the following relationship:

$$CV = 100 * (e^{VAR} - 1)^{0.5} \qquad (13.4)$$

where:
- CV = coefficient of variation in percent,
- VAR = variance — s^2, and
- e = base of natural logarithm.

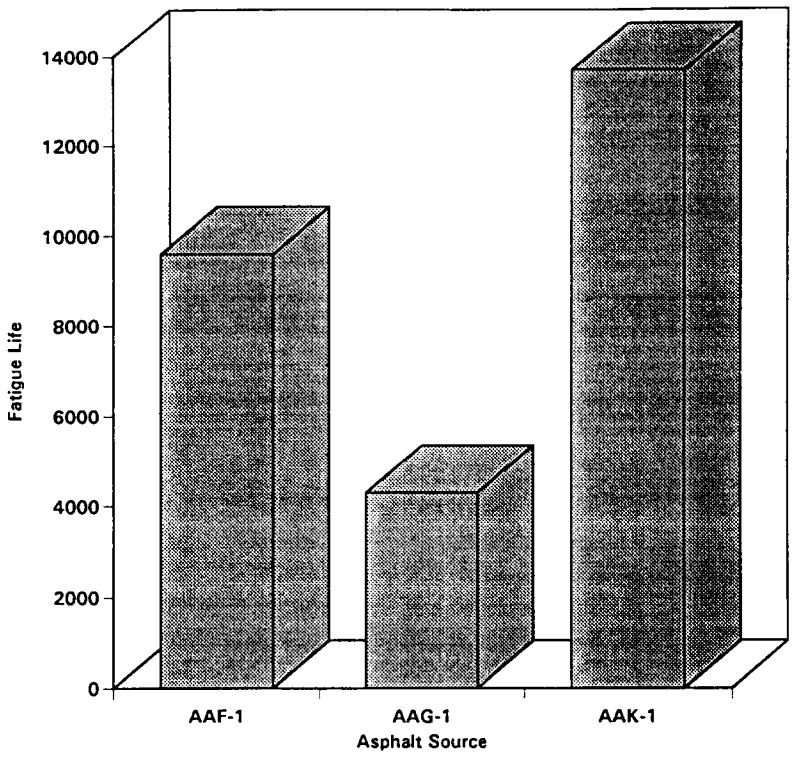

Figure 13.5. Average fatigue life versus asphalt source

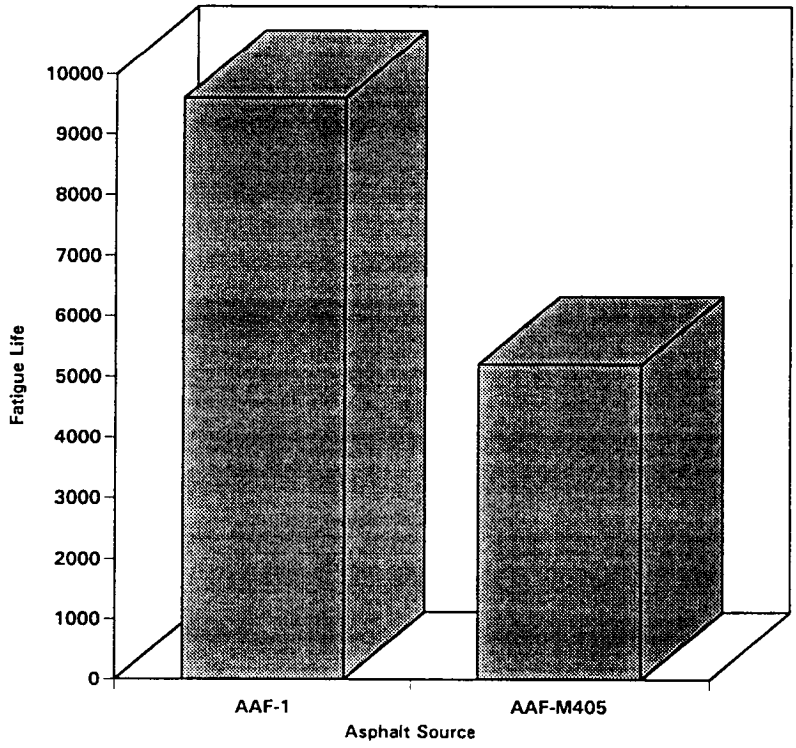

Figure 13.6. Effect of modifier type on fatigue life (at 500 micro in./in.) for mixes containing AAF-1 asphalt binder and M-405 modifier

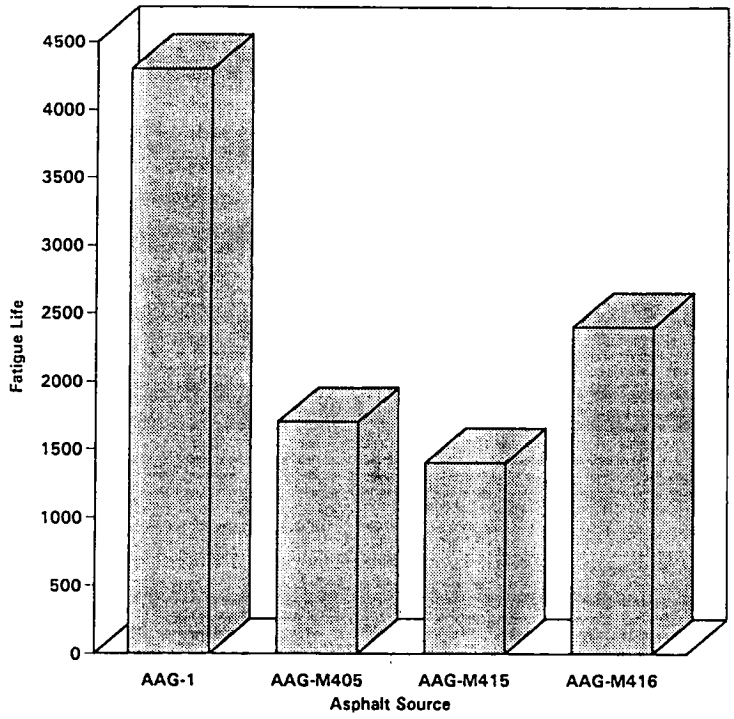

Figure 13.7. Effect of modifier type on fatigue life (at 500 micro in./in.) for mixes containing AAG-1 asphalt binder and M-405, M-415, and M-416 modifiers

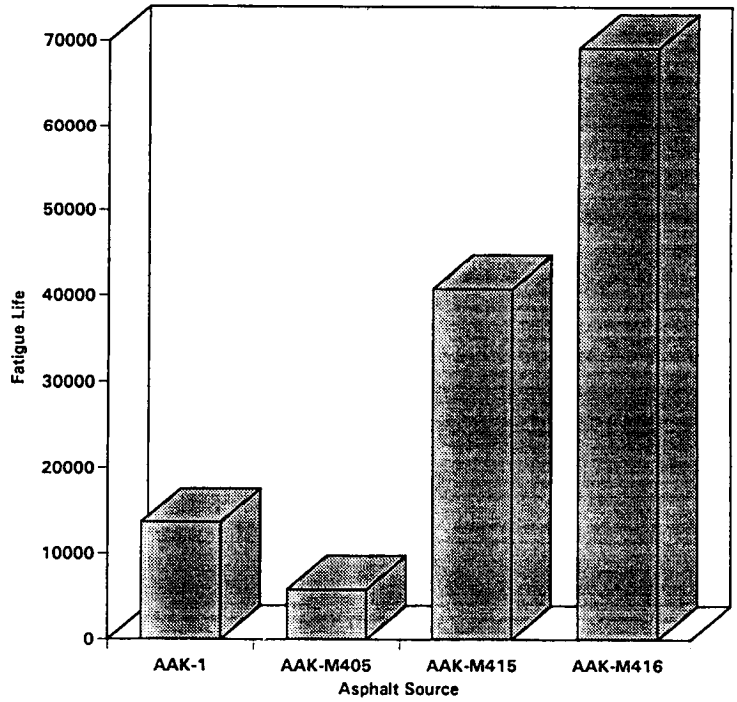

Figure 13.8. Effect of modifier type fatigue life (at 500 micro in./in.) for mixes containing AAK-1 asphalt binder and M-405, M-415, and M-416 modifiers

Computation of the variance and coefficient of variation for MAME are summarized below:

Response Variable	MAME Kneading Compaction, CV (%)	8×2 Expanded Study Rolling-Wheel Compaction, CV (%)
Stiffness	19	12
Fatigue Life	54	40
Cumulative Dissipated Energy	57	41

The coefficients of variation for all three response variables—stiffness, fatigue life, and cumulative dissipated energy—are higher for this study than the results from the 8×2 expanded study. Since the testing procedure, equipment, and operators remained the same for both studies, higher coefficients of variation may be attributed to differences in laboratory specimen fabrication (i.e., the method of compaction).

13.4 Model Calibrations

A stepwise-regression model fitted to the MAME data, with fatigue life as the dependent variable, is as follows:

$$N_f = 424.11 \exp^{(-0.239\ VFB)} (\epsilon_o)^{-4.593} (S_o'')^{-1.374} \quad R^2 = 0.61 \quad CV = 170\% \tag{13.5}$$

where:
- N_f = fatigue life,
- ϵ_o = initial tensile strain, in./in.,
- S_o'' = initial loss stiffness, psi, and
- VFB = percent voids filled with asphalt.

Fitting the strain-based model was generally judged to be inadequate for the MAME results, as indicated by a coefficient of determination of 0.61 and coefficient of variation of 170 percent. Model fit improved when regression calibration was based on the results from the conventional unmodified mixes only. The coefficient of determination improved from 0.61 to 0.82, whereas the coefficient of variation decreased from 170 to 70 percent. The strain-based fatigue life model for the conventional mixes is

$$N_f = 4.51 (\epsilon_o)^{-3.818} (S_o'')^{-1.721} \quad R^2 = 0.82 \quad CV = 70\% \tag{13.6}$$

Regression results based on this study indicate that strain and loss stiffness do not fully account for the variation in the fatigue life of mixes containing modified asphalt binders.

13.5 Summary

MAME was conducted to investigate whether changes in the fatigue characteristics of modified mixes could be evaluated using the new fatigue equipment. Results of this study indicate that both asphalt source and modifier type substantially affect stiffness, fatigue life, and cumulative dissipated energy.

For conventional (unmodified) mixes, stiffness decreased from mixes containing asphalt AAG-1 to mixes containing asphalt AAF-1, followed by mixes containing asphalt AAK-1. Mix stiffness generally decreased with the addition of modifiers, except for mixes containing asphalts AAF-1 or AAK-1 and modified with M-405.

Without exception, fatigue life for mixes containing asphalts AAF-1 and AAG-1 decreased with the addition of modifiers. For mixes containing asphalt AAK-1, fatigue life substantially increased with the presence of modifiers M-415 and M-416. With M-405 modification, the fatigue life of mixes containing asphalt AAK-1 decreased. These results suggest that addition of modifiers to conventional asphalt mixes may not always enhance fatigue characteristics.

For conventional mixes, fatigue life increased with decreasing stiffness in the controlled-strain mode of loading used in this study. For modified mixes, this trend was not apparent. For some mixes, such as those containing asphalts AAK-1 and modifiers M-415 and M-416, fatigue life increased with decreasing stiffness. For other mixes, such as those containing asphalt AAG-1 and modifiers M-415 and M-416, fatigue life decreased with decreasing stiffness.

The modeling effort using the results of this study was generally judged inadequate: strain and loss stiffness were unable to fully account for variations in fatigue life. Because specimens were prepared using kneading compaction and replicate specimens were tested at each strain level, comparison of variations due to method of specimen fabrication—kneading versus rolling-wheel compaction—could be made. The coefficient of variation in fatigue life for specimens fabricated using kneading compaction was approximately 30 percent higher (54 percent versus 40 percent) compared to that for specimens fabricated using rolling-wheel compaction.

14

Validation Studies

14.1 Introduction

In the previous chapters of this report, specific conclusions and relationships concerning the fatigue properties of asphalt-aggregate mixes were developed on the basis of results of the controlled-strain, flexural beam fatigue test. In order to confirm the applicability of the results from such testing to field conditions, a series of validation tests was conducted. Because of time and resource constraints, it was not possible to conduct full-scale experiments. In lieu of using full-scale, in-service pavements, an effort was made to compare results from specific accelerated test facilities with predictions obtained by testing asphalt-aggregate mixes using the laboratory accelerated performance test (APT). The specific facilities involved included the accelerated loading facility (ALF) of the Federal Highway Administration located in McLean, Virginia; the Laboratoire Central des Ponts et Chaussées (LCPC) circular test track in Nantes, France; and laboratory wheel track test device at the SWK slab testing facility, in Nottingham, United Kingdom.

Asphalts and aggregates used in the ALF and LCPC studies were non-MRL materials. Samples of these materials were provided to A-003A, where test specimens were prepared using rolling-wheel compaction and tested using the controlled-strain, flexural beam test procedure. The fatigue properties obtained from the laboratory were then compared to the validation study results.

In making comparisons, it should be recognized that quantitative comparisons may not be possible for the following reasons:

- The performance of the pavement being tested is based on an observed level of distress and the laboratory fatigue test measures damage in terms of flexural stiffness reduction.

- In order to compute the maximum tensile strain in the asphalt-concrete layer, it is necessary to have material properties for each supporting layer. Therefore,

the testing agency supplied the maximum tensile strain. However, the methods used to arrive at the supplied tensile strain may not be compatible with the methods A-003A investigators used to calculate the tensile strain in the asphalt-concrete.

- ALFs are subject to a number of variables which are not specifically included in the analysis of the laboratory test data. These variables include aging, changes in temperature during loading of the pavement, rain, and periods of no simulated traffic due to equipment maintenance or data collection requirements.

For these reasons, a qualitative comparison or ranking was used to validate the proposed fatigue test.

The use of a laboratory-scale, wheel tracking device offered the fastest and least expensive form of validation. Such devices permit the evaluation of asphalt mixes without the confounding effects encountered in full-scale facilities or in-service pavements. By using this device, researchers could control or measure a number of variables, for example, temperature, exposure to water, loads, repetitions, tire inflation pressures, direction of tracking or loading the pavement, response in terms of deflection, stress and strain at various locations, and the properties of the supporting materials or layers.

The specific objective of this validation study was to compare the ranking of asphalts obtained in the laboratory- or full-scale, wheel track testing to the ranking obtained from the flexural beam controlled-strain fatigue tests. A brief description and summary of results for each of the validation studies are presented in the following sections.

14.2 SWK Wheel Track Study

This study was conducted to evaluate the fatigue properties of slabs of asphalt-aggregate mixes using the wheel tracking device shown in Figure 14.1 by SWK Pavement Engineering at the University of Nottingham, United Kingdom. The work included two experiments: one for the validation of core MRL asphalts; the other, for modified asphalt binders. Details of both studies are reported by Rowe et al. (1993a,b,c) and are summarized below.

Testing for this validation study consisted of applying a moving load to asphalt slabs with the following dimensions—1000 mm (39.4 in.) length, 500 mm (19.7 in.) width, and 50 mm (1.97 in.) height—placed directly over a weak base, a 92 mm (3.6 in.) thick rubber sheet with a modulus of approximately 10 MPa (1,450 psi).

The asphalt slabs were instrumented with strain gages on the slab underside, and the induced strains were monitored during testing. Evaluation of mix performance was made by considering the tensile strain versus the number of wheel load applications required to produce a predefined degree of fatigue damage (fatigue life, N1). Figure 14.2 shows the general experimental arrangement for the fatigue wheel tracking tests in the STF.

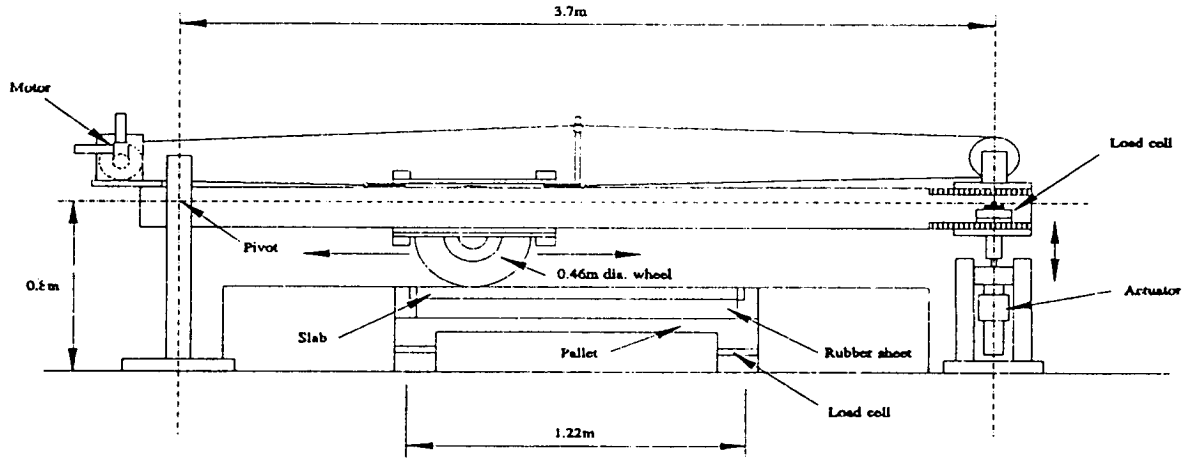

Figure 14.1. The slab testing facility (after Rowe et. al 1993a)

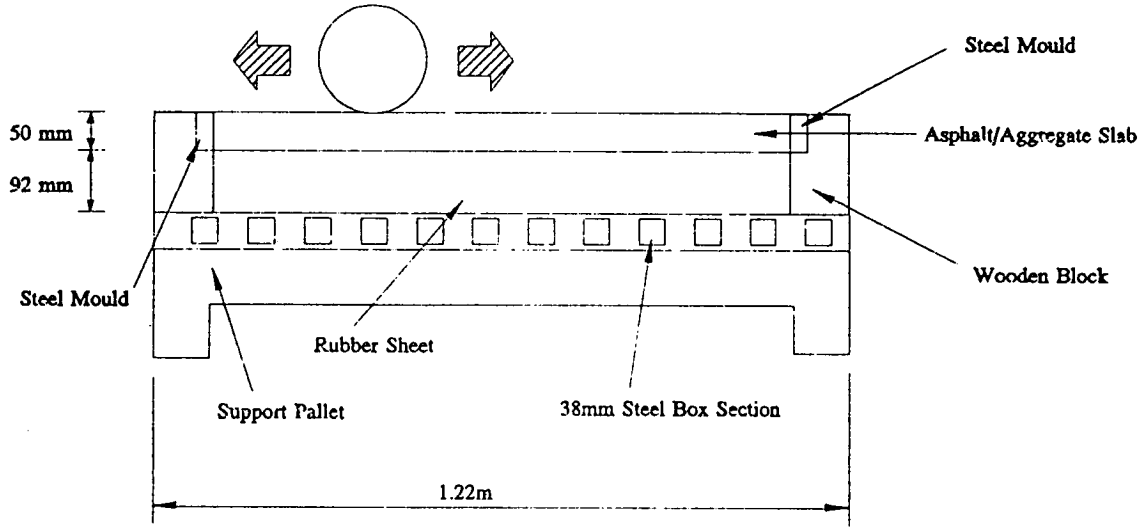

Figure 14.2. General experimental arrangement for fatigue wheel track tests in the slab testing facility (after Rowe et. al 1993a)

An elastic analysis of the slab configuration for stress and strain indicated that the mode factor[7] for this structure would be in the range of -0.70 to -0.77. Thus, the conditions simulated are closer to those obtained in a controlled-stress mode of loading. A similar mode factor for a typical full-scale pavement structure would be associated with a thick (greater than 10.2 to 15.2 cm [4 to 6 in.]) structural layer. Thus, the use of a thin asphalt layer over a weak base used in the laboratory STF represented a relatively thick, full-scale, in-service pavement structure.

14.2.1 Validation of A-003A Fatigue Test Using MRL Core Asphalts

14.2.1.1 Selection of Materials and Variables

The mix and testing variables included in this part of the validation testing program were as follows:

- **Asphalts.** Six MRL asphalts were used: AAA-1, AAC-1, AAF-1, AAG-1, AAK-1, and AAM-1.
- **Aggregates.** One MRL aggregate was used: RD, a crushed limestone, the same material used for the 8×2 expanded test program.
- **Asphalt Content.** A single asphalt content of 4.31 percent by weight of mix was used.
- **Air-Void Content.** An average air-void content of approximately 9.3 percent was achieved.
- **Replicates.** One slab for each of the six core asphalt and RD aggregate combinations was tested.
- **Tire Pressure and Test Frequency.** Tire pressure used was approximately 94 psi (650 kPa), and the frequency of loading was 30 passes per minute.
- **Test Temperature.** The tests were conducted at 20°C (68°F).
- **Compaction Procedure.** Slabs were compacted using a single-drum vibratory roller (in the nonvibratory mode), a procedure similar to the UCB compaction procedure used in the 8×2 expanded test program.

---

[7]The mode factor assumes a value of -1 for a controlled-stress condition and +1 for a controlled-strain condition (Monismith and Deacon 1969).

14.2.1.2 Test Results

Tables 14.1 and 14.2 show the stiffness characteristics and the fatigue life for each of the slabs, respectively. Stiffness was measured at 20°C (68°F) using the indirect tensile test (ITT) on specimens cored from the nonfatigued sections of the slabs. A Poisson's ratio of 0.35 was assumed for the stiffness computation.

Table 14.1. Average indirect tensile stiffness and air-void contents for each of the slabs tested

Asphalt Source	Aggregate Source	Indirect Tensile Stiffness (20°C) (68°F), psi		Average Air-Void Contents (%)
		Average	Standard Deviation	
AAA-1	RD	243,200	21,200	11.1
AAC-1	RD	598,900	50,600	8.1
AAF-1	RD	1,166,700	61,000	9.4
AAG-1	RD	1,072,700	87,400	9.6
AAK-1	RD	806,400	21,600	9.1
AAM-1	RD	668,900	142,100	8.4

Table 14.2. Average fatigue lives normalized to 200 micron tensile strain

Asphalt Source	Aggregate Source	Fatigue Life N1 at 20°C (68°F) Normalized to 200 micron Tensile Strain		
		Average	Average (log)	Standard Deviation (log)
AAA-1	RD	219,300	5.341	0.505
AAC-1	RD	54,200	4.734	0.756
AAF-1	RD	10,100	4.006	0.381
AAG-1	RD	3170	3.501	0.116
AAK-1	RD	55,700	4.746	0.223
AAM-1	RD	28,300	4.452	0.170

Fatigue life, N1, considered the point where cracking initiates (defined as the coalescence of micro-cracks to form a sharp crack which then propagates) was determined from the strain versus the number of wheel passes relationship for each of the strain gages. Average fatigue lives (N1) normalized to 200 micron tensile strain for each of the slabs tested are presented in Table 14.2.

Stiffness. For the 8×2 expanded test program (Chapter 10), flexural stiffness of mixes containing asphalts AAG-1 and AAF-1 were consistently the highest, regardless of the aggregate source or air-void level. Similarly, mixes containing asphalt AAA-1 consistently showed the lowest stiffness. The remaining mixes fell between these two extremes. Based on graphical and statistical analysis, mixes were grouped for flexural stiffness in the following manner:

(Lowest Flexural Stiffness) Group 1	Group 2	(Highest Flexural Stiffness) Group 3
AAA-1	AAC-1	AAF-1
	AAK-1	AAG-1
	AAM-1	

Similar groupings were also observed for specimens cored from asphalt-concrete slabs, based on the ITT stiffness, shown in Figure 14.3. The mix containing asphalt AAA-1 showed the lowest average stiffness and those containing asphalts AAG-1 and AAF-1 showed the highest average stiffness. Mixes containing asphalts AAC-1, AAM-1, and AAK-1 fell between the two extremes. Based on Figure 14.3, for indirect tensile stiffness, mixes were grouped in the following manner:

(Lowest ITT Stiffness) Group 1	Group 2	(Highest ITT Stiffness) Group 3
AAA-1	AAC-1	AAG-1
	AAM-1	AAF-1
	AAK-1	

It may be noted that within a group, the ranking of asphalts differs slightly between flexural stiffness and indirect tensile stiffness. For example, the mix containing asphalt AAM-1 showed higher stiffness than mixes with asphalts AAC-1 and AAK-1 in the flexural test, but ranked between mixes containing asphalts AAC-1 and AAK-1 for indirect tensile stiffness. Considering the variability due to specimen preparation, specimen geometry, test equipment, testing procedure, operator, and air-void content, such differences in ranking are not unreasonable.

Fatigue Life. Results from the 8×2 experiment indicated that for fatigue life (defined as the number of cycles to a 50 percent reduction in stiffness) based on the controlled-strain, flexural beam test, mixes containing asphalts AAG-1 and AAF-1 showed the lowest fatigue lives and those containing asphalt AAA-1 showed the highest fatigue lives. For the flexural beam test, mixes were ranked in the following manner:

(Lowest Beam Fatigue Life) Group 1	Group 2	Group 3	Group 4	(Highest Beam Fatigue Life) Group 5
AAG-1	AAF-1	AAC-1	AAM-1	AAA-1
		AAK-1		

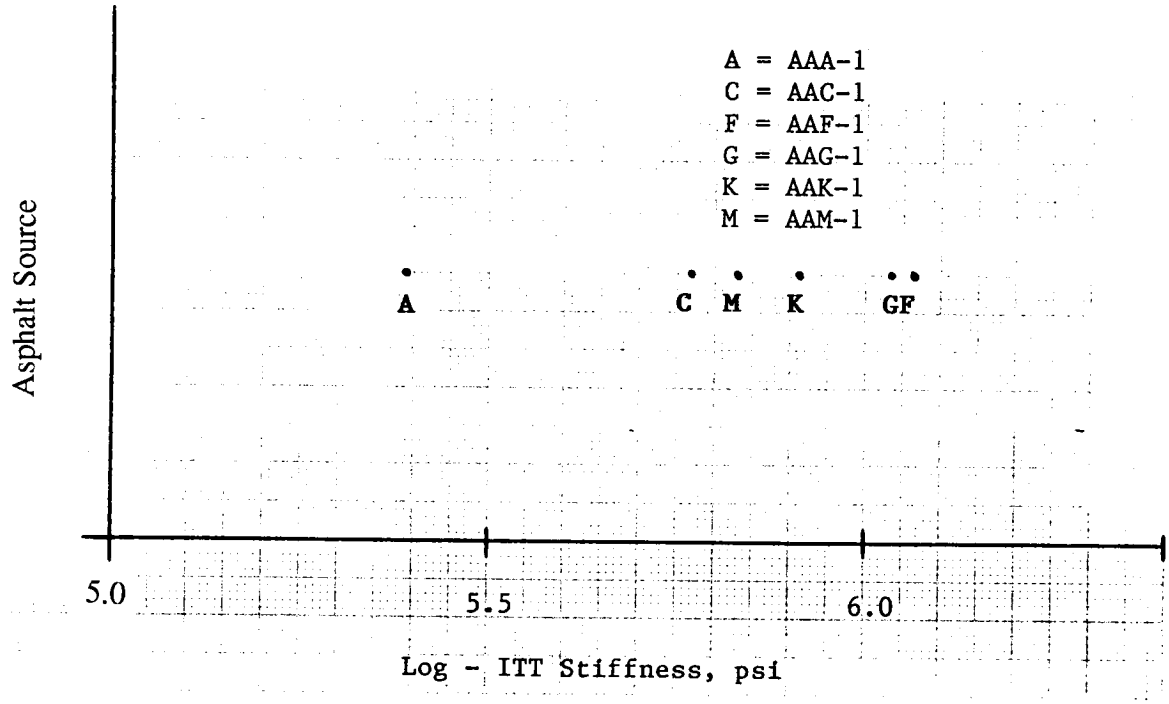

Figure 14.3. Ranking of mixes based on indirect tensile stiffness at 20°C (68°F)

Results from the wheel track testing also suggest five groupings in which the asphalt-concrete slab containing asphalt AAA-1 shows the highest fatigue life (N1) and that containing asphalt AAG-1 shows the lowest as shown in Table 14.2 and Figure 14.4. Based on Figure 14.4, mixes tested in the wheel track device were ranked in the following manner:

(Lowest Wheel Track Fatigue Life) Group 1	Group 2	Group 3	Group 4	(Highest Wheel Track Fatigue Life) Group 5
AAG-1	AAF-1	AAM-1	AAC-1 AAK-1	AAA-1

This ranking is similar to that based on the flexural beam test with the exception of the mix containing asphalt AAM-1. For the flexural fatigue test, the mix containing asphalt AAM-1 ranked fourth highest (5 being the best performance), ahead of mixes containing asphalts AAC-1 and AAK-1, whereas, in the wheel track device, it ranked third, behind mixes containing asphalts AAC-1 and AAK-1.

It may be noted that the wheel track experiment was fairly limited, with only one slab tested for each mix. Moreover, evaluation of fatigue life (N1) for the slabs was difficult to judge, as reported by Rowe et al. (1993a,b,c). There was a relatively high variability in fatigue life normalized to a constant strain level, as indicated in Table 14.2. Regardless of these shortcomings, the wheel track test does validate the flexural beam fatigue test as far as the ranking of asphalts is concerned.

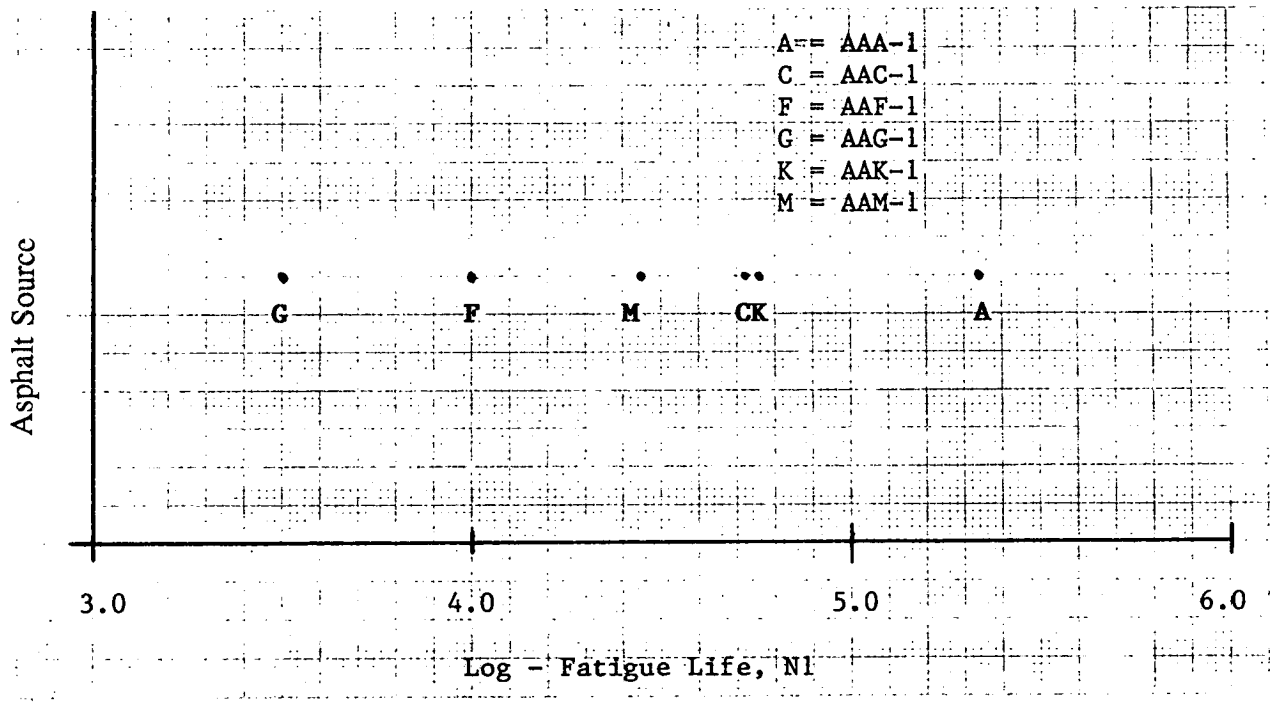

Figure 14.4. Ranking of mixes based on fatigue life (N1) at 200 microstrain

14.2.2 Ranking of Mixes With Modified Asphalts

14.2.2.1 Selection of Materials and Variables

The mix and testing variables included in this part of the validation testing program were as follows:

- **Asphalts and Modifiers.** One MRL asphalt, AAG-1, and three modifiers, M-405, M-415, and M-416, were used.
- **Aggregates.** One MRL aggregate was used: RB, a crushed granite.
- **Asphalt Content.** A single asphalt content of 5.1 percent by weight of mix was used.
- **Air-Void Content.** An average air-void content of approximately 7.7 percent was achieved.
- **Replicates.** Three slabs for each of the four asphalt types were tested.

- **Tire Pressure and Test Frequency.** The tire pressure used was approximately 94 psi (650 kPa), and the frequency of loading was 30 passes per minute.

- **Test Temperature.** All tests were performed at 20°C (68°F).

- **Compaction Procedure.** Slabs were compacted using a single-drum vibratory roller (in the nonvibratory mode).

14.2.2.2 Test Results

Since three slabs were tested at different initial strain levels, a relationship between fatigue life and strain could be developed for each mix tested in the wheel track device. Results presented in Table 14.3 show strong regression fits, with coefficients of determination varying between 0.81 and 0.99. Each fatigue relationship is a linear regression calibration of the following form:

$$N1 = K_1 \epsilon^{K2} \qquad (14.1)$$

where: $N1$ = fatigue life to crack initiation,
ϵ = average initial tensile microstrain underneath the slab, and
K_1, K_2 = regression coefficients.

Fatigue life (N1) at 200 microstrain was determined using the relationships of Table 14.3. Results are presented in Table 14.4, which also shows the average indirect tensile stiffness and air-void contents.

Table 14.3. Fatigue life versus microstrain calibrations for different mixes

Mix Type			K_1	K_2	R^2
Asphalt Source	Modifier	Aggregate Source			
AAG-1	None	RB	$5.767*10^9$	-2.6364	0.98
AAG-1	M-405	RB	$8.770*10^9$	-2.7506	0.81
AAG-1	M-415	RB	$2.551*10^{10}$	-2.6501	0.99
AAG-1	M-416	RB	$1.539*10^9$	-2.2279	0.96

Table 14.4. Average stiffness, fatigue life, and air-void contents

Mix Type			Indirect Tensile Stiffness (psi)	Fatigue Life, N1 at 200 Microstrain	Air Voids (%)
Asphalt Source	Modifier	Aggregate Source			
AAG-1	None	RB	801,900	4950	7.6
AAG-1	M-405	RB	1,657,000	4109	8.2
AAG-1	M-415	RB	602,000	20,353	7.9
AAG-1	M-416	RB	826,500	11,503	7.0

Stiffness. The effects of adding modifiers on the mix stiffness are summarized below for indirect tensile stiffness and flexural stiffness.

		Modifier		
Asphalt Source	**Test**	M-405	M-415	M-416
AAG-1	Indirect Tensile	+52%	-25%	+3%
AAG-1	Flexural Beam	-19%	-23%	-10%
AAK-1	Flexural Beam	+12%	-37%	-39%

Note: Percentage difference computed as a percentage of the larger value.

The ITT results for mixes containing AAG-1 asphalt indicated an increase in stiffness of 52 and 3 percent with modifiers M-405 and M-416, respectively, and a decrease in stiffness of 25 percent with modifier M-415. Results from the flexural beam test (Chapter 13) indicated a reduction in flexural stiffness of 19, 23, and 10 percent for the modification with M-405, M-415, and M-416, respectively, of mixes containing AAG-1 asphalt. However, flexural stiffness for mixes containing M-405-modified AAK-1 asphalt was observed to increase by 12 percent, whereas flexural stiffness for mixes containing M-415- and M-416-modified AAK-1 asphalt decreased by approximately 38 percent. For mixes containing AAG-1 asphalt, the indirect tensile stiffness and flexural stiffness do not appear to have similar trends in stiffness except for the mix containing M-415-modified AAG-1 asphalt.

Fatigue Life. The effects of adding modifiers on fatigue life are summarized below for both the wheel track and the flexural beam fatigue tests.

Asphalt Source	Test	Modifier		
		M-405	M-415	M-416
AAG-1	Slab Wheel Track	-17%	+75%	+57%
AAG-1	Flexural Beam	-61%	-67%	-44%
AAK-1	Flexural Beam	-58%	+66%	+80%

Note: Percentage difference computed as percentage of the larger value.

Both the wheel track test and flexural beam test show a decrease in fatigue life for mixes containing M-405-modified AAG-1 asphalt. For the flexural beam test, this decrease is also found for mixes with M-405-modified AAK-1 asphalt.

For mixes of AAG-1 asphalt modified with M-415 and M-416, results from the wheel track device and flexural beam test are generally opposite. For the wheel track test, fatigue life performance increases with modification, whereas for the flexural test, fatigue life performance decreases with modification. Beam test specimens prepared by SWL, Houston, were made using a kneading compaction procedure, while the slabs used in the wheel track test were prepared using rolling-wheel compaction. For the validation of the six core MRL asphalts described in the previous sections, beam specimens were prepared using the UCB rolling-wheel compaction procedure. Although mixes containing AAK-1 asphalt and modified with M-415 and M-416 showed improved fatigue performance in the flexural beam fatigue test, the results could not be validated because no asphalt-concrete slabs containing these asphalts were tested in the wheel track device. In general, the results from the validation effort for modified asphalt binders appear inconclusive.

14.2.3 Summary

The objective of this part of the validation effort was to compare the rankings of asphalt mixes tested in the wheel track device to those obtained in the flexural beam fatigue test in the controlled-strain mode of loading.

Wheel track tests were conducted on asphalt mixes containing six core MRL asphalts and one MRL aggregate. The experimental arrangement of the thin asphalt-concrete slab in the STF was such that the resulting structure represented a relatively thick, full-scale, in-service pavement structure and *controlled-stress* mode of loading. Findings and conclusions of this validation effort include the following:

- For mix stiffness, the ranking of core MRL asphalts based on indirect tensile stiffness at 20°C (68°F) was similar to the ranking obtained based on the flexural stiffness.

- For fatigue life, the rankings of core MRL asphalts based on fatigue life (N1) from wheel track testing were similar to those based on fatigue life obtained from the flexural beam fatigue tests.

- For modified mixes, validation results were generally inconclusive, except that both wheel track and flexural beam test results suggest that modification with M-405 is detrimental to the fatigue life of mixes containing AAG-1 asphalt.

14.3 LCPC-Nantes Wheel Track Study

This study was conducted to compare the fatigue performance of mixes containing two 60/70 penetration graded asphalts, designated as A and B. Rheological properties of the asphalt binders determined at the LCPC laboratory suggested the following:

- Asphalt B is more structured than asphalt A.

- Asphalt B is less temperature susceptible than asphalt A.

- Asphalt B has a smaller loss tangent than asphalt A over a range in dynamic stiffness, particularly at lower values of stiffness.

Based on the binder properties, it was hypothesized that mixes containing asphalt binder B would show better fatigue response than mixes containing asphalt binder A at the same asphalt content and air-void level. A 10/20 penetration grade asphalt was also evaluated to produce a high modulus mix for comparison with the fatigue performance of a mix containing asphalt A (4.6 percent asphalt content by weight of aggregate compared to the 5.4 percent used in conventional mixes).

Laboratory fatigue tests conducted on trapezoidal cantilever specimens at LCPC confirmed the hypotheses that mixes containing asphalt B are more fatigue resistant than mixes containing asphalt A and that the high-modulus mix will also show better fatigue performance than the mix containing asphalt A (4.6 percent asphalt content). In a cooperative effort, these same materials were also sent for further evaluation to the SHELL-KSLA laboratory, SWK Pavement Engineering, and the UCB. Results of these laboratory studies follow.

In order to validate the laboratory fatigue test results, a full-scale wheel track test was conducted by LCPC at the Nantes test track facility. This circular test track has a 20.5 m (67.25 ft) outer radius and a 14.5 m (47.6 ft) inner radius and is divided into four pavement sections that are subjected to full-scale loading. Figure 14.5 provides a general indication of the test layout, Figure 14.6 provides the schematics of the pavement structural sections.

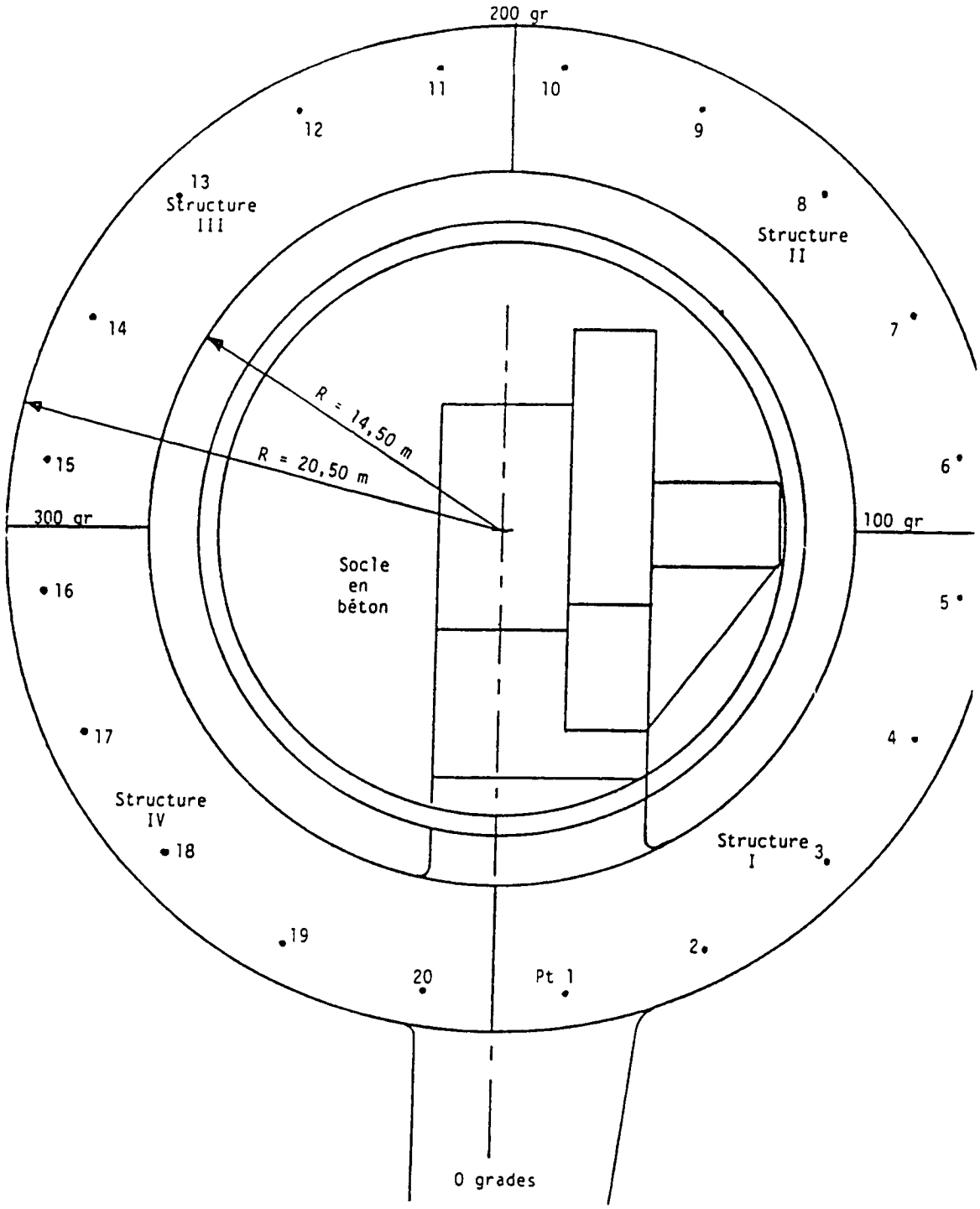

Figure 14.5. Test layout for pavement sections at Nantes wheel track facility

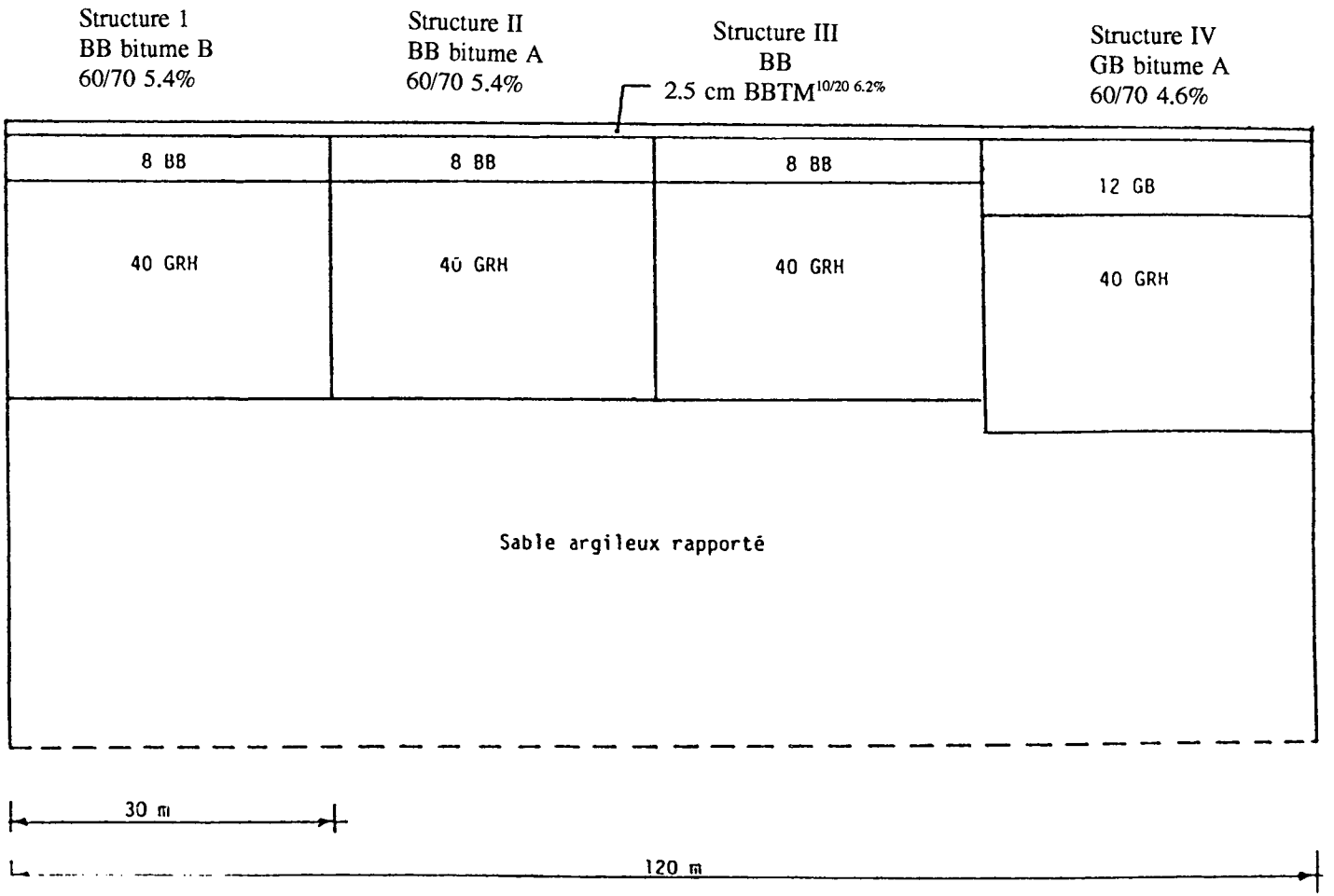

Figure 14.6. Schematics of the structural pavement sections

The four structural sections, I to IV, were constructed using the following materials:

Test Section	Binder	Asphalt Content by Weight of Aggregate (%)	Air-Void Content (%)
I	60/70 pen. grade asphalt B	5.4	3.5
II	60/70 pen. grade asphalt A	5.4	4.3
III	10/20 pen. grade asphalt	6.2	1.8
IV	60/70 pen. grade asphalt A	4.6	4.3

An 8 cm (3.2 in.) thick asphalt-concrete layer was used for structures I, II, and III over a 40 cm (16 in.) granular base layer. For structure IV, a 12 cm (4.7 in.) asphalt-concrete layer was selected to produce a fatigue life similar to that of the high-modulus mix structure. For all structures, the subgrade layer consisted of clayey sand with a stiffness of approximately 14,500 psi. The asphalt-concrete layer was overlaid with a thin wearing course consisting of a stone mastic asphalt (SMA) containing modified binder (fibers are included in the binder). The actual layer thicknesses and material properties of each structural section are summarized in Table 14.5.

Table 14.5. Layer thickness and material properties for pavement sections

Layer	Section I		Section II		Section III		Section IV	
	Thick-ness (in.)	Stiffness (psi)	Thick-ness (in.)	Stiffness (psi)	Thick-ness (in.)	Stiffness (psi)	Thick-ness (in.)	Stiffness (psi)
Wearing Course	0.80	650,000	0.5	650,000	0.5	650,000	0.6	650,000
Asphalt Concrete	2.65	[a]	2.9	[a]	3.0	[a]	3.9	[a]
Aggregate Base	17.20	48,000	16.6	48,000	16.5	48,000	17.2	48,000
Subgrade		14,500		14,500		14,500		14,500

[a]Asphalt layer stiffness obtained from laboratory fatigue tests.

Pavement loading was transmitted through dual tires with 6.5 metric tonnes (14,300 lb) load, representative of one-half of a single-axle load moving at a speed of 70 km/h (39 mph). An 8 bars (116 psi) tire pressure was used, giving a resulting contact area of 651 cm^2 (100 in^2) per tire.

Results of the fatigue tests conducted at the various laboratories are presented in the following section. Following the discussion of laboratory tests, results from the wheel track study are summarized and compared with the laboratory test results.

Results presented in this report are summarized from various published documents as well as unpublished memorandums from various agencies, including notes from J. Bonnot's (1991) presentations at UCB. Details of each experiment can be obtained from the following references: Gramsammer and Kerzreho (1992), Robertus et al. (1992), and Rowe (1992). Results of fatigue test conducted at LCPC are contained in Appendix F.

14.3.1 Laboratory Fatigue Test Results

14.3.1.1 Selection of Materials and Variables

The mix and testing variables included in this part of the validation testing program were as follows:

- **Asphalts.** The non-MRL asphalts supplied by LCPC were used: asphalt A (60/70 pen.), asphalt B (60/70 pen.), and a high-modulus material (10/20 pen.).

- **Aggregates.** One non-MRL aggregate supplied by LCPC was used.

- **Asphalt Content.** For asphalt A, two asphalt contents—5.4 and 4.6 percent by weight of aggregate—were used. The mix with asphalt B contained 5.4 percent, while that with the high-modulus material contained 6.2 percent, both by weight of aggregate.

- **Air-Void Contents.** One air-void content was used. The average air-void levels achieved for the different mixes were: 3.8 percent for mixes containing asphalt A (5.4 percent asphalt content); 4.1 percent for mixes containing asphalt B; 1.7 percent for mixes containing 10/20 pen. high modulus asphalt; and 5.3 percent for mixes containing asphalt A (4.6 percent asphalt content). These air-void contents are similar to those reported for the in situ pavement structures.

- **Strain Levels.** Strain levels varied between 200 and 1200 micro in./in.

- **Test Frequency.** All tests at UCB were performed under the controlled-strain mode of loading at a frequency of 10 Hz under sinusoidal loading with no rest periods.

- **Test Temperature.** All tests were performed at 20°C (68°F).

- **Compaction Procedure**. Specimens were 6.4 cm (2.5 in.) wide, 5.1 cm (2.0 in.) tall, and 40.7 cm (15.0 in.) long and were sawed from slabs prepared using rolling-wheel compaction.

The response variables measured included 1) initial flexural stiffness measured at the 50th load cycle, 2) fatigue life—the number of cycles to a 50 percent reduction in initial stiffness, 3) initial dissipated energy per cycle measured at 50th load cycle, and 4) cumulative dissipated energy associated with the fatigue life.

14.3.1.2 Test Results

Apart from the flexural beam fatigue tests at UCB, fatigue tests were also conducted at LCPC, SHELL-KSLA, and SWK. Test type, specimen configuration, mode of loading, temperature, and frequency used for these different studies are summarized below:

Variable	**UCB**	**SHELL-KSLA**	**LCPC**	**SWK**
Test Type	Flexural Beam	Flexural Beam	Trapezoidal Cantilever	Trapezoidal Cantilever
Mode of Loading	Controlled-Strain (tension only)	Controlled-Stress (tension-compression)	Controlled-Strain (tension-compression)	Controlled-Stress (tension-compression)
Temperature	20°C (68°F)	20°C (68°F)	20°C (68°F)	20°C (68°F)
Test Frequency	10 Hz	40 Hz	25 Hz	20 Hz

For each fatigue study, test results are summarized for each mix in the form of following relationships:

$$N = K_1 \epsilon^{K_2} \tag{14.2}$$

and/or

$$N = K_3 \sigma^{K_4} \tag{14.3}$$

where: N = fatigue life,
σ = initial tensile stress amplitude, psi,
ϵ = initial tensile strain amplitude, in./in., and
K_1 to K_4 = experimentally determined coefficients.

Linear regression calibration results for fatigue life as a function of strain and stress are presented in Tables 14.6 and 14.7. Regression fits for most mixes were good; coefficients of determination vary between 0.84 and 0.99.

Table 14.6. Regression coefficients for strain-life relationships

Pavement Section	K_1	K_2	R^2
UCB controlled-strain, flexural beam test, 20°C (68°F), 10 Hz			
I — asphalt B	$2.988*10^{-13}$	-5.0102	0.96
II — asphalt A (5.4%)	$7.386*10^{-13}$	-4.7042	0.99
III — high-modulus mix	$4.054*10^{-15}$	-5.4843	0.99
IV — asphalt A (4.6%)	$2.831*10^{-11}$	-4.1660	0.99
SHELL-KSLA controlled-stress, flexural beam test, 20°C (68°F), 40 Hz			
I — asphalt B	$2.203*10^{-10}$	-4.1432	0.95
II — asphalt A (5.4%)	$5.071*10^{-16}$	-5.4286	0.93
III — high-modulus mix	$6.657*10^{-14}$	-5.0665	0.84
LCPC controlled-strain, trapezoidal cantilever test, 20°C (68°F), 25 Hz			
I — asphalt B	$1.45*10^{-9}$	-4.064	-
II — asphalt A (5.4%)	$8.10*10^{-7}$	-3.128	-
III — high-modulus mix	$6.94*10^{-9}$	-3.871	-
IV — asphalt A (4.6%)	$6.954*10^{-3}$	-2.098	-
SWK controlled-stress, trapezoidal cantilever test, 20°C (68°F), 20 Hz			
I — asphalt B	$2.404*10^{-12}$	-4.2975	0.97
II — asphalt A (5.4%)	$7.877*10^{-17}$	-5.3752	0.94
III — high-modulus mix	$1.139*10^{-16}$	-5.5434	0.98
IV — asphalt A (4.6%)	$1.372*10^{-17}$	-5.5585	0.98

Table 14.7. Regression coefficients for stress-life relationships

Pavement Section	K_1	K_2	R^2
UCB controlled-strain, flexural beam test, 20°C (68°F), 10 Hz			
I — asphalt B	$4.663*10^{22}$	-7.9672	0.98
II — asphalt A (5.4%)	$2.345*10^{16}$	-5.1550	0.98
III — high-modulus mix	$7.562*10^{21}$	-6.4611	0.99
IV — asphalt A (4.6%)	$6.822*10^{15}$	-4.9662	0.99
SWK controlled-stress, trapezoidal cantilever test, 20°C (68°F), 20 Hz			
I — asphalt B	$3.800*10^{15}$	-4.8824	0.97
II — asphalt A (5.4%)	$1.470*10^{17}$	-5.5280	0.96
III — high-modulus mix	$3.007*10^{20}$	-6.4020	0.97
IV — asphalt A (4.6%)	$3.346*10^{18}$	-6.0080	0.98

Stiffness. Average stiffnesses for the four mixes are shown in Table 14.8. For all tests, specimens containing 60/70 pen. asphalt B showed the lowest stiffness, and those containing 10/20 pen. asphalt (high-modulus mix) showed the highest stiffness. Specimens containing 60/70 pen. asphalt A showed stiffnesses between the two extremes. As expected, specimens with a higher asphalt content (asphalt A at 5.4 percent) exhibited lower average stiffness than specimens with a lower asphalt content (asphalt A at 4.6 percent).

Table 14.8. Average pavement section stiffness

Pavement Section	UCB Controlled-Strain Test, 20°C (68°F), 10 Hz	SHELL-KSLA Controlled-Stress Test, 20°C (68°F), 40 Hz	LCPC Controlled-Strain Test, 20°C (68°F), 25 Hz	SWK Controlled-Stress Test, 20°C (68°F), 20 Hz
I — asphalt B	$5.35*10^5$	$1.005*10^6$	$9.96*10^5$	$1.053*10^6$
II — asphalt A (5.4%)	$7.00*10^5$	$1.35*10^6$	$1.167*10^6$	$1.337*10^6$
III — high-modulus mix	$1.35*10^5$	$1.653*10^6$	$1.602*10^6$	$1.572*10^6$
IV — asphalt A (4.6%)	$7.95*10^5$	-	$1.392*10^6$	$1.518*10^6$

Stiffness comparisons between laboratories indicate that the average stiffnesses of mixes tested at the UCB laboratory are lower than those tested at the other laboratories. These lower stiffnesses are attributed to two factors: 1) the test frequency used at UCB was lower than those used at the other laboratories—10 Hz versus 40, 25, and 20 Hz used at SHELL-KSLA, LCPC, and SWK, respectively, and 2) the average air-void content of beam

specimens prepared at UCB was higher than that of specimens obtained from the field and tested at other laboratories. Stiffness results suggest the following ranking:

(Lowest Stiffness) 1	2	3	(Highest Stiffness) 4
Asphalt B	Asphalt A (5.4%)	Asphalt A (4.6%)	High-modulus mix

Tensile Strain at 10^6 Load Repetitions. Table 14.9 shows the tensile strains corresponding to a million load repetitions for different asphalt mixes. Conventional wisdom would dictate that for controlled-strain tests, mixes exhibiting lower stiffness and higher asphalt content will show better fatigue performance. For the 60/70 pen. asphalts, A and B, this observation was confirmed by both UCB and LCPC controlled-strain fatigue test results, where mixes containing asphalt B outperformed mixes containing asphalt A. For mixes containing asphalt A, the tensile strain corresponding to a million load repetitions decreased with decreasing asphalt content for both tests as anticipated. The high-modulus mix containing 10/20 pen. asphalt was anticipated to exhibit the poorest fatigue performance because of its higher stiffness, but was observed to exhibit the second best performance, following mixes containing asphalt B. The high-modulus mix had the lowest air-void content and a higher asphalt content, both known to improve the fatigue characteristics of asphalt-aggregate mixes. On the other hand, asphalt A with its 4.6 percent asphalt content generally had higher stiffness values than mixes containing higher asphalt contents (5.4 percent), but it had the poorest fatigue performance.

Table 14.9. Tensile microstrain to 10^6 cycles

Pavement Section	UCB Controlled-Strain Test, 20°C (68°F), 10 Hz	SHELL-KSLA Controlled-Stress Test, 20°C (68°F), 40 Hz	LCPC Controlled-Strain Test, 20°C (68°F), 25 Hz	SWK Controlled-Stress Test, 20°C (68°F), 20 Hz
I — asphalt B	200	171	169	80
II — asphalt A (5.4%)	140	120	104	77
III — high-modulus mix	191	164	159	110
IV — asphalt A (4.6%)	106	-	91	77

Controlled-stress fatigue tests at SHELL-KSLA show trends for tensile strain at a million repetitions similar to those observed for the controlled-strain tests (i.e., mixes containing asphalt B showed the best performance, followed by the high-modulus mix and mixes containing asphalt A). In contrast, controlled-stress fatigue test results at SWK indicate that the high-modulus mix will perform better, followed by mixes containing asphalt B and A, respectively. No difference was found between asphalt A mixes with different asphalt

contents. Based on test results from UCB, SHELL-KSLA, and LCPC, the fatigue performance of the mixes may be ranked as follows:

(Lowest Fatigue Performance)			(Highest Fatigue Performance)
1	2	3	4
Asphalt A (4.6%)	Asphalt A (5.4%)	High-Modulus Mix	Asphalt B

Fatigue Life at 200 Microstrain. Table 14.10 shows the fatigue life of different mixes at the 200 microstrain level. These values were computed using the strain-life relationships presented in Table 14.6. UCB, SHELL-KSLA, and LCPC results indicate that mixes containing asphalt B will show the highest fatigue life at 200 microstrain, followed by the high-modulus mix and mixes containing asphalt A. SWK controlled-stress tests indicate that at 200 microstrain the high-modulus mix will show the highest fatigue life, followed by mixes containing asphalt B and both mixes containing asphalt A, respectively. With respect to asphalt content, UCB and SWK results indicate a decrease in fatigue life with decreasing asphalt content. LCPC test results indicate an increase in fatigue life with decreasing asphalt content. Based on the UCB fatigue test results, mix rankings are similar to those obtained based on the tensile strain at a million load repetitions as shown above.

Table 14.10. Fatigue life at 200 microstrain

Pavement Section	UCB Controlled-Strain Test, 20°C (68°F), 10 Hz	SHELL-KSLA Controlled-Stress Test, 20°C (68°F), 40 Hz	LCPC Controlled-Strain Test, 20°C (68°F), 25 Hz	SWK Controlled-Stress Tests, 20°C (68°F), 20 Hz
I — asphalt B	1,019,000	500,000	1,558,600	19,000
II — asphalt A (5.4%)	186,000	63,000	300,000	6000
III — high-modulus mix	784,000	363,000	1,441,000	36,500
IV — asphalt A (4.6%)	72,000	-	400,000	5000

Fatigue Life at 1750 kPa (254 psi) Stress Level. Table 14.11 shows the fatigue life of different mixes at the 1750 kPa (254 psi) stress level. These values were computed using the stress-life relationships presented in Table 14.7. UCB and SWK test results indicate that, based on a given stress level, a high-modulus mix will exhibit the longest fatigue life, followed by both mixes containing asphalt A and mixes containing asphalt B. SHELL-KSLA test results indicate that mixes containing asphalt B will show better fatigue performance than mixes containing asphalt A (5.4 percent).

Table 14.11. Fatigue life at 1750 kPa (254 psi) stress level

Pavement Section	UCB Controlled-Strain Test, 20°C (68°F), 10 Hz	SHELL-KSLA Controlled-Stress Test, 20°C (68°F), 40 Hz	LCPC Controlled-Strain Test, 20°C (68°F), 25 Hz	SWK Controlled-Stress Test, 20°C (68°F), 20 Hz
I — asphalt B	3200	94,000	-	6900
II — asphalt A (5.4%)	9400	67,000	-	7500
III — high-modulus mix	2,191,000	1,670,000	-	121,000
IV — asphalt A (4.6%)	7800	-	-	11,900

With respect to asphalt content, UCB test results indicate that decreasing the asphalt content will decrease fatigue life, whereas SWK results indicate the opposite. Based on the UCB results at a given stress level, mixes may be ranked as follows:

(Lowest Fatigue Performance)			**(Highest Fatigue Performance)**
1	**2**	**3**	**4**
Asphalt B	Asphalt A (4.6%)	Asphalt A (5.4%)	High-modulus mix

14.3.1.3 In Situ Fatigue Life Estimate Using Laboratory Test Results

In situ mix performance was simulated by linear elastic layer analysis (ELSYM) of the response of the four pavement structures identified in Table 14.5 and Figure 14.6. A 6.5 metric tonne (14,300 lb) wheel load on dual tires with 651 cm^2 (100 in^2) contact area (per tire) was used for this analysis.

For each pavement structure, the maximum tensile strain at the bottom of the asphalt layer was determined from the elastic analysis. These results are summarized in Table 14.12. Using these tensile strains and the laboratory fatigue relationships between strain and fatigue life presented in Table 14.6, cycles to failure in the pavement structures were determined. These results from all laboratories, presented in Table 14.13, indicate that fatigue performance for pavements containing asphalt B will be better than the pavement containing asphalt A (5.4 percent). Also, a pavement containing the high-modulus mix will not perform as well as pavement containing asphalt A (4.6 percent).

Table 14.12. Maximum tensile microstrains under asphalt layer

Pavement Section	UCB	SHELL-KSLA	LCPC	SWK
I — asphalt B	192	158	157	155
II — asphalt A (5.4%)	178	151	143	143
III — high-modulus mix	141	132	130	133
IV — asphalt A (4.6%)	150	-	119	114

Table 14.13. Cycles to failure simulated using the laboratory test results

Pavement Section	UCB	SHELL-KSLA	LCPC	SWK
I — asphalt B	$4.03*10^7$	$4.06*10^6$	$4.17*10^6$	$5.66*10^4$
II — asphalt A (5.4%)	$8.38*10^6$	$7.23*10^5$	$8.57*10^5$	$3.65*10^4$
III — high-modulus mix	$2.38*10^8$	$7.20*10^6$	$7.64*10^6$	$3.50*10^5$
IV — asphalt A (4.6%)	$4.33*10^6$	-	$1.19*10^6$	$1.14*10^5$

Table 14.14 presents the estimated fatigue lives of pavement sections using the surrogate fatigue model (see Chapter 15). Performance rankings are similar to those based on the laboratory fatigue tests (i.e., the mix containing asphalt B outperforms the mix containing asphalt A [5.4 percent] and the high-modulus mix outperforms the mix containing asphalt A [4.6 percent]).

Table 14.14. Cycles to failure simulated using the surrogate fatigue model

Pavement Section	UCB Surrogate Fatigue Model
I — asphalt B	$2.82*10^6$
II — asphalt A (5.4%)	$2.14*10^6$
III — high-modulus mix	$9.89*10^6$
IV — asphalt A (4.6%)	$1.66*10^6$

14.3.2 Wheel Track Test Results

Results of the laboratory fatigue tests indicate that pavement structures containing asphalt B (5.4 percent) will perform better than structures containing asphalt A (5.4 percent), and the structure containing the high-modulus mix will perform better than that containing asphalt A (4.6 percent). As discussed earlier, in order to validate the laboratory findings, a full-scale, circular wheel track test containing these different materials was subjected to repeated wheel loads. Surface cracking in each section was monitored at periodic intervals as wheel

passages increased. Table 14.15 and Figure 14.7 summarize the evolution of percentage of cracked surface in each section.

Table 14.15. Evolution of percentage of cracked surface with load applications

Traffic	Section I Asphalt B (5.4%)	Section II Asphalt A (5.4%)	Section III High-Modulus Mix (6.2%)	Section IV Asphalt A (4.6%)
1,165,000	45	34	11	2
1,902,000	80	57	60	2
2,124,000	81	59	61	2
2,310,000	97	71	72	11
2,666,000	100	72	74	47

The pavement section containing asphalt B showed the worst performance; 100 percent of its surface cracked at the end of approximately 2.67 million load applications. The pavement section containing asphalt A (4.6 percent) at a lower asphalt content showed the best performance; less than 50 percent of its surface cracked at approximately 2.67 million load applications. The sections containing the mixes with asphalt A (5.4 percent) and the high-modulus mix showed similar performance; approximately 73 percent of its surface cracking at the same number of wheel load applications.

Because of the discrepancy between the laboratory test results and the wheel track test results, a second test track was constructed with structural sections similar to the first. However, in the second pavement section the asphalt wearing surface was excluded and the asphalt-concrete layer was loaded directly. Results (Figure 14.8) from the second wheel track experiment are generally similar to those of the first experiment.

14.3.3 Summary

The objective of this part of the validation effort was to compare the ranking of mixes tested in the full-scale, circular wheel track test facility at LCPC to the ranking obtained from the controlled-stress and controlled-strain flexural fatigue tests using beam and trapezoidal cantilever specimens. Findings of this validation effort include the following:

- The flexural beam fatigue testing in controlled-strain and controlled-stress modes of loading at UCB and SHELL-KSLA, respectively, and trapezoidal cantilever fatigue tests in controlled-strain and controlled-stress modes of loading at LCPC and SWK, respectively, predicted better fatigue performance

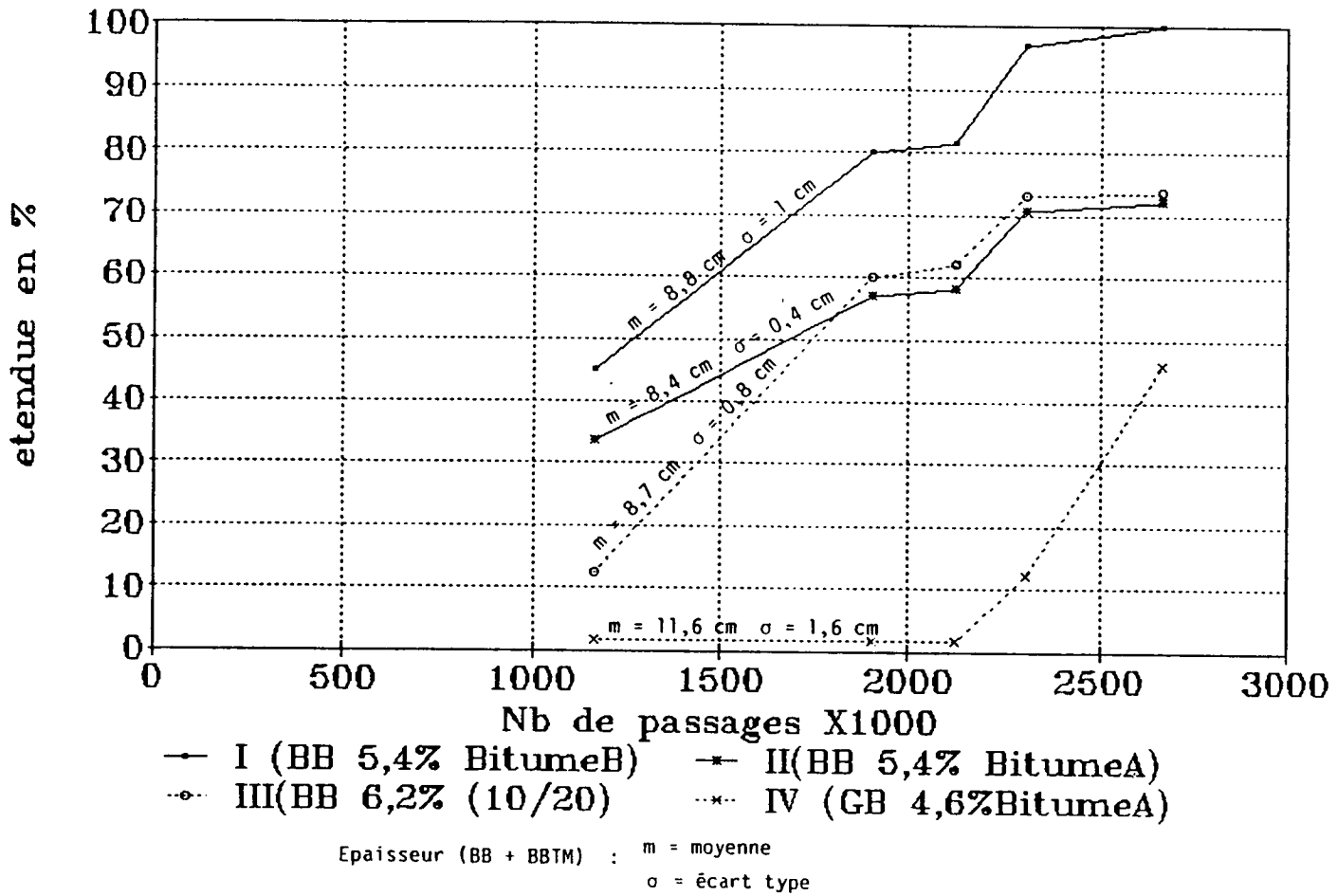

Figure 14.7. Evolution of surface cracking with wheel passes (experiment 1) (after Gramsammer and Kerzreho 1992)

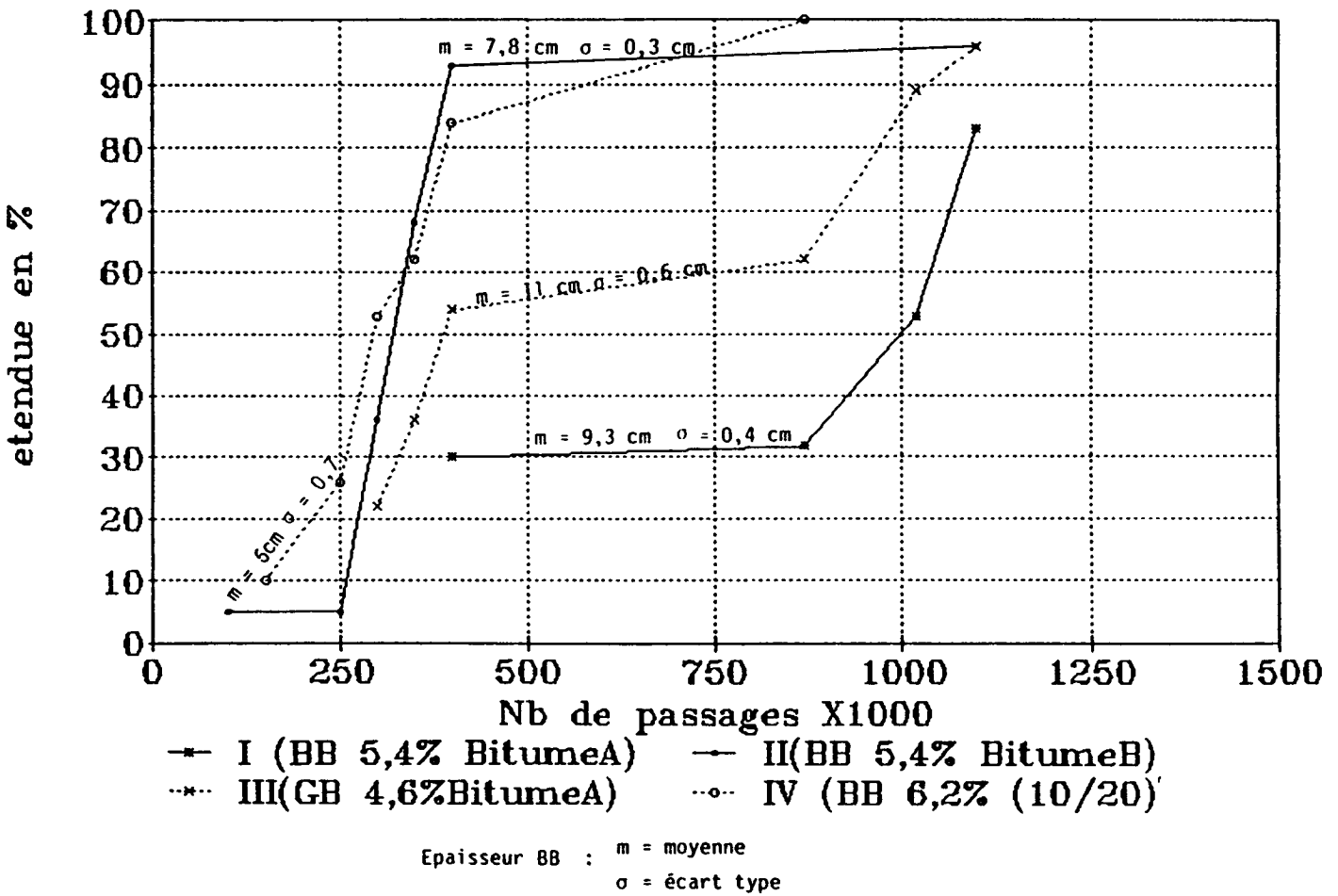

Figure 14.8. Evolution of surface cracking with wheel passes (experiment 2) (after Gramsammer and Kerzreho 1992)

for mixes containing asphalt B (5.4 percent) than mixes containing asphalt A (5.4 percent). Similarly, fatigue tests indicated better fatigue performance for the high-modulus mix than mixes containing asphalt A (4.6 percent).

- Fatigue life estimated for the in situ structures containing these different mixes, based on both the laboratory fatigue tests and the surrogate fatigue model, also confirmed the above ranking of the asphalt mixes.

- Wheel track test results do not support the ranking of the mixes obtained from laboratory fatigue test results. Because of the concern that the asphalt wearing course may have affected the test results in the first wheel track experiment, a second wheel track experiment was conducted without the asphalt wearing course. Results of the second wheel track test were generally identical to those of the first experiment. The pavement section containing asphalt B (5.4 percent) had more surface cracking than the section containing asphalt A (5.4 percent) at the same number of wheel load passes; the section containing the high-modulus mix had more surface cracking than the section containing asphalt A (4.6 percent) at the same number of wheel load passes.

14.4 FHWA Accelerated Loading Facility

The objective of the FHWA-ALF pavement test study was to evaluate the fatigue performance of a thin asphalt pavement section (8.9 cm [3.5 in.] asphalt-concrete layer over a 30.5 cm [12 in.] base) when subjected to dual- versus single-tire loading.

Sawed slab sections of asphalt-concrete from this facility were received at UCB. Beam specimens 63.5 mm × 50.8 mm × 381.0 mm (2.5 in. × 2.0 in. × 15.0 in.) were sawed from the asphalt-concrete slab, and controlled-strain fatigue tests were performed on these specimens using the UCB fatigue test apparatus. The asphalt and aggregate used for this study were non-MRL materials. The average asphalt content was 4.6 percent by weight of mix, and the average air-void content was 4.2 percent. Testing variables for this study included the following:

- **Strain Level.** Four strain levels were used: 200, 400, 600, and 800 micro in./in.

- **Test Frequency.** All tests were performed under a controlled-strain mode of loading at a frequency of 10 Hz under sinusoidal loading with no rest periods.

- **Test Temperature.** All tests were performed at 20°C (68°F).

- **Replicates.** Two replicate specimens were tested at each strain level.

The response variables measured included 1) initial flexural stiffness at the 50th load cycle, 2) fatigue life—the number of cycles to a 50 percent reduction in initial stiffness, 3) initial

dissipated energy per cycle measured at the 50th load cycle, and 4) cumulative dissipated energy associated with fatigue life. Results of the fatigue tests for this part of the test program are presented in Appendix G.

Fatigue test results are summarized below in the form of relationships between fatigue life and initial strain, initial dissipated energy per cycle, and cumulative dissipated energy to failure, respectively, developed using linear regression calibrations:

$$N_f = 8.959*10^{-8} (\epsilon_o)^{-3.5741} \qquad R^2 = 0.987 \qquad (14.4)$$

$$N_f = 425.81 (w_o)^{-1.8459} \qquad R^2 = 0.987 \qquad (14.5)$$

$$N_f = 0.0012 (W_N)^{-2.2225} \qquad R^2 = 0.987 \qquad (14.6)$$

where: N_f = fatigue life,
ϵ_o = initial peak-to-peak tensile strain,
w_o = initial dissipated energy per cycle, psi, and
W_N = cumulative dissipated energy to N_f, psi.

In situ mix performance was simulated using an elastic analysis of the response of the given pavement section under single and dual tires with 53.3 kN (12,000 lb) wheel load (24 kip axle load) and a 965 kPa (140 psi) tire pressure. An average asphalt-concrete layer stiffness of 700,000 psi and an aggregate base layer stiffness of 15,000 psi were used. Two subgrade stiffnesses—35 MPa and 70 MPa (5000 and 10,000 psi)—were used. The maximum tensile strain at the bottom of the asphalt layer was determined from the elastic analysis, and the fatigue life was determined using Equation 14.4, as well as the surrogate fatigue model (Equation 15.1, see Chapter 15). Results are presented in Table 14.16, and indicate an estimated fatigue life of approximately 40,000 to 50,000 load repetitions for a single-tire configuration, and 70,000 to 90,000 load repetitions for a dual-tire configuration, depending on the subgrade stiffness.

Table 14.16. Estimated fatigue life for the in situ pavement (FHWA-ALF study)

Tire Configuration	Subgrade Stiffness (psi)	Tensile Strain Under AC Layer	Fatigue Life Estimate, Using Lab Relationship ϵ-Nf	Fatigue Life Estimate, Using Surrogate Model
Single	5000	$5.51*10^{-4}$	40,000	36,000
Single	10,000	$5.26*10^{-4}$	47,000	43,000
Dual	5000	$4.67*10^{-4}$	72,000	66,000
Dual	10,000	$4.43*10^{-4}$	87,000	80,000

Preliminary results from the pavement testing reported by the FHWA, shown in Figure 14.9, indicate a fatigue life to surface crack initiation of approximately 55,000 and 110,000 load repetitions for the single- and dual-tire configurations, respectively. Detailed comparison of the actual and estimated fatigue life was not possible when this report was prepared because

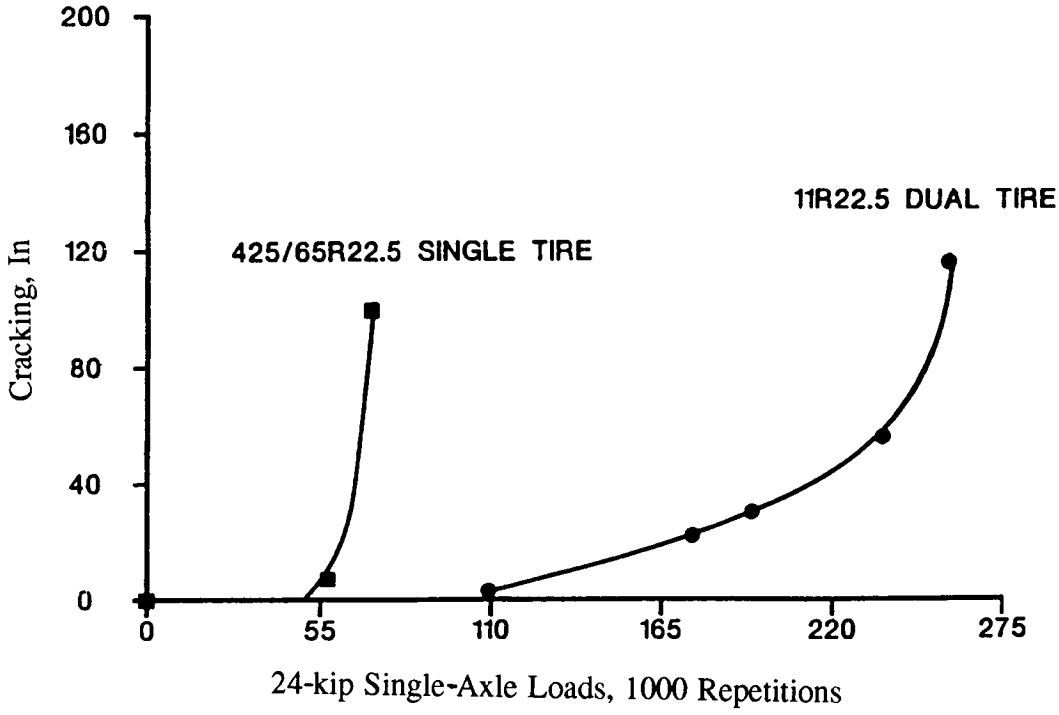

Figure 14.9. Surface cracking versus number of 24-kip single-axle load repetitions (FHWA-ALF pavement study)

the details of the experimental results, such as variations in temperature and the material properties of the various structural layers, were unavailable from the FHWA. Findings from this validation effort may be summarized as follows:

- Estimated fatigue life for the in situ pavement based on the laboratory strain-life relationship compares well with the estimated fatigue life based on the surrogate fatigue model.
- Estimated fatigue life for the in situ pavement is approximately double for the dual-tire configuration compared to the single-tire configuration.
- Actual pavement fatigue life to surface crack initiation is approximately double that for the dual-tire configuration compared to the single-tire configuration.

14.5 Summary

Validation studies were conducted to compare results and rankings of asphalt mixes from specific accelerated wheel track test facilities to those obtained from the SHRP Project A-003A laboratory controlled-strain, flexural beam fatigue test. The specific wheel track facilities involved included the SWK laboratory wheel track device in Nottingham, United Kingdom; a full-scale, LCPC circular test track at Nantes, France; and the FHWA-ALF in Mclean, Virginia.

Results of the laboratory wheel track tests conducted at SWK on asphalt mixes containing six core MRL asphalts and one MRL aggregate are summarized as follows:

- For mix stiffness, ranking of core MRL asphalts based on indirect tensile stiffness at 20°C (68°F) was similar to the ranking obtained based on flexural stiffness.

- For fatigue life, ranking of core MRL asphalts based on fatigue life (N1) from wheel track testing was similar to the ranking based on fatigue life obtained from flexural beam fatigue tests.

Validation results for the modified asphalt-aggregate mixes were generally inconclusive, except that both wheel track tests and flexural beam test results suggest that modification with M-405 is detrimental to the fatigue life of mixes containing AAG-1 asphalt.

Results from SHRP A-003A's controlled-strain, flexural beam fatigue test on mixes from the LCPC-Nantes test facility are in good agreement with test results obtained by SHELL-KSLA as well as LCPC. The rankings of asphalt mixes observed in the circular wheel track test section, however, are not in agreement with the in situ fatigue life estimated using any of the laboratory test methods and the surrogate fatigue model. Findings from the LCPC-Nantes validation study are summarized as follows:

- Flexural beam fatigue testing in controlled-strain and controlled-stress modes of loading at UCB and SHELL-KSLA, respectively, and trapezoidal cantilever fatigue testing in controlled-strain and controlled-stress modes of loading at LCPC and SWK, respectively, predicted that mixes containing asphalt B (5.4 percent) will show better fatigue performance than mixes containing asphalt A (5.4 percent). Similarly, fatigue tests indicated that the high-modulus mix will also show better fatigue performance than mixes containing asphalt A (4.6 percent).

- Fatigue life estimated for the in situ structures containing these different mixes, based on both the laboratory fatigue tests and the surrogate fatigue model, also confirmed the above ranking of the asphalt mixes.

- Wheel track test results do not support the ranking of the mixes that was based on the laboratory fatigue test results. Because of the concern that the asphalt wearing course may have affected the test results in the first wheel track experiment, a second wheel track experiment was conducted without the asphalt wearing course. Results of the second wheel track test were generally identical to those of the first experiment. The pavement section containing asphalt B (5.4 percent) exhibited more surface cracking than the section containing asphalt A (5.4 percent) at the same number of wheel load passes; the section containing the high-modulus mix exhibited more surface cracking than the section containing asphalt A (4.6 percent) at the same number of wheel load passes.

For the FHWA-ALF validation study, comparison of the actual and estimated fatigue life was limited by the unavailability of the details, including the variations in temperature and material properties of the various structural layers, of the experimental results from the FHWA. Preliminary results from the pavement testing reported by the FHWA indicate a fatigue life to surface crack initiation of approximately 55,000 and 110,000 load repetitions for the single- and dual-tire configurations, respectively. These results are in good agreement with the laboratory-based estimate of fatigue lives of approximately 45,000 load repetitions for single-tire and 80,000 for dual-tire loadings.

15

Calibration of Surrogate Fatigue Models Using All Applicable A-003A Fatigue Data

15.1 Introduction

The applicability of the surrogate fatigue models developed during the expanded test program detailed in Chapter 10 was examined using the mix design study and Nantes validation study. Details of the validation effort can be found in various chapters of this report as well as in the study by Deacon and Tayebali (1992a). Results of these efforts are summarized in following sections.

The primary conclusion of the validation analysis was that models developed during the 8×2 expanded test program do not accurately simulate the behavior observed during the mix design experiment. No likely cause for such discrepancies was readily apparent.

Basic strain-based fatigue models were calibrated independently for the expanded test program, the mix design experiment, and the Nantes validation test program since each of these experiments included different materials and variables. A fatigue model was also calibrated from the combined data from these three experiments. These results, summarized in Table 15.1, show that the fatigue life of the Nantes mixes is much more sensitive to flexural strain than the other mixes. Predictions using the composite model are compared with measurements for each of the tested mixes in Table 15.2 and in Figures 15.1 through 15.21.

Table 15.1. Effect of testing program on regression model calibration

Testing Program	Regression Model	R^2	Std. Error of Estimate
8×2 Expanded Program	$N_f = 470.4\ \exp^{0.052\ VFB}\ \epsilon^{-3.948}\ S''^{-2.271}$	0.84	0.578
Nantes	$N_f = 1.208\times10^{13}\ \exp^{0.097\ VFB}\ \epsilon^{-4.967}\ S''^{-4.950}$	0.95	0.561
Mix Design	$N_f = 638.1\ \exp^{0.107\ VFB}\ \epsilon^{-3.309}\ S''^{-2.309}$	0.94	0.467
Combined	$N_f = 2.015\times10^{6}\ \exp^{0.080\ VFB}\ \epsilon^{-3.525}\ S''^{-2.838}$	0.77	0.800

Table 15.2. Comparison of predicted life with measured life

Mix	Average Ratio of Predicted to Measured Fatigue Life
AH	1.42
BH	1.46
CH	1.04
DH	1.43
FH	1.48
GH	1.53
KH	1.16
MH	1.34
AD	1.45
BD	0.94
CD	0.73
DD	0.79
FD	0.54
GD	1.32
KD	0.53
MD	0.41
Nantes B	0.56
Nantes A (5.4%)	0.68
Nantes Modified	0.93
Nantes A (4.6%)	0.76
Mix Design—FM	3.5

Note: Mix type AH denotes MRL asphalt A and MRL aggregate RH.
Mix type AD denotes MRL asphalt A and MRL aggregate RD.

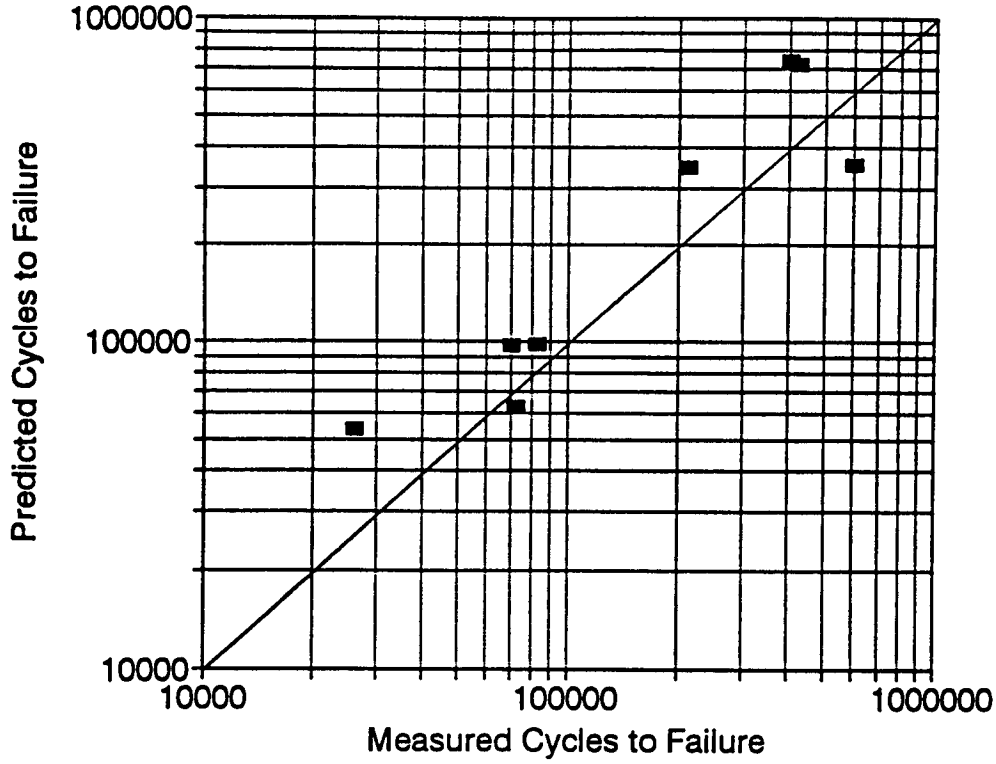

Figure 15.1. Measured cycles to failure versus predicted cycles to failure for mix containing AAA-1 asphalt and RH aggregate

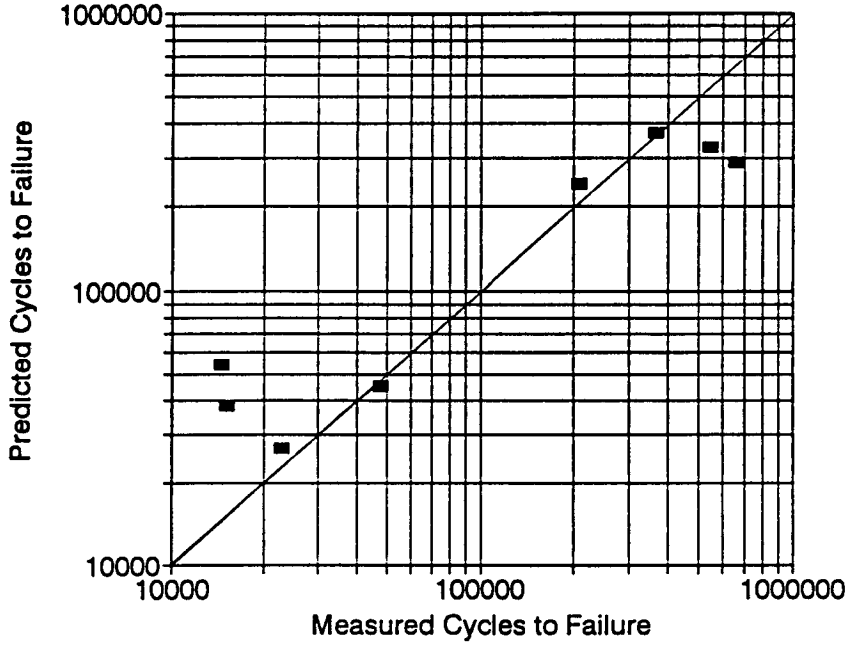

Figure 15.2. Measured cycles to failure versus predicted cycles to failure for mix containing AAB-1 asphalt and RH aggregate

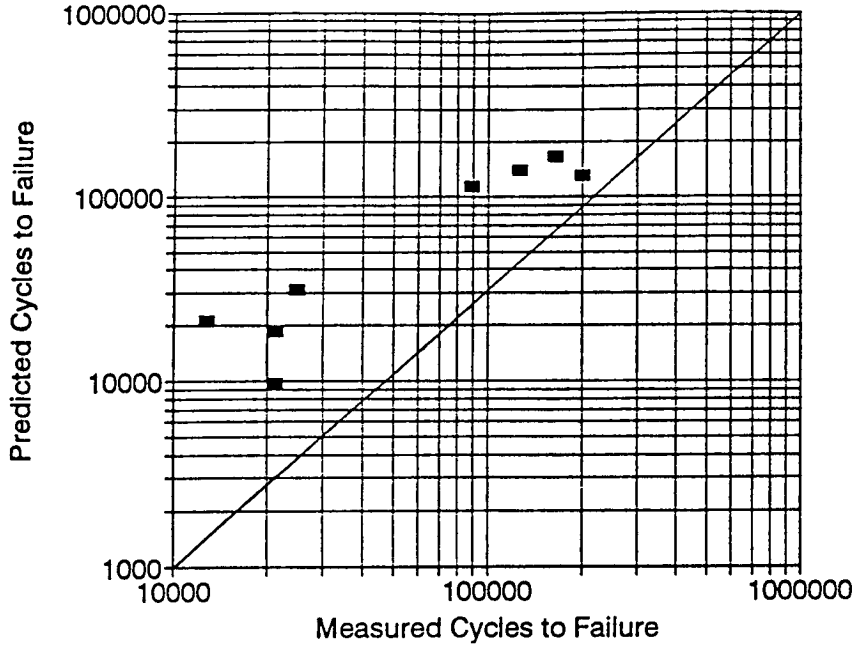

Figure 15.3. Measured cycles to failure versus predicted cycles to failure for mix containing AAC-1 asphalt and RH aggregate

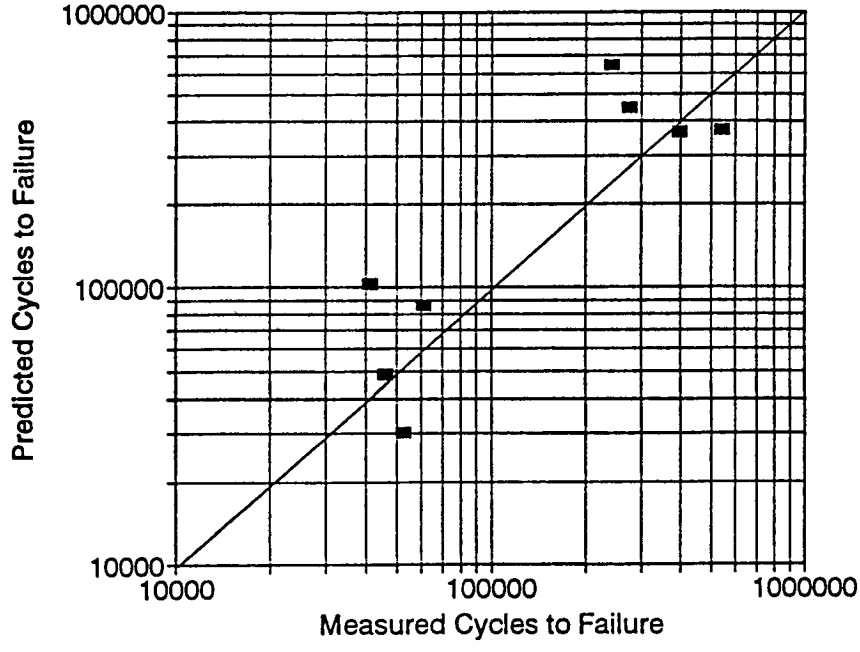

Figure 15.4. Measured cycles to failure versus predicted cycles to failure for mix containing AAD-1 asphalt and RH aggregate

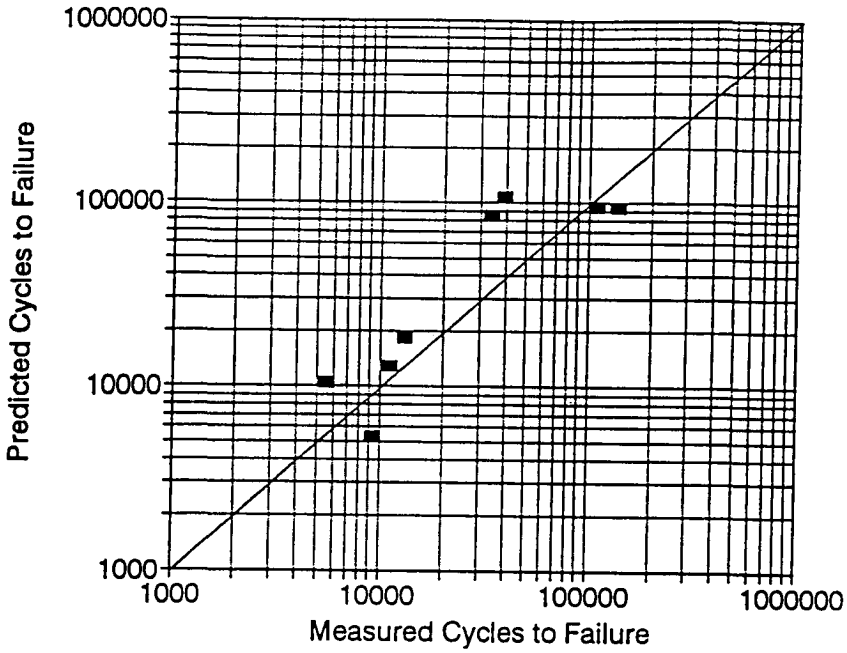

Figure 15.5. Measured cycles to failure versus predicted cycles to failure for mix containing AAF-1 asphalt and RH aggregate

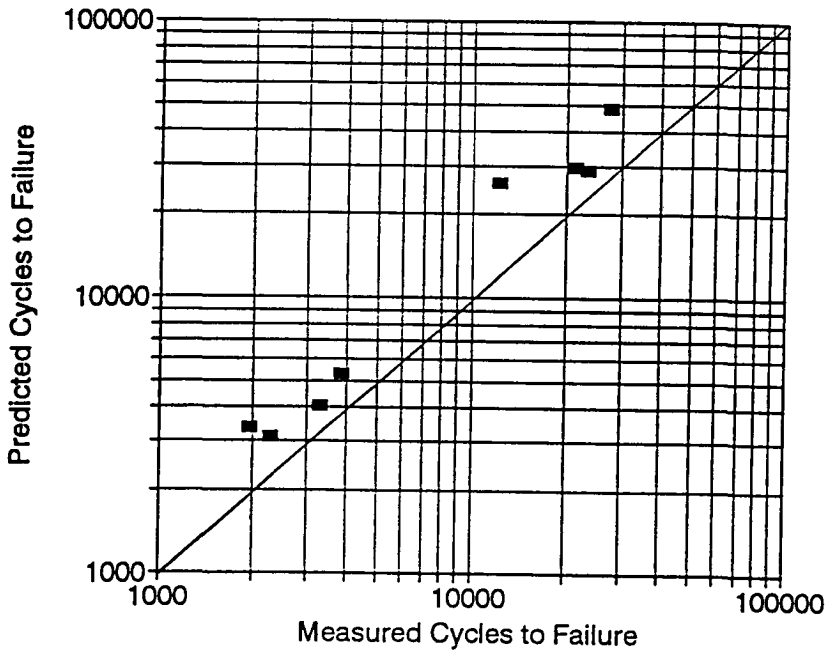

Figure 15.6. Measured cycles to failure versus predicted cycles to failure for mix containing AAG-1 asphalt and RH aggregate

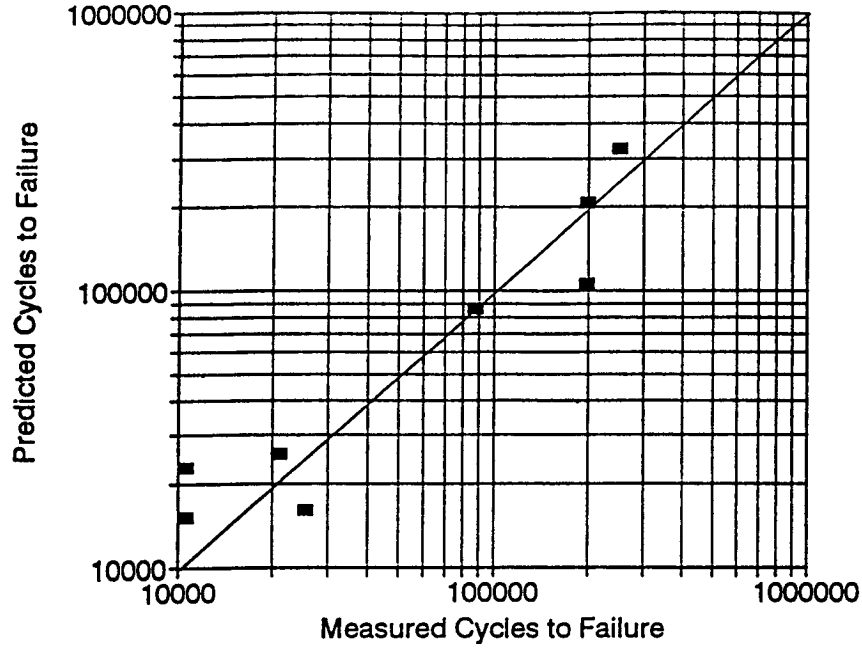

Figure 15.7. Measured cycles to failure versus predicted cycles to failure for mix containing AAK-1 asphalt and RH aggregate

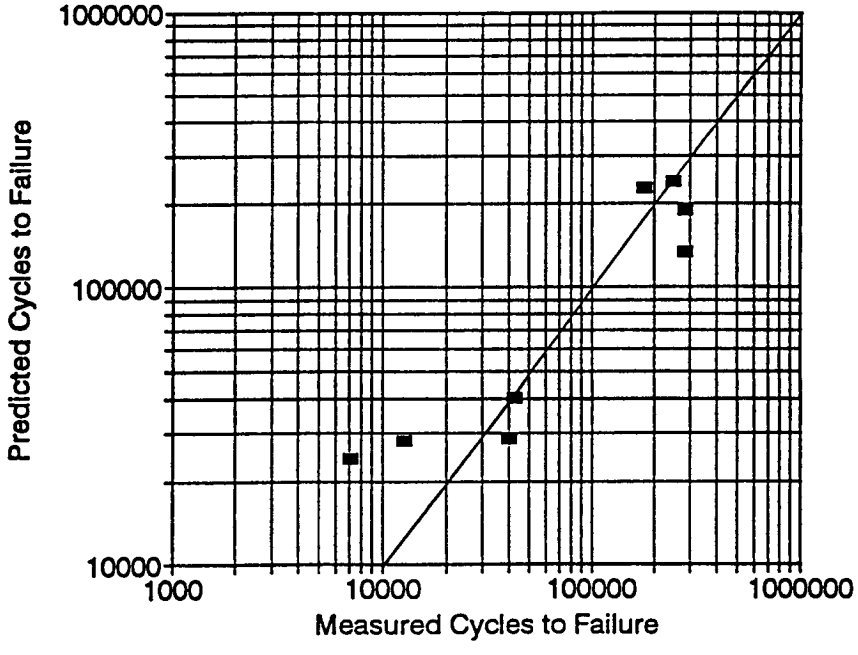

Figure 15.8. Measured cycles to failure versus predicted cycles to failure for mix containing AAM-1 asphalt and RH aggregate

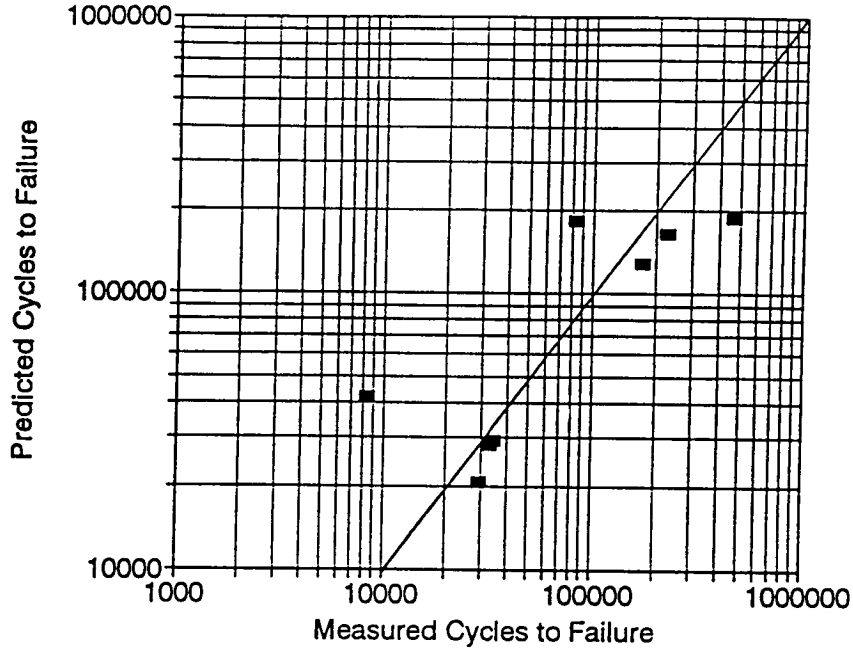

Figure 15.9. Measured cycles to failure versus predicted cycles to failure for mix containing AAA-1 asphalt and RD aggregate

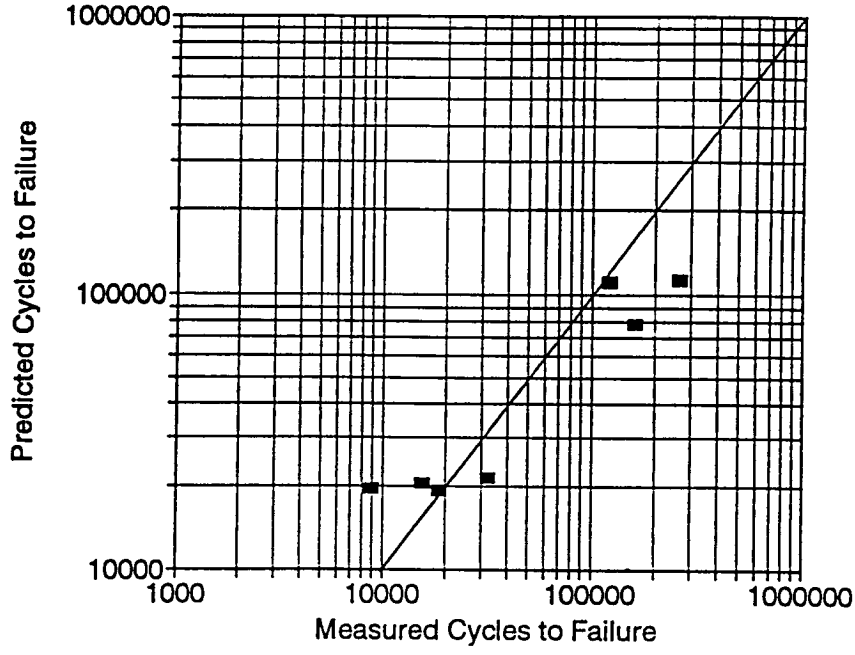

Figure 15.10. Measured cycles to failure versus predicted cycles to failure for mix containing AAB-1 asphalt and RD aggregate

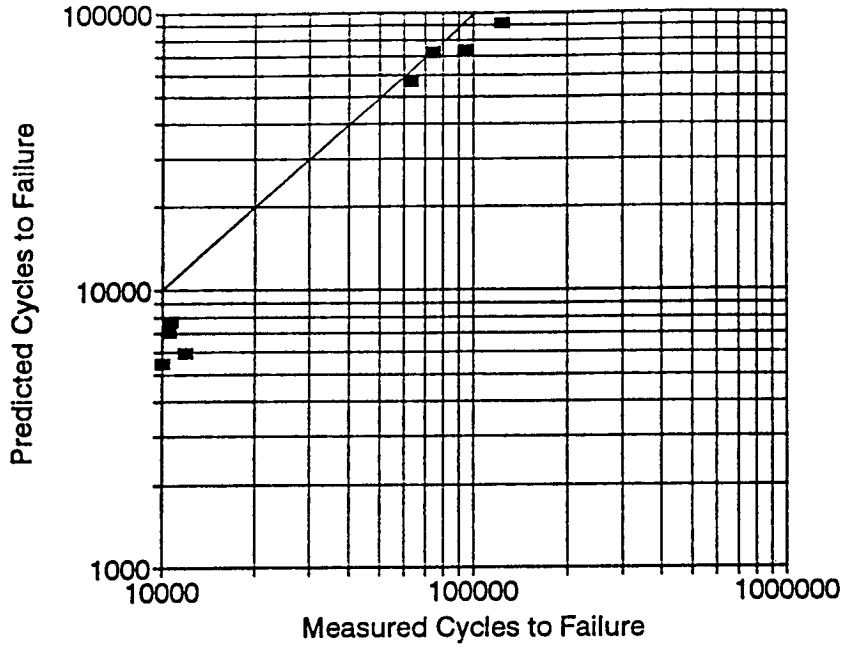

Figure 15.11. Measured cycles to failure versus predicted cycles to failure for mix containing AAC-1 asphalt and RD aggregate

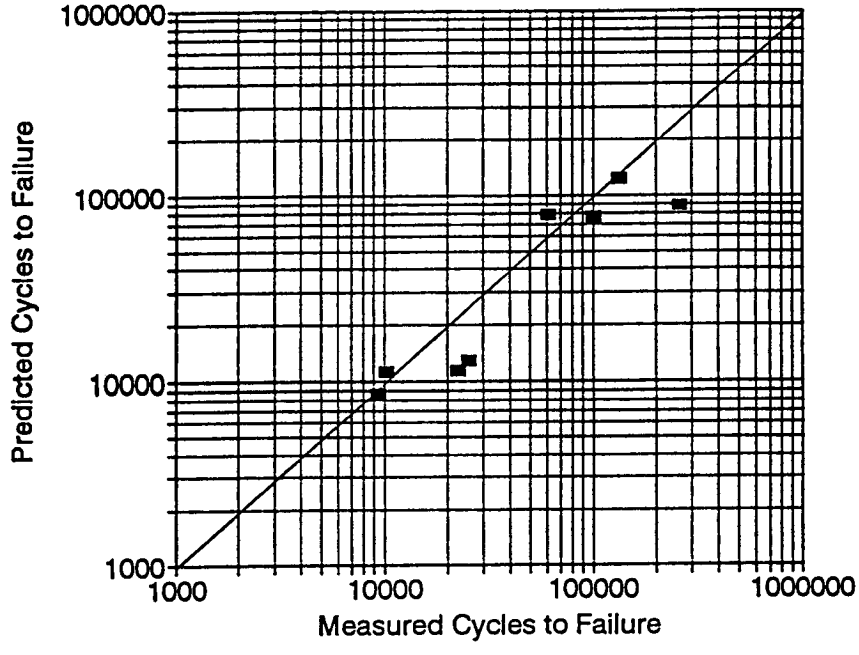

Figure 15.12. Measured cycles to failure versus predicted cycles to failure for mix containing AAD-1 asphalt and RD aggregate

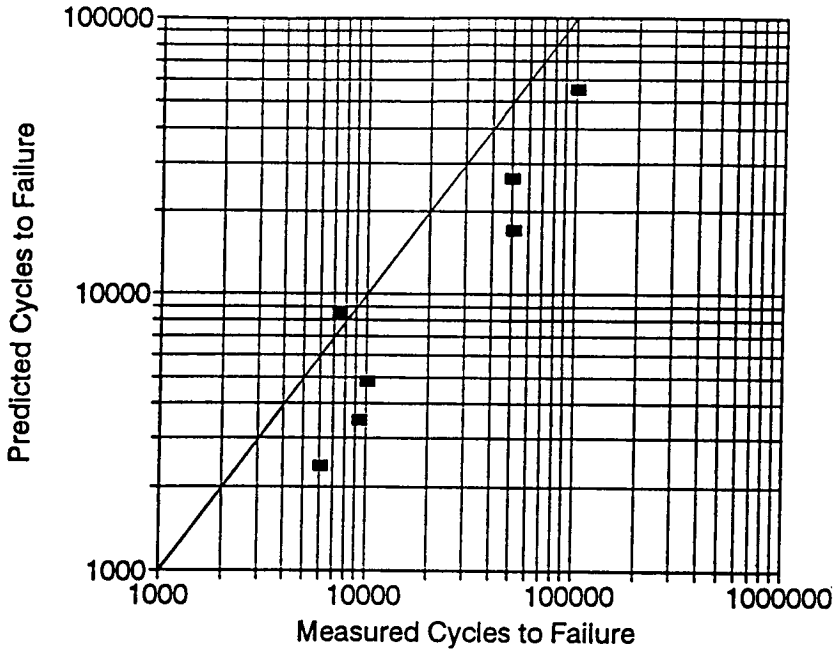

Figure 15.13. Measured cycles to failure versus predicted cycles to failure for mix containing AAF-1 asphalt and RD aggregate

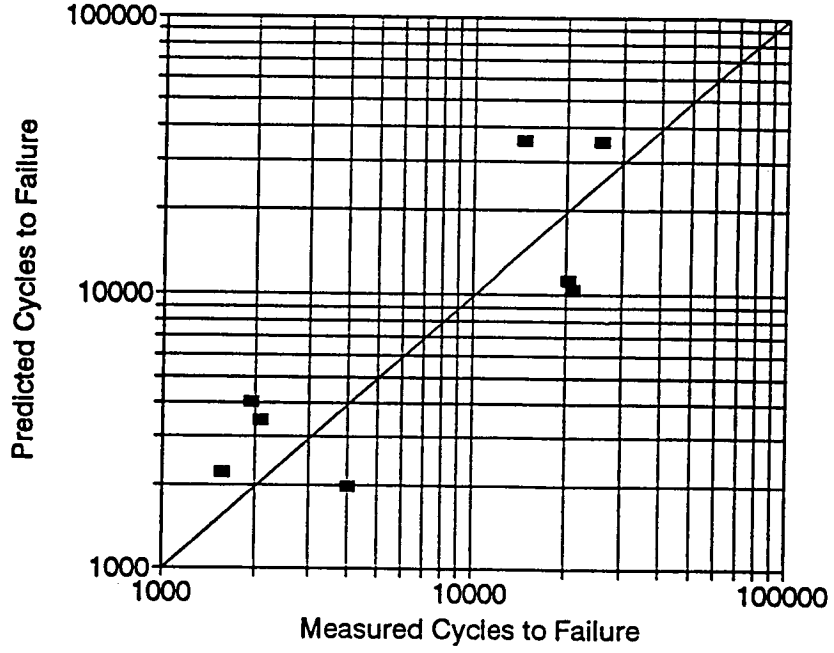

Figure 15.14. Measured cycles to failure versus predicted cycles to failure for mix containing AAG-1 asphalt and RD aggregate

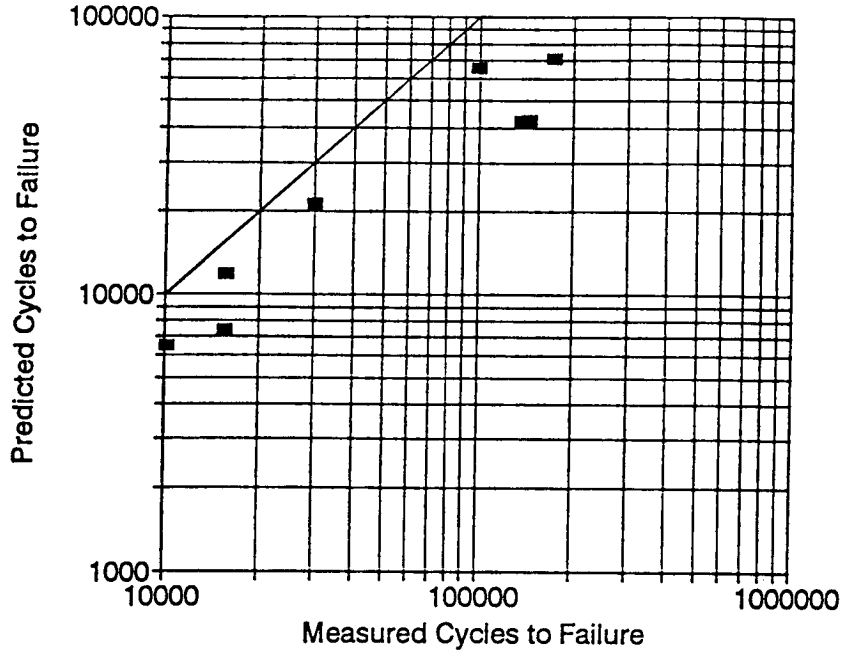

Figure 15.15. Measured cycles to failure versus predicted cycles to failure for mix containing AAK-1 asphalt and RD aggregate

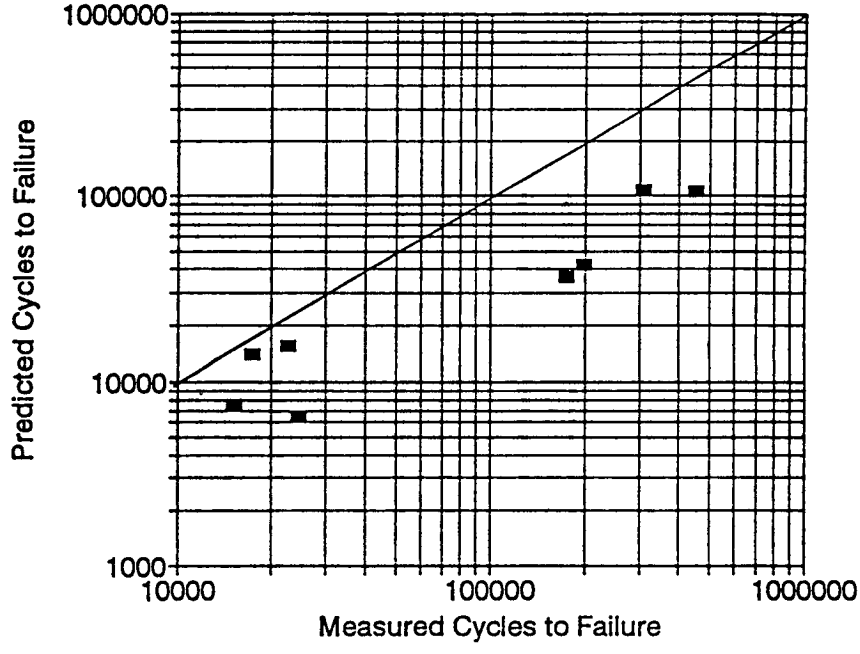

Figure 15.16. Measured cycles to failure versus predicted cycles to failure for mix containing AAM-1 asphalt and RD aggregate

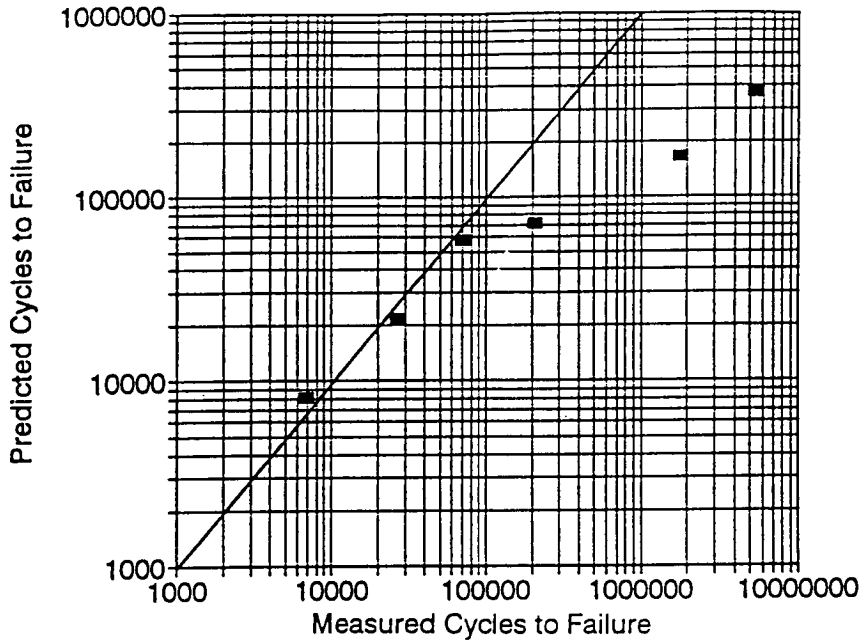

Figure 15.17. Measured cycles to failure versus predicted cycles to failure for mix containing Nantes asphalt B

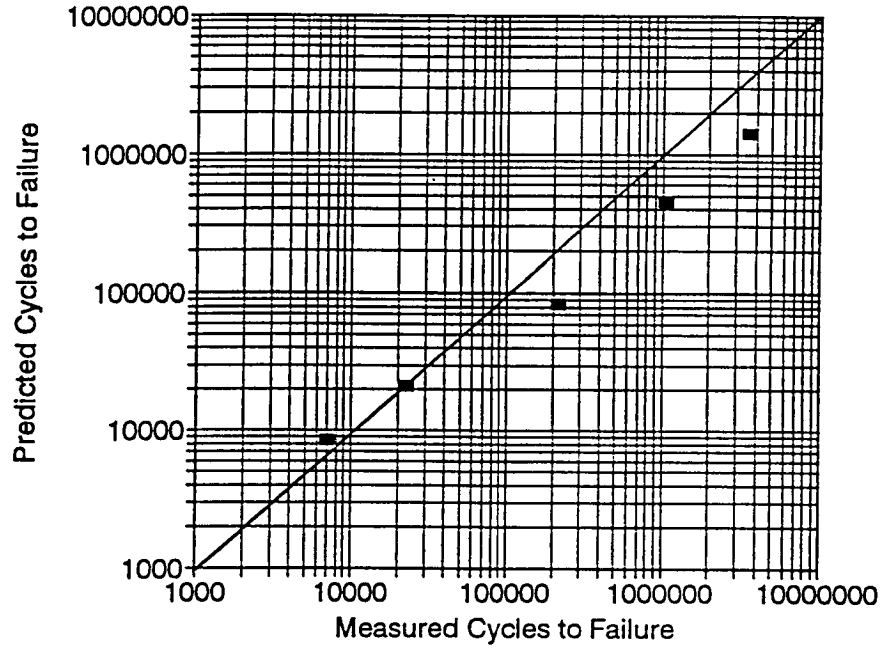

Figure 15.18. Measured cycles to failure versus predicted cycles to failure for mix containing Nantes asphalt A (5.4 percent)

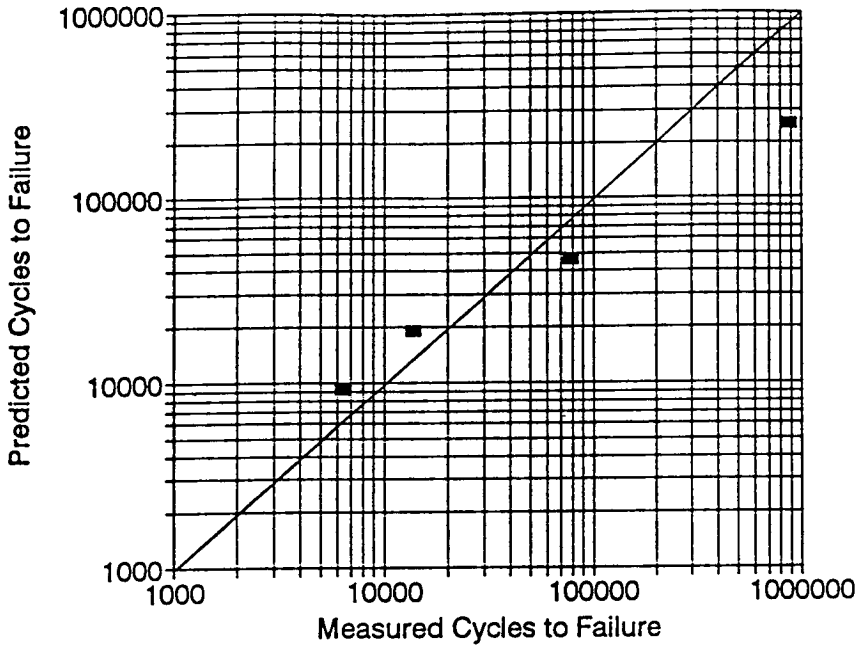

Figure 15.19. Measured cycles to failure versus predicted cycles to failure for mix containing Nantes modified asphalt

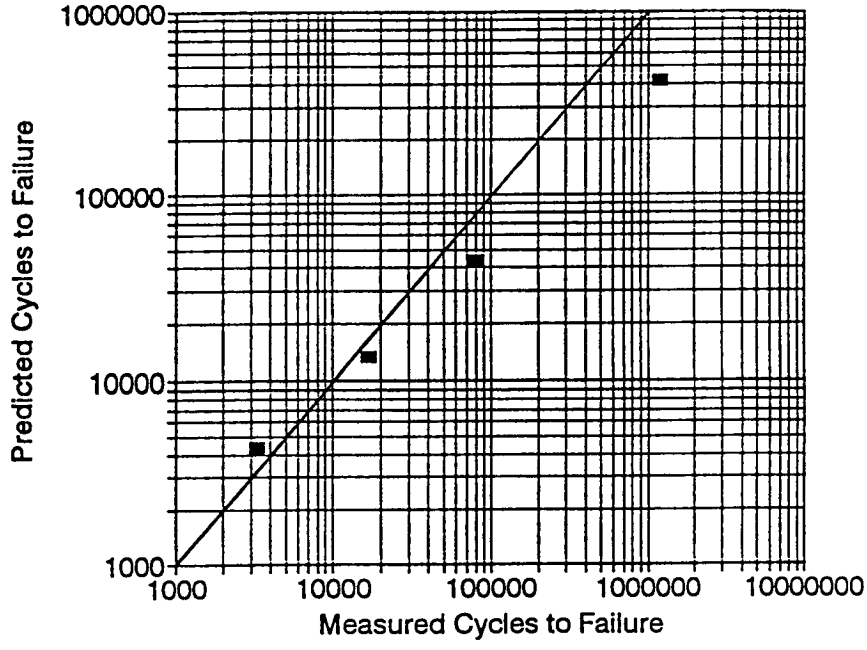

Figure 15.20. Measured cycles to failure versus predicted cycles to failure for mix containing Nantes asphalt A (4.6 percent)

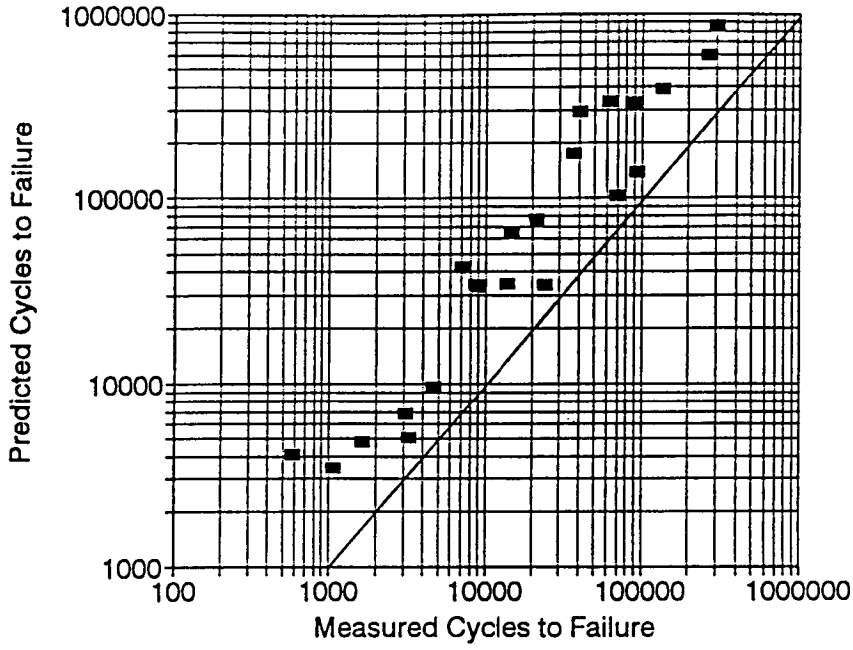

Figure 15.21. Measured cycles to failure versus predicted cycles to failure for mix design experiment

Further efforts were made to determine whether the basic model could be improved. There was some indication that the exponent on the strain and loss stiffness terms was sensitive to mix stiffness. Model calibrations for the data set consisting of combined data from the three experiments tentatively confirmed this finding (Table 15.3). The following model, calibrated using dummy variables to represent the effects of mix stiffness, also tentatively confirms the stiffness effect:

$$N_f = 1.548*10^5 \exp^{0.076\,VFB} \epsilon_0^{-3.908\,D1\,-3.785\,D2\,-3.385\,D3\,-2.796\,D4} S_0''^{-2.855\,D1\,-2.752\,D2\,-2.561\,D3\,-2.182\,D4}$$

where: D1 = 1 if stiffness < = 400,000 psi, 0 if otherwise,
D2 = 1 if 400,000 < stiffness < = 800,000 psi, 0 if otherwise,
D3 = 1 if 800,000 < stiffness < = 1,200,000 psi, 0 if otherwise, and
D4 = 1 if stiffness > 1,200,000 psi, 0 if otherwise.

Table 15.3. Effect of stiffness on regression model calibration

Mix Stiffness (psi)	Regression Model	R^2	Std. Error of Estimate
< 400,000	$N_f = 1.742 \exp^{0.043\,VFB} \epsilon^{-3.994} S''^{-1.803}$	0.87	0.525
400,000 to 800,000	$N_f = 291.0 \exp^{0.105\,VFB} \epsilon^{-3.845} S''^{-2.452}$	0.79	0.769
800,000 to 1,200,000	$N_f = 7.294\times10^{19} \exp^{0.074\,VFB} \epsilon^{-3.138} S''^{-4.997}$	0.82	0.782
> 1,200,000	$N_f = 8.742\times10^{-7} \exp^{0.064\,VFB} \epsilon^{-2.554}$	0.68	0.849

Although this calibration demonstrated the effect of stiffness, it did not significantly improve its accuracy (R^2=0.80; standard error of estimate = 0.769). Figure 15.22 provides a graphical demonstration of the effect of stiffness using this model.

Based on the results of the validation effort, it was concluded that the mixes selected in the 8×2 expanded test program were not sufficiently diverse to yield a representative model together with an accurate estimate of residual error. The surrogate model must capture, as well as possible, the effect of mix properties and strain level on fatigue life. At the same time it must yield accurate measurements of residual errors or variability. It therefore seemed desirable to include all applicable A-003A fatigue data in calibrating the surrogate fatigue model presented in the following section.

15.2 Calibration of Surrogate Fatigue Models Using Combined Data

The objective of this section is to present the results of an effort to recalibrate the strain- and energy-based surrogate fatigue models using all applicable A-003A fatigue data. Included in the calibration process are data sets from the following studies:

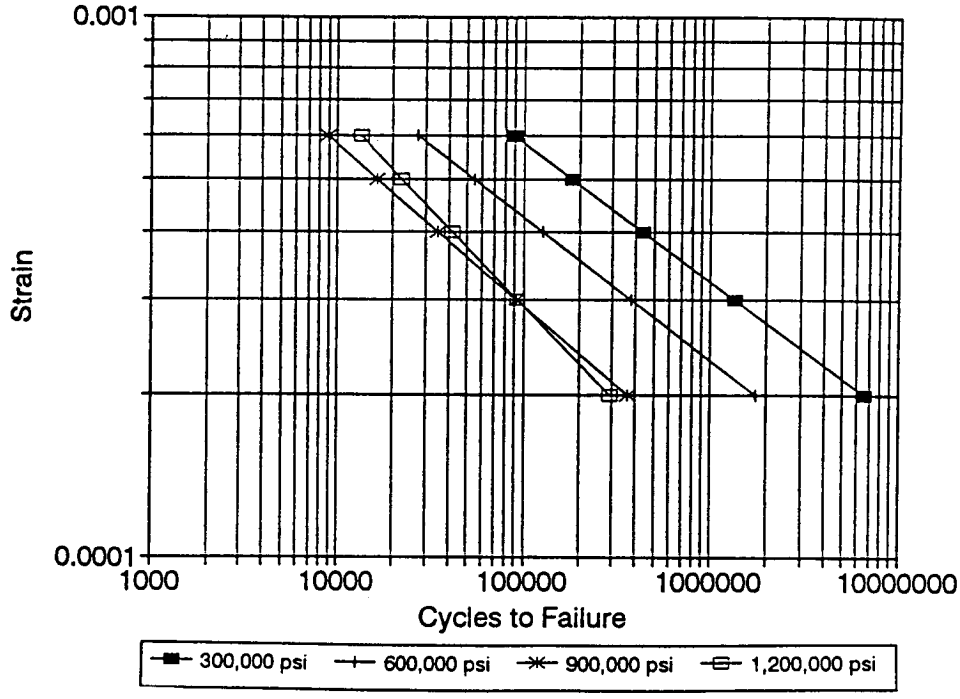

Figure 15.22. Strain versus cycles to failure relationship for different mix stiffnesses

- 8×2 expanded test program.
- Mix design study.
- Temperature equivalency factor experiment.
- Nantes validation study.
- FHWA-ALF validation study.

The details of each experiment were presented earlier. Table 15.4 shows the summary of the combined data used to recalibrate of the surrogate model.

An assumption necessary for GLM is that the variables are normally distributed—especially in this case, since five different data sets have been combined. Variables were found to be log-normally distributed as indicated in Figure 15.23, which shows a probability plot for log-fatigue life. Since the data lie on a straight line, the assumption of log-normal distribution is justified in this case. Therefore, log-transformed (natural logarithms) data were used for the GLM.

Table 15.4. Summary of the overall data used to recalibrate the surrogate fatigue models

Number of Asphalts	12
Number of Aggregates	5
Asphalt Content	8 — 4.5 to 6.2 percent by weight of aggregate, depending on the type of aggregate used
Air-Void Levels	Variable — 2 to 9 percent
Voids Filled with Asphalt	Variable — 54 to 90 percent
Strain Levels	Variable — 200 to 1200 micro in./in.
Temperature	4 — 5°, 10°, 20°, and 25°C (41°, 50°, 68°, and 77°F)
Frequency	1 — 10 Hz (sinusoidal)
Specimen Size	2.0 in. (5.1 cm) height, 2.5 in. (6.4 cm) width, 15.0 in. (38.1 cm) length
Total Number of Mixes	44
Total Number of Specimens	196
Range of Fatigue Life	1000 to 5,400,000 cycles
Range of Loss Stiffness	120,000 to 650,000 psi

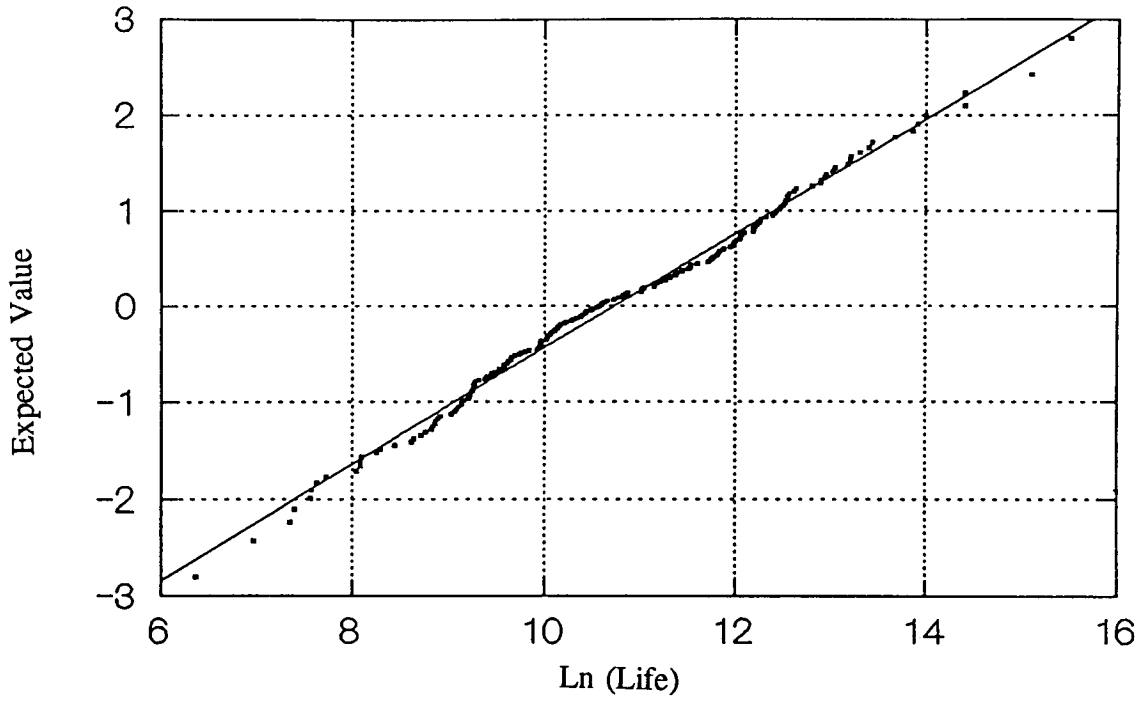

Figure 15.23. Probability plot for fatigue life for combined data

Table 15.5 shows the Pearson correlation matrix for the variables used for the GLM. Strain- and energy-based surrogate fatigue models are shown in Table 15.6. The coefficient of determination for the strain-based model is 0.79 with a coefficient of variation of 90 percent. For the energy-based model, the coefficient of determination is 0.76 with a coefficient of variation of 99 percent.

Table 15.5. Pearson correlation matrix for the dependent and independent variables

	Ln (N_f)	Ln (w_o)	Ln (ϵ_o)	Ln (S_o'')	V_o	VFB
Ln (N_f)	1.000					
Ln (w_o)	-0.811	1.000				
Ln (ϵ_o)	-0.687	0.905	1.000			
Ln (S_o'')	-0.267	0.198	-0.238	1.000		
V_o	-0.202	-0.141	-0.039	-0.233	1.000	
VFB	0.216	0.117	0.025	0.209	-0.970	1.000

Table 15.6. Surrogate fatigue life models from the combined data

Model	R^2	Ln (SEE)	CV %
Strain-Dependent			
$N_f = 6.816*10^8 \exp^{-0.373\ V_o} (\epsilon_o)^{-3.661} (S_o'')^{-2.789}$	0.79	0.762	89
$N_f = 2.738*10^5 \exp^{0.077\ VFB} (\epsilon_o)^{-3.624} (S_o'')^{-2.720}$	0.79	0.776	90
Energy-Dependent			
$N_f = 1495.18 \exp^{-0.332\ V_o} (w_o)^{-1.901}$	0.76	0.818	97
$N_f = 2.365 \exp^{0.069\ VFB} (w_o)^{-1.882}$	0.76	0.825	99

Strain- and energy-dependent models recommended for use in surrogate mix analysis are the following:

$$N_f = 2.738*10^5 \exp^{0.077\ VFB} (\epsilon_o)^{-3.624} (S_o'')^{-2.720} \quad (15.1)$$

$$N_f = 2.365 \exp^{0.069\ VFB} (w_o)^{-1.882} \quad (15.2)$$

where:
- N_f = fatigue life,
- ϵ_o = initial strain in./in.,
- S_o'' = initial loss-stiffness, psi,
- w_o = initial dissipated energy per cycle, psi,
- VFB = percentage of voids filled with asphalt, and
- exp = exponent of the natural logarithm.

Results of the regression analysis for the two models above are included in Tables 15.7 and 15.8.

Table 15.7. Results of the regression analysis for the strain-based surrogate model

Dep Var = Ln(N_f) N = 196 Multiple R = 0.886 Squared Multiple R = 0.785
Adjusted Squared Multiple R = 0.782 Standard Error of Estimate = 0.776

Variable	Coefficient	STD Error	STD Coef	Tolerance	T	P (2 Tail)
Constant	12.520	2.247	0.000	.	5.573	0.000
Ln (ϵ_o)	-3.624	0.152	-0.824	0.9374	-23.850	0.000
Ln (S_o'')	-2.720	0.179	-0.537	0.8968	-15.193	0.000
VFB	0.077	0.008	0.349	0.9502	10.1620	0.000

Analysis of Variance

Source	Sum-of-Squares	DF	Mean-Square	F-Ratio	P
Regression	422.090	3	140.697	233.88	0.000
Residual	115.503	192	0.602		

Table 15.8. Results of the regression analysis for the energy-based surrogate model

Dep Var = $Ln(N_f)$	N = 196	Multiple R = 0.869		Squared Multiple R = 0.755	
Adjusted Squared Multiple R = 0.753				Standard Error of Estimate = 0.825	
Variable	Coefficient	STD Error	STD Coef	Tolerance	T	P (2 Tail)
Constant	0.861	0.610	0.000	.	1.411	0.160
$Ln(w_o)$	-1.882	0.080	-0.848	0.9863	-23.653	0.000
VFB	0.069	0.008	0.315	0.9863	8.785	0.000
Analysis of Variance						
Source	Sum-of-Squares	DF	Mean-Square	F-Ratio	P	
Regression	405.717	2	202.858	296.884	0.000	
Residual	131.875	193	0.683			

15.3 Surrogate Stiffness Models Based on Shear Stiffness Using Combined Data

As indicated earlier in Chapter 10, Level 1 of the abridged procedure for the mix design and analysis requires an estimate of the flexural stiffness of the asphalt-aggregate mixes at 20°C (68°F). This estimate is used with multilayer elastic analysis to determine the critical level of strain to which the mix is subjected under traffic load and, with the surrogate fatigue models, to estimate the fatigue lives of mixes.

The SHRP materials testing protocol is expected to specify the use of a shear frequency sweep test for Level 1 of the abridged procedure. Presented in this section are regression calibrations for estimating flexural stiffness and phase angle from the shear stiffness and shear phase angle at 20°C (68°F) and 10 Hz frequency by using the combined data.

In order to calibrate these models, shear stiffness tests were conducted on prismatic specimens 5.1 cm (2.0 in.) wide, 6.4 cm (2.5 in.) tall, and 15.2 cm (6.0 in.) long. One specimen from each of the mixes tested in the following experiments was used:

- 8×2 expanded test program—flexural stiffness testing at 20°C (68°F) and 10 Hz.
- 8×2 expanded test program—frequency sweep test results.
- Nantes validation study.
- FHWA-ALF validation study.

Shear stiffness results from the mix design and TEF experiments were not available and could not be included in these model calibrations. Shear and flexural stiffness data for each of the studies mentioned above may be obtained from "Stiffness Characteristics of Asphalt-

Aggregate Mixes" (Tayebali et al. 1994). Details of model calibration are presented by Tayebali (1992a).

Model calibrations using the combined data set, which included a total of 70 observations, yielded the following relationships:

$$S_o = 8.560\ (G_o)^{0.913} \qquad R^2 = 0.712 \qquad (15.3)$$

$$\sin\phi_{S_o} = 1.040\ (\sin\phi_{G_o})^{0.817} \qquad R^2 = 0.810 \qquad (15.4)$$

$$S''_o = 81.125\ (G''_o)^{0.725} \qquad R^2 = 0.512 \qquad (15.5)$$

where:

S_o	=	initial flexural stiffness, psi,
S''_o	=	initial flexural loss stiffness, psi,
G_o	=	initial shear stiffness, psi,
G''_o	=	initial shear loss stiffness, psi,
$\sin\phi_{S_o}$	=	initial sine of phase angle in flexural test, and
$\sin\phi_{G_o}$	=	initial sine of phase angle in shear test.

Table 15.9 shows the Pearson correlation matrix, and Tables 15.10 and 15.11 show the results of regression calibration for the above models.

Table 15.9. Pearson correlation matrix for the dependent and independent variables for stiffness and phase angle

	$Ln(S_o)$	$Ln(G_o)$	$Ln(\sin\phi_{S_o})$	$Ln(\sin\phi_{G_o})$	VFB	V_o
$Ln(S_o)$	1.000					
$Ln(G_o)$	0.844	1.000				
$Ln(\sin\phi_{S_o})$	-0.893	-0.770	1.000			
$Ln(\sin\phi_{G_o})$	-0.767	-0.770	0.898	1.000		
VFB	0.247	0.189	-0.091	-0.025	1.000	
V_o	-0.296	-0.234	0.097	0.017	-0.977	1.000

Table 15.10. Results of the regression calibration for flexural stiffness (S_0)

Dep Var = Ln(S_o)	N = 70	Multiple R = 0.844		Squared Multiple R = 0.712	
Adjusted Squared Multiple R = 0.708			Standard Error of Estimate = 0.277		
Variable	Coefficient	STD Error	STD Coef	Tolerance	T	P (2 Tail)
Constant	2.147	0.858	0.000	.	2.502	0.015
Ln(G_o)	0.913	0.070	0.844	1.000	12.968	0.000
Analysis of Variance						
Source	Sum-of-Squares	DF	Mean-Square	F-Ratio	P	
Regression	12.908	1	12.908	168.168	0.000	
Residual	5.129	68	0.077			

Table 15.11. Results of the regression calibrations for flexural sine of the phase angle

Dep Var = Ln(sinϕ_{S_o})	N = 70	Multiple R = 0.898		Squared Multiple R = 0.806	
Adjusted Squared Multiple R = 0.803			Standard Error of Estimate = 0.098		
Variable	Coefficient	STD Error	STD Coef	Tolerance	T	P (2 Tail)
Constant	0.039	0.039	0.000	.	0.981	0.330
Ln(sinϕ_{G_o})	0.817	0.049	0.898	1.000	16.825	0.000
Analysis of Variance						
Source	Sum-of-Squares	DF	Mean-Square	F-Ratio	P	
Regression	2.720	1	2.720	283.070	0.000	
Residual	0.635	68	0.010			

15.4 Summary

This chapter has summarized the effort toward validation of the basic strain-based, surrogate model and calibration of both the fatigue and stiffness models using a data set which included all applicable fatigue tests conducted as part of SHRP Project A-003A. The strain-based, surrogate, fatigue model obtained using the combined data set is

$$N_f = 2.738*10^5 \exp^{0.077\ VFB} (\epsilon_o)^{-3.624} (S_o'')^{-2.720} \qquad R^2 = 0.79$$

where:

N_f	=	fatigue life,
ϵ_o	=	initial strain in./in.,
S_o''	=	initial loss-stiffness, psi,
VFB	=	percentage of voids filled with asphalt, and
exp	=	exponent of the natural logarithm.

The recommended steps for using shear stiffness testing in the surrogate fatigue procedure are as follows:

1. Convert the shear loss-stiffness (G''_o) at 20°C (68°F) and 10 Hz frequency to a flexural loss-stiffness (S''_o) at the same temperature and frequency using Equation 15.5.

2. Estimate the fatigue resistance from the above surrogate fatigue model.

16

Summary

The primary objectives of SHRP Project A-003A, entitled "Performance Related Testing and Measuring of Asphalt-Aggregate Interactions and Mixes," were to develop a series of accelerated performance tests for asphalt-aggregate mixes, together with methods for analyzing asphalt-aggregate interactions which significantly affect pavement performance. This report enumerates the results of a series of laboratory fatigue tests and wheel track tests conducted to validate the A-003A's accelerated performance test for fatigue.

Improvements and changes in test equipment and procedures significantly improved the repeatability of the test, as indicated by a coefficient of variation of 40 percent for fatigue life versus a value of approximately 90 percent observed during the earlier pilot test program. These improvements in test repeatability allowed a short fatigue test procedure to be developed in which a mix could be characterized in as little as 24 hours with a minimum of four fatigue tests.

The most extensive series of tests in this extended phase was the expanded test program, which included testing with eight MRL core asphalts and two MRL core aggregates. This series of tests provided vital information not only for evaluating and validating the fatigue test itself, but also for confirming the SHRP Project A-002A fatigue hypothesis and developing surrogate fatigue models.

Comparison of the A-003A laboratory fatigue test results to those of the laboratory wheel track test results indicated that for fatigue life, ranking of core MRL asphalts from the wheel track testing was similar to the ranking based on the fatigue life obtained from the SHRP Project A-003A flexural beam fatigue tests.

For modified MRL asphalts as well as for the non-MRL Nantes materials, validation results were inconclusive. However, it should be noted that for the Nantes materials, ranking of mixes based on the A-003A fatigue tests was similar to the ranking based on tests conducted by LCPC as well as those conducted by SHELL-KSLA.

Specific findings and conclusions based on the results of the extended test program include the following:

- Conventional wisdom generally suggests that lower stiffness asphalt-aggregate mixes are likely to demonstrate better fatigue resistance under controlled-strain loading than their higher stiffness counterparts. Although binder effects on stiffness and fatigue life confirmed this concept, the effects of air-void content and aggregate type did not. Lower air-void content and crushed, rough-textured aggregates showed increased stiffness *and* increased fatigue life.

- A detailed analysis of asphalt effects indicated that the loss stiffness of the aged binder provides a good indication of the relative laboratory fatigue resistance of otherwise identical mixes. Accordingly, binder loss stiffness seems to be an attractive candidate for inclusion in binder specifications.

- The loss stiffness of the binder, however, is generally not a sufficient indication of the relative fatigue resistance of mixes. Other mix characteristics, such as asphalt content, aggregate type, and air-void content, also contribute significantly to laboratory fatigue resistance. Accordingly, a binder specification alone is insufficient to ensure satisfactory pavement performance.

- Having laboratory test data on mixes is necessary for characterizing fatigue behavior. However, laboratory testing must be interpreted using mechanistic analyses to determine how mixes are likely to perform in the pavement structure under anticipated traffic loads and environmental conditions. Accordingly, mix specifications must address the composite effects of mix, structure, loading, and environment on pavement performance.

- Calibrations of surrogate fatigue models suggest the following: 1) the effects of initial mix stiffness and phase angle on fatigue life can be expressed with equivalent accuracy by the initial mix loss stiffness, 2) the effect of mix voids on fatigue life can be expressed with equivalent accuracy by either the air-void content or the percentage of voids filled with asphalt, and 3) the effects of initial strain level, mix stiffness, and phase angle on fatigue life can be expressed with equivalent accuracy by the initial dissipated energy per cycle.

- In general, the slope (K_2) of the strain-life relationship was found to be highly temperature sensitive. This temperature sensitivity of the strain-life slope is expected to increase with an increase in the temperature susceptibility of the asphalt binder.

- Fatigue life estimates from the strain- and energy-based surrogate fatigue models developed during the 8×2 expanded test program compared well with life measurements from the TEF experiment. However, the surrogate models were unable to reproduce the observed effect of temperature on the strain-life slope (K_2).

- The ranking of six core MRL asphalts based on fatigue life (N1) from laboratory wheel track testing was similar to the ranking based on fatigue life obtained from laboratory flexural beam fatigue tests.

- For LCPC-Nantes (non-MRL) materials, the SHRP A-003A flexural beam fatigue tests ranked mixes similar to those based on the SHELL-KSLA flexural beam fatigue tests and the LCPC trapezoidal cantilever tests.

- The ranking of LCPC-Nantes mixes based on full-scale, circular wheel track test results does not agree with the ranking of mixes based on any of the laboratory test results.

- Estimated pavement fatigue lives for the FHWA-ALF experiment based on the SHRP A-003A laboratory accelerated performance test, as well as the surrogate models, are in good agreement with the observed pavement fatigue life to surface crack initiation.

- Based on the combined laboratory fatigue data, the strain-dependent model that could be used for surrogate mix analysis is the following:

$$N_f = 2.738*10^5 \exp^{0.077\,VFB} (\epsilon_o)^{-3.624} (S''_o)^{-2.720}$$

where:

N_f	=	fatigue life,
ϵ_o	=	initial strain, in./in.,
S''_o	=	initial loss-stiffness, psi,
VFB	=	percentage of voids filled with asphalt, and
exp	=	exponent of the natural logarithm.

- Based on the combined laboratory data, models that could be used for estimating flexural stiffness and loss-stiffness from shear stiffness and shear loss-stiffness are the following:

$$S_o = 8.560\ (G_o)^{0.913}$$

$$S''_o = 81.125\ (G''_o)^{0.725}$$

where:

S_o	=	initial flexural stiffness, psi,
G_o	=	initial shear stiffness, psi,
S''_o	=	initial flexural loss-stiffness, psi, and
G''_o	=	initial shear loss-stiffness, psi.

- The recommended steps for using shear stiffness testing in the surrogate fatigue procedure are as follows:

  1. Convert the shear loss-stiffness (G''_o) at 20°C (68°F) and 10 Hz frequency to a flexural loss-stiffness (S''_o) at the same temperature and frequency.

2. Estimate the fatigue resistance from the surrogate fatigue model.

- The effects of mix composition on fatigue resistance can be determined most accurately by laboratory fatigue testing. Fatigue testing may be required in order to assess the fatigue resistance of new and unconventional mixes. At the same time, the fatigue resistance of conventional mixes can be estimated, although often less accurately, using precalibrated regression models.

Part III Mix Design and Analysis

John A. Deacon
Akhtarhusein A. Tayebali
John S. Coplantz
Fred N. Finn
Carl L. Monismith

17

Introduction

The primary objectives of SHRP Project A-003A include the development of a series of accelerated performance-related tests for asphalt-aggregate mixes together with methods for analyzing asphalt-aggregate interactions which significantly affect pavement performance. Included within the scope of A-003A is fatigue cracking—one of the major distress mechanisms affecting asphalt pavement performance. The primary test methods for fatigue analysis include the flexural beam test for fatigue distress measurement and a dynamic shear test for measuring complex moduli. In addition to mix testing in the laboratory, an analysis system is necessary for properly interpreting test results and for determining the effect of important asphalt-aggregate interactions on pavement performance.

The analysis system developed by A-003A researchers recognizes that mix performance in situ may depend on critical interactions between mix properties and in situ conditions (pavement structure, traffic loading, and environmental conditions). It thus provides not only sensitivity to mix behavior but also sensitivity to the in situ traffic, climatic, and structural environment as well. Because a hierarchical approach has been adopted, the analysis system is relatively simple for routine purposes but permits more exhaustive investigation when necessary; reliability is a key ingredient at all levels and for all applications. The structure of the analysis system provides the flexibility necessary to accommodate future refinements and extensions.

The purpose of this report is to describe in detail the fatigue analysis system developed by A-003A researchers. A discussion of general concepts, including an overview of the analysis system, immediately follows.

18

General Concepts

The analysis system assumes that a trial mix has been proportioned, that traffic and environmental conditions have been determined, and that the pavement cross-section has been designed. The analysis system seeks to judge, with predetermined reliability, whether the trial mix would perform satisfactorily in service. If the mix would not, the designer may redesign the mix, strengthen the pavement section, or repeat the analysis using more refined measurements and/or estimates. The several steps of the analysis system are as follows:

1. Determine design requirements for reliability (probability of avoiding the acceptance of a deficient mix) and performance (extent of permissible fatigue cracking).

2. Determine the expected distribution of in situ pavement temperatures.

3. Estimate design traffic demand ([ESALs]).

4. Select trial mix.

5. Prepare test specimens and condition as required.

6. Measure stiffness of trial mix.

7. Design pavement structural section.

8. Determine design strain under standard axle load.

9. Determine the resistance of the trial mix to fatigue (N_{supply}) in the laboratory or by regression estimate.

10. Apply a shift factor to the travel demand (ESALs) to account for differences between laboratory and in situ conditions (such as traffic wander and crack propagation).

11. Compare traffic demand (N_{demand}) with mix resistance (N_{supply}).

12. If N_{demand} exceeds N_{supply}, reanalyze current trial mix with procedures that yield greater accuracy or alter trial mix and/or structural section and iterate.

Key features of the design and analysis system are briefly described in the following sections.

18.1 Levels of Analysis

Although mix designs must recognize not only material properties but also in situ traffic, climatic, and structural conditions, testing and analysis need not be extensive for most routine applications. However, simplistic systems do not yield the greatest possible accuracy, nor are they capable of reliably testing unconventional mixes or uncommon design applications. As a result, testing and analysis details must vary depending on design requirements. For routine use, surrogate or accelerated fatigue testing at a single temperature is recommended. For complex designs, on the other hand, the testing needs to be extensive, and the full range of in situ temperatures must be investigated.

The analysis process described herein is thus hierarchic. The first level requires only stiffness testing and uses a previously calibrated regression model to estimate fatigue life. The second level replaces regression estimates with fatigue test measurements but limits the testing and analysis to a single temperature. The third and most complex level requires a complete battery of fatigue tests at multiple temperatures.

18.2 Traffic Loading and Temperature Considerations

For the purposes of structural design, traffic loading is typically expressed as the number of ESALs per lane that is expected during the pavement's design life. The analysis system uses this convention for mix design purposes as well. Although distress-dependent load equivalency factors eventually may be developed, American Association of State Highway and Transportation Officials (AASHTO) load equivalency factors are recommended for initial use. Thus, the load equivalency factors used for pavement structural design will also be used for mix design.

Testing and analysis over a range of temperatures is both unnecessary and unacceptable for most routine mix designs. For mixes of typical temperature sensitivity, testing at a single temperature is recommended. This procedure requires conversion of the design ESALs to their equivalents at the test temperature. Predetermined temperature frequency distributions (by climatic region) and predetermined temperature equivalency factors (TEFs) should suffice for most purposes. For mixes of atypical temperature sensitivity, testing over a range of temperatures representative of in situ conditions is necessary.

The most desirable temperature for testing normal mixes would be at or near the *critical* temperature anticipated at highly stressed locations within the pavement structure.[8] The critical temperature is the one at which more fatigue damage occurs than at any other temperature. More damage occurs at this temperature because of both the frequency of its occurrence and the sensitivity of the mix to damage at this temperature. Any imprecision in TEFs that are referenced to the critical temperature is likely to have a negligible effect on damage estimates, since most damage accumulates when temperatures are at and near the critical temperature—conditions when TEFs have the smallest possible error. However, a major disadvantage of testing at the critical temperature is that test results are not generally transferable because this temperature is location- and pavement structure-specific.

Accordingly, a temperature of 20°C (68°F) is recommended for testing typical mixes in fatigue. Not only is this temperature convenient for production testing in the laboratory, it is expected to be near the critical temperature level at many locations within the continental United States. The advantage of single-temperature testing in production laboratories outweighs the possible loss in accuracy from testing at temperatures different from (although near to) the critical temperature.

18.3 Reliability

Decisions about anticipated mix performance cannot be made with absolute certainty. Although large safety factors can reduce the likelihood of error, their cost consequences can be considerable. Reliability analysis offers the potential for ensuring an acceptable level of risk in mix analysis without the costs of excessive safety factors.

The analysis system requires that mix resistance (N_{supply}, the laboratory fatigue life) exceeds traffic demand (N_{demand}, the adjusted field ESAL estimate) by an amount which is carefully chosen to meet reliability requirements. This task is accomplished by applying a reliability multiplier to N_{demand} before it is compared to N_{supply}. The reliability multiplier (M) increases with increases in design reliability level as well as with increases in the variabilities of mix-resistance and traffic-demand estimates. A mix initially judged marginal may ultimately be judged acceptable by more accurate estimates of mix resistance (for example, by increasing sample size in the laboratory testing) or, if possible, by relaxing requirements for the acceptable level of risk.

---

[8]Testing at an "effective" temperature is also a possible alternative. Effective temperature is defined as the one at which single temperature testing and analysis would yield results identical to multitemperature testing with analytical accumulations of distress over the range of temperatures anticipated in situ. Identifying effective temperatures is similar in many respects to the process of developing TEFs. The latter process, however, is more transparent to the mix designer and is expected to permit fatigue testing at a common temperature for applications covering much of the continental United States.

18.4 Mechanistic Analysis

The maximum principal tensile strain at the underside of the asphalt layer governs the initiation of fatigue cracking in situ. Mixes will perform adequately only if they can sustain the necessary repetitions of this strain level without cracking. For mix analysis purposes, the multilayer elastic theory provides a convenient and sufficiently accurate means for estimating the maximum strain anticipated in situ at 20°C (68°F) under the standard axle load. Laboratory testing or regression estimation is then used to establish the fatigue resistance at this critical strain level.

18.5 Overview of Analysis System

Distinguishing characteristics of the fatigue analysis system are displayed in Table 18.1. The three levels of the analysis hierarchy are differentiated primarily by the extent of required testing, the treatment of temperature, and analytical requirements. Mixes of typical temperature sensitivity can be analyzed at a single temperature (Level 1 or 2). Level 1, based on shear frequency sweeps instead of fatigue testing, is applicable to conventional dense graded mixes. Unconventional mixes require fatigue testing and analysis of the type characteristic of Level 2. Finally, the multiple temperature testing and analysis of Level 3 are necessary for mixes of atypical temperature sensitivity. Table 18.2 summarizes the recommended level of fatigue testing and analysis for mixes of varying types.

Table 18.1. Distinguishing characteristics of the fatigue analysis system

Variables		Level 1 Abbreviated analysis with surrogate testing	Level 2 Abbreviated analysis with limited fatigue testing	Level 3 Comprehensive analysis with full fatigue testing
Testing	Type	Dynamic properties from shear frequency sweeps	Flexural beam fatigue	Flexural beam fatigue
	Temperature	20°C (68°F)	20°C (68°F)	Multiple
In Situ Conditions	Traffic	Equivalent ESALs at 20°C (68°F)	Equivalent ESALs at 20°C (68°F)	Equivalent ESALs at 20°C (68°F)
	Structure	Tensile strain under standard load at 20°C (68°F)	Tensile strain under standard load at 20°C (68°F)	Tensile strain under standard load at 20°C (68°F)
	Temperature	Frequency distribution at bottom of surface layer	Frequency distribution at bottom of surface layer	Frequency distribution at bottom of surface layer
Analysis	Mechanistic	Multilayer elastic	Multilayer elastic	Multilayer elastic
	Damage	Preanalysis (TEFs for design ESALs)	Preanalysis (TEFs for design ESALs)	Development of unique TEFs for design ESALs

Table 18.2. Recommended level of fatigue testing and analysis

	Level 1	Level 2	Level 3
Mix Characteristics	Abbreviated analysis with surrogate testing	Abbreviated analysis with limited fatigue testing	Comprehensive analysis with full fatigue testing
Dense graded mixes with conventional binders of typical temperature sensitivity	Recommended	Optional for increased accuracy	Optional for increased accuracy or complete mix cataloging
Unconventional mixes with binders of typical temperature sensitivity	Not applicable	Recommended	Optional for increased accuracy, complete mix cataloging, or investigative analyses
Mixes with binders of atypical temperature sensitivity	Not applicable	Not applicable	Required

For all levels, the design traffic is expressed in terms of the number of AASHTO ESALs in the critical lane during the pavement's design life, adjusted to its equivalent at 20°C (68°F). A shift factor must be applied to this traffic estimate to enable direct comparisons between the design traffic estimate and laboratory measurements. The shift factor accounts for such effects as crack progression, traffic wander, construction variability, differences between field and laboratory modes of loading. The end result of the traffic analysis is an estimate of traffic demand (N_{demand}) that is commensurate with laboratory fatigue measurements.

Mix resistance to fatigue distress (N_{supply}) is ascertained from laboratory measurements using either surrogate testing and a regression model (Level 1) or direct fatigue testing (Levels 2 and 3). In either case, the mix is characterized as a linearly elastic material, and the appropriate strain level is determined by simulating the pavement response to the standard axle load at a temperature of 20°C (68°F).

Conceptual development of the mix analysis system has been completed as part of SHRP Project A-003A, and considerable progress has been made toward establishing a readily implementable package for use by material engineers nationwide. In addition to completing the calibration process, one of the key remaining tasks is to validate the process by demonstrating its ability to reliably discriminate between suitable and unsuitable mixes. Before the mix design and analysis system is described in detail herein, key concepts regarding TEFs, reliability, and shift factors are explored in depth.

19

Temperature Equivalency Factors

The purpose of this section is to describe the concept and demonstrate the feasibility of A-003A's approach to incorporating temperature into the mix design and analysis system for fatigue. The intent is to demonstrate the process as well as to document the development of a preliminary set of TEFs applicable to conventional mixes of normal temperature sensitivity. As future investigation reveals the sensitivity of TEFs to such factors as mix properties, pavement thickness, and climate, a complete set of factors can eventually be developed. Interim results to date demonstrate the validity of the concepts presented herein.

Conventional fatigue analyses typically accommodate variations in temperature by means of the linear-summation-of-cycle-ratios hypothesis. Using this methodology, the temperature is approximated by a limited number of discrete categories (such as average temperature by month), and the ratio of the predicted to permissible fatigue damage is summed over all categories. The design is considered satisfactory if the summation does not exceed unity. Although such procedures have been reasonably successful, they are considered too cumbersome for routine mix analysis. Instead, it is proposed to limit, where possible, fatigue testing or other estimates of fatigue life to a single temperature and to express the destructive effects of anticipated traffic in the field as equivalent ESALs at that temperature. These tasks are accomplished through the use of TEFs—an approach that simplifies testing, which, in turn, increases productivity and reduces costs.

The TEFs, as developed herein, build on the AASHTO load equivalency concept. TEF_i is defined as the number of ESALs at a common temperature, T_c, that is equivalent in destructive effect to one ESAL applied at some other temperature, T_i. If $ESAL_i$ represents the number of ESALs anticipated when the temperature is T_i, then the product, $ESAL_i \cdot TEF_i$, represents the equivalent effect of the loading at the common temperature, T_c. Therefore,

$$ESAL_i \cdot TEF_i = \text{Equivalent } ESAL_c \tag{19.1}$$

or, alternatively,

$$TEF_i = [\text{Fatigue Life at } T_c]/[\text{Fatigue Life at } T_i] \tag{19.2}$$

In the context of the analysis procedures for mix design, T_c is the single temperature at which fatigue testing is conducted, and the T_i values are related to the annual distribution of in situ pavement temperatures at the bottom of the asphalt layer.

TEFs are expected to depend on mix properties, location (environment), and structural section (thickness). In order to demonstrate the temperature equivalency concept, specific assumptions have been made for each of these factors. The sensitivity of mix properties to location and structural section has been partially evaluated by simulating 10.16 and 20.32 cm (4 and 8 in.) asphalt pavements in nine climatic regions of the United States (Lytton et al. 1990). For simplicity, detailed results are presented herein for only two: Region I-A in the colder Northeast and Region III-B in the hotter Southwest. Also, as indicated previously, the factors developed herein are based on a conventional asphalt-aggregate mix of normal temperature sensitivity.

19.1 Approach

To develop TEFs, conditions within the hypothetical pavements were evaluated for 4,380 of 8,760 hours (one-half) in a typical year. For each of these 4,380 hours, the load-induced tensile strain at the bottom of the asphalt layer and the corresponding number of repetitions of cycles to fatigue failure (N_f) under controlled-strain conditions in the laboratory were determined. Then, by categorizing the hours into discrete temperature categories, the average number of sustainable repetitions was determined for each category. From these averages, TEFs were computed using Equation 19.2. The common reference temperature (T_c) corresponded to the 20°C (68°F) temperature interval.

Because of the varying temperature profile, material properties and pavement responses are generally different for each of the 4,380 hours; however, they may be characterized by the temperature at a fixed depth within the structure together with the temperature gradient through the pavement surface. For the purpose of these analyses, the fixed depth is at the bottom of the asphalt layer, and the temperature gradient is defined as the difference in temperature between the bottom of the asphalt layer and the temperature at a 5 cm (2 in.) depth divided by the total asphalt thickness minus 5 cm (2 in.). The 5 cm (2 in.) depth was chosen as a means for defining temperature gradient to lessen surface effects on temperature-gradient computations. Units of temperature gradient are °C per inch.

To keep the number of computations manageable, 72 separate analyses were conducted using all combinations of nine different temperature categories at the bottom of the asphalt layer and eight different temperature gradients. The resulting 72 estimates of N_f were modeled as a function of temperature at the bottom of the asphalt layer and temperature gradient. Then, for each of the 4,380 hours, N_f was determined from this regression model by using the computed values for in situ pavement temperature at the bottom of the asphalt layer and for temperature gradient. Following this, the 4,380 hours were grouped by pavement temperature category, and the average N_f was determined for each category. Finally, TEFs, expressed by the ratio of the average values of N_f at two different temperatures, were determined and tabulated.

19.1.1 Fatigue Testing

To support the development of TEFs, an experimental fatigue testing program was carried out by UCB. Testing was limited to an asphalt mix incorporating 5.2 percent AAD asphalt by weight of aggregate, RH aggregate, and approximately 4 percent air-void contents. This mix, which incorporates an asphalt of normal temperature sensitivity, is typical of the dense graded mixes currently used throughout much of the United States. Testing was conducted with flexural beam specimens under controlled-strain loading at temperatures of 5°, 10°, 20°, and 25°C (41°, 50°, 68°, and 77°F). Fatigue lives were measured at several levels of strain.

19.1.2 Pavement Temperature Profiles

Estimates of pavement temperature were made with the FHWA's computer program, "Integrated Model of the Climatic Effects of Pavements" (Lytton et al. 1990). The program is based on average climatological data for a period of approximately 30 years. The analysis resulted in estimates of pavement temperature at the surface and at 5 cm (2 in.) incremental depths below the surface at 2 hour intervals for each day of the year, a total of 4,380 pavement temperature profiles. The minimum and maximum pavement temperatures at the bottom of the asphalt layer for Regions I-A and III-B, respectively, were determined to be as follows:

Region	Pavement Structure	Minimum Temperature at Bottom of Slab (°C)	Maximum Temperature at Bottom of Slab (°C)
I-A	20 cm (8 in.) Asphalt	-2.0	31.3
	10 cm (4 in.) Asphalt	-3.7	37.7
III-B	20 cm (8 in.) Asphalt	4.6	38.8
	10 cm (4 in.) Asphalt	2.0	46.5

The distribution of annual pavement temperature frequency computed for each pavement structure in each region is presented in Tables 19.1 through 19.4. This type of information was used to establish the pavement temperature categories and the temperature gradients to be used for the analysis. Nine bottom-surface temperatures were investigated ranging from -5° to 35°C (23° to 95°F) in increments of 5°C (9°F), and eight temperature gradients, ranging from -1.5°C to 0.6°C (29° to 33°F) per inch in increments of 0.3°C (0.5°F) per inch. These conditions bracket those most commonly occurring throughout the United States and are sufficiently small in number to be manageable. As stated earlier, the temperature gradient is arbitrarily defined as the difference between the temperature at the bottom surface of the asphalt layer and that at a 5 cm (2 in.) depth divided by the distance separating these locations.

Table 19.1. Annual pavement temperature distribution, Region I-A, northeastern United States, 20 cm (8 in.) pavement

Midrange Temperature (°C)	Percentage of Time in Temperature Range				
	Surface	5 cm (2 in.) Depth	10 cm (4 in.) Depth	15 cm (6 in.) Depth	20 cm (8 in.) Depth
-7.5	0.9	0.0	0.0	0.0	0.0
-5.0	3.0	2.0	0.1	0.0	0.0
-2.5	5.4	4.5	4.3	3.4	2.1
0.0	8.9	12.4	15.7	18.3	20.8
2.5	5.4	5.4	5.1	4.5	3.4
5.0	5.5	5.2	4.8	3.8	3.9
7.5	5.3	5.1	4.7	4.5	4.6
10.0	5.7	5.2	4.9	5.2	5.4
12.5	5.7	5.3	5.5	5.7	5.8
15.0	6.2	5.7	5.9	6.0	6.2
17.5	7.5	6.5	6.4	6.5	6.8
20.0	8.2	8.5	7.4	7.5	7.6
22.5	5.9	8.6	9.6	10.2	10.8
25.0	5.4	6.4	8.4	9.2	9.4
27.5	3.1	5.7	6.5	7.0	7.1
30.0	3.8	3.3	4.9	5.7	5.6
32.5	3.3	4.5	4.8	2.3	0.3
35.0	2.6	3.6	1.0	0.0	0.0
37.5	4.3	2.0	0.0	0.0	0.0
40.0	2.3	0.0	0.0	0.0	0.0
42.5	1.5	0.0	0.0	0.0	0.0

Table 19.2. Annual pavement temperature distribution, Region I-A, northeastern United States, 10 cm (4 in.) pavement

Midrange Temperature (°C)	Percentage of Time in Temperature Range		
	Surface	5 cm (2 in.) Depth	10 cm (4 in.) Depth
-7.5	1.3	0.0	0.0
-5.0	3.4	2.4	0.0
-2.5	5.5	5.6	7.6
0.0	9.5	13.7	17.8
2.5	5.1	5.0	2.9
5.0	5.4	5.1	3.9
7.5	5.3	4.7	4.3
10.0	5.5	4.6	4.6
12.5	5.9	5.2	5.2
15.0	6.3	5.7	5.8
17.5	8.2	6.8	6.9
20.0	6.3	8.7	9.0
22.5	5.8	6.5	7.0
25.0	5.2	5.8	5.9
27.5	3.0	4.5	5.2
30.0	3.9	3.8	4.6
32.5	3.2	3.7	3.8
35.0	2.5	3.5	3.4
37.5	3.8	3.2	2.0
40.0	2.5	1.3	0.0
42.5	2.4	0.0	0.0

Table 19.3. Annual pavement temperature distribution, Region III-B, southwestern United States, 20 cm (8 in.) pavement

Midrange Temperature (°C)	Percentage of Time in Temperature Range				
	Surface	5 cm (2 in.) Depth	10 cm (4 in.) Depth	15 cm (6 in.) Depth	20 cm (8 in.) Depth
0.0	0.3	0.0	0.0	0.0	0.0
2.5	1.8	0.5	0.0	0.0	0.0
5.0	2.5	2.2	1.6	1.0	0.8
7.5	3.7	3.4	3.4	3.4	3.5
10.0	4.7	4.7	5.0	5.7	6.4
12.5	5.2	5.5	6.7	7.3	7.4
15.0	5.7	6.6	6.9	6.8	6.9
17.5	6.1	6.8	6.7	6.8	6.9
20.0	7.7	6.9	6.7	6.8	6.9
22.5	9.3	7.2	7.1	7.1	7.4
25.0	8.4	8.7	7.9	8.0	8.3
27.5	7.6	10.7	10.7	10.0	10.4
30.0	7.3	7.2	10.2	11.3	12.6
32.5	4.2	6.8	7.4	9.2	9.0
35.0	3.7	5.8	7.0	7.9	8.0
37.5	3.7	3.9	5.7	5.8	5.2
40.0	3.7	5.0	4.6	2.9	0.1
42.5	2.6	3.3	2.4	0.0	0.0
45.0	3.6	3.9	0.0	0.0	0.0
47.5	3.6	0.6	0.0	0.0	0.0
50.0	2.9	0.0	0.0	0.0	0.0
52.5	1.4	0.0	0.0	0.0	0.0

Table 19.4. Annual pavement temperature distribution, Region III-B, southwestern United States, 10 cm (4 in.) pavement

Midrange Temperature (°C)	Percentage of Time in Temperature Range		
	Surface	5 cm (2 in.) Depth	10 cm (4 in.) Depth
0.0	0.8	0.0	0.0
2.5	1.8	1.2	0.8
5.0	2.6	2.7	2.4
7.5	3.8	3.4	3.6
10.0	4.6	4.6	4.6
12.5	5.0	5.4	5.8
15.0	6.0	6.1	6.8
17.5	6.2	7.0	7.1
20.0	7.9	7.2	7.1
22.5	9.1	8.1	7.8
25.0	8.2	9.5	10.6
27.5	7.2	8.0	8.0
30.0	6.4	6.5	7.8
32.5	4.6	6.8	5.3
35.0	3.5	4.4	6.0
37.5	4.4	4.0	4.5
40.0	3.2	4.2	4.0
42.5	2.4	3.8	4.2
45.0	3.3	3.5	3.1
47.5	4.1	3.4	0.5
50.0	2.3	0.2	0.0
52.5	2.6	0.0	0.0

19.1.3 Pavement Analysis

The standard traffic loading consisted of an 80 kN (18,000 lb) standard axle with dual tires spaced at 30.5 cm (12 in.) center to center and having a contact pressure of 587 kPa (85 psi). Maximum principal tensile strains at the bottom of the asphalt layer were computed for the 72 pavement sections via the ELSYM (multilayered elastic) program. Three output locations were examined: 1) the centerline of one tire of the dual set, 2) the inside edge of one tire, and 3) the midpoint between the two tires. The largest (most critical) maximum principal tensile strain was then used to estimate fatigue life.

Each of the two pavement structures was modeled as a multilayer elastic system. The first comprised a 20 cm (8 in.) surface course on a subgrade having a stiffness of 69 MPa (10,000 psi). The second comprised a 10 cm (4 in.) surface course on a subgrade having a stiffness of 173 MPa (25,000 psi). Poisson's ratios of 0.35 and 0.40 were employed for surface and subgrade materials, respectively. In analyzing each structure, the subgrade modulus was assumed to remain constant throughout the period of analysis, that is, a typical annual cycle.

19.1.4 Stiffness Moduli

For the ELSYM analyses, the asphalt layers were represented by four sublayers of varying stiffness moduli as a function of temperature. Five centimeter (2 in.) thick sublayers were used for the 20.32 cm (8 in.) pavement, and 2.54 cm (1 in.) thick sublayers were used for the 10.16 cm (4 in.) pavement. The representative stiffness for each sublayer was computed from the temperature at the midpoint of each layer using the following stiffness-temperature model which had been calibrated using data from the TEF fatigue experiment:

$$S_o = 2.1621 \cdot 10^6 \cdot e^{-0.09385\,T} \qquad R^2 = 0.92 \qquad (19.3)$$

where: S_o = initial flexural stiffness in psi after 50 load cycles at 10 Hz,
e = base of natural logarithms, and
T = temperature in °C.

All stiffness measurements were taken at 10 Hz frequency, which simulates in-pavement stress pulses corresponding to vehicle speeds in the 15 to 30 mph range.

19.1.5 Fatigue Life Calculations

The fatigue lives (N_f) of the 72 pavement sections were computed from the critical maximum principal tensile strain using a model which incorporated both temperature and tensile strain. The model, developed from data obtained during the TEF fatigue experiment, follows:

$$N_f = 10^{(20.0341 - 0.2261\,T)} \cdot \epsilon^{(-5.9138 + 0.1056\,T)} \qquad R^2 = 0.94 \qquad (19.4)$$

where: N_f = number of cycles to 50-percent reduction in stiffness (fatigue life),
ϵ = maximum principal tensile strain in units of 10^{-6} in./in., and
T = temperature in °C.

Because of testing limitations, this fatigue life model was developed using data obtained within a temperature range of 5° to 25°C (41° to 77°F). Extrapolations of model predictions beyond this temperature range are recognized as a source of potential error, especially at elevated temperatures.

The 72 estimates of N_f were next modeled as a function of pavement temperature at the bottom of the asphalt layer and temperature gradient. Relationships between N_f, pavement temperature, and temperature gradient are illustrated graphically in Figures 19.1 and 19.2. Because these relationships are parabolic, they can be modeled by a second-order polynomial. For the 20.32 cm (8 in.) pavement, the regression model is

$$Ln(N_f) = 22.702-0.55674 \cdot T+1.0481 \cdot G+0.0088228 \cdot T^2-0.024482 \cdot T \cdot G \quad R^2 = 0.99 \quad (19.5)$$

and for the 10.16 cm (4 in.) pavement

$$Ln(N_f) = 18.405-0.37039 \cdot T+0.44504 \cdot G+0.0068057 \cdot T^2-0.010977 \cdot T \cdot G \quad R^2 = 0.99 \quad (19.6)$$

where: T = temperature in °C, and
G = temperature gradient in °C per inch.

Each term of these equations is statistically significant at a level of 5 percent or less.

19.2 Temperature Equivalency Factors

In situ fatigue lives were estimated for each of the 4,380 hours using the models of Equations 19.5 and 19.6, and the average fatigue life within each pavement temperature category was computed. TEFs, representing ESAL conversions to a temperature of 20°C (68°F), were then determined using these averages. Results are tabulated in Table 19.5.

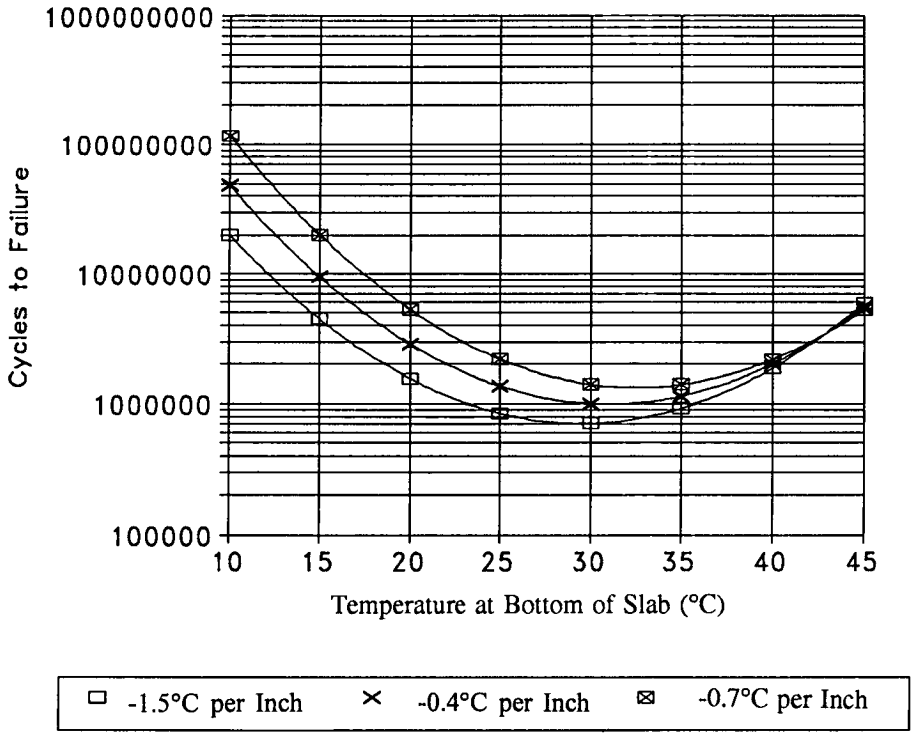

Figure 19.1. Effect of temperature and temperature gradient on fatigue life (N_f), 8 in. pavement

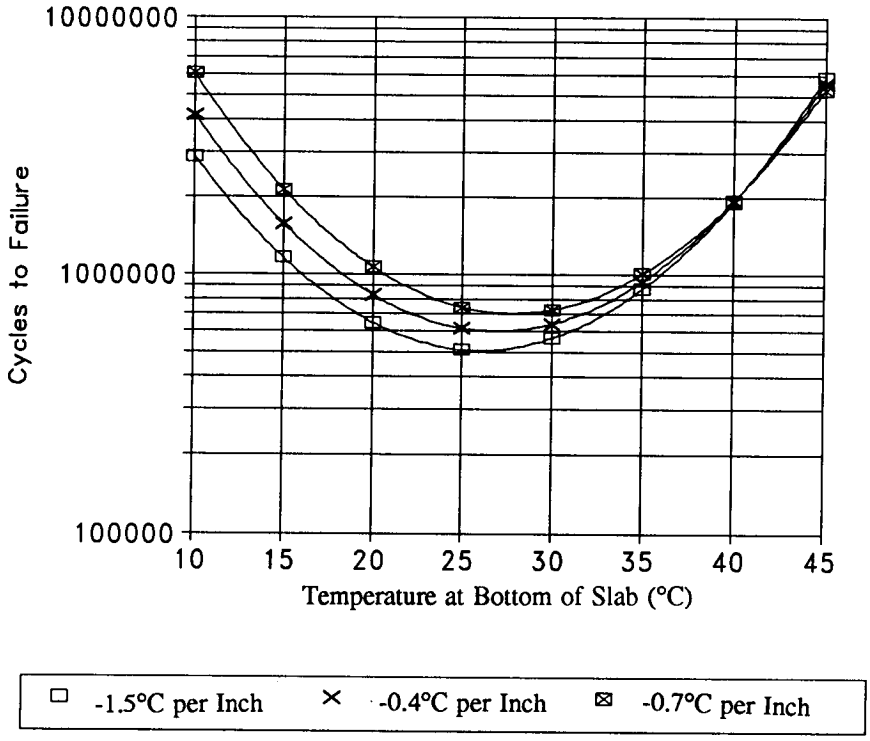

Figure 19.2. Effect of temperature and temperature gradient on fatigue life (N_f), 4 in. pavement

Table 19.5. Temperature equivalency factors (reference temperature of 20°C [68°F])

Midrange Temperature at Bottom of Asphalt Layer (°C)	Northeastern United States (Region I-A)		Southwestern United States (Region III-B)	
	10 cm (4 in.) Asphalt Layer	20 cm (8 in.) Asphalt Layer	10 cm (4 in.) Asphalt Layer	20 cm (8 in.) Asphalt Layer
-2.5	0.002872	0.0001337	---	---
0.0	0.008739	0.0003449	---	---
2.5	0.021140	0.0016160	0.02390	---
5.0	0.048220	0.0056510	0.04321	0.009227
7.5	0.098770	0.0175800	0.09462	0.018180
10.0	0.185500	0.0490700	0.17560	0.050300
12.5	0.319300	0.1225000	0.31730	0.122800
15.0	0.512600	0.2754000	0.51270	0.277100
17.5	0.753900	0.5568000	0.74740	0.560800
20.0	1.000000	1.0000000	1.00000	1.000000
22.5	1.239000	1.6280000	1.22400	1.604000
25.0	1.407000	2.1690000	1.36900	2.298000
27.5	1.492000	2.8850000	1.42000	2.951000
30.0	1.398000	3.2200000	1.37600	3.289000
32.5	1.260000	3.3590000	1.18300	3.334000
35.0	0.963200	---	0.97300	2.965000
37.5	0.772400	---	0.68240	2.405000
40.0	---	---	0.44880	2.059000
42.5	---	---	0.27640	---
45.0	---	---	0.14940	---
47.5	---	---	0.11010	---

20

Reliability

Decisions about anticipated mix performance cannot be made with absolute certainty. Although large safety factors can reduce the likelihood of error, their cost consequences can be considerable. Reliability analysis can ensure an acceptable level of risk in mix analysis without the cost of excessively large safety factors.

The AASHTO guide for pavement design (AASHTO 1986) provides the following description of the reliability concept as it applies to pavement structural design:

> The reliability of a pavement design-performance process is the probability that a pavement section designed using the process will perform satisfactorily over the traffic and environmental conditions for the design period.

A similar concept can be used for asphalt-aggregate mix design. In this case, reliability is considered to be the probability that the mix will provide satisfactory performance for the design period. Acceptable levels of risk (1 - probability levels) may be selected by the designer. For example, reliability levels could be specified at 60, 80, 90, or 95 percent; these would correspond to risk levels of 40, 20, 10, or 5 percent, respectively. Higher levels of reliability would reduce the chances of accepting deficient mixes; however, the tradeoff is the potentially higher cost associated with reducing the number of acceptable materials or mixes.

20.1 Approach

The safety factor associated with a specified level of reliability can be defined in terms of a multiplier (M) to be applied to traffic demand (N_{demand}). This multiplier is always greater than 1. The estimated fatigue life of the mix (N_{supply}) must exceed the product of the multiplier and the traffic demand ($M \cdot N_{demand}$). This condition is expressed in equation form as follows:

$$N_{supply} \geq M \cdot N_{demand} \quad (20.1)$$

where: M = the reliability multiplier (greater than 1) whose magnitude depends on variabilities of the estimated fatigue life and the traffic demand estimate and upon the desired reliability of the design.

Primarily because of the use of logarithmic transformations in modeling fatigue response, it is convenient to rewrite Equation 20.1 as follows:

$$Ln(N_{supply}) \geq Ln(N_{demand}) + \delta \quad (20.2)$$

where: Ln = natural logarithmic function, and
δ = an increment (greater than 0) whose value is equal to Ln(M).

The increment (δ) may be thought of as a positive spacing factor between $Ln(N_{supply})$ and $Ln(N_{demand})$. The δ increment increases with increases in the reliability level as well as with increases in the variabilities of the estimated fatigue life (N_{supply}) and the estimated traffic demand (N_{demand}). A marginal mix may ultimately be judged acceptable by more accurate estimates of mix resistance (for example, by increasing sample size in laboratory testing) or, if allowed, by relaxing requirements for the permissible level of risk.

The variability in the estimated fatigue life (N_{supply}) will reflect uncertainties in fatigue testing as well as extrapolation of test results to in situ levels of strain. The variability in the traffic demand estimates (N_{demand}) reflects uncertainty in the forecasted number and distribution of traffic loads across the pavement as well as a shift factor to bring laboratory estimates of fatigue life in line with pavement performance. The variability of N_{supply} may be estimated from fatigue test data generated in the A-003A project, as discussed below. The variability of N_{demand} must be estimated based on input by the traffic engineer.

20.2 Calculation of Variability of N_{supply}

Fatigue testing or surrogate model development is usually conducted at relatively large strain levels in order to minimize the required laboratory testing time. Then, assuming linearity in the $Ln(N_f)$-$Ln(\epsilon)$ relationship, a regression line or surrogate model is fitted to the data and an extrapolation is made to the design strain level, the in situ tensile strain under the standard traffic load. Estimates of field strain levels may be made under simulated field conditions utilizing layered elastic analysis. All analyses are conducted at a single temperature, and the stiffness modulus of the asphalt-aggregate layers can be measured from frequency sweep tests. The basic task is to determine the variability in the extrapolated cycles to failure given the nature of the testing program, the extent of the extrapolation, and the variability of the fatigue test data or surrogate model.

Two methods are available to predict N_{supply} at field strain levels: 1) extrapolation of the $Ln(N_f)$-$Ln(\epsilon)$ fatigue lines from laboratory tests for an individual mix or 2) extrapolation of

the surrogate fatigue model based on the mix's loss modulus (S_o'') and on the tensile strain (ϵ) in the pavement. In either case, the variance associated with the prediction must be determined.

20.2.1 Laboratory Testing

The variance associated with the fatigue life predicted from a linear regression of $Ln(N_f)$ versus $Ln(\epsilon)$ may be determined by standard analytical techniques as follows (Neter et al. 1983):

$$Var\{Y\} = \sigma^2 \left[\frac{1}{n} + \frac{X-\bar{x})^2}{\Sigma\ (x_i-\bar{x})^2} \right] \tag{20.3}$$

where:

$Var\{Y\}$	=	variance of predicted $Ln(N_{supply})$,
σ^2	=	variance of $Ln(N_f)$ in fatigue testing,
n	=	number of test specimens,
X	=	Ln(strain) at which predicted $Ln(N_{supply})$ is estimated,
$\bar{x}$	=	average Ln(test strain), and
x_i	=	ith level of test strain.

With p levels of test strain and q repeats at each level, Equation 20.3 becomes

$$Var\{Y\} = \sigma^2 \left[\frac{1}{n} + \frac{X-\bar{x})^2}{q\ \Sigma\ (x_p-\bar{x})^2} \right] \tag{20.4}$$

where:

q	=	number of replicate specimens at each test strain level,
p	=	number of strain levels, and
x_p	=	Ln(strain) at the pth strain level.

Equations 20.3 and 20.4 permit the calculation of the variance about the prediction of $Ln(N_{supply})$ for a given strain level. However, when an actual pavement is built, it is the variance between the new observed value and the predicted value that is of interest. This variance is computed by adding the variance of the new observed value to the variance of the prediction, as shown in the following modification of Equation 20.4:

$$Var\{Y\} = \sigma^2 \left[1 + \frac{1}{n} + \frac{X-\bar{x})^2}{q\ \Sigma\ (x_p-\bar{x})^2} \right] \tag{20.5}$$

20.2.2 Surrogate Model

The variance associated with the fatigue life predicted from the surrogate model (incorporating ϵ, S_o'', and the percentage of voids filled with asphalt) may be computed using essentially the same analytical techniques as for the regression of laboratory test data. Instead of σ^2, the mean square error (MSE) of the surrogate model regression is used. The resulting equation is as follows:

$$\text{Var}\{Y\} = \text{MSE}\left[1 + \frac{1}{n} + \sum_{i}^{k} c_{ii}x_i^2 + 2\sum_{i}^{k}\sum_{j>i}^{k} c_{ij}x_i x_j\right] \qquad (20.6)$$

where:

	$\text{Var}\{Y\}$	=	variance of predicted $\text{Ln}(N_{supply})$,
	MSE	=	mean square error of $\text{Ln}(N_f)$ from surrogate model,
	n	=	number of observations used for surrogate-model calibration,
	x	=	$\text{Ln}(\epsilon)$, $\text{Ln}(S_o'')$, and VFB at which predicted $\text{Ln}(N_{supply})$ is estimated,
	k	=	number of independent variables (3), and
	c	=	variance and covariance of the regression coefficients expressed as a fraction of the MSE.

For the extended fatigue test program data, it should be noted that interactions between strain and mix effects were found to be negligible. This finding suggests that there is minimal danger in extrapolating to the relatively low strain levels associated with field conditions.

20.3 Calculations of M and δ

The calculations of M and δ are similar to those used in the AASHTO pavement design procedure (AASHTO 1986). Recall from Equation 20.2 that, for mixes to be judged acceptable for a given level of reliability, $\text{Ln}(N_{supply})$ must be greater than $\text{Ln}(N_{demand})$ by an increment δ. The reliability level together with the standard deviations (or variances) of both fatigue life estimates (Ln)—one for laboratory data and the other for design traffic—determine the required value of δ.

To determine δ, Equation 20.2 may be written in the following form:

$$\text{Ln}(N_{supply}) - \text{Ln}(N_{demand}) \geq \delta \qquad (20.7)$$

Because the variance of a difference is the sum of the variances,

$$\text{Var}\{\text{Ln}(N_{supply}) - \text{Ln}(N_{demand})\} = \text{Var}\{\text{Ln}(N_{supply})\} + \text{Var}\{\text{Ln}(N_{demand})\} \qquad (20.8)$$

and

$$\text{Var}\{\delta\} = \text{Var}\{\text{Ln}(N_{\text{supply}})\} + \text{Var}\{\text{Ln}(N_{\text{demand}})\} \quad (20.9)$$

The probability distribution of δ, illustrated graphically in Figure 20.1, forms the basis for solving for δ and M. The area underneath the distribution curve where $\delta \geq 0$ corresponds to the probability that $\text{Ln}(N_{\text{supply}}) \geq \text{Ln}(N_{\text{demand}})$. This probability is defined to be the reliability level (R), which is expressed as a percentage. The equation for R is as follows:

$$R \text{ (percent)} = \text{Prob } [\text{Ln}(N_{\text{supply}}) \geq \text{Ln}(N_{\text{demand}})] \quad (20.10)$$

$$= \text{Prob } [\delta \geq 0] \quad (20.11)$$

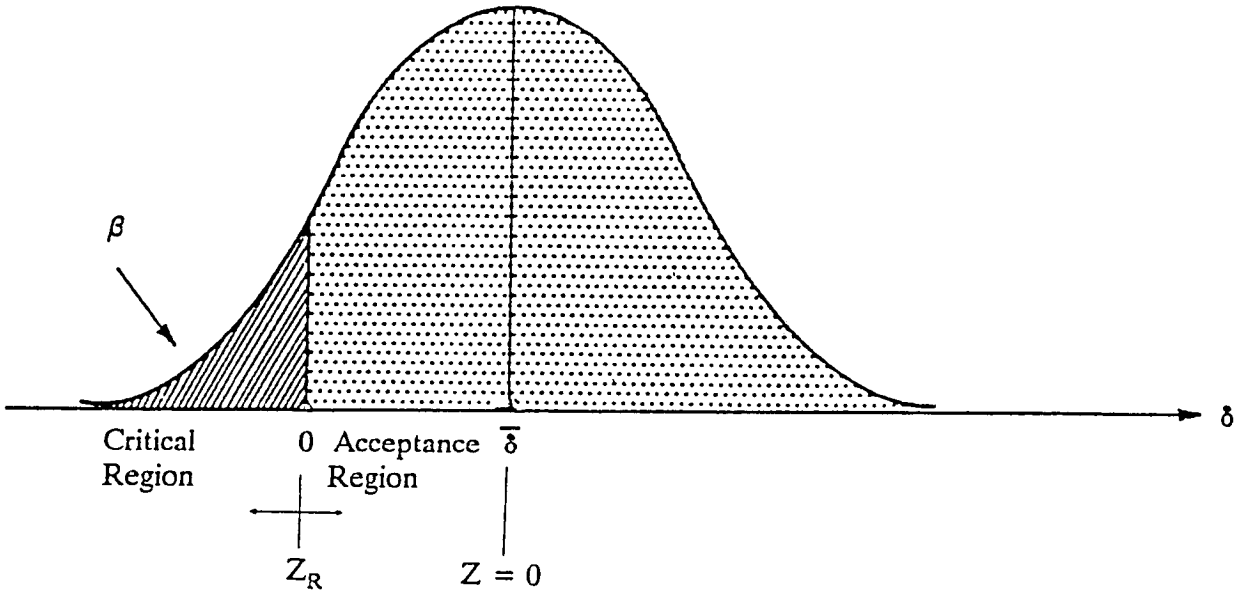

Distribution of $\text{Ln}(N_{\text{supply}}) - \text{LnN}(_{\text{demand}})$

H_0: Mix Acceptable $\quad \delta \geq \text{Ln}(N_{\text{supply}}) - \text{Ln}(N_{\text{demand}})$

H_1: Mix Unacceptable $\quad \delta < \text{Ln}(N_{\text{supply}}) - \text{Ln}(N_{\text{demand}})$

If reality is H_1 and we accept H_0, we have committed a Type II error. The probability of a Type II error P (Type II) is β. For Reliability Level R, choose δ such that $\beta < 1\text{-R}$.

Figure 20.1. Illustration of one-sided tolerance limit for determining δ

Referring to Figure 20.1, a Z-scale corresponding to a standard normal deviate may be applied to the distribution of δ by the following relationship:

$$Z = \frac{\delta - \bar{\delta}}{S_\delta} \tag{20.12}$$

where: s_δ = the standard deviation of the δ distribution.

At the point where $\delta = 0$, Z becomes Z_R where

$$Z_R = -\bar{\delta}/s_\delta \tag{20.13}$$

Since the standard deviation is the square root of the variance,

$$\bar{\delta} = -Z_R \cdot \sqrt{Var\{\delta\}} \tag{20.14}$$

And finally, the reliability multiplier, M, is the anti-log (Ln) of $\bar{\delta}$,

$$M = EXP\ (-Z_R \cdot \sqrt{Var\{\delta\}}\ ) \tag{20.15}$$

where: EXP = a power function of e such that EXP [x] refers to $e^{[x]}$.

Combining Equations 20.9 and 20.15 yields

$$M = EXP\ (-Z_R * \sqrt{Var\{Ln\ (N_{supply})\} + Var\{Ln\ (N_{demand})\}}\ ) \tag{20.16}$$

Note that Z_R depends solely on the desired reliability level. For reliabilities of 60, 80, 90, and 95 percent, for example, Z_R is -0.253, -0.841, -1.28, and -1.64, respectively. To solve for M or δ, the designer needs only to know the reliability level and variance estimates for traffic and fatigue life. Typically, the designer knows variance estimates for these latter two items in terms of standard deviation, which is the square root of the variance.

20.4 Comparisons Between Laboratory Testing and Surrogate Models

20.4.1 Laboratory Test Program

Variances associated with A-003A laboratory fatigue testing can be quantified using results from the expanded fatigue test program. The expanded test program involved 32 different mixes tested at each of two strain levels with full replication. The 64 pairs of replicates allow the sample variance to be estimated by pooling variances between replicate tests as follows:

$$s^2 = \{\Sigma\ [Ln(N_{rep1}/N_{rep2})]^2/2\}/(\#\ Obs) \tag{20.17}$$

where: s^2 = sample variance of $Ln(N_f)$ associated with fatigue testing,
N_{rep1} = fatigue life of first replicate,

N_{rep2} = fatigue life of second replicate, and
Obs = number of pairs of replicates.

The sample variance, as obtained by Equation 20.17 above, is the best estimate of the variance associated with fatigue tests on replicate beam specimens; that is, beam-to-beam variance. Slab-to-slab variance would be expected to be somewhat larger than beam-to-beam variance. Due to the particular design of the expanded test program, however, the variance associated with replicate slabs could not be estimated.

The best estimate of the sample variance of $Ln(N_f)$—obtained from the expanded fatigue testing program—was 0.1521. This variance reflects measurements obtained with the fatigue testing equipment and procedures developed by A-003A researchers.

With this estimate of sample variance from laboratory fatigue testing, variance estimates for predicted N_{supply} values can be made for a variety of testing program scenarios using Equation 20.5. To illustrate, standard deviation (square root of variance) estimates for predicted $Ln(N_{supply})$ values at 1, 3.5, 10, and 35 million cycles were computed for several different testing program scenarios.[9] Results are tabulated below.

Predicted N_{supply}	Standard Deviation of Predicted $Ln(N_{supply})$					
	4 Strain Levels			2 Strain Levels		
	4 Tests	8 Tests	12 Tests	4 Tests	8 Tests	12 Tests
1,000,000	0.606	0.510	0.473	0.535	0.468	0.444
3,500,000	0.747	0.596	0.536	0.625	0.521	0.481
10,000,000	0.879	0.680	0.599	0.712	0.574	0.520
35,000,000	1.045	0.789	0.682	0.825	0.645	0.573

For the same number of tests, testing at two strain levels instead of four obviously produces more accurate (less variable) estimates of $Ln(N_{supply})$. The cost for this added accuracy is an increase in the required duration of testing.

20.4.2 Surrogate Model

The reliability of surrogate models can be evaluated using a procedure similar to that for laboratory testing. The A-003A surrogate model was developed from a composite data set

---

[9]This example assumes that laboratory testing is conducted at strains which induce failure at approximately 10,000, 35,000, 100,000, and 350,000 cycles for testing at four strain levels and 10,000 and 350,000 cycles for testing at two strain levels. For these computations, the regression model of Equation 20.18 was used to relate tensile strain and fatigue life. VFB was taken to be the average, 69 percent, of 200 specimens from which the regression model was calibrated, and S''_o was assumed to be the approximate measured average of 2.4 GPa (350,000 psi).

which included 1) the 8×2 expanded experiment (128 specimens), 2) the mix design experiment (22 specimens), 3) the Nantes validation study (19 specimens), 4) the FHWA-ALF validation study (8 specimens), and 5) the TEF experiment (23 specimens). Controlled-strain loading at 10 Hz was used throughout. Least-squares calibration yielded the following regression model:

$$N_{supply} = 2.738 \cdot 10^5 \cdot e^{0.077 \cdot VFB} \cdot \epsilon_o^{-3.624} \cdot S_o''^{-2.720} \quad R^2 = 0.79 \qquad (20.18)$$

The MSE was estimated to be 0.6341. Again, this error estimate represents beam-to-beam variance only. Slab-to-slab variance could not be estimated due to the nature of the experiment.

From the MSE estimate, variance estimates for predicted N_{supply} values from the surrogate model can be developed using Equation 20.6. Using the same example used earlier for laboratory testing, the standard deviation (square root of variance) estimates for predicted N_{supply} values of 1, 3.5, 10, and 35 million cycles were computed. For these computations, the voids filled with asphalt was assumed to be 70 percent, and S_o'' was assumed to be 1.5 GPa (250,000 psi). The results are tabulated below.

Predicted N_{supply}	Standard Deviation of $Ln(N_{supply})$
	Surrogate Model
1,000,000	0.807
3,500,000	0.816
10,000,000	0.827
35,000,000	0.842

20.4.3 Comparisons

To characterize the fatigue behavior of an asphalt-aggregate mix, the minimum testing which can be completed within 24 hours involves four specimens, each tested at a different strain level. The accuracy of estimates developed from such testing relative to the accuracy of estimates developed from the composite regression model is illustrated as follows:

Predicted N_{supply}	Standard Deviation of $Ln(N_{supply})$	
	Laboratory Testing 4 Tests, 4 Strains	Surrogate Model
1,000,000	0.606	0.807
3,500,000	0.747	0.816
10,000,000	0.879	0.827
35,000,000	1.045	0.842

This form of laboratory testing yields less variable estimates of fatigue life than the composite regression model when the extent of the required extrapolation is relatively small. For larger extrapolations, the surrogate model is actually superior. However, by testing more specimens and relaxing the 24 hour testing restriction, the relative superiority of laboratory testing can be restored. For example, adding only two specimens to the laboratory test program while eliminating the two most middle strain levels makes testing estimates better than surrogate model estimates for all predictions, as illustrated below:

Predicted N_{supply}	Standard Deviation of $Ln(N_{supply})$	
	Laboratory Testing 6 Tests, 2 Strains	Surrogate Model
1,000,000	0.491	0.807
3,500,000	0.558	0.816
10,000,000	0.623	0.827
35,000,000	0.710	0.842

Using the standard deviations above with a design reliability of 80 percent to determine M and assuming a standard deviation in N_{demand} of 0.2, the required N_{supply} for acceptable mixes would be as follows:

N_{demand}	Minimum Required N_{supply} for Acceptable Mix		
	Laboratory Testing 4 Tests, 4 Strains	Laboratory Testing 6 Tests, 2 Strains	Surrogate Model
1,000,000	1,700,000	1,600,000	2,000,000
3,500,000	6,700,000	5,800,000	7,100,000
10,000,000	21,300,000	17,300,000	20,400,000
35,000,000	85,600,000	65,100,000	72,500,000

A comparison of the predictive accuracy of fatigue life estimates among the various laboratory test programs and the surrogate model is illustrated graphically in Figure 20.2. If the laboratory fatigue test program is limited to four tests, one at each of four strain levels, better reliability can be achieved through the surrogate model beyond a traffic level of about 6 million cycles. By changing the laboratory testing program (for example, by adding more tests and/or reducing the number of strain levels from four to two by eliminating the most middle levels), the accuracy of laboratory testing relative to the surrogate model can be significantly improved.

20.5 Use of Beam Fatigue Tests

The mix designer will typically want to substitute stiffness testing and regression estimates for fatigue testing in order to complete the design process more quickly and less expensively. Fatigue testing will be necessary, however, not only for unconventional mixes and those with atypical temperature sensitivity but also to increase the accuracy of the estimated fatigue life.

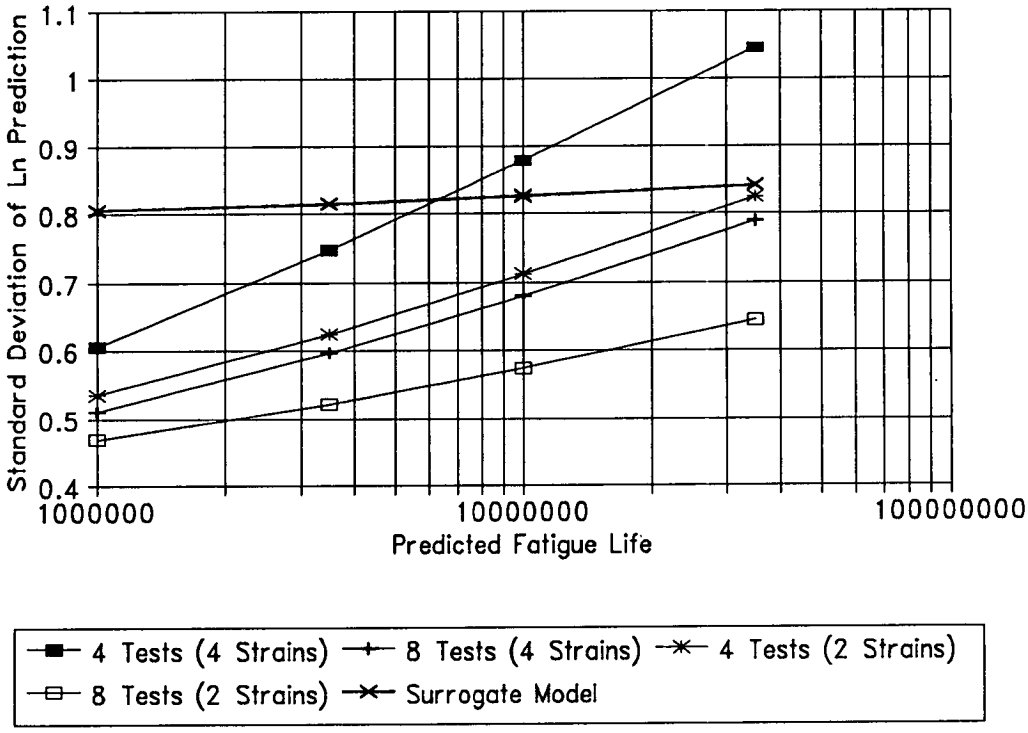

Figure 20.2. Comparison of predictive accuracy of various laboratory test programs and the surrogate model

The techniques described before enable the designer to quantify the relative accuracy of fatigue testing programs and the composite surrogate model and make reasonable choices from among them.

21

Shift Factor

As a result of such factors as crack progression, traffic wander, and even periodic "healing," highway pavements have been found to sustain from 10 to perhaps as much as 100 times the number of load applications that are estimated by procedures similar to those used herein before pavements become seriously distressed. As a result, laboratory estimates (N_{supply}) can be compared with service requirements ($ESAL_{20°C}$) only after applying a suitable shift factor. Proposed herein is the use of such a shift factor that is defined as follows:

$$N_{demand} = ESAL_{20°C}/SF \quad (21.1)$$

where:
- N_{demand} = design traffic demand (laboratory-equivalent repetitions of standard load),
- $ESAL_{20°C}$ = design ESALs adjusted to a constant temperature of 20°C (68°F), and
- SF = empirically determined shift factor.

One of the most definitive examinations of shift factors was conducted for the National Cooperative Highway Research Program (NCHRP) by Finn et al. (1986). These researchers developed shift factors to bring fatigue life estimates from mechanistic analysis in line with measurements of Class 2 fatigue cracking from 19 sections of the AASHTO road test. Laboratory fatigue life was characterized by a model reported by Monismith et al. (1972)[10]; multilayer elastic characterization (with stress dependency) was employed. The detailed analysis produced the following recommended shift factors: 13.0 for 10 percent

---

[10]The NCHRP model is identified as follows:

$$\log N_f = 14.82 - 3.291 \log(\epsilon/10^{-6}) - 0.854 \log(|E^*|/10^3)$$

where:
- N_f = load applications of constant stress to cause fatigue failure,
- ϵ = initial strain on the underside of the asphalt-concrete, and
- $|E^*|$ = complex modulus, in psi.

Class 2 cracking in the wheel path area and 18.4 for 45 percent cracking in the wheel path area. Although the analysis indicated that changes in the thickness of the asphalt-concrete from 10.16 to 15.24 cm (4 to 6 in.) would not likely alter the magnitudes of the shift factors, the authors suggested that a different set of reference fatigue curves would likely yield a different set of shift factors. They suggested further study to verify or refine these shift-factor recommendations.

Although detailed study has not been possible within the scope of the A-003A project, a limited effort was made to validate this recommendation. The attempt was to demonstrate whether a shift factor of 13 would produce reasonable mix-acceptance results for mixes tested by A-003A staff and for several different pavements designed according to current AASHTO procedures (AASHTO 1986). Five pavement structures were examined. Two incorporated 10.16 cm (4 in.) surfaces with granular bases of sufficient thickness to resist 1,000,000 and 4,000,000 design ESALs. The remaining three incorporated 20.32 cm (8 in.) surfaces with granular bases of sufficient thickness to resist 1,000,000; 4,000,000; and 16,000,000 design ESALs. Other design variables are identified in Table 21.1.

Table 21.1. Simulated designs for shift-factor validation

Pavement Structural Section	Asphalt Layer	Thickness	10 cm and 20 cm (4 in. and 8 in.)
		Modulus of Elasticity	Varies With Mix
		Poisson's Ratio	0.35
		Layer Coefficent	0.44
	Granular Base	Thickness	Varies as Necessary
		Modulus of Elasticity	207 MPa (30,000 psi)
		Poisson's Ratio	0.40
		Layer Coefficient	0.14
		Drainage Coefficient	1.10
	Subgrade	Modulus of Elasticity	52 MPa (7500 psi)
		Poisson's Ratio	0.45
Design Criteria	Design Traffic		1,000,000 to 16,000,000 ESALs
	Reliability		90 Percent
	Standard Deviation		0.45
	Initial Serviceability		4.20
	Terminal Serviceability		2.50
Locations	Northeastern United States (Region I-A) and Southwestern United States (Region III-B)		

Using the NCHRP fatigue life model, a determination was first made of the expected performance of each of the 44 mixes within each of the five pavement structures. Climatic Region I-A was selected for the analysis because the AASHTO road test was located within it. Assuming that the AASHTO mix typified a normal paving mix, one would expect approximately one half of the A-003A mixes to perform better than the AASHTO mix and approximately one half to perform worse. Except for the most substantial structures and the most damaging traffic loading, the analysis generally confirmed this expectation and demonstrated the reasonableness of a shift factor of 13 in modeling average pavement performance (Table 21.2).

Table 21.2. A-003A mix suitability for northeastern United States (Region I-A), using NCHRP 291 model

Variable	Pavement Structure				
	10 cm (4 in.) Surface, 30 cm (12 in.) Base	10 cm (4 in.) Surface, 43 cm (17 in.) Base	20 cm (8 in.) Surface, No Base	20 cm (8 in.) Surface, 15 cm (6 in.) Base	20 cm (8 in.) Surface, 30 cm (12 in.) Base
Design ESALs	1,000,000	4,000,000	1,000,000	4,000,000	16,000,000
Temperature Conversion Factor (Table 22.3)	0.614	0.614	0.920	0.920	0.920
$ESALs_{20°C}$	614,000	2,456,000	920,000	3,680,000	14,720,000
Shift Factor	13.0	13.0	13.0	13.0	13.0
N_{design}	47,000	189,000	71,000	283,000	1,132,000
Percentage of A-003A Mixes With Fatigue Life Greater Than N_{design}	41	0	84	55	0

Detailed procedures for evaluating the fatigue resistance of the 44 A-003A mixes, each of which had been tested for fatigue resistance at 20°C (68°F) in the laboratory, followed the abridged, Level 2 analysis. Separate determinations were made for the northeastern and southwestern regions of the United States because of the influence of thermal environment on the conversion of design ESALs to their equivalent at 20°C [68°F].[11] Additional computations were also made using the NCHRP fatigue life model.

The design ESALs were first converted to their equivalent at 20°C (68°F) by a temperature conversion factor. Described subsequently, the temperature conversion factor is a convenient and simple way to combine the effects of the frequency distribution of pavement temperatures with the TEFs reported earlier. Applying the shift factor of 13 to $ESAL_{20°C}$

[11]As a simplification, the same basic pavement designs were used for both northeastern and southwestern states. The detailed refinements necessary to produce the location-specific pavement designs of AASHTO procedures were considered unnecessary for this investigation.

yielded N_{design}, a measure of the design traffic loading commensurate with laboratory measurements. Because the reliability multiplier depends on $Var\{Ln(N_{supply})\}$ which in turn depends on the extent of the necessary extrapolation from laboratory testing, a two-step procedure using a trial reliability multiplier of 3 was followed. To determine $Var\{Ln(N_{supply})\}$, it was also assumed that four specimens of each mix had been tested in the laboratory: two at each of two levels of strain.[12] Although such a scheme was not always followed, most of the laboratory tests were performed this way. For lack of more definitive information, $Var\{Ln(N_{demand})\}$ was simply assumed to be 0.3. For this analysis, a reliability of 90 percent was selected as the acceptable minimum. The above procedure yielded the minimum N_{supply} considered necessary for acceptable performance in situ.

To determine the acceptability of each of the 44 mixes, their average flexural stiffnesses were computed together with the constants K1 and K2, which described their fatigue resistance (Equation 22.4). Using the stiffness average for each mix, the critical tensile strains in the five structures were computed together with the mix-specific N_{supply} (Equation 22.4). A mix was judged adequate when N_{supply} exceeded the minimum requirement. A similar procedure was followed to test the NCHRP model, except that model estimates replaced those obtained from laboratory testing.

Computations are summarized in Tables 21.3 and 21.4 for the northeastern and southwestern regions, respectively. Percentages of the 44 mixes that had acceptable fatigue resistance are tabulated on the last rows of these tables. The effect of method of characterization of the mixes, either the NCHRP model or laboratory fatigue testing, is plainly evident. Using the NCHRP model, most of the 44 mixes were found unsuitable for use in the trial structures. On the other hand, most were found suitable when their fatigue lives were determined from laboratory testing. This remarkably different behavior is likely due to the fact that the NCHRP model was developed from controlled-stress testing instead of the controlled-strain testing utilized and recommended by A-003A staff. At a given level of initial strain, fatigue lives are considerably longer under controlled-strain than under controlled-stress testing. Direct comparison of fatigue lives of the 44 mixes in the five trial pavement structures, summarized below, demonstrates that controlled-strain testing yields much larger fatigue-life estimates than controlled-stress modeling. Thus, different shift factors are required for the two different modes of loading.

Median Ratio of A-003A Fatigue Life to NCHRP Fatigue Life

10 cm (4 in.) Surface, 30 cm (12 in.) Base	10 cm (4 in.) Surface, 43 cm (17 in.) Base	20 cm (8 in.) Surface, No Base	20 cm (8 in.) Surface, 15 cm (6 in.) Base	20 cm (8 in.) Surface, 30 cm (12 in.) Base
22.0	22.6	25.8	27.2	28.6

[12]Variability of NCHRP-model estimates was treated similarly merely because more accurate estimates were unavailable.

Table 21.3. A-003A mix suitability for northeastern United States (Region I-A)

Variable		Pavement Structure				
		10 cm (4 in.) Surface, 30 cm (12 in.) Base	10 cm (4 in.) Surface, 43 cm (17 in.) Base	20 cm (8 in.) Surface, No Base	20 cm (8 in.) Surface, 15 cm (6 in.) Base	20 cm (8 in.) Surface, 30 cm (12 in.) Base
Design ESALs		1,000,000	4,000,000	1,000,000	4,000,000	16,000,000
Temperature Conversion Factor (Table 22.3)		0.614	0.614	0.920	0.920	0.920
$ESALs_{20°C}$		614,000	2,456,000	920,000	3,680,000	14,720,000
Shift Factor		13	13	13	13	13
N_{design}		47,000	189,000	71,000	283,000	1,132,000
Trial Reliability Multiplier		3	3	3	3	3
Trial Minimum N_{supply}		141,000	567,000	213,000	849,000	3,396,000
$Var\{Ln(N_{supply})\}$ (Table 22.5)		0.177	0.250	0.196	0.276	0.387
Reliability Multiplier (Equation 22.7 for $Var\{Ln(N_{demand})\} = 0.3$ and 90% Reliability)		2.42	2.58	2.46	2.64	2.89
Minimum N_{supply} $(M \cdot N_{demand})$		114,000	488,000	175,000	747,000	3,271,000
Percentage of Suitable A-003A Mixes	NCHRP 291	0	0	55	11	0
	A-003A	95	73	100	95	75

Table 21.4. A-003A mix suitability for southwestern United States (Region III-B)

Variable		Pavement Structure				
		10 cm (4 in.) Surface, 30 cm (12 in.) Base	10 cm (4 in.) Surface, 43 cm (17 in.) Base	20 cm (8 in.) Surface, No Base	20 cm (8 in.) Surface, 15 cm (6 in.) Base	20 cm (8 in.) Surface, 30 cm (12 in.) Base
Design ESALs		1,000,000	4,000,000	1,000,000	4,000,000	16,000,000
Temperature Conversion Factor (Table 22.3)		0.838	0.838	1.839	1.839	1.839
$ESALs_{20°C}$		838,000	3,352,000	1,839,000	7,356,000	29,424,000
Shift Factor		13	13	13	13	13
N_{design}		64,000	258,000	141,000	566,000	2,263,000
Trial Reliability Multiplier		3	3	3	3	3
Trial Minimum N_{supply}		192,000	774,000	423,000	1,698,000	6,789,000
$Var\{Ln(N_{supply})\}$ (Table 22.5)		0.191	0.269	0.232	0.327	0.459
Reliability Multiplier (Equation 22.7 for $Var\{Ln(N_{demand})\} = 0.3$ and 90% Reliability)		2.45	2.63	2.54	2.76	3.05
Minimum N_{supply} $(M \cdot N_{demand})$		157,000	678,000	358,000	1,562,000	6,902,000
Percentage of Suitable A-003A Mixes	NCHRP 291	0	0	25	0	0
	A-003A	91	66	98	91	61

When using the NCHRP model (controlled-stress loading), a shift factor of 13, previously found suitable for characterizing average behavior, seems unreasonably small for the mix design and analysis process recommended herein, at least when highly reliable performance is required. When the A-003A mixes are evaluated and conventional structural design procedures are employed, an inordinately large percentage of the mixes appears to be unsuitable at a reliability level of 90 percent. More acceptable percentages would have been expected were it not for the large variability in fatigue life and fatigue life measurements.

When using A-003A laboratory measurements (controlled-strain loading), a shift factor of 13 produced much more reasonable results, at least for performance at a reliability level of 90 percent. Although the bulk of the mixes is acceptable at the smallest traffic loading (1,000,000 ESALs), the percentage of suitable mixes decreases with increases in traffic loading. Although this seems to indicate that AASHTO design procedures are more conservative (vis-à-vis fatigue cracking) at smaller traffic levels than at larger ones, it also

suggests that requirements for mix quality increase with increases in traffic level (despite the AASHTO requirements for thicker pavement sections with increased loading). The analysis also suggests that the loading environment is more severe in the southwestern United States than in the Northeast. Although such differences might be reduced or possibly even eliminated by region-specific structural designs, it is not unreasonable to expect that mixes suitable for one region of the country might not be suitable for another.

Considering the fact that the A-003A mixes intentionally spanned a wide range of likely mix performance, a shift factor of 13 is certainly within an acceptable range for use with the mix design and analysis procedures recommended herein. However, a factor of 10 would be somewhat more discriminating and is recommended initially for design applications. For 45 percent cracking, a shift factor of about 14 is consistent with NCHRP 291 findings.

Because AASHTO structural design procedures are based on overall pavement serviceability rather than on specific distress mechanisms, analyses such as the one above cannot yield accurate shift-factor estimates. At the same time, the analysis above has confirmed that the shift factors recommended by Finn et al. (1986) generally allow reasonable modeling and, following adjustments to reflect a different mode of loading and to accommodate reliability analysis, reasonable judgments about the adequacy of specific mixes to resist fatigue cracking in service. Such shift factors certainly provide an effective place to begin, and design agencies are encouraged to start with these shift factors and make refinements based on local experiences. Analysis of selected General Pavement Studies (GPS) test sites, currently under way by the SHRP A-005 contractor, should provide invaluable information for added refinement. Ultimately, the shift factors are expected to depend on the extent of permissible cracking and possibly such added factors as the structural section, rate of accumulation of traffic loading, mode of loading, and perhaps mix properties as well.

22

Abridged Analysis System

The abridged analysis system, which includes Levels 1 and 2, is generally applicable to mixes having binders of typical temperature sensitivity. The evaluation of conventional mixes relies initially on Level 1 analysis. Fatigue testing and Level 2 analysis would be employed only when added accuracy was desired or for evaluating unconventional mixes. Described below are the steps necessary for undertaking the abridged analysis system.

22.1 Determine Design Requirements for Reliability and Performance

Design reliability and performance requirements are set by the individual design agency. Presumably, they reflect in part the importance of the paving project as evidenced by such factors as highway functional classification and traffic volumes as well as the tradeoffs between benefits and costs. The analysis system proposed herein enables the designer to select any level of reliability—the probability that an asphalt mix will provide satisfactory performance throughout the design period. However, because of the highly variable nature of asphalt mixes and of conditions encountered in situ, the costs associated with designs of high reliability are likely to be quite large.

Performance requirements in fatigue generally specify the extent of permissible fatigue cracking expressed as a percentage of the pavement or wheel track surface area. Unfortunately, the analysis system proposed herein has not yet been calibrated to the extent that would permit the designer to evaluate the possible effects of varying performance levels. The recommended level targeted by the current procedure limits cracking to approximately 5 percent of the pavement surface area within the design lane or approximately 10 percent within the wheel tracks.

22.2 Determine Expected Distribution of In Situ Temperatures

Pavement analysis in the abridged procedure assumes a uniform temperature of 20°C (68°F) throughout the asphalt layer. However, to effectively treat the destructive effects of traffic

under other temperature conditions, it is necessary to know the expected frequency distribution of in situ temperatures at the underside of the asphalt layer. FHWA's integrated model provides a relatively convenient way to determine this distribution at any location in the continental United States. Computation time can be reduced without seriously jeopardizing accuracy by limiting the analysis to one-half of the annual total of 8,760 hours. Regional estimates, as exemplified by Table 22.1, may eventually prove sufficient for most applications.

Table 22.1. Frequency distribution (percentage) of pavement temperature

Midrange Temperature at Bottom of Asphalt Layer (°C)	Northeastern United States (Region I-A)		Southwestern United States (Region III-B)	
	10 cm (4 in.) Asphalt Layer	20 cm (8 in.) Asphalt Layer	10 cm (4 in.) Asphalt Layer	20 cm (8 in.) Asphalt Layer
-2.5	7.6	2.1	—	—
0.0	17.8	20.8	—	—
2.5	2.9	3.4	0.8	—
5.0	3.9	3.9	2.4	0.8
7.5	4.3	4.6	3.6	3.5
10.0	4.6	5.4	4.6	6.4
12.5	5.2	5.8	5.8	7.4
15.0	5.8	6.2	6.8	6.9
17.5	6.9	6.8	7.1	6.9
20.0	9.0	7.6	7.1	6.9
22.5	7.0	10.8	7.8	7.4
25.0	5.9	9.4	10.6	8.3
27.5	5.2	7.1	8.0	10.4
30.0	4.6	5.6	7.8	12.6
32.5	3.8	0.3	5.3	9.0
35.0	3.4	—	6.0	8.0
37.5	2.0	—	4.5	5.2
40.0	—	—	4.0	0.1
42.5	—	—	4.2	—
45.0	—	—	3.1	—
47.5	—	—	0.5	—

Each design agency is required to determine temperature distributions within its geographical jurisdiction only when initially setting up its mix design and analysis system. The process need not be repeated each time a new mix is analyzed. For mixes with typical temperature

sensitivities, the design and analysis computations are shortened by the use of temperature conversion factors (see Table 22.3).

22.3 Estimate Design Traffic Demand

The starting point for estimating the traffic demand (ESALs) for mix design is the ESAL estimate that drives the AASHTO structural design process; that is, the number of ESALs anticipated within the design lane during the design period. Adjusting this estimate to yield the equivalent number of ESALs *at a pavement temperature of 20°C (68°F)* requires the use of the temperature frequency distribution (exemplified in Table 22.1), TEFs (exemplified in Table 19.5), and the assumption, in the absence of other information, that the accumulation of ESALs is uniformly distributed through the hours of the year. Table 22.2 illustrates the required computations. If detailed traffic forecasts are available, nonuniform ESAL accumulations can easily be handled as well.

Table 22.2. Illustrative computation of equivalent ESALs at 20°C (68°F)

Midrange Temperature (°C)	Frequency	ESALs	Temperature Equivalency Factor	Equivalent Design ESALs
-2.5	f_1	$ESAL_d \times f_1$	TEF_1	$ESAL_1 \times TEF_1$
0.0	f_2	$ESAL_d \times f_2$	TEF_2	$ESAL_2 \times TEF_2$
2.5	f_3	$ESAL_d \times f_3$	TEF_3	$ESAL_3 \times TEF_3$
...	...	...	...	...
42.5	f_{n-2}	$ESAL_d \times f_{n-2}$	TEF_{n-2}	$ESAL_{n-2} \times TEF_{n-2}$
45.0	f_{n-1}	$ESAL_d \times f_{n-1}$	TEF_{n-1}	$ESAL_{n-1} \times TEF_{n-1}$
47.5	f_n	$ESAL_d \times f_n$	TEF_n	$ESAL_n \times TEF_n$
Equivalent ESALs at 20°C ($ESAL_{20°C}$)				$\Sigma(ESAL_i \times TEF_i)$

Although the process of calibrating TEFs is rather tedious (see Appendix H), it too is a one-time process that need not be repeated for other mixes which employ binders of normal temperature sensitivity. Ultimately, when temperature conversion factors such as those illustrated by Table 22.3 are developed for a particular jurisdiction, the detailed computations of Table 22.2 will be unnecessary. A single factor that is sensitive to asphalt layer thickness and geographical area would then be available to convert design ESALs to their equivalents at 20°C (68°F).

Table 22.3. Temperature conversion factor for design ESALs

Region	10 cm (4 in.) Pavement	20 cm (8 in.) Pavement
I-A	0.614	0.920
I-B	0.760	1.422
I-C	0.826	1.130
II-A	0.531	0.848
II-B	0.740	1.473
II-C	0.859	1.816
III-A	0.564	0.849
III-B	0.838	1.839
III-C	0.934	1.922

22.4 Select Trial Mix

Using preselected asphalt, additives, and aggregate, the trial mix is initially designed either by the design agency's conventional practice or by SHRP's volumetric proportioning procedure (SHRP Asphalt Program Final Report, Volume I, 1994). Subsequent redesigns are evaluated at the discretion of the materials engineer.

22.5 Prepare Test Specimens and Condition as Required

Briquette specimens (5 × 15 cm [2 × 6 in.] round) for shear frequency sweep testing and beams (8.25 × 8.9 × 38 cm [3.25 × 3.50 × 15 in.]) for flexural fatigue testing are prepared by rolling-wheel compaction in accordance with SHRP Test Method M-008. Before testing, all specimens are subjected to short-term, oven aging in accordance with SHRP Test Method M-007. Level 2 analysis requires flexural fatigue testing, while Level 1 analysis uses shear frequency sweep testing as a surrogate for fatigue testing.

22.6 Measure Stiffness of Trial Mix

The abridged procedure requires an estimate of the flexural stiffness modulus of the asphalt-aggregate mix at 20°C (68°F). This estimate is used in the multilayer elastic analysis to determine the critical level of strain to which the mix is subjected under the standard traffic load.

The SHRP materials testing protocol is expected to specify shear frequency sweep tests for all conditions, that is, all distress modes, all mixes, and all levels of analysis. For measurements at 20°C (68°F) and 10 Hz, flexural properties can be reliably estimated from shear properties through the following regression equations:

$$S_o = 8.560(G_o)^{0.913} \qquad R^2 = 0.712 \qquad (22.1)$$

$$S''_o = 81.125(G''_o)^{0.725} \qquad R^2 = 0.512 \qquad (22.2)$$

where:
- S_o = initial flexural stiffness at the 50th loading cycle in psi,
- G_o = shear stiffness at 10 Hz in psi,
- S''_o = initial flexural loss stiffness at the 50th loading cycle in psi, and
- G''_o = shear loss stiffness at 10 Hz in psi.

For Level 1 analysis, estimates of flexural stiffness and flexural loss stiffness are determined using the equations above. Shear frequency sweep tests, conducted in accordance with SHRP Test Method M-003, allow sufficiently accurate estimates of G_o and G''_o from measurements on a single briquette specimen. For Level 2 analysis, fatigue testing at 20°C (68°F) and 10 Hz yields direct estimates of all necessary flexural properties.

22.7 Design Structural Section

Because mix performance in fatigue depends on the pavement's structure, the pavement cross-section must be known or assumed before evaluating the mix. Structural design is accomplished according to the design agency's normal procedures.

22.8 Determine Design Strain Under Standard Axle Load

Multilayer elastic analysis is used to determine the design strain, the maximum principal tensile strain at the bottom of the asphalt layer, under the standard AASHTO axle load. The standard load is an 80 kN (18,000 lb), single-axle, dual-tire load. A uniform contact pressure of 585 kPa (85 psi) and a tire spacing of 30.5 cm (12 in.) are assumed. The analysis is based on a temperature of 20°C (68°F) distributed uniformly throughout the pavement section. The flexural stiffness modulus of the asphalt-aggregate layer is measured directly (Level 2) or estimated using Equation 22.1 from shear stiffness measurements (Level 1); its Poisson's ratio is assumed to be 0.35. Moduli and Poisson's ratios of other layers, representing annual average conditions, are determined in accordance with standard AASHTO procedures (AASHTO T-285). Laboratory testing of substrata materials is considered unnecessary for designing the asphalt-aggregate mix.

22.9 Determine the Resistance of the Trial Mix to Fatigue

For Level 1 analysis, fatigue resistance is estimated from the following, previously calibrated regression model:

$$N_{supply} = 2.738 \cdot 10^5 \cdot e^{0.077 \cdot VFB} \cdot \epsilon_o^{-3.624} \cdot S''^{-2.720}_o \qquad R^2 = 0.79 \qquad (22.3)$$

where:

N_{supply}	=	the number of load repetitions to a 50 percent reduction in stiffness (crack initiation),
e	=	base of the natural logarithms,
ϵ	=	the flexural strain in in./in.,
S''_o	=	the initial flexural loss stiffness at the 50th loading cycle in psi (estimated by Equation 22.2), and
VFB	=	the voids filled with bitumen expressed as a percentage and measured using the frequency-sweep specimens or determined from the volumetric proportioning process.

For Level 2 analysis, fatigue resistance is measured in the laboratory by subjecting beam specimens to repeated flexure (20°C [68°F] at 10 Hz frequency) in accordance with SHRP Test Method M-009. The minimum testing program, which can usually be completed within 24 hours, involves four specimens subjected to strain levels expected to induce failure at approximately 10,000; 35,000; 100,000; and 350,000 load cycles (or 20 minutes, 1 hour, 3 hours, and 10 hours, respectively). If the required accuracy cannot be achieved by testing four specimens, additional specimens must be tested. At the completion of testing, a model of the following form is fit to the data:

$$N_f = K1 \cdot \epsilon^{K2} \tag{22.4}$$

The fatigue life (N_{supply}) corresponding to the design strain is then computed using Equation 22.4.

22.10 Apply a Shift Factor to the Travel Demand

Laboratory estimates of fatigue life (N_{supply}) can be compared with service requirements ($ESAL_{20°C}$) only after the application of a suitable shift factor. The shift factor is applied as follows:

$$N_{demand} = ESAL_{20°C}/SF \tag{22.5}$$

where:

N_{demand}	=	design traffic demand (laboratory-equivalent repetitions of standard load),
$ESAL_{20°C}$	=	design ESALs adjusted to a constant temperature of 20°C (68°F), and
SF	=	empirically determined shift factor.

Shift factors recommended for application initially depend upon the amount of cracking that is permissible so that shift factors of 10.0 for 10 percent cracking in the wheel paths and 14.0 for 45 percent cracking in the wheel paths are allowed.

Because experience with these recommendations is limited, design agencies are encouraged to consider adjustments that reflect their experience with both adequately and inadequately performing mixes. Future research should eventually help to guide these efforts.

22.11 Compare Traffic Demand (N_{demand}) With Mix Resistance (N_{supply})

Satisfactory mix performance requires that the mix resistance (N_{supply}) equal or exceed the traffic demand (N_{demand}). A multiplicative safety factor is applied to N_{demand} to account for the fact that neither N_{supply} nor N_{demand} is known with certainty and to accommodate the desired level of design reliability. Thus, for a mix to be satisfactory,

$$N_{supply} \geq M \cdot N_{demand} \tag{22.6}$$

where: M = a multiplier whose value depends on the design reliability and on the variabilities of the estimates of N_{supply} and N_{demand}.

The reliability multiplier can be estimated from Table 22.4 or calculated from the following equation:

$$Ln(M) = Z_R \cdot [Var\{Ln(N_{supply})\} + Var\{Ln(N_{demand})\}]^{0.5} \tag{22.7}$$

where:
- Z_R = a function of the reliability level which assumes values of 0.253, 0.841, 1.280, and 1.640 for reliability levels of 60, 80, 90, and 95 percent, respectively;
- $Var\{Ln(N_{supply})\}$ = variance of the natural logarithm of N_{supply}; and
- $Var\{Ln(N_{demand})\}$ = variance of the natural logarithm of N_{demand}.

For Level 1 analysis (surrogate testing and regression model), $Var\{Ln(N_{supply})\}$ depends upon the extent of extrapolation. Disregarding the variability associated with surrogate stiffness testing, $Var\{Ln(N_{supply})\}$ is approximated as follows:

Predicted N_{supply}	Variance of $Ln(N_{supply})$
	Surrogate Model
1,000,000	0.651
3,500,000	0.666
10,000,000	0.684
35,000,000	0.709

For Levels 2 and 3 analyses (laboratory fatigue testing), $Var\{Ln(N_{supply})\}$, which depends on the nature of the testing program, can be determined from Equation 22.8 ($\sigma^2 = 0.1521$) or estimated from Table 22.5.

Table 22.4. Reliability multipliers

Level of Analysis	Variance of $Ln(N_{supply})$	Variance of $Ln(N_{demand})$	Reliability Multiplier			
			60 Percent Reliablity (Z_R = 0.253)	80 Percent Reliability (Z_R = 0.841)	90 Percent Reliability (Z_R = 1.280)	95 Percent Reliability (Z_R = 1.640)
Level 1 (Surrogate Testing With Regression Model)	0.6	0.2	1.254	2.122	3.142	4.336
		0.4	1.288	2.319	3.597	5.155
		0.6	1.319	2.512	4.064	6.029
		1.0	1.377	2.897	5.048	7.960
	0.7	0.2	1.271	2.221	3.368	4.739
		0.4	1.304	2.416	3.829	5.585
		0.6	1.334	2.609	4.303	6.488
		1.0	1.391	2.994	5.306	8.485
Levels 2 and 3 (Fatigue Testing)	0.2	0.2	1.74	1.702	2.247	2.821
		0.4	1.216	1.918	2.695	3.562
		0.6	1.254	2.122	3.142	4.336
		1.0	1.319	2.512	4.064	6.029
	0.4	0.2	1.216	1.918	2.695	3.562
		0.4	1.254	2.122	3.142	4.336
		0.6	1.288	2.319	3.597	5.155
		1.0	1.349	2.705	4.547	6.962
	0.6	0.2	1.254	2.122	3.142	4.336
		0.4	1.288	2.319	3.597	5.155
		0.6	1.319	2.512	4.064	6.029
		1.0	1.377	2.897	5.048	7.960
	0.8	0.2	1.271	2.221	3.368	4.739
		0.4	1.304	2.416	3.829	5.585
		0.6	1.319	2.512	4.064	6.029
		1.0	1.377	2.897	5.048	7.960
	1.0	0.2	1.319	2.512	4.064	6.029
		0.4	1.349	2.705	4.547	6.962
		0.6	1.377	2.897	5.048	7.960
		1.0	1.430	3.285	6.112	10.169

Table 22.5. Variance of $Ln(N_{supply})$

Extrapolated Fatigue Life (N_{supply})	Number of Replicate Specimens					
	1	2	3	4	5	6
Laboratory Testing at Four Levels of Strain (Corresponding to 10,000, 35,000, 100,000, and 350,000 Load Cycles)						
1,000,000	0.367	0.260	0.224	0.206	0.195	0.188
1,500,000	0.421	0.287	0.242	0.219	0.206	0.197
2,000,000	0.464	0.308	0.256	0.230	0.214	0.204
3,000,000	0.531	0.342	0.278	0.247	0.228	0.215
4,000,000	0.583	0.368	0.296	0.260	0.238	0.223
6,000,000	0.662	0.407	0.322	0.280	0.254	0.237
8,000,000	0.723	0.438	0.342	0.295	0.266	0.247
12,000,000	0.817	0.483	0.373	0.318	0.285	0.262
16,000,000	0.884	0.518	0.396	0.335	0.298	0.274
24,000,000	0.988	0.570	0.431	0.361	0.319	0.291
32,000,000	1.067	0.609	0.457	0.381	0.335	0.304
Laboratory Testing at Two Levels of Strain (Corresponding to 10,000 and 350,000 Load Cycles)						
1,000,000	0.420	0.286	0.242	0.219	0.206	0.197
1,500,000	0.480	0.316	0.261	0.234	0.218	0.207
2,000,000	0.526	0.339	0.277	0.246	0.227	0.214
3,000,000	0.599	0.376	0.301	0.264	0.242	0.227
4,000,000	0.655	0.404	0.320	0.278	0.253	0.236
6,000,000	0.742	0.447	0.347	0.299	0.270	0.250
8,000,000	0.808	0.480	0.371	0.316	0.283	0.261
12,000,000	0.907	0.530	0.404	0.341	0.303	0.278
16,000,000	0.983	0.567	0.429	0.360	0.318	0.290
24,000,000	1.096	0.624	0.467	0.388	0.341	0.309
32,000,000	1.181	0.667	0.495	0.409	0.358	0.324

$$\text{Var}\{\text{Ln}(N_{supply})\} = \sigma^2 \left[1 + \frac{1}{n} + \frac{(X-\bar{x})^2}{q \, \Sigma \, (x_p-\bar{x})^2} \right] \qquad (22.8)$$

where:

	$\text{VAR}\{\text{Ln}(N_{supply})\}$	=	variance of the extrapolated fatigue life (Ln),
	σ^2	=	variance of laboratory fatigue life (Ln) (use 0.1521 for A-003A testing procedures and equipment),
	n	=	total number of test specimens,
	X	=	strain (Ln) at which extrapolated fatigue life (Ln) is required,
	$\bar{x}$	=	average test strain (Ln),
	q	=	number of specimens tested at each strain level, and
	x_p	=	strain (Ln) at pth strain level.

For both fatigue testing and the surrogate regression model, the variance can also be estimated using the approximate equations of Table 22.6.

$\text{Var}\{\text{Ln}(N_{demand})\}$ is a function primarily of the accuracy of the traffic estimates and, as a consequence, will vary from agency to agency.

22.12 If Inadequate, Alter Trial Mix and/or Structural Section and Iterate

If a particular mix is judged inadequate for a specific application, several options are available to the designer, including the following:

- Repeat the analysis with a less demanding level of design reliability.
- Reduce $\text{Var}\{\text{Ln}(N_{supply})\}$ by adding laboratory testing or by expanding its scope.
- Redesign the pavement structure to reduce tensile strain levels within the asphalt mix.
- Modify the mix design to improve its fatigue resistance.

Table 22.6. Regression equations for computing variance of $Ln(N_{supply})$

Estimation Procedure	Number of Replicate Specimens	$Var\{Ln(N_{supply})\}$
Laboratory Testing at Four Levels of Strain (Corresponding to 10,000; 35,000; 100,000; and 350,000 Load Cycles)	1	$0.005283\ (N_{supply})^{0.3085}$
	2	$0.008558\ (N_{supply})^{0.2472}$
	3	$0.01263\ (N_{supply})^{0.2076}$
	4	$0.01713\ (N_{supply})^{0.1792}$
	5	$0.02186\ (N_{supply})^{0.1575}$
	6	$0.02673\ (N_{supply})^{0.1402}$
Laboratory Testing at Two Levels of Strain (Corresponding to 10,000 and 350,000 Load Cycles)	1	$0.006903\ (N_{supply})^{0.2988}$
	2	$0.009653\ (N_{supply})^{0.2455}$
	3	$0.01345\ (N_{supply})^{0.2086}$
	4	$0.01764\ (N_{supply})^{0.1817}$
	5	$0.02213\ (N_{supply})^{0.1607}$
	6	$0.02643\ (N_{supply})^{0.1444}$
Regression Model		$0.4656\ (N_{supply})^{0.02401}$

23

General (Unabridged) Analysis System

The general analysis system (Level 3), used primarily for evaluation of mixes having binders of atypical temperature sensitivity, requires fatigue testing over a range of temperatures. The analysis process becomes quite complex as a result of the necessity to simulate the broad range of in situ temperature conditions. The accumulation of fatigue damage over the range of temperature levels is usually estimated using the linear-summation-of-cycle-ratios principle.

The recommended approach, which applies similar tools and is based on principles similar to those of more conventional approaches, is designed to produce mix-specific (and possibly site-specific as well) TEFs which can subsequently be used in a single-temperature analysis. This approach is recommended so that both abridged and unabridged analysis systems are similar in structure and in application.[13] Although the development of specific TEFs is a relatively detailed process (see Appendix J), it is no more complex than other approaches of comparable accuracy. Once the TEFs have been developed, the process of mix evaluation parallels that of Level 2 analysis.

To support the general analysis system, fatigue testing is generally recommended at four temperature levels: 10°, 15°, 20°, and 25°C (50°, 59°, 68°, and 77°F). Much of the expected in situ damage occurs within this span, and laboratory testing is facilitated by avoiding more extreme conditions. It may sometimes be desirable to test a larger number of specimens at 20°C (68°F)—that temperature at which the basic analysis is performed—than at the other temperatures to reduce the variability of the estimated fatigue life.

---

[13]Knowing the TEFs for new or unconventional mixes may also eliminate the need for comprehensive analysis when their use is being evaluated for other, subsequent applications.

24

Summary

Described herein is an innovative design and analysis system for evaluating the fatigue resistance of asphalt-aggregate mixes. This system provides an effective mechanism for interpreting laboratory fatigue measurements and determining the impact of asphalt-aggregate interactions on expected pavement performance. The analysis system assumes that a trial mix has been identified, that traffic loading (repetitions, wheel loads, and tire pressures) and environmental conditions (temperature) have been determined, and that the pavement cross-section has been designed. It then seeks to judge, with predetermined reliability, whether the trial mix would perform satisfactorily in service. If it would not, the designer can opt to redesign the mix, strengthen the pavement section, or repeat the analysis using more refined measurements and/or estimates.

For routine mix designs, the testing and analysis system has been simplified to the maximum possible extent. Laboratory testing is limited to stiffness measurements, and the primary analysis requires only a single estimate of in situ strains using traditional assumptions of linear elasticity. Unconventional mixes or uncommon applications, on the other hand, require more extensive testing and analysis for reliable decision making. Multiple-temperature fatigue testing must be performed, and analysis must address the complex thermal environment anticipated in situ.

Key features of the mix analysis system include the use of temperature conversion factors and quantitative reliability concepts. Temperature conversion factors—used to convert design ESALs to their equivalents at a common reference temperature of 20°C (68°F)—have been found to be an effective but simple way of treating environmental temperature effects and of reducing the necessity for extensive multiple temperature testing. Reliability concepts provide a quantitative means for comparatively judging the adequacy of surrogate testing-regression models vis-à-vis laboratory fatigue testing; they thus permit and encourage a hierarchical approach to mix design, which routinely simplifies the process but permits detailed analysis where necessary.

Conceptual development of the mix analysis system has been completed as part of SHRP Project A-003A, and considerable progress has been made toward establishing a readily

implementable package for use by material engineers nationwide. In addition to completing the calibration process, one of the key remaining tasks is to validate the analysis system by demonstrating its ability to reliably discriminate among suitable and unsuitable mixes.

References

American Association of State Highway and Transportation Officials (AASHTO) (1986). AASHTO guide for design of pavement structures—1986. American Association of State Highway and Transportation Officials, Washington, DC.

Bell, C. A., Y. AbWahab, M. E. Cristi, and D. Sosnovske (1994). *Selection of Laboratory Aging Procedures for Asphalt-Aggregate Mixtures*. Report No. SHRP-A-383. Strategic Highway Research Program, National Research Council, Washington, DC.

Bonnot, J. (1991). Based on conversation and presentation notes. SHRP Project A-003A, Richmond Field Station, University of California, Berkeley.

Bronstein, M., and J. B. Sousa (1987). Computer software ATS—testing system. SHRP Equipment Inc., Walnut Creek, CA.

Chomton, G., and P. J. Valayer (1972). Applied rheology of asphalt mixes, practical applications. *Proceedings*, Third International Conference on the Structural Design of Asphalt Pavements, London, vol. I, September.

Coplantz, J. S., and A. A. Tayebali (1992a). Statistical analysis of flexural fatigue validation testing. Technical memorandum TM-ARE-A-003A-92-2, prepared for SHRP Project A-003A. Asphalt Research Program, Institute of Transportation Studies, University of California, Berkeley, June.

Coplantz, J. S., and A. A. Tayebali (1992b). Comparison of A-002A parameters to field predicted fatigue life from ELSYM and SAPSI (elastic case). Technical memorandum TM-ARE-A-003A-92-6, prepared for SHRP Project A-003A. Asphalt Research Program, Institute of Transportation Studies, University of California, Berkeley.

Deacon, J. A., and A. A. Tayebali (1992a). Validation of surrogate fatigue model using mix design experiment. Technical memorandum prepared for SHRP Project A-003A. Institute of Transportation Studies, University of California, Berkeley, August.

Deacon, J. A., and A. A. Tayebali (1992b). Surrogate fatigue model. Technical memorandum prepared for SHRP Project A-003A. Institute of Transportation Studies, University of California, Berkeley, August.

Finn, F. N., C. Saraf, R. Kulkarni, K. Nair, W. Smith, and A. Abdullah (1977). The use of distress prediction subsystem for the design of pavement structures. *Proceedings*, Fourth International Conference on the Structural Design of Asphalt Pavements, University of Michigan, Ann Arbor, August.

Finn, F. N., C. L. Saraf, R. Kulkarni, K. Nair, W. Smith, and A. Abdullah (1986). Development of pavement structural subsystems. NCHRP Report 291. Transportation Research Board, Washington, DC.

Gramsammer, J. C., and J. P. Kerzreho (1992). Expérience fatigue des enrobés. Laboratoire Central des Ponts et Chaussées, Paris, France.

Harrigan, E. T., R. B. Leahy, and J. S. Youtcheff, ed. (1994). *The SUPERPAVE™ Mix Design System Manual of Specifications, Test Methods, and Practices*. Report No. SHRP-A-379. SHRP, National Research Council, Washington, DC.

Harvey, J. T. (1991). University of California at Berkeley SHRP A-003A asphalt concrete specimen preparation protocol, version 3.0. Technical memorandum no. TM-UCB-A-003A-91-2, prepared for the Strategic Highway Research Program, National Research Council, Washington, DC.

Hudson, W. R., and T. W. Kennedy (1968). An indirect tensile test for stabilized materials. Research report 9801. Center for Highway Research, The University of Texas, Austin.

Kennedy, T. W., G. A. Huber, E. T. Harrigan, R. J. Cominsky, D. A. Anderson, C.S. Hughes, H. von Quintus, and J. S. Moulthorp (1994). *SUPERPAVE™ System: The Product of the SHRP Asphalt Research Program*. SHRP, National Research Council, Washington, DC.

Lytton, R. L., D. Pufahl, C. Michalak, H. Liang, and B. Dempsey (1990). An integrated model of the climatic effects in pavements. FHWA-RD-90-33, Federal Highway Administration, Washington, DC.

Monismith, C. L., J. A. Epps, D. A. Kasianchuk, and D. B. McLean (1972). Asphalt mixture behavior in repeated flexure. Report No. TE70-5. Institute of Transportation and Traffic Engineering, University of California, Berkeley.

Monismith, C. L., J. A. Epps, and F. N. Finn (1985). Improved asphalt mix design. *Proceedings*, Association of Asphalt Paving Technologists, vol. 54, February.

Neter, J., W. Wasserman, and M. Kutner (1983). Applied statistical models: regression analysis of variance and experimental designs.

Porter, B. P., and T. W. Kennedy (1975). Comparison of fatigue test methods for asphaltic materials. Research Report 183-4. Center for Highway Research, The University of Texas, Austin.

Pronk, A. C., and P. C. Hopman (1990). Energy dissipation: The leading factor of fatigue. *Proceedings*, United States Strategic Highway Research Program—Sharing the Benefits, October 29-31, London.

Raithby, K. D., and A. B. Sterling (1972). Some effects of loading history on the performance of rolled asphalt. TRRL-LR-496. Transport and Road Research Laboratory, Crowthorne, England.

Robertus, C., J. S. Hughes, and D. J. Jongeneel (1992). Fatigue testing in laboratory and pavement cracking in Nantes Carrousel: Cooperative programme with LCPC, phase II. AMER.92.010, Code 500.50.310.SM3102-IN 31815. SHELL Internationale Research, Maatschappij, B.V.

Rowe, G. M. (1992). LCPC—fatigue tests at Nottingham. Report prepared for SHRP Project A-003A. SWK Pavement Engineering Ltd., Notthingham, United Kingdom.

Rowe, G. M, S. F. Brown, P. S. Pell, and R. J. Armitage (1993a). Fatigue wheel tracking—validation studies, volume I. Report prepared for SHRP Project A-003A. SWK Pavement Engineering Ltd., Nottingham, United Kingdom.

Rowe, G. M, S. F. Brown, P. S. Pell, and R. J. Armitage (1993b). Fatigue wheel tracking—validation studies, volume II. Report prepared for SHRP Project A-003A. SWK Pavement Engineering Ltd., Nottingham, United Kingdom.

Rowe, G. M, S. F. Brown, P. S. Pell, and R. J. Armitage (1993c). Fatigue wheel tracking—validation studies, volume III. Report prepared for SHRP Project A-003A. SWK Pavement Engineering Ltd., Nottingham, United Kingdom.

SHELL International (1978). Shell pavement design manual. London.

Sousa, J. B., R. Taylor, and A. Tanco (1991a). Analysis of some laboratory testing systems for asphalt-aggregate mixtures. TRB Paper No. 91-0743, presented at the annual meeting of the Transportation Research Board, Washington, D.C.

Sousa, J. B., J. Harvey, L. Painter, J. A. Deacon, and C. L. Monismith (1991b). Evaluation of laboratory procedures for compacting asphalt-aggregate mixtures. Technical Memorandum No. TM-UCB-A003A-90-1, prepared for SHRP Project A-003A. Institute of Transportation Studies, University of California, Berkeley.

Sousa, J. B., A. A. Tayebali, J. Harvey, P. Hendricks, and C. L. Monismith (1993). Sensitivity of SHRP A-003A testing equipment to mix design parameters for permanent deformation and fatigue. Paper presented at the annual meeting of the Transportation Research Board, January.

Tangella, R., J. Crauss, J. A. Deacon, and C. L. Monismith (1990). Summary report of fatigue response of asphalt mixtures. Technical Memorandum No. TM-UCB-A-003A-89-3M, prepared for SHRP Project A-003A. Institute of Transportation Studies, University of California, Berkeley.

Tayebali, A. A. (1991). Influence of shear deformation in flexural fatigue beam compared to the deformation due to bending. Technical memorandum prepared for SHRP Project A-003A. Asphalt Research Program, Institute of Transportation Studies, University of California, Berkeley, January.

Tayebali, A. A. (1992a). Surrogate flexural stiffness models based on shear stiffness. Technical memorandum prepared for SHRP Project A-003A. Institute of Transportation Studies, University of California, Berkeley.

Tayebali, A. A. (1992b). Re-calibration of surrogate fatigue models using all applicable A-003A fatigue data. Technical memorandum prepared for SHRP Project A-003A. Institute of Transportation Studies, University of California, Berkeley.

Tayebali, A. A. (1992c). Surrogate fatigue models based on flexural and shear loss stiffness and dissipated energy. Prepared for SHRP Project A-003A. Institute of Transportation Studies, University of California, Berkeley.

Tayebali, A., J. S. Coplantz, J. T. Harvey, and C. L. Monismith (1992a). Interim report on fatigue response of asphalt-aggregate mixtures. Report TM-UCB-A-003A-92-1, SHRP Project A-003A. Asphalt Research Program, Institute of Transportation Studies, University of California, Berkeley.

Tayebali, A., G. Rowe, and J. Sousa (1992b). Fatigue response of asphalt-aggregate mixtures. Paper presented at the annual meeting of the Association of Asphalt Paving Technologists, Charleston, SC, February.

The Asphalt Institute (1981). Manual Series No. 1 (MS-1), ninth edition. College Park, MD.

Tsai, B. W., and A. A. Tayebali (1992). Computer software for fatigue test data analysis for SHRP Project A-003A. Prepared for SHRP Project A-003A. Asphalt Research Program, Institute of Transportation Studies, University of California, Berkeley, January.

van Dijk, W. (1975). Practical fatigue characterization of bituminous mixes. *Proceedings*, Association of Asphalt Paving Technologists, vol. 44, Phoenix, AZ, February.

van Dijk, W., and W. Visser (1977). The energy approach to fatigue for pavement design. *Proceedings*, Association of Asphalt Paving Technologists, San Antonio, TX, February.

van Dijk, W., H. Moreaud, A. Quedeville, and P. Ugé (1972). The fatigue of bitumen and bituminous mixes. *Proceedings*, Third International Conference on the Structural Design of Asphalt Pavements, vol. 1, London, September 11-15.

Appendix A

Fatigue Test Results for the Expanded Test Program

Dynamic Flexural Fatigue, Controlled–strain Tests
20 C, 10 Hz Frequency
8x2 Expanded Test Program

Specimen Designation					Strain (in/in)	Stress (psi)	Stiffness (psi)	Life Nf 50% Ini. Stiff	Cumulative Dissipated Energy (psi)	Phase Angle (degrees)	Voids (%)	Voids Filled With Bitumen (%)
AT	AG	VO	ST	RP								
AAA	RH	0	0	0	0.0004	112.0	280000	400000	7242	50	3.4	77.8
AAA	RH	0	0	1	0.0004	102.5	256300	421270	6195	48	4.3	73.3
AAA	RH	0	1	0	0.0007	196.7	281000	82300	4530	52	3.3	78.3
AAA	RH	0	1	1	0.0007	212.7	303903	69885	4195	51	2.9	80.5
AAA	RH	1	0	0	0.0004	92.2	230586	600001	7958	48	7.4	60.7
AAA	RH	1	0	1	0.0004	103.7	259305	211666	3469	47	6.5	64.0
AAA	RH	1	1	0	0.0007	132.1	188702	71829	2648	52	8.0	58.7
AAA	RH	1	1	1	0.0007	159.1	227334	26050	1171	49	7.1	61.8
AAB	RH	0	0	0	0.0004	203.0	507619	661045	17420	36	3.4	77.7
AAB	RH	0	0	1	0.0004	167.9	419727	208387	4388	38	4.9	70.4
AAB	RH	0	1	0	0.0007	337.3	481812	47783	3904	39	3.0	79.8
AAB	RH	0	1	1	0.0007	396.4	566296	22770	2013	38	3.3	78.2
AAB	RH	1	0	0	0.0004	104.3	260759	364241	5477	42	7.0	61.9
AAB	RH	1	0	1	0.0004	123.5	308749	547203	8553	40	6.2	64.9
AAB	RH	1	1	0	0.0007	172.4	246346	14476	606	42	7.4	60.5
AAB	RH	1	1	1	0.0007	202.8	289686	15001	754	41	7.2	61.2
AAC	RH	0	0	0	0.0004	192.5	481278	163309	4660	41	4.4	72.8
AAC	RH	0	0	1	0.0004	201.5	503664	200001	5792	39	5.0	70.0
AAC	RH	0	1	0	0.0007	303.2	433204	24634	1806	43	4.1	74.2
AAC	RH	0	1	1	0.0007	341.0	487116	21082	1796	41	4.9	70.5
AAC	RH	1	0	0	0.0004	171.0	427567	88289	2011	37	7.3	61.0
AAC	RH	1	0	1	0.0004	157.6	394031	126269	2679	37	7.4	60.6
AAC	RH	1	1	0	0.0007	318.5	455067	21112	1691	39	8.0	58.6
AAC	RH	1	1	1	0.0007	261.3	373261	12766	846	41	6.8	62.8
AAD	RH	0	0	0	0.0004	112.1	280138	275001	4820	47	5.0	69.9
AAD	RH	0	0	1	0.0004	104.5	261154	240436	3703	46	4.7	71.3
AAD	RH	0	1	0	0.0007	226.4	323421	41068	2400	43	3.2	78.7
AAD	RH	0	1	1	0.0007	189.9	271282	60813	3060	46	4.5	72.2
AAD	RH	1	0	0	0.0004	99.9	249680	398575	5649	44	7.1	61.5
AAD	RH	1	0	1	0.0004	104.7	261827	542580	8062	44	6.6	63.4
AAD	RH	1	1	0	0.0007	209.6	299443	52273	2740	43	7.3	60.8
AAD	RH	1	1	1	0.0007	197.7	282460	45780	2307	44	6.1	65.3
AAF	RH	0	0	0	0.0004	380.6	951616	137775	5060	22	5.0	70.0
AAF	RH	0	0	1	0.0004	393.5	983642	109169	4347	23	4.4	72.8
AAF	RH	0	1	0	0.0007	674.7	963905	11159	1406	23	4.6	71.8
AAF	RH	0	1	1	0.0007	677.1	967305	13159	1666	23	3.7	76.2
AAF	RH	1	0	0	0.0004	278.4	696083	33854	921	23	7.8	59.2
AAF	RH	1	0	1	0.0004	292.9	732152	39119	1149	24	6.1	65.4
AAF	RH	1	1	0	0.0007	613.2	875958	9303	600	25	7.5	60.2
AAF	RH	1	1	1	0.0007	486.3	694703	5540	450	26	7.1	61.7

Note: AT = asphalt type
AG = aggregate type
VO = air void content (level)
ST = strain level
RP = replicate

Dynamic Flexural Fatigue, Controlled–strain Tests
20 C, 10 Hz Frequency
8x2 Expanded Test Program

Specimen Designation					Strain (in/in)	Stress (psi)	Stiffness (psi)	Life Nf 50% Ini. Stiff	Cumulative Dissipated Energy (psi)	Phase Angle (degrees)	Voids (%)	Voids Filled With Bitumen (%)
AT	AG	VO	ST	RP								
AAG	RH	0	0	0	0.0004	524.2	1310386	27537	1644	27	3.0	80.0
AAG	RH	0	0	1	0.0004	501.6	1254039	21284	1285	28	4.3	73.4
AAG	RH	0	1	0	0.0007	697.4	996218	3845	583	30	4.9	70.6
AAG	RH	0	1	1	0.0007	773.2	1104506	3291	578	31	4.6	72.0
AAG	RH	1	0	0	0.0004	412.4	1031115	12162	555	25	7.3	61.1
AAG	RH	1	0	1	0.0004	346.3	865633	23393	914	27	8.0	58.8
AAG	RH	1	1	0	0.0007	644.3	920395	1947	258	27	8.0	58.8
AAG	RH	1	1	1	0.0007	705.2	1007440	2270	325	28	7.0	62.2
AAK	RH	0	0	0	0.0004	235.0	587528	197801	5446	33	3.7	76.1
AAK	RH	0	0	1	0.0004	197.8	494481	250001	6385	36	3.3	78.2
AAK	RH	0	1	0	0.0007	441.9	631334	25364	2423	32	4.9	70.4
AAK	RH	0	1	1	0.0007	331.0	472869	20858	1613	37	4.9	70.4
AAK	RH	1	0	0	0.0004	198.7	496642	197559	5023	36	6.3	64.5
AAK	RH	1	0	1	0.0004	231.9	579684	86837	2468	31	6.8	62.7
AAK	RH	1	1	0	0.0007	300.0	428538	10567	679	35	6.5	63.8
AAK	RH	1	1	1	0.0007	402.3	574656	10572	883	30	6.4	64.2
AAM	RH	0	0	0	0.0004	216.5	541269	178627	4515	30	4.7	71.4
AAM	RH	0	0	1	0.0004	235.6	589103	246103	6383	28	4.4	72.8
AAM	RH	0	1	0	0.0007	366.7	523793	40105	3100	31	5.0	70.0
AAM	RH	0	1	1	0.0007	383.3	547619	42280	3216	30	4.0	74.7
AAM	RH	1	0	0	0.0004	172.4	430974	281790	5583	32	6.7	63.1
AAM	RH	1	0	1	0.0004	209.3	523354	281278	6471	30	6.6	63.5
AAM	RH	1	1	0	0.0007	272.4	389168	12764	799	33	7.2	61.3
AAM	RH	1	1	1	0.0007	287.9	411262	7099	477	35	6.7	63.1
AAA	RD	0	0	0	0.0004	166.2	415618	462500	10874	45	4.1	71.9
AAA	RD	0	0	1	0.0004	203.0	507463	81983	2268	43	3.1	77.3
AAA	RD	0	1	0	0.0007	264.3	377607	8378	537	39	4.4	70.3
AAA	RD	0	1	1	0.0007	275.6	393676	29127	2061	45	5.1	67.0
AAA	RD	1	0	0	0.0004	129.2	323089	225000	4204	44	6.6	60.7
AAA	RD	1	0	1	0.0004	138.9	347197	171401	3575	45	6.6	60.7
AAA	RD	1	1	0	0.0007	186.4	266311	32814	1668	50	6.8	59.9
AAA	RD	1	1	1	0.0007	170.7	243852	34228	1641	51	7.4	57.7
AAB	RD	0	0	0	0.0004	217.5	543824	121949	3725	39	4.3	70.7
AAB	RD	0	0	1	0.0004	203.4	508482	261776	6965	37	5.1	66.8
AAB	RD	0	1	0	0.0007	428.8	612567	15521	1533	36	3.3	76.0
AAB	RD	0	1	1	0.0007	349.8	499714	32000	2564	37	4.4	70.2
AAB	RD	1	0	0	0.0004	158.0	395042	160527	3279	40	7.9	55.8
AAB	RD	1	0	1	0.0004	158.0	395042	160527	3279	40	7.9	55.8
AAB	RD	1	1	0	0.0007	240.9	344118	18734	1141	43	6.7	60.1
AAB	RD	1	1	1	0.0007	259.0	370023	8856	560	43	6.0	62.9
AAC	RD	0	0	0	0.0004	363.6	909111	93634	3892	29	3.6	74.5
AAC	RD	0	0	1	0.0004	335.9	839788	123706	5062	33	2.9	78.5
AAC	RD	0	1	0	0.0007	609.6	870873	11873	1614	33	4.4	70.3
AAC	RD	0	1	1	0.0007	615.1	878704	10724	1486	33	3.7	73.9

Dynamic Flexural Fatigue, Controlled–strain Tests
20 C, 10 Hz Frequency
8x2 Expanded Test Program

Specimen Designation					Strain (in/in)	Stress (psi)	Stiffness (psi)	Life Nf 50% Ini. Stiff	Cumulative Dissipated Energy (psi)	Phase Angle (degrees)	Voids (%)	Voids Filled With Bitumen (%)
AT	AG	VO	ST	RP								
AAC	RD	1	0	0	0.0004	190.2	475605	73979	1939	39	6.6	60.6
AAC	RD	1	0	1	0.0004	206.0	515054	62742	1645	37	7.1	58.8
AAC	RD	1	1	0	0.0007	410.3	586150	10000	946	36	7.3	58.0
AAC	RD	1	1	1	0.0007	381.7	545290	10530	944	37	6.9	59.5
AAD	RD	0	0	0	0.0004	281.1	702675	100425	3491	34	4.3	70.9
AAD	RD	0	0	1	0.0004	246.9	617258	133653	4360	36	3.7	74.0
AAD	RD	0	1	0	0.0007	469.9	671325	9337	1052	36	4.8	68.4
AAD	RD	0	1	1	0.0007	444.3	634694	10254	1120	36	4.5	69.9
AAD	RD	1	0	0	0.0004	210.5	526142	60835	1609	36	6.1	62.7
AAD	RD	1	0	1	0.0004	163.0	407570	258846	5849	41	7.0	59.2
AAD	RD	1	1	0	0.0007	287.4	410614	22412	1585	42	7.0	59.2
AAD	RD	1	1	1	0.0007	278.8	398256	25327	1669	42	6.9	59.6
AAF	RD	0	0	0	0.0004	541.6	1354033	101844	5545	23	3.1	77.4
AAF	RD	0	0	1	0.0004	541.6	1354033	101844	5545	23	3.1	77.4
AAF	RD	0	1	0	0.0007	917.2	1310302	10173	1603	23	4.4	70.4
AAF	RD	0	1	1	0.0007	766.5	1094966	7460	1006	24	4.0	72.4
AAF	RD	1	0	0	0.0004	465.8	1164535	49655	2149	20	7.3	58.1
AAF	RD	1	0	1	0.0004	502.9	1257144	51285	2422	21	7.6	57.1
AAF	RD	1	1	0	0.0007	842.0	1202883	6111	898	24	6.8	60.0
AAF	RD	1	1	1	0.0007	869.9	1242772	9425	1386	22	6.0	63.1
AAG	RD	0	0	0	0.0004	658.4	1645964	25765	1526	18	4.4	70.4
AAG	RD	0	0	1	0.0004	441.1	1102628	14553	850	34	3.1	77.3
AAG	RD	0	1	0	0.0007	833.5	1190716	1933	361	31	3.6	74.5
AAG	RD	0	1	1	0.0007	818.9	1169842	2065	377	33	3.7	74.0
AAG	RD	1	0	0	0.0004	556.2	1390451	20964	836	22	7.9	56.0
AAG	RD	1	0	1	0.0004	554.1	1385351	20365	1000	21	8.1	55.3
AAG	RD	1	1	0	0.0007	784.2	1120251	4000	682	26	7.4	57.8
AAG	RD	1	1	1	0.0007	845.6	1207954	1560	218	22	7.8	56.4
AAK	RD	0	0	0	0.0004	266.3	665762	99511	3395	35	4.8	68.0
AAK	RD	0	0	1	0.0004	313.9	784823	172019	6320	31	4.2	71.0
AAK	RD	0	1	0	0.0007	489.0	698510	15688	1702	34	4.0	72.0
AAK	RD	0	1	1	0.0007	450.1	642944	29779	3019	34	3.2	76.4
AAK	RD	1	0	0	0.0004	254.6	636436	144005	4486	35	6.4	61.1
AAK	RD	1	0	1	0.0004	286.3	715710	136335	4766	32	6.1	62.3
AAK	RD	1	1	0	0.0007	415.5	593598	15566	1470	36	6.1	62.3
AAK	RD	1	1	1	0.0007	397.8	568229	10206	954	36	6.9	59.1
AAM	RD	0	0	0	0.0004	291.2	728105	307500	9593	29	4.2	71.2
AAM	RD	0	0	1	0.0004	288.1	720310	452960	14189	30	4.1	71.8
AAM	RD	0	1	0	0.0007	510.7	729574	17279	1850	31	3.9	72.8
AAM	RD	0	1	1	0.0007	471.1	672964	22547	2226	32	4.0	72.3
AAM	RD	1	0	0	0.0004	376.4	941019	196378	6790	24	6.1	62.6
AAM	RD	1	0	1	0.0004	355.2	888063	174250	6345	25	6.7	60.2
AAM	RD	1	1	0	0.0007	435.7	622358	24455	2183	30	7.7	56.6
AAM	RD	1	1	1	0.0007	496.7	709638	15145	1577	30	6.0	63.0

Appendix B

Flexural and Shear Stiffnesses and Phase Angles at 20°C and 10 Hz Frequency for the 8x2 Experiment

Specimen Designation	Flexural Stiffness (psi)	Shear Stiffness (psi)	Flexural Phase Angle (degrees)	Shear Phase Angle (degrees)	Voids (%)	Voids Filled With Bitumen (%)
AAARH	303903	109200	51	42.8	2.9	80.5
AAARH	188702	63642	52	38.0	8.0	58.7
AABRH	566296	127490	38	28.6	3.3	78.2
AABRH	246346	98022	42	27.5	7.4	60.5
AACRH	503664	188845	39	26.6	5.0	70.0
AACRH	373261	201755	41	26.9	6.8	62.8
AADRH	323421	158084	43	30.5	3.2	78.7
AADRH	249680	129422	44	35.2	7.1	61.5
AAFRH	983642	222269	23	17.8	4.4	72.8
AAFRH	694703	310157	26	17.8	7.1	61.7
AAGRH	1310386	306830	27	22.0	3.0	80.0
AAGRH	865633	251426	27	21.3	8.0	58.8
AAKRH	472869	188585	37	28.8	4.9	70.4
AAKRH	428538	144878	35	25.5	6.5	63.8
AAMRH	589103	185809	28	23.6	4.4	72.8
AAMRH	389168	132065	33	24.9	7.2	61.3
AAARD	507463	161836	43	35.8	3.1	77.3
AAARD	347197	95994	45	40.9	6.6	60.7
AABRD	612567	195195	36	26.5	3.3	76.0
AABRD	344118	162592	43	28.3	6.7	60.1
AACRD	909111	247035	29	24.6	3.6	74.5
AACRD	475605	222357	39	27.3	6.6	60.6
AADRD	702675	206752	34	33.7	4.3	70.9
AADRD	398256	158678	42	36.9	6.9	59.6
AAFRD	1354033	400018	23	17.2	3.1	77.4
AAFRD	1164535	369987	20	17.6	7.3	58.1
AAGRD	1645964	520149	18	17.7	4.4	70.4
AAGRD	1120251	408234	26	19.4	7.4	57.8
AAKRD	784823	258925	31	27.2	4.2	71.0
AAKRD	568229	238221	36	28.0	6.9	59.1
AAMRD	729574	340757	31	21.5	3.9	72.8
AAMRD	622358	191167	30	20.3	7.7	56.6

Appendix C

Fatigue Test Results for the Mix Design Study

Dynamic Flexural–Fatigue, Controlled–Strain Test,
20 C, 10 Hz Frequency
Mix Design Study

Specimen Designation	Micro Strain (in/in)	Stress (psi)	Stiffness (psi)	Life Nf 50% Ini. Stiff	Cumulative Dissipated Energy (psi)	Phase Angle (degrees)	Voids (%)	Voids Filled With Bitumen (%)
C1	700	626.7	914891	1628	223	31.4	5.0	67.8
C3	400	383.5	934678	7079	316	30.0	4.6	69.7
C3	200	290.4	1432829	86987	1122	22.0	4.6	69.7
C4	300	366.1	1314269	36602	1020	18.0	4.6	69.7
G1	700	604.9	844472	4661	633	33.5	4.4	75.6
G2	400	332.0	812505	21060	910	33.6	4.4	75.6
G3	200	187.5	916362	300000	3323	30.4	4.2	76.5
C1	700	788.4	1112430	1067	155	26.2	5.7	64.7
C2	400	339.0	854359	8633	362	30.8	5.7	64.7
C3	200	197.8	968740	61593	663	28.0	5.9	63.9
G2	700	666.7	926546	3114	444	31.7	5.0	73.1
G3	400	391.4	1006416	23837	1200	31.7	5.4	71.5
G4	300	330.0	1079377	93032	2564	27.5	4.8	73.9
G5	200	208.0	1023180	267723	3332	28.6	4.8	73.9
C1	300	295.1	1034504	14432	349	25.8	6.6	61.1
C2	700	555.5	766760	581	58	28.7	7.8	56.7
C3	400	227.0	586680	9010	279	35.4	8.2	55.4
C4	200	124.9	623386	39982	320	34.5	8.8	53.5
G1	200	165.5	821402	135125	1650	32.1	7.3	64.5
G2	700	510.3	711476	3250	352	32.0	8.6	60.3
G3	400	324.2	778908	13742	554	32.0	7.8	62.8
G4	300	246.9	838106	69507	1557	31.0	7.1	65.2

Note: All mixes with binder AAG and aggregate RB
C – asphalt content = 4.5%
G – asphalt content = 6.0%
1 = air void level 4 – 5%
2 = air void level 5 – 6%
3 = air void level 6 – 7%
4 = air void level 7 – 9%
5 = air void level > 9%

Appendix D

Fatigue Test Results for the Temperature Equivalency Factors Experiment

Dynamic Flexural–Fatigue, Controlled–Strain Test
5, 10, 20 and 25 C, 10 Hz Frequency
Temperature Equivalency Factors Experiment

Test No	Test Temperature (degrees C)	Micro Strain (in/in)	Stress (psi)	Stiffness (psi)	Life Nf 50% Ini. Stiff	Cumulative Dissipated Energy (psi)	Phase Angle (degrees)	Voids (%)	Voids Filled With Bitumen (%)
1	25	1200	177.2	147658	23584	2074	55.0	4.4	72.6
2	25	1000	204.0	203980	30787	2325	49.0	4.1	74.1
3	25	620	137.9	222412	159340	5200	47.0	2.8	80.9
4	25	600	151.8	253012	273544	8755	47.0	3.1	79.3
5	20	1000	298.3	298283	10403	1230	44.2	5.3	68.6
6	20	900	310.5	345009	16137	1751	43.6	3.5	77.1
7	20	700	226.4	323421	41068	2400	43.0	3.2	78.7
8	20	700	189.9	271282	60813	3060	46.0	4.5	72.2
9	20	600	246.6	411001	154573	8316	40.0	3.5	77.1
10	20	400	196.8	491877	684892	15848	35.5	4.3	73.1
11	20	400	112.7	280138	275001	4820	47.0	5.0	69.9
12	20	400	103.4	261154	240436	3703	46.0	4.7	71.3
13	10	700	618.4	883392	5689	674	25.2	4.4	72.6
14	10	600	608.8	1014712	18042	1558	22.0	3.8	75.6
15	10	600	505.9	843099	32395	2524	26.2	4.6	71.7
16	10	500	369.5	739051	49826	2701	28.5	5.2	69.0
17	10	350	341.2	974812	285619	8466	24.0	4.5	72.2
18	10	300	344.0	1146564	528808	12349	20.3	3.2	78.7
19	5	500	697.7	1395319	35822	2178	17.2	5.3	68.6
20	5	400	331.9	829764	45141	1375	24.1	3.1	79.3
21	5	350	406.7	1162135	142332	4182	18.7	4.6	71.7
22	5	350	558.1	1594451	170816	6538	18.2	3.5	77.1
23	5	300	431.5	1438183	416981	9402	16.0	5.1	69.5

Appendix E

Fatigue Test Results for the Modified Asphalt Mix Experiment

Dynamic Flexural–Fatigue, Controlled–Strain Test
20 C, 10 Hz Frequency
Modified Asphalt Mixture Experiment

Control–F	700	376.2	530933	2131	146.4	7.60	25.3	59.9
Control–F	700	417.6	601026	1940	157.8	7.10	27.1	61.6
Control–F	400	291.8	712882	37563	985.3	6.70	21.6	63.1
Control–F	400	195.5	481087	19344	393.5	6.70	28.0	63.1
Control–G	700	411.8	603759	640	52.9	7.10	29.2	61.5
Control–G	700	622.2	894513	2063	244.8	6.30	26.2	64.5
Control–G	400	397.9	973220	15869	563.2	6.00	22.4	65.7
Control–G	400	273.8	669110	6496	210.3	6.00	29.7	65.7
Control–K	700	303.2	438144	5152	350.6	6.80	32.0	62.7
Control–K	700	308.8	433651	4029	295.5	6.30	34.4	64.6
Control–K	400	166.5	418174	16783	356.6	6.40	33.6	64.2
Control–K	400	152.2	374896	47907	806.4	7.70	31.6	59.5
M405–F	700	314.6	452239	461	18.6	6.50	19.2	64.5
M405–F	700	607.7	830791	939	62.8	6.10	16.2	66.0
M405–F	400	321.9	797959	13978	278.2	7.00	14.6	62.6
M405–F	400	266.2	645576	28881	378.2	6.80	12.9	63.4
M405–G	700	530.3	751979	551	31.4	6.60	17.5	64.3
M405–G	700	457.9	638971	437	20.8	7.10	17.1	62.5
M405–G	400	217.2	548826	8333	109.4	6.60	18.4	64.3
M405–G	400	232.8	603014	1763	49.1	6.00	29.8	66.6
M405–K	700	273.7	379353	496	16.3	6.70	20.5	63.9
M405–K	700	286.3	402260	924	30.8	7.40	18.5	61.4
M405–K	400	195.3	489838	15525	204.7	7.70	19.5	60.4
M405–K	400	256.3	621717	36385	753.3	6.50	19.6	64.6
M415–G	700	351.7	516148	235	15.8	6.30	35.6	65.4
M415–G	700	456.7	636496	452	38.5	6.10	30.5	66.2
M415–G	400	249.2	629529	2553	81.1	6.20	31.6	65.8
M415–G	400	252.6	644332	4949	151.1	6.80	31.1	63.5
M415–K	700	162.7	230227	12955	541.6	7.80	42.1	60.1

Dynamic Flexural–Fatigue, Controlled–Strain Test
20 C, 10 Hz Frequency
Modified Asphalt Mixture Experiment

M415–K	700	154.1	214069	15848	592.2	7.10	41.2	62.5
M415–K	400	105.6	271712	105308	1466.7	7.40	38.0	61.5
M415–K	400	128.6	338694	63336	1120.5	6.90	37.6	63.2
M416–G	700	513.6	746800	829	89.7	6.80	32.3	63.7
M416–G	400	292.9	727757	4861	171.4	6.00	31.9	66.7
M416–G	400	245.2	622198	4637	145.6	6.90	33.9	63.3
M416–K	700	148.5	210757	21007	807.6	7.30	46.3	61.9
M416–K	700	204.1	296825	19330	983.8	7.20	42.6	62.2
M416–K	400	99.4	242388	164627	2076.3	6.50	37.6	64.8
M416–K	400	104.4	266626	150000	2260.1	6.80	42.1	63.7

Note: F = binder AAF
G = binder AAG
K = binder AAK

Appendix F

Fatigue Test Results for the LCPC-Nantes Study

Dynamic Flexural–Fatigue, Controlled–Strain Test
20 C, 10Hz Frequency,
Tests for Nantes (LCPC) Fatigue Test Program

Test Sections	Micro Strain (in/in)	Stress (psi)	Stiffness (psi)	Life Nf 50% Ini. Stiff	Cumulative Dissipated Energy (psi)	Phase Angle (degrees)	Voids Filled With Bitumen (%)	Voids (%)
Asphalt–B	300	193.8	635096	5404900	88606	33.0	73.4	4.60
60/70 pen	400	242.0	581833	1800000	53562	35.0	74.8	4.30
5.4% a/c	500	305.7	592623	204202	9616	34.0	73.9	4.50
	600	350.4	558024	69847	4692	37.0	79.6	3.30
	800	365.2	462077	27016	2823	40.0	75.7	4.10
	1200	470.0	370588	6814	1367	43.0	75.7	4.10
Asphalt–A	200	153.8	741831	3600000	29500	33.5	78.3	3.50
60/70 pen	300	216.0	704516	1047510	21578	35.0	81.5	2.90
5.4% a/c	400	274.2	677054	213097	7540	36.3	72.7	4.70
	600	460.5	742027	22888	2040	37.1	77.3	3.70
	800	497.3	636699	6907	985	39.4	74.9	4.20
High Mod. Mix	400	580.2	1421325	869452	40226	18.0	89.6	1.70
10/20 pen	600	870.1	1384725	78154	8711	20.0	89.0	1.80
6.2% a/c	800	1112.8	1348857	13748	2888	20.0	89.6	1.70
	1000	1239.4	1219685	6405	1857	22.0	90.1	1.60
Asphalt–A	200	190.2	935086	1199150	12112	30.0	67.7	5.20
60/70 pen	400	314.1	784160	78416	3168	33.0	66.9	5.40
4.6% a/c	600	408.1	701081	16893	1411	34.0	66.9	5.40
	800	634.2	754282	3254	550	33.0	67.3	5.30

Appendix G

Fatigue Test Results for the FHWA-ALF Study

Dynamic Flexural–Fatigue, Controlled–Strain Test
20 C, 10 Hz Frequency,
FHWA (ALF) Study

Section Identification	Micro Strain (in/in)	Stress (psi)	Stiffness (psi)	Life Nf 50% Ini. Stiff	Cumulative Dissipated Energy (psi)	Phase Angle (degrees)	Voids (%)	Voids Filled With Bitumen (%)
ALF–A	800	475.1	616285	7275	921	35.9	3.8	75.2
ALF–B	800	501.9	630939	10745	1386	33.8	3.7	75.7
ALF–C	600	397.4	631725	37925	2741	33.6	4.3	72.7
ALF–D	600	415.0	670141	33636	2493	32.8	4.7	70.9
ALF–E	400	284.1	685005	129581	4131	30.7	5.3	68.2
ALF–F	400	294.1	713270	128231	4313	30.7	4.3	72.7
ALF–G	200	169.1	845500	1800000	13192	27.6	3.6	76.2
ALF–H	200	145.8	779080	1100000	9197	29.6	3.6	76.2

Appendix H

Development of Temperature Equivalency Factors

1. Objective

The objective is to develop a set of temperature equivalency factors (TEFs) that can be used in Level 3 analysis. Level 3 analysis requires fatigue testing over a range of temperatures representative of in situ conditions. Level 3 analysis is necessary when using modified binders or binders of atypical temperature sensitivity and is optional for increased accuracy and complete mix cataloging.

2. Definition

The TEF is a multiplicative factor used to convert the number of load applications at one temperature, i, to an equivalent number of load applications at a common reference temperature of 20°C (68°F). Thus

$$TEF_i \times ESAL_i = \text{Equivalent } ESAL_{20°C} \quad \text{(H.1)}$$

where:

TEF_i	=	temperature equivalency factor for ith temperature category, and
$ESAL_i$	=	design ESALs accumulating during ith temperature interval.

TEFs must be developed for a number of temperature categories (2.5°C [36.5°F] range) based on the temperature at the bottom of the asphalt layer.

3. Approach

The approach described herein is rather detailed; it doesn't rely on many arbitrary assumptions. However, examination of only one half of the 8,760 hours in each year reduces the computational effort without sacrificing accuracy. For each of these 4380 hours, the number of repetitions of a standard load that will initiate fatigue cracking must be determined. Then by categorizing the hours into approximately 25

temperature categories, the average number of repetitions (N_i) is determined for each category. The computation of TEFs is as follows:

$$TEF_i = N_{20°C}/N_i \quad \text{(H.2)}$$

where: $N_{20°C}$ = the number of load repetitions to failure at 20°C (68°F), and

N_i = the number of load repetitions to failure at the ith temperature.

4. Fatigue Testing

Level 3 analysis requires laboratory fatigue testing over a range of temperatures that reasonably represent in situ conditions. Testing is generally recommended at four levels (10°, 15°, 20°, and 25°C [50°, 59°, 68°, and 77°F]). Much of the expected in situ damage occurs within this span, and laboratory testing is facilitated by avoiding more extreme conditions. Testing at each temperature can be completed within a span of 24 hours by using a single replicate and selecting four test strains expected to induce failure at about 10,000; 35,000; 100,000; and 350,000 repetitions. It may sometimes be desirable to test a larger number of specimens at 20°C (68°F)—the temperature at which the basic analysis is performed—than at the other temperatures. A second replicate at 20°C (68°F) will reduce the variability in the fatigue life estimate by 30 to 40 percent, depending on the required extent of extrapolation, without extending testing beyond a 5-day work week.

5. Conditions for Analysis

a. Location/temperature

Pavement temperatures, sensitive to local climatic conditions, are determined using the Federal Highway Administration's (FHWA's) integrated model.

b. Pavement structure

For temperature analysis with FHWA's integrated model, the pavement structure can be represented by as many as five different layers. For stress analysis, the maximum number of layers is limited by the capabilities of the computer software that is used. The number of layers for temperature analysis may differ from the number for stress analysis.

c. Pavement analysis

Multilayered elastic analysis is used to estimate pavement strains under a standard axle load. Although any suitable computer program can be used, ELSYM—and other packages with five-layer limitations—requires the structure to be represented as a two- or at most a three-layer system. The surface layer

is in turn represented by four or perhaps three individual sublayers to reflect as accurately as possible the temperature-profile effects on modulus and fatigue life.

d. Stiffness model

Initial flexural stiffnesses, measured during the fatigue testing, are used in the multilayered elastic analysis. Using laboratory data, a regression model is developed relating flexural stiffness to temperature. A model of the following form has proved sufficient for prior analysis and should serve as an effective point to begin future work:

$$S_o = K1 \cdot T^{K2} \quad \text{(H.3)}$$

where: S_o = initial flexural stiffness in psi after 50 loading cycles, and
T = temperature.

e. Fatigue model

The laboratory fatigue data are also used to characterize the fatigue behavior of the asphalt-aggregate mix. A regression model is developed relating fatigue life to both tensile strain and test temperature. A model of the following form has proved sufficient for prior analysis and should serve as an effective point to begin future work:

$$N_f = 10^{(K1 + K2 \cdot T)} \cdot \epsilon^{(K3 + K4 \cdot T)} \quad \text{(H.4)}$$

where: N_f = number of cycles to a 50 percent reduction in stiffness,
ϵ = maximum tensile strain in the specimen, and
T = temperature.

f. Load

The standard load is an 18,000 lb, single-axle load supported by dual tires 30 cm (12 in.) spacing having a contact pressure of 85 psi.

6. Temperature Profiles

Temperatures are computed using FHWA's integrated model for 0100, 0300, ..., 2100 hours for each of the 365 days in a typical year. Twelve runs of the program are required for each specific location. A 0.125 hour time step is used, and times of minimum and maximum temperatures are measured at 0600 and 1500 hours, respectively. The constant deep ground temperature depends on the geographic location of the pavement.

Output can be documented in tables and graphs, and a computer file should be generated for use in later analyses.

7. Standard Sections

Because of the varying temperature profile, the pavement section is a bit different for each of the 4380 hours. To keep the ELSYM runs manageable, approximately 72 standard sections are developed. The 72 sections represent all possible combinations of nine bottom-surface temperature categories (ranging from -5° to 35°C [23° to 95°F] in increments of 5°C [9°F]) and eight temperature gradient categories (ranging from -1.5° to 0.6°C per inch [29° to 33°F] in increments of 0.3°C [0.5°F] per inch). Although the temperature gradient can represent the difference in temperatures between any two arbitrary depths, it is recommended that temperatures at the bottom surface of the asphalt layer and at a 5 cm (2 in.) depth be used. The gradient must be computed for each of the 4380 hours being analyzed.

In performing ELSYM computations, it is not necessary to assume a *linear* temperature gradient, even though each of the 4380 hours will have been characterized that way. Instead temperatures for the 72 ELSYM computations should be averages computed by first grouping each of the 4380 hours of data into 1 of the 72 categories (excluding the few extreme hours).

For each of the 72 sections, asphalt-layer stiffnesses are computed at the midpoints of each of four sublayers,[14] and ELSYM computations are performed assuming the standard axle load. The ELSYM output of interest is the maximum principal tensile strain at the bottom of the asphalt layer. It is sufficient to examine locations beneath the centerline of one tire of the dual set, at the inside edge of one tire, and at the midpoint location.

8. Fatigue Life for Standard Sections

Fatigue life is computed directly using Equation H.4. Independent variables are the temperature and the maximum principal tensile strain at the bottom of the asphalt layer.

9. Regression Analysis

The fatigue life calculations of section 8 yield 72 estimates of N_f, varying by temperature level at the bottom surface and by temperature gradient. A regression model must be calibrated to determine N_f as a function of these two variables. A

[14]The asphalt layer is typically divided into four layers of equal thickness, regardless of the total layer thickness. Midpoint temperatures of each of the four sublayers are determined by interpolation.

model of the following form has proved sufficient for prior analysis and should serve as an effective point to begin future work:

$$Ln(N_f) = K1 + K2 \cdot T + K3 \cdot G + K4 \cdot T^2 + K5 \cdot G^2 + K6 \cdot T \cdot G \qquad (H.5)$$

where: $Ln(N_f)$ = natural logarithm of fatigue life,
T = temperature at the bottom of the asphalt layer, and
G = temperature gradient through the asphalt layer.

10. Fatigue Life for Each Hour

Using the regression model, determine the fatigue life (N_f) for each of the 4380 hours.

11. Average Fatigue Life for Each Temperature

Categorize the 4380 hours into approximately 25 temperature categories (at bottom of asphalt layer) and compute the average fatigue life for each category. In past work, temperature categories having a range of 2.5°C (36.5°F) and centered on -15°C, -12.5°, -10.0°, ... , 40.0°, 42.5°, and 45.0°C (5°, 9.5°, 14°, ... , 104°, 108.5°, 113°F) have proven satisfactory.

12. Temperature Equivalency Factors

Compute and tabulate TEFs (Step 3) for a common reference temperature of 20°C (68°F).

13. Temperature Conversion Factor for ESALs

Finally, if the analysis is being performed for a single application rather than general cataloging, the temperature conversion factor for ESALs can be easily determined. This factor is the summation of the products of frequency of temperature occurrence and the temperature equivalency factor for each temperature interval.